THE DEVELOPMENT OF AN EXPERIMENTAL PATHWAY FOR THE SYNTHESIS OF ORGANIC SEQUENTIAL INTERPENETRATING POLYMER NETWORK (IPN) MICROGEL DISPERSIONS

by

Simon Richard Washbrook

A Doctoral Thesis

Submitted in partial fulfilment of the requirements

for the award of

Doctor of Philosophy

of

Loughborough University

10 December 1998

M0001026LB

ABSTRACT

Research into the synthesis of sequential, poly(n-butyl acrylate), PnBA/polystyrene, PS, IPN microgel (μ-gel) dispersions in organic media was performed. Poly(styrene-co-divinylbenzene), PS/DVB (0, 1, 5 & 10 weight % DVB), particles were synthesised by emulsion copolymerisation and these microgels were characterised by dynamic mechanical thermal analysis (DMTA), gel permeation chromatography and diffuse reflectance Fourier transform infrared (DRIFT) spectroscopy.

DMTA studies of acrylic microgel and macrogel samples, PnBA crosslinked with neopentyl glycol diacrylate, NPGDA ($\leq$ 20 wt.%), and ethylene glycol dimethacrylate ($\leq$ 20 wt.%), indicated that NPGDA was the more suitable crosslinking agent.

The solubility of styrene and n-butyl acrylate (nBA) monomers in a wide range of organic liquids was determined (25°C). Monomers were found to be miscible (at all compositions) with each of the liquids. Polymerisation within μ-gel dispersions could not, therefore, be performed ideally (under modified quasi-emulsion conditions).

Fourier transform infrared (FTIR) spectroscopy analysis of PS macrogels (1, 5 & 10 wt.% DVB) swollen with benzyl alcohol/nBA mixtures (10 wt.% nBA) showed that networks were not preferentially swollen with monomer (25°C). Free radical (FR) initiation of acrylic polymerisation within organic microgel dispersions could not, therefore, readily generate IPN particles (macrogel synthesis would also occur).

Attempts were, therefore, made at synthesising FR initiators within microgel particles. The peroxide monomers, t-butylperoxy-2-methacryloyloxyethyl carbonate (PMEC), di-t-butylperoxy fumarate and t-butylperoxyallyl carbonate were synthesised. Peroxides were characterised by ^{1}H/^{13}C nuclear magnetic resonance and FTIR spectroscopies. Emulsion copolymerisation of styrene with each peroxide (5 mole % peroxide) was performed (75°C). FTIR spectroscopy and differential scanning calorimetry showed that PMEC was the most suitable peroxide monomer. Analysis of poly(styrene/DVB/PMEC) microgels dispersed in nBA/NPGDA mixtures demonstrated that thermally-induced copolymerisation of the comonomers occurred at temperatures (T) required for peroxide decomposition (T $\geq$ 110°C).

To Melissa Hynes

.

Am I in earth, in heaven, or in hell ?

Sleeping or waking ? mad or well advised ?

Known unto these, and to myself disguised !

I 'll say as they say, and persever so,

And in this midst at all adventures go.

William Shakespeare (1564 - 1616 AD)

ACKNOWLEDGEMENTS

CONTENTS

CHAPTER 3 - POLYSTYRENE MICROGELS

CHAPTER 8

CHAPTER 1

INTRODUCTION

1.1 - INITIAL OBJECTIVES FOR THIS EXPERIMENTAL INVESTIGATION

Microgels, intramolecularly crosslinked polymer particles of sub-micron dimensions, are used as rheological modifiers for high-solid organic coatings (section 1.7.2).

The objectives of this project were:

1.   To synthesise and characterise polystyrene microgel particles.

2.   To synthesise and characterise P*n*BA microgel particles.

3.   To characterise organic PS and acrylic microgel dispersions.

4.   To determine the monomer-swelling behaviour of microgel particles dispersed in organic diluent/monomer mixtures.

5.   To synthesise sequential PS/P*n*BA IPN microgels from second-stage polymerisations within the particles of organic microgel dispersions.

6.   To characterise PS/P*n*BA IPN particles and IPN microgel dispersions.

IPNs, with one elastomeric component and one glassy component at the use temperature, can behave as reinforced rubbers or impact-resistant plastics, to a degree dependent upon which of the components is the more continuous phase for the blend (section 1.4). One method for synthesising sequential IPNs involves the initial preparation of a macrogel sample. The network is subsequently swollen with monomer/crosslinking agent (along with free radical initiator) and polymerisation of the second monomer is then initiated - in an attempt to synthesise a composite material where the first and second networks are intimately mixed (section 1.4). One drawback of this procedure is that the IPN product cannot be dispersed in an organic medium (the material is merely swollen by organic diluent). Consequently, thin polymer films cannot be prepared by spraying high-solid IPN coating formulations onto a substrate, followed by particle coalescence during diluent evaporation, as would be the case for IPN microgel formulations.

IPNs can also be synthesised by sequential emulsion polymerisation (section 1.6.4). Such, latex, IPNs are synthesised by the addition of monomer to a microgel emulsion followed by polymerisation of the monomer within the first-formed latex particles. The second-stage monomer is, in general terms, practically immiscible with the aqueous phase of the latex, and the monomer constitutes a droplet phase during latex

2

agitation. At equilibrium, the system contains partially monomer-swollen gel particles and monomer droplets, with a small amount of monomer dissolved in the aqueous phase (sections 1.6.1 and 1.6.2). Addition of a continuum-soluble free radical initiator is considered to generate initially water-soluble oligomeric radicals which propagate within the continuous phase until they reach a certain, critical, chain-length, when they precipitate from solution (sections 1.6.1 and 1.6.3). It is considered that each macro-radical adheres to the surface of a first-formed network particle and propagates, as monomer molecules dissolved in the aqueous phase, and monomer within the gel particle, diffuse toward the radical. (Macro-radicals are not considered to diffuse into the swollen particles and then propagate, as a consequence of chain entanglement effects). Consequently, a low level of molecular-mixing between the two network components is often found for latex IPN systems (section 1.6.4).

Polymerisation of second-stage monomer within the particles of an organic microgel dispersion was to be undertaken within this project. Employment of an organic continuous phase was considered desirable, since interfacial tensions within the system would be considerably lower than for latex IPN synthesis. It was anticipated that polymerisation within perfectly-swollen network particles could yield IPN microgels of ideal structure (particles with notable degrees of mixing between the two components). The partitioning of monomer within organic microgel dispersions was of fundamental importance for this investigation. If monomer exclusively partitioned within the gel particles, conventional free radical (FR) initiators could be used for IPN synthesis. If significant levels of monomer were to partition within the microgel particles, and the remaining monomer were to constitute a droplet phase, polymerisation could then have been attempted under a modified form of quasi-emulsion conditions (if an organic dispersant-soluble/monomer-insoluble FR initiator had been available). Partial monomer swelling of microgels, with significant monomer levels in the continuous phase (an organic diluent/monomer mixture), would not generate IPN microgel dispersions, if conventional FR initiators were employed (macrogel synthesis would also occur). This swelling behaviour would have been undesirable, and the synthesis of microgels containing polymer-bound FR initiator groups, located within the gel particle-interior, would have then been required for the synthesis of IPNs.

1.2 - POLYMER NETWORKS

Polymer networks, or "gels", have been prepared from a large number of contrasting synthetic reactions [1-8, 15, 16]. In general terms, however, a given polymer network sample will have been generated either from a modification procedure, where a linear polymer is crosslinked as a result of a chemical/physical treatment process, or, it will have been synthesised directly [6, 7]. Linear polymer modification methods are widely used in the rubber industry [5], where homopolymer [2, 3] or copolymer [4] molecules containing sites of unsaturation are chemically cured (intermolecularly crosslinked) to generate elastomeric materials. Vulcanisation (cure) of both natural [9] and synthetic [10] rubbers with sulphur has found extensive commercial employment. The formation of short sulphur atom bridges [11], sulphur linkages which are randomly incorporated between adjacent polymer chains, is considered to impart elasticity [11] on these materials. Peroxide cures [5, 12, 13], thermal decomposition of organic peroxides in the presence of linear polymer molecules, are an additional class of crosslinking reactions which have found significant commercial employment [11]. Gamma irradiation of linear polymer samples [14, 15] has also been used to cure randomly polymeric materials. A common feature of each of these three distinct curing processes is that the polymer sample is initially attacked at random by a low molecular weight free radical [1]. Polymer-bound radicals are subsequently generated [1] and the combination of free radicals located on adjacent polymer chains results in the formation of a covalent bond linkage between two polymer molecules [1]. Non-radical crosslinking processes have also been reported [8, 16]. For example, Friedmann *et al.* [8] have selectively cured polybutadiene, PBD, samples with 1,1,3,3-tetramethylsiloxane [8]. The crosslinking reaction was found to have exclusively occurred via the addition of the hydrogenosilyl group on to the pendant (1,2-addition) double bonds of PBD [8], as depicted in figure 1.1 (where R represents an alkyl group present in the polymer main-chain). The synthesis of polystyrene network samples via Friedel-Crafts crosslinking of dilute polystyrene solutions with dichloroxylylene [16] has also been reported.

4

Figure 1.1 - Representation of PBD Reaction with Tetramethyl Siloxane [8]

$$\begin{array}{ccc} R & & H \\ \diagdown & & \diagup \\ & C = C & \\ \diagup & & \diagdown \\ H & & H \end{array} \quad + \quad H'-\underset{\underset{CH_3}{|}}{\overset{\overset{CH_3}{|}}{Si}}-O-\underset{\underset{CH_3}{|}}{\overset{\overset{CH_3}{|}}{Si}}-H' \quad \longrightarrow \quad H'-\underset{\underset{H}{|}}{\overset{\overset{R}{|}}{C}}-\underset{\underset{H}{|}}{\overset{\overset{H}{|}}{C}}-\underset{\underset{CH_3}{|}}{\overset{\overset{CH_3}{|}}{Si}}-O-\underset{\underset{CH_3}{|}}{\overset{\overset{CH_3}{|}}{Si}}-H'$$
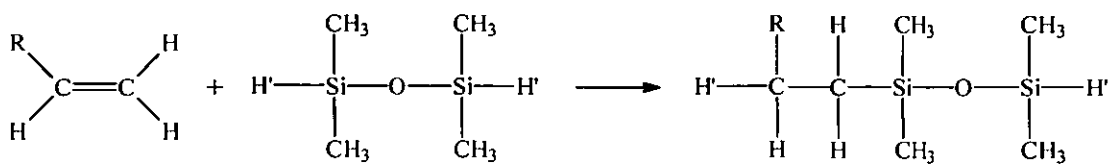
Each polymer network synthesised in this particular investigation was prepared from a polyaddition process. A general description of network formation from polyaddition techniques is briefly outlined below.

The synthesis of a polymer network from a chain-addition polymerisation requires a polyfunctional monomer to be present within the system. For example, gels can be synthesised from homopolymerisations of divinyl or trivinyl monomers, e.g. polymerisation of *para*-divinylbenzene [17-19], ethylene glycol dimethacrylate [20] or trimethylolpropane trimethacrylate [21]. More commonly, however, networks are synthesised from copolymerisation processes, e.g. copolymerisation of styrene/divinylbenzene [22-24] or methyl methacrylate/ethylene glycol dimethacrylate [25, 26]. Free radical copolymerisation of a monofunctional and difunctional pair of vinyl comonomers is the most commonly employed method for polymer network synthesis from polyaddition processes [22-26], although structured networks have also been prepared from anionic polymerisation techniques [27]. Networks can also be directly synthesised from polycondensation reactions [11, 28-30]. For example, Kienle and Petke [28] synthesised polyester gels from polycondensation of glycerol with dibasic acids, and Flory [29] prepared polyester networks from the reaction of ethylene glycol and tricarballylic acid.

A critical point, where the viscosity of the polymerisation medium is found to increase rapidly, is often observed during the course of a multifunctional monomer-containing polymerisation process (whether it be a polyaddition or a polycondensation reaction). Such a phenomenon is only observed in systems where the polyfunctional material is present at a sufficiently high concentration [11]. This viscosity transition is commonly called the gel-point [11] and it has been classified as the instant where a critical number of intermolecular crosslinks has been exceeded [29]. It is generally considered that the gel-point occurs when infinitely large networks are first formed in

the reaction mixture [29]. For polycondensation reactions involving two difunctional components, A-A and B-B, and a trifunctional component, A-A-A, polymer chain-branching processes occur during the early stages of the reaction [11]. Flory [29, 31] derived a theoretical relation between the branching coefficient (the probability that a given functional group on a branch unit would be connected to a branch on a second polymer chain), α, and the gel-point, for simple polycondensation reactions involving two difunctional components and one polyfunctional material [31]. Predictions of gelation behaviour were developed [31] with the assumption that all unreacted functional groups within the system were equally reactive, regardless of the size of the molecule to which they were attached [29, 31]. From statistical considerations [31], the critical value of α at which macro-gelation becomes theoretically possible, α_c, is given by:

$$\alpha_c = 1 \, / \, (f - 1) \tag{1.1}$$

where f is the functionality of the polyfunctional monomer [31].

The extent of reaction, for a polycondensation process involving one difunctional material of type A-A, a trifunctional component (A-A-A), and a second difunctional material, of type B-B, can be related to α by [11]:

$$\alpha \;=\; \frac{p_B^2 \, \rho}{r - p_B^2 (1 - \rho)} \tag{1.2}$$

where p_B is the extent of reaction for the B groups, ρ is the ratio of A groups on branch units to the total number of A groups in the mixture, and r is the ratio of all A to B groups [31].

The gel-point is readily determined experimentally, as it corresponds to the instant where the polymerisation mixture suddenly loses fluidity [11]. Additionally, the extent of reaction in a polycondensation process can be simply determined by titrating samples of the reaction mixture, in order to determine the number of functional groups present in the system [31]. Flory compared α values determined experimentally at the polymerisation gel-point [31] with theoretical α_c values, for several polycondensation

6

processes [31]. Each reaction system was found to proceed appreciably beyond the critical point before gelation was observed [31]. Experimental deviations from theoretical gel-point behaviour [31] were attributed to the presence of additional, intramolecular, polycondensation reactions occurring within the polymerisation system. Coupling between a branch and a functional group within the same polymer chain [11], an intramolecular reaction process, is one example of how network imperfections (figure 1.2) can develop during network synthesis [1].

Figure 1.2 - Representation of Perfect and Observed Network Structures [1]
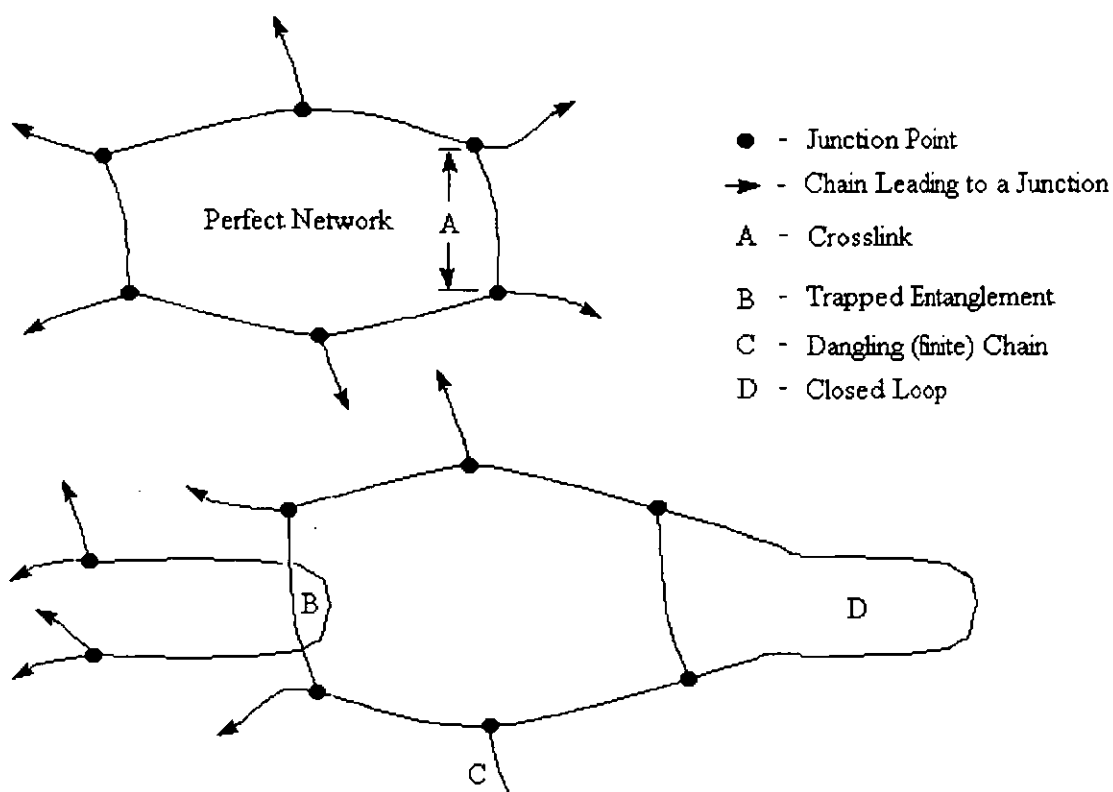
Gelation in free radical polyaddition processes [32] has been found to deviate significantly from Flory's [31] predicted gel-point behaviour (equation 1.1). Extensive cyclisation [33] (intramolecular reaction processes) and reduced pendant vinyl group reactivity [34, 35] phenomena have been found to occur within several of these polymerisation systems, thus negating the assumptions made during the derivation of the theoretical gelation equation [31]. Landin and Macosko [35] employed ^{1}H NMR spectroscopy to follow the free radical copolymerisation of methyl

7

methacrylate (MMA) and ethylene glycol dimethacrylate (EGDMA) in solution. Pendant vinyl groups [35], structures formed when only one bond of EGDMA had been incorporated within the copolymer chain, were found to promote cyclisation during the early stages of the reaction [35], especially in dilute systems [35], and the average reactivity of pendant vinyls was found to be approximately half that of monomeric vinyl bonds [35]. Dotsen *et al.* [36] demonstrated that the gel-point in MMA/EGDMA copolymerisation occurred very much later than predicted from ideal network theory. Li *et al.* [37, 38] investigated the kinetics of bulk MMA/EGDMA free radical copolymerisation at different crosslinker concentrations, and gelation was found to be accurately predicted by a kinetic model [38]. Hild and Okasha [39] investigated the kinetics of free radical styrene/*m*-divinylbenzene and styrene/*p*-divinylbenzene solution copolymerisations in the pre-gel state. Difunctional comonomers were found to be consumed more rapidly than styrene [39] and the presence of crosslinking agent was found to significantly increase the rate of polymerisation [39]. Okasha *et al.* [40] characterised soluble styrene/divinylbenzene copolymers prepared from free radical copolymerisation in the presence of chain-transfer agent [40]. Antonietti and Rosenauer [41] synthesised styrene/divinylbenzene copolymers from free radical copolymerisation in solution [41]. Walczynski *et al.* [42], Kast and Funke [43] and Okay *et al.* [44, 45] have reported the free radical solution polymerisation of divinylbenzene isomers.

Copolymers, and homopolymers, synthesised from free radical polymerisations involving divinylbenzene, or ethylene glycol dimethacrylate, can be classed into two distinct categories, those materials which are soluble in organic diluents and those which are insoluble [46]. Soluble materials, polymers recovered before macro-gelation, are a unique form of polymer networks, microgels [47]. Several authors have reported [18, 33, 43-45] that approximately half of the divinyl units from the crosslinking agent are incorporated within networks via intramolecular, cyclisation, reactions. Additionally, pendant vinyl groups are often found [34, 35, 39] to remain within networks prepared from free radical polyaddition processes. Consequently, functional microgels [47], intramolecularly crosslinked polymer particles which contain pendant vinyl groups [47], can be recovered from solution polymerisation processes, prior to macro-gelation [40-42]. Okay *et al.* [45] have postulated that

irregular macrogel structures are prepared from free radical polymerisation processes [45], as macro-gelation corresponds to the point where intermolecularly crosslinked microgel particle clusters [45] begin to extend throughout the whole volume of the system.

Polystyrene and poly(n-butyl acrylate) microgel particles were synthesised via emulsion copolymerisation techniques in this particular investigation (sections 2.2.1 and 2.3.1). The synthesis of crosslinked polymer particles from heterogeneous free radical polymerisation methods will be considered in section 1.7.1. Organic microgel dispersions are discussed in section 1.7.2.

1.3 - THERMODYNAMICS OF MIXING FOR POLYMER BLENDS

The physical properties of a polymer blend are critically dependent upon the mutual thermodynamic miscibility of its constituent components [48, 49]. The majority of polymer blends exhibit macroscopic phase separation [48, 50-52]. Efforts at minimising the size of the domains in heterogeneous polymer blends, in order to enhance the bulk properties of the materials [53-57], have been made. The influence of graft [53-55] and block copolymers [56, 57] has been extensively investigated, and reductions in the size of blend phase domains have been considered to arise from decreased blend interfacial tensions [48, 54]. Interpenetrating polymer networks are a unique form of polymer blend that can show significant mixing between the two, or more, network components (section 1.4).

Convention has classified polymer pairs as being either miscible or immiscible on a macroscopic level, with the term miscible defining systems which show only one glass transition [48]. Complete mixing of two dissimilar materials is observed for systems with negative Gibbs free energy of mixing, ΔG^M (J mol^{-1}), values, where the free energy of mixing is governed by the entropy change ΔS^M (J mol^{-1} K^{-1}) and enthalpy change ΔH^M (J mol^{-1}) of the system:

$$\Delta G^M = \Delta H^M - T(\Delta S^M) \tag{1.3}$$

where T is the absolute temperature of the system (K).

For mixtures of two simple liquids, denoted as liquids A and B (figure 1.3), there are four common examples [58] of temperature (T)-composition phase diagram.

Figure 1.3 - Phase Diagrams for Binary Liquid Mixtures at Constant Pressure
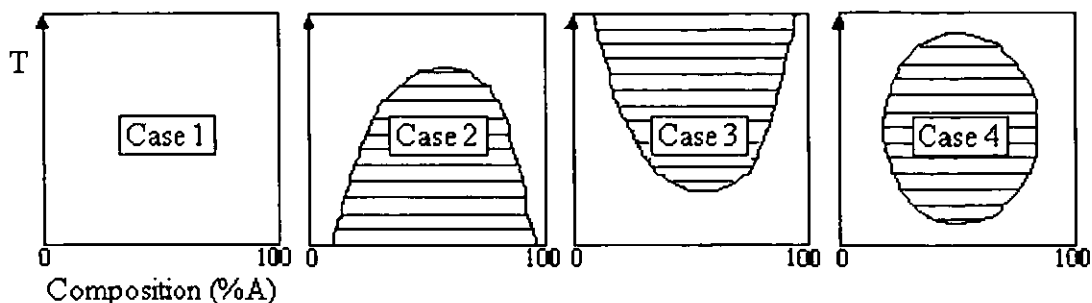
The shaded regions indicate the presence of two, separate, liquid phases.

Case 1-type phase diagrams are observed for two liquids that are miscible at all mixture compositions and at all temperatures between the melting and vaporisation points. This behaviour is relatively rare. Carbon tetrachloride/cyclohexane [58] is one such system. In Case 2, the phase boundary curve exhibits a maximum, defined as the upper critical solution temperature (UCST), the temperature above which phase separation does not occur [58]. Such phase behaviour is common, n-butanol/water shows UCST behaviour [58]. The phase boundary illustrated in Case 3 has a minimum, defined as the lower critical solution temperature (LCST) [58]. Ethylamine/water follows this kind of phase behaviour, although it is not commonly observed for pairs of simple liquids [58]. The temperature-composition phase diagram denoted as Case 4, exhibits both a UCST and a LCST. One system that exhibits this behaviour is water/nicotine [58]. Each of these phase responses has been found for certain binary polymer mixtures and many other variations have been observed [48, 49, 59-61].

Ideal solution behaviour [58], observed seldomly in practice, requires athermal mixing between the two, or more, materials, and, hence, the free energy change on mixing solely results from an entropy gain for each of the components (the entropy change results from an increase in component degree of freedom on dissolution [48]). Polymer solutions are non-ideal and show strong negative deviations from Raoult's law [48]. For polymer/liquid and polymer/polymer mixtures, the volume fraction of

each component must be considered [48]. A lattice concept was introduced for such systems (each central segment of a polymer molecule must have at least two adjacently occupied lattice sites, and, hence, the number of ways that the two components can be arranged in the lattice is minimised), due to the unique behaviour of high chain-length molecules [62, 63]. Flory and Huggins developed a mean field, rigid lattice, theory [64] to predict the molar free energy on mixing two polymers, A and B:

$$\frac{\Delta G^M}{RT} = \left(\frac{V}{V_R}\right)[(\phi_A/r_A)\ln\phi_A + (\phi_B/r_B)\ln\phi_B + \chi\phi_A\phi_B] \qquad (1.4)$$

where ϕ_i is the volume fraction and r_i is the degree of polymerisation of component i, respectively, χ is the Flory segmental interaction parameter, V is the system volume, V_R is a reference volume related to the size of the unit cell of the lattice, and R and T have their usual significance.

The van Laar-type [48] ($\chi\phi_A\phi_B$) term (equation 1.4) represents an estimate of the enthalpic contribution toward the free energy of mixing [48]. The two other terms in the square brackets (equation 1.4) describe the entropy of athermal mixing for a binary, monodisperse, polymer pair [48]. In this approach, the entropic contribution to the free energy of mixing is combinatorial and the entropy becomes negligibly small as the molecular weight of each component increases (r_i becomes large). Consequently, blend miscibility is largely influenced by the interactional free energy, the segmental interaction parameter (χ), which is required to be either of very low magnitude or negative if a homogeneous blend is to result [48]. The χ parameter is assumed to be a composite term that is influenced by dispersive (intermolecular) forces, specific interactions, and blend compressibility effects [48, 65]. It is important to note that the Flory interaction parameter (χ) has been found to be dependent on temperature, pressure, blend composition and component molecular weight [48]. The Flory-Huggins approach has been widely employed for predicting the miscibility behaviour of polymer blends [66-70]. Accurate predictions of the phase behaviour of binary, and ternary, copolymer blends involving N-phenylitaconamide, methyl methacrylate, styrene and acrylonitrile comonomers have been made by consideration of the Flory-Huggins method [66, 67].

Segmental (χ) interaction parameters cannot be readily determined from analytical characterisation of polymer blends [67]. Heats of mixing between polymers can be estimated, however, from the enthalpies of mixing for liquid pairs whose structures model the repeat segments of each polymer [71]. This calorimetric approach can be useful for prediction of the phase behaviour of polymer blends [72, 73]. Polymer blend phase behaviour has also been estimated by utilising statistical mechanics, the equation-of-state approach [48], to predict the free energy of mixing.

A specific exothermic intermolecular interaction is generally required for complete mixing between two homopolymers [48]. Hydrogen bonding is the driving force for miscibility in many polymer systems [74-79]. The miscibility of poly(vinyl chloride), PVC, with a large number of carbonyl group-containing polymer samples [74-78] has been considered to arise from intermolecular hydrogen bonding interactions. Experimental studies by Koleske and Lundberg [74] have demonstrated the miscibility of PVC with poly(ε-caprolactone) over all blend compositions. These findings were attributed to specific interactions between the α-hydrogens of PVC with the carbonyl groups of the polyester. Many other, non-hydrogen bonding, polymer pairs exhibit characteristics of miscibility [48, 79-81]. Blends of polystyrene, PS, with poly(vinyl methyl ether), PVME, have been extensively investigated [80, 82-84]. Solid-state one dimensional nuclear Overhauser effect (NOE) spectroscopy has been used to study PS/PVME blends [82]. The relative intensity of intermolecular ^{13}C NOE enhancements determined that the methoxy carbon of PVME was specifically oriented near the aromatic ring of PS [82]. Blends of poly(1,2-butadiene), 1,2-PBD, and polyisoprene have been found to be miscible at all compositions [81, 85]. Solid-state 2D NMR studies at temperatures above T_g [85] have discovered that weak specific intermolecular interactions between the methyl group of polyisoprene and the pendant vinyl bond of 1,2-PBD occur.

Equilibrium thermodynamics can only predict the overall, macroscopic, phase structure of a given polymer blend [48]. Investigations into the dynamics of the system can allow for both a determination of the rate of the phase separation process [48] and for a prediction of the blend morphology [48]. The mechanism of the phase separation process is one factor which can influence the phase structure of a polymer blend [86]. The nucleation and growth mechanism involves the initial generation of

nuclei of a new, more stable, phase within a metastable host, mother, phase [48]. Each individual nucleus possesses an excess surface free energy compared to neighbouring molecules in the matrix [48]. Gibbs defined the excess surface energy as the sum of the work expended in generation of the surface and the work gained in forming the interior mass of the nucleus [87]. Matsuda proposed that the activation energy for the generation of such critical nuclei has a contribution from the free energy of mixing for the system, as well as the contribution from the excess surface free energy (interfacial energy) [88]. Once a nucleus has been generated, the free energy of the system decays away and each of the nuclei then grows [48]. The overall effect is that a finely-dispersed heterogeneous phase structure is generated [48]. Final domain sizes and the separation between them are dependent upon the rate of diffusion and the time scale of the process [48]. Domain sizes increase throughout the process, initially through growth and later by coalescence or ripening [89, 90], until two substantial phases are present.

Phase separation by spinodal decomposition [48] involves phase growth from statistical compositional fluctuations. The theory, originally developed by Cahn and Hilliard to predict the phase structure of metallic alloys [91, 92], estimates the contribution from concentration fluctuations in heterogeneous solutions to the system free energy. Differences in local free energy lead to an interdiffusion flux, which allows for continuous growth of the sinusoidally-fluctuating composition modulation with a certain, maximum, wavelength [91]. The general solution of the Cahn-Hilliard relation [91] expresses the time (t) dependence of the apparent structure function (determined by the time-dependent, spatial concentration fluctuation of one component), $S(\beta)$, as:

$$S(\beta) = S_0\{\exp[R(\beta).t]\}$$

(1.5)

where S_0 is the structure factor at time $t = 0$ and the growth rate, $R(\beta)$, is:

$$R(\beta) = -\Omega\beta^2\left(\frac{\partial^2 G'}{\partial\psi_1^2} + 2K\beta^2\right)$$

(1.6)

where β is the wave vector, defined by the wavelength (λ) observed for each fluctuation in solution composition ($\beta = 2/\lambda$), Ω is an Onsager-type phenomenological

coefficient [91], G' is the free energy density for the homogeneous system, ψ_i is the segment fraction of component i, and K is the gradient energy coefficient (J m^{-1}) [91].

As the gradient energy coefficient is positive, the growth rate relation is governed by the sign of the derivative, $\partial^2 G'/\partial \psi_1^2$. Positive values give negative values for the growth rate and subsequently all such instabilities rapidly decay. As the derivative becomes negative, certain wavelengths, predominately the longer ones, will grow. As the values become more and more negative, the shorter wavelengths also have the capacity for growth. Consequently, the phase separation process leads to a significant level of phase interconnectivity in the system [48, 93]. The presence of such interwoven structures does not necessarily prove a spinodal decomposition mechanism, interconnected regions can coarsen to give somewhat dispersed structures and the influence of shear during a nucleation and growth mechanism can generate interwoven-style blend morphologies [48]. Consequently, spinodal kinetics is the most suitable method for determining whether the phase separated regions of a polymer blend have resulted from spinodal decomposition [48, 94]. This property of the Cahn-Hilliard approach to spinodal decomposition is readily determined, if the rate of growth, R(β), is plotted as a function of wavelength (λ). For certain values of $\partial^2 G'/\partial \psi_1^2$ and K, the growth rate exhibits a maximum and this most rapidly propagating wavelength (λ_m) dominates the spinodal decomposition process [91, 94]:

$$\lambda_m = 2\sqrt{2}\pi \left((-1/2K) \frac{\partial^2 G'}{\partial \psi_1^2} \right) \tag{1.7}$$

This relation can be considered to characterise the initial spinodal instability and to also determine the magnitude of the growing precipitate [48, 94]. A significant number of investigations into the dynamics of phase separation have concluded that both spinodal decomposition and nucleation and growth mechanisms can contribute to the overall phase separation process, and, hence, both of the mechanisms can have an influence on the morphology of the blend [48, 94-97]. Research into the thermally-induced phase separation behaviour of PS/PVME blends [95] and styrene/acrylonitrile (28% acrylonitrile) copolymer blends with poly(methyl methacrylate) [96, 97], concluded that spinodal decomposition was the mechanism of phase separation in certain regions of the temperature-composition phase diagram, whilst other regions underwent phase separation via the nucleation and growth mechanism [96].

1.4 - INTERPENETRATING POLYMER NETWORKS (IPNs)

An interpenetrating polymer network (IPN) is a unique kind of polymer blend which can show, under certain conditions, significant degrees of phase-mixing between the two, or more, polymer network components [98-100]. IPNs have historically [98] been defined as combinations of two polymers in network form, at least one of which is synthesised and/or crosslinked in the immediate presence of the other [98]. IPNs, where one component is elastomeric and the other glassy at the use temperature, can behave as reinforced rubbers or impact resistant plastics, to a degree dependent upon which of the components is the more continuous phase for the blend [99, 100]. For the synthesis of IPNs of two incompatible polymers (such as the PnBA/PS system), a degree of phase separation results [98]. The two components remain intimately mixed [98], however, with phase domains being of the order of tens of nanometers [99] (as opposed to domains of μm size that are commonly observed for conventional polymer blends). There are a number of modes of IPN synthesis [94, 98] including sequential IPNs, where polymerisation of the second monomer (with crosslinking agent) is performed within (monomer-swollen) first-stage networks [98] and simultaneous interpenetrating networks (SINs) [98], where both polymerisations are performed concurrently but by independent (and non-interfering) pathways (for example, one network is synthesised by a polycondensation reaction whilst a second network is generated by a, vinyl, polyaddition process [98]). Other IPN synthetic procedures include latex IPN [101, 102] processes (section 1.6.4), interpenetrating elastomeric network (IEN) synthesis, where two latex polymers are mixed and subsequently crosslinked [98], and thermoplastic IPN systems [99]. Sequential IPNs were the class of materials to be investigated within this project and reports of sequential IPN synthesis, published in the scientific literature, will be exclusively reviewed in this text. Comprehensive treatises on the synthesis of each IPN-type (e.g. simultaneous, thermoplastic and sequential) have been written by Sperling [94, 98-100].

As with conventional polymer blends, the size of the phase domains in IPNs is dependent upon the compatibility of the two polymer components [98] and the weight fraction of each of the components in the composite material [98]. Morphologies of IPNs can also be significantly influenced by the degree of crosslinking (the average

molecular weight between crosslinks) of both the first- [103] and second-formed [104, 105] networks. The inward-shifting of the glass transition temperatures of the two polymer network components in an IPN has long been recognised [98]. Phase domain sizes within IPN materials were found to be significantly smaller than domain sizes within their corresponding blends [98], and consequently, it was postulated that increased inter-phase mixing lead to the unique glass transition behaviour of IPNs [94]. IPNs can undergo phase separation by both nucleation and growth and spinodal decomposition mechanisms concurrently [94], although spinodal decomposition kinetics often dominate the phase separation process [94]. Phase separation by nucleation and growth tends to generate finely dispersed, spherical, domains of the second phase within the matrix of the first, mother, phase [48] (section 1.3). Spinodal decomposition kinetics tends to yield interconnected, cylindrical-like, domains of the second phase within the matrix of the first phase [48, 94]. Coarsening [90] and coalescence [89] processes, leading to an increase in the size of phase domains, can occur during the later stages of phase separation [94]. It was considered that, provided gelation preceded phase separation during polymerisation, the extent of phase separation within IPNs could have been restricted by crosslinking [94] (the presence of crosslinks could have impeded phase-coarsening processes, which would, subsequently, have lead to the maintenance of small domain sizes [94]), and, hence, an increase in the apparent miscibility between the two components would result [94].

Advances in the understanding of IPN morphologies [94] resulted from a number of investigations into IPN systems where the two polymeric components were known to be miscible in the conventional blend [106-109]. Briber and Bauer [106] investigated the small angle neutron scattering behaviour of polystyrene, PS/poly(deuterated styrene) semi-II IPNs (networks of deuterated styrene were synthesised in the presence of linear PS). IPNs were found to be immiscible at lower PS molecular weights than was found for the blends (phase separation of the blend occurred at a PS molecular weight of 800,000 g mol^{-1}, whereas semi-II IPNs phase-separated when the molecular weight of PS exceeded 40,000 g mol^{-1}) [106]. Phase separation was considered to have arisen from an endothermic contribution to the free energy of mixing (which also lead to phase separation in the blend at high molecular weights), as defined by a positive Flory (χ) interaction parameter, and also, more significantly, to have resulted

from an unfavourable contribution to the free energy from elastic stretching of the network component [106]. This behaviour was ascribed to the fact that each of the propagating network chains had fewer available conformational states to adopt, than they would have had, if they had been generated in the relaxed state [106]. Several investigations into the phase separation of polystyrene/poly(vinyl methyl ether) IPNs have been reported [107-109]. A decrease in miscibility between the two components of the IPNs [109] was observed, when compared to the degree of mixing in each of the blends [108].

The observation that, in general, IPNs exhibit greater miscibility characteristics than their corresponding blend, whereas certain IPNs (materials consisting of two components that are miscible in the blend) are less homogeneous than their linear blend analogues, has been considered by Sperling [94] to be non-dichotomous. The presence of crosslinks may lead to the presence of small phase domains in IPN materials. In the instance that the blend is miscible, the chain deformation of the networks could lead toward demixing between the two components [94]. Theoretical predictions into the phase behaviour of AB-crosslinked polymers [110] (materials where two polymers, A and B, make up one network) have concluded that these materials should be more miscible than their corresponding blends, as a consequence of the requirement that the network chains would have to be extended in order for phase separation to occur [110]. The assumption that IPNs could mirror this behaviour would also predict that a greater degree of phase-mixing would be found for the IPN [94], when compared to the corresponding blend (both of the network chains must be extended, i.e. of lower entropy, to enable phase separation). This theoretical approach assumes that phase separation takes place long after gelation, namely that the rate of network formation is significantly more rapid than the rate of phase separation [94]. For simultaneous IPN synthesis, the relative rates of network formation and phase separation have a significant influence on the final morphology of the material [100]. If phase separation precedes gelation, then the phase domains, generally, will be of large size [100]. Once gelation occurs, domains are found to remain separated from one another [94, 100]. In cases where gelation precedes phase separation, the presence of crosslinks tends to lead to the retention of the small domain size [94] (phase coarsening and ripening processes, often found during the

17

later stages of phase separation, are suppressed). For sequential IPNs, the presence of the first-formed network ensures that gelation occurs before phase separation, and finely dispersed IPN morphologies often result (to a degree dominated by the crosslink-density of the first network [94], although the crosslink-density of the second-formed network can also influence the final morphology [99]).

A considerable number of latex IPN systems, IPNs prepared by sequential emulsion polymerisation processes, have been investigated [101, 102, 111-120]. The synthesis of latex IPNs will be considered separately (section 1.6.4) to other modes of sequential IPN synthesis. A second method for the synthesis of sequential IPNs involves the initial preparation of a macrogel sample, this network is subsequently swollen with monomer (along with a crosslinking agent and a free radical initiator) and polymerisation of the monomer is then initiated, with the aim of synthesising a composite network material where the first and second networks are intimately mixed [98]. Eschbach and Huang [121] reported the synthesis of sequential poly(ϵ-caprolactone), PCL/poly(2-hydroxyethyl methacrylate), PHEMA, IPNs [121]. PCL (M_n = 40,000 g mol^{-1}) was mixed with dicumyl peroxide in methylene chloride [121]. After solvent evaporation, networks were synthesised by heating PCL films at 130°C. The crosslinking mechanism was considered to have resulted from combination of PCL macro-radicals, generated by abstraction of main-chain hydrogen atoms by peroxy free radicals (figure 1.4) [121]. Equilibrium swelling of PCL networks with 2-hydroxyethyl methacrylate (2-HEMA) and ethylene glycol dimethacrylate (EGDMA), containing 2,2'-azobisisobutyronitrile (AIBN), was performed over 24 hour periods (99 wt.% 2-HEMA/1 wt.% EGDMA) [121]. Polymerisation of 2-HEMA was performed at 90°C [121], leading to the generation of an IPN with a PHEMA content of 10 weight %. Detailed investigations into the structure of PCL/PHEMA IPNs were not undertaken, but tensile tests on the PCL networks, PHEMA networks, and the IPN, were performed. The high tensile modulus observed for the IPN was attributed to an increase in the effective crosslink-density of PCL which had resulted from interpenetration of the two network components [121].

Figure 1.4 - Illustration of Poly(ε-caprolactone) Peroxide Curing Reactions

$$\text{ROOR} \xrightarrow{\text{Heat}} 2\text{ RO}\bullet$$

$$\text{RO}\bullet + \text{\small{mmm}}CH_2-CH_2\text{\small{mmm}} \longrightarrow \text{ROH} + \text{\small{mmm}}CH_2-CH\bullet\text{\small{mmm}}$$

$$2 \text{\small{mmm}}CH_2-CH\bullet\text{\small{mmm}} \longrightarrow \begin{array}{c} \text{\small{mmm}}CH_2-CH\text{\small{mmm}} \\ | \\ | \\ \text{\small{mmm}}CH_2-CH\text{\small{mmm}} \end{array}$$

(Most probable site for hydrogen abstraction)

$$-(\underset{\displaystyle \overset{\|}{O}}{C}-CH_2-CH_2-CH_2-CH_2-CH_2-O)_{\overline{N}}-$$
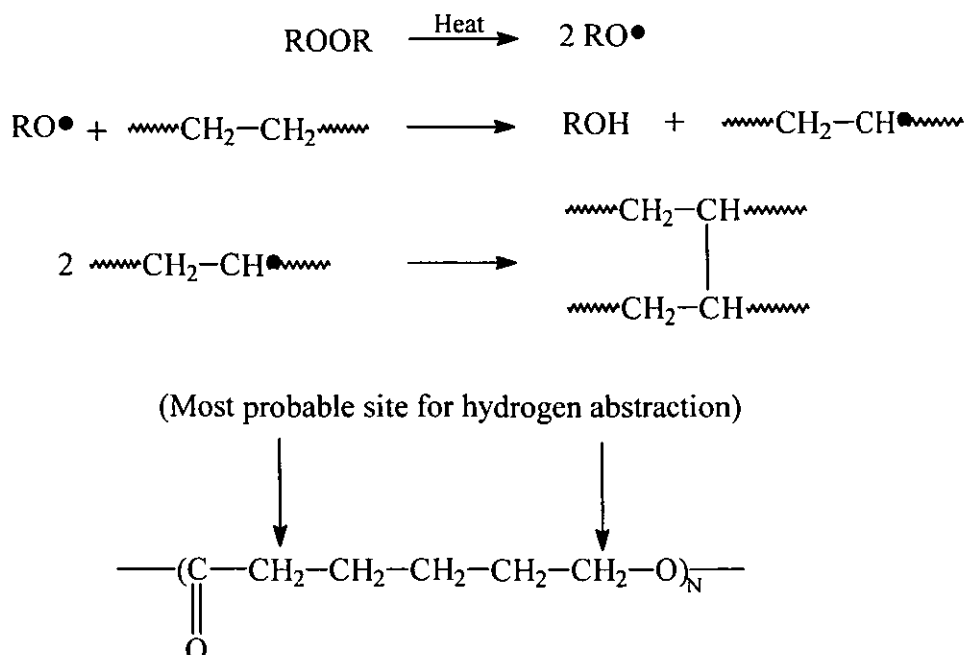
Yeo *et al.* [122-124] have extensively reported the synthesis and characterisation of P*n*BA/PS sequential IPN materials. Several urethane grafted poly(*n*-butyl acrylate)/polystyrene semi-I IPNs were prepared [122]. Mixtures of 2-hydroxyethyl acrylate (2-HEA) and 2,4-toluene diisocyanate were initially coupled in the presence of catalyst and *n*BA monomer. AIBN and tetraethylene glycol dimethacrylate were then added, and systems were subsequently heated at 70-80°C [122] for synthesis of the first network component. Elastomer sheets were then swollen with styrene, 2-HEA, AIBN and polycondensation catalyst before thermal polymerisation of the second components was initiated [122]. A series of semi-II IPNs was also synthesised with controlled P*n*BA molecular weights (*n*-butyl mercaptan was employed as chain-transfer agent in these systems) [122]. After the acrylic polymer components had been dissolved in styrene/DVB/benzoin mixtures, the second polymerisation process was photoinitiated [122]. Semi-I IPNs were selectively stained with osmium tetroxide and the samples were characterised by transmission electron microscopy (TEM) [122, 123]. The glass transition behaviour of both semi-I and semi-II IPN samples was determined from dynamic mechanical analysis [123]. Grafted semi-I IPN samples were found to exhibit significant degrees of phase-mixing

between the two components at the molecular level. The appreciable levels of miscibility induced by grafting resulted in single mechanical transitions for the samples at intermediate compositions [122]. Semi-II IPN samples with high P*n*BA molecular weights were found to exhibit two distinct glass transitions [124], whereas IPNs with the lowest acrylic polymer molecular weights exhibited only one α-relaxation [124]. Semi-II IPNs which displayed only a single glass transition were found to have P*n*BA viscosity average molecular weights (M_v) of 20,000 g mol^{-1}, or less, and such acrylic polymer components were considered to have acted as polymeric plasticisers [122]. Two general types of phase structure were observed for semi-II IPNs with heterogeneous morphologies [193]. At higher P*n*BA molecular weights, coarse cellular structures were observed from TEM analysis of IPN samples. IPNs with low molecular weight acrylic components exhibited finer, phase-inverted, phase structures [123]. Cellular domain structures were observed for IPN and semi-I IPN samples with low crosslink-densities and intermediate composition ratios [122]. Small, irregular, phase-domains were found for IPN and semi-II IPN samples with higher crosslink-densities and this phase behaviour was also followed by materials where extensive grafting between the two network components had occurred [123]. Glass transition broadening effects were observed for IPN samples with low crosslink densities [122] and single, broad, transitions were found at higher crosslink levels. The stress-strain behaviour of IPN and semi-I IPN samples with high PS content was found to generally mirror the tensile behaviour of toughened thermoplastic samples, whereas P*n*BA-rich samples behaved as reinforced elastomers [124].

A number of studies into the synthesis of poly(ethyl acrylate)/poly(methyl methacrylate), PEA/PMMA, IPNs have been reported [125-127]. Sperling *et al.* [125] synthesised PEA elastomer (PEA crosslinked with tetraethylene glycol dimethacrylate, TEGDMA) with benzoin as photoinitiator [125]. Sheets of elastomer were subsequently swollen with controlled amounts of methyl methacrylate and TEGDMA, with benzoin [125]. This procedure was subsequently followed by photoinitiated polymerisation. The glass transition behaviour of PEA/PMMA IPNs was explored over a broad range of IPN compositions and the results were compared to those obtained from statistical copolymer samples [125]. Only one glass transition was observed for each of the IPN samples, with unusually broad transitions resulting from

materials with intermediate/mid-range compositions [125]. The broad transition behaviour of certain IPN samples [125] was attributed to a near-continuous connected phase structure [125] in these materials, where each phase composition had made a specific contribution to the relaxation process [125]. Adachi and Kotaka [127] synthesised PEA elastomers (PEA crosslinked with EGDMA) by bulk copolymerisation processes [196]. PEA networks were swollen with methyl methacrylate, EGDMA and AIBN, before thermal polymerisation [127]. The PEA/PMMA IPNs exhibited only one, broad, glass transition, as determined by dynamic mechanical analysis - indicating a micro-heterogeneous morphology for the material [127]. The corresponding semi-I IPNs (i.e. linear PMMA was the second component synthesised) exhibited two glass transitions, indicating that phase separated materials had been generated [127].

Widmaier and Tabka [128] synthesised a series of sequential polystyrene/polybutadiene, PS/PBD, IPNs. PS macrogels were synthesised with variable DVB content (1-5 mole % DVB), from copolymerisations containing variable benzene content (0-65 volume %) with four different methods of free radical initiation (benzoyl peroxide at 80°C, AIBN at 60°C, and photolysis of benzophenone or benzoin at 20°C) [128]. Dry PS macrogel samples were initially swollen in benzene/PBD-precursor (M_n = 1,000 g mol^{-1}) mixtures, containing 1,1,3,3-tetramethyl siloxane crosslinking agent and chloroplatinic acid catalyst [128]. Crosslinking of PBD was performed over 48 hour periods [128]. The crosslinking reaction (figure 1.1) has been found to exclusively occur via addition of the hydrogenosilyl group on to pendant (1,2-addition) double bonds of PBD [8]. PS/PBD IPNs were preferentially stained with osmium tetroxide and samples were characterised by transmission electron microscopy [128]. Electron micrographs indicated that phase separation between the two network components was significantly reduced at the highest polystyrene crosslink-densities [128].

Parizel *et al.* [129] have characterised polyurethane, PU/PMMA sequential IPNs by measurement of ^{1}H nuclear magnetic resonance (NMR) spin-lattice relaxation times. PU elastomer was synthesised [129] from a 1,1,1-trimethylolpropane/toluene diisocyanate adduct and poly(oxypropylene glycol), POPG, in the presence of MMA, TRIM (1,1,1-trimethyloylpropane trimethacrylate), AIBN and stannous octoate

catalyst, at 25°C. After gelation of the polyurethane component had been observed [129], the systems were heated at 60°C for 16 hours, followed by 3 hours of heating at 120°C. ^{1}H NMR spin-lattice relaxation times predicted that the materials were of co-continuous morphology and average domain sizes of less than 10 nm were evaluated for both the PU and the PMMA components [129]. Simultaneous polymerisation of the two network components generated materials which exhibited higher degrees of phase separation. A PU-rich matrix, containing PMMA inclusions of at least 30 nm domain size, was predicted from ^{1}H NMR relaxation times [129]. Lal *et al.* [130] synthesised polyurethane/deuterated-polystyrene sequential IPNs. The influence of the first and second network crosslink-density on the small angle neutron scattering behaviour of the materials [130] was investigated. PU elastomers were synthesised from the reaction between an aliphatic trifunctional isocyanate adduct and POPG derivatives in the presence of deuterated (d_8) styrene, divinylbenzene, AIBN and stannous octoate catalyst [130]. Gelation of the PU networks occurred within 30 minutes (25°C) and the systems were subsequently heated for 15 hours at 60°C, followed by 2 hours of heating at 120°C [130]. Small angle neutron scattering analysis determined that the two network components of the IPN showed significant molecular mixing [130]. An increase in the crosslink-density of each of the two networks [130] was found to reduce the size of IPN phase domains.

1.5 - COPOLYMERISATION KINETICS

Each polymer network generated within this project was synthesised by a vinyl, polyaddition, free radical copolymerisation technique. The synthesis of networks of ideal structure (networks of homogeneous crosslink-density) requires either the employment of two comonomers that copolymerise ideally (in the case of bulk copolymerisation, especially) [131], or, the controlled, continuous, addition of comonomers to the polymerisation vessel [132] (e.g. the starve-fed addition of comonomers in emulsion copolymerisation). For polymerisation systems involving two monomers, M_1 and M_2, each propagating copolymer radical that last reacted with a molecule of monomer M_1 ($PM_1\bullet$) can react once more with a M_1 molecule or, alternatively, it can react with a molecule of M_2 (to generate a $PM_1M_2\bullet$ radical).

Additionally, each propagating radical that last incorporated a M_2 molecule ($PM_2\bullet$) has the opportunity to either add a second consecutive M_2 moiety (yielding a $PM_2M_2\bullet$ radical), or, it can react with a molecule of M_1. If it is assumed that the reactivity of a given radical, to either M_1 or M_2, is purely dependent on the last monomer unit that the radical incorporated (i.e. there are no penultimate group effects [133]), then only four (generalised) propagation processes need be considered:

$$PM_1\bullet \ + \ M_1 \ \xrightarrow{\ k_{11}\ } \ PM_1M_1\bullet \tag{1.8}$$

$$PM_1\bullet \ + \ M_2 \ \xrightarrow{\ k_{12}\ } \ PM_1M_2\bullet \tag{1.9}$$

$$PM_2\bullet \ + \ M_1 \ \xrightarrow{\ k_{21}\ } \ PM_2M_1\bullet \tag{1.10}$$

$$PM_2\bullet \ + \ M_2 \ \xrightarrow{\ k_{22}\ } \ PM_2M_2\bullet \tag{1.11}$$

where k_{ij} is the propagation rate constant (s^{-1}) for the reaction between components i and j. The value of each of the rate constants is considered to be independent of the chain length [11]. This assumption, with the exception of cases of very short (ca. 1-5 monomer units) chain lengths [11], has been shown to be experimentally valid.

Provided that high molecular weight copolymer is synthesised, the consumption of each of the monomers, M_1 and M_2, can be expressed by [202]:

$$\frac{-d[M_1]}{dt} = k_{11}[PM_1\bullet][M_1] + k_{21}[PM_2\bullet][M_1] \tag{1.12}$$

$$\frac{-d[M_2]}{dt} = k_{12}[PM_1\bullet][M_2] + k_{22}[PM_2\bullet][M_2] \tag{1.13}$$

If we assume that a steady-state in each macro-radical concentration is attained, then:

$$k_{21}[PM_2\bullet][M_1] = k_{12}[PM_1\bullet][M_2] \tag{1.14}$$

The division of equation 1.12 with equation 1.13, followed by substitution with equation 1.14, generates the Mayo-Lewis [134] equation for copolymer composition (equation 1.15).

$$\frac{d[M_1]}{d[M_2]} = \left(\frac{M_1}{M_2}\right)_{Cop} = \left(\frac{[M_1]}{[M_2]}\right)_{Feed} \cdot \left\{\frac{(r_1[M_1] + [M_2])}{(r_2[M_2] + [M_1])}\right\} \tag{1.15}$$

where $(M_1/M_2)_{Cop}$ is the instantaneous composition of the copolymer and $r_1 = k_{11}/k_{12}$ and $r_2 = k_{22}/k_{21}$ are the comonomer reactivity ratios, the ratio of the rate constants for a given macro-radical adding an additional molecule of the same monomer (e.g. $PM_{2\bullet}$ reacting with M_2), to the rate constant for the addition of the second monomer (e.g. $PM_{2\bullet}$ reacting with M_1).

The Mayo-Lewis equation predicts the composition of copolymer molecules at a given instant [134]. Bulk (or solution) copolymerisation of two monomers (M_1 and M_2) that have a large difference in their comonomer reactivity ratios (e.g. $r_1 = 0.05$ and $r_2 = 20$), leads to a drift in the composition of the copolymer molecules, as the copolymerisation proceeds (e.g. if r_1 was 0.05 and r_2 was 20, M_2 would be preferentially consumed during the initial stages of copolymer synthesis and M_1 would be consumed to a greater extent during the later stages of copolymerisation). Consequently, bulk copolymerisations are, almost always, terminated at low (≤ 10 weight %) conversion [11]. Starve-fed addition of comonomers [135] (where the rate of comonomer addition is equal to the rate of consumption) is often employed to minimise compositional drift during emulsion copolymerisation.

1.6.1 - EMULSION POLYMERISATION

Emulsion polymerisation techniques are extensively employed industrially for the production of polymer latices [136]. For example, styrene/butadiene synthetic rubber latex and poly(vinyl acetate)-based emulsion paint manufacturing processes both utilise emulsion polymerisation methods [136]. An emulsion polymerisation process typically has four major components, namely; water, monomer, emulsifier and free radical initiator [136]. Emulsifier (surfactant) molecules are, generally, comprised of hydrophobic "tails" and hydrophilic "heads". The chosen surfactant has one of four generalised types of hydrophilic group [136] - anionic (e.g. alkyl sulphates and sulphonates [137, 138]), cationic (e.g. alkyl ammonium halides [139]), non-ionic (e.g. low molecular weight polyethylene glycols [140]) or zwitterionic (e.g. amino acid derivatives [141]). Free radicals are generated in the continuous phase, the aqueous phase, of the latex [136]. Thermal decomposition of water-soluble initiator molecules, e.g. ammonium/potassium persulphate, is commonly used for the

generation of free radicals [136, 142]. Persulphates are most commonly used in conjunction with emulsifier for the emulsion polymerisation process [136]. "Soap-free" polymer latices can also be synthesised, if high persulphate concentrations are employed [136]. Sulphate radical anions are initially generated from the decomposition of persulphate molecules [143, 144] and sulphate groups are found to concentrate at the latex particle surface [144, 145]. Provided that the surface charge is sufficiently high [145], colloidally-stable dispersions of polymer particles are recovered. Sodium lauryl sulphate was used as emulsion polymerisation emulsifier in this project and, consequently, anionically-stabilised polymer latices will be exclusively considered in this text.

Before initiation of an idealised, batch, emulsion polymerisation process, water, surfactant and monomer are mechanically agitated in a reaction vessel. The emulsifier forms aggregates, micelles, which are comprised of 50-100 molecules in water, if the concentration of surfactant in the aqueous phase is greater than its critical micelle concentration (CMC) [136]. The emulsifier is predominantly found as soap micelles, although a number of monomolecular surfactant molecules are also present in the aqueous phase and emulsifier molecules can be additionally adsorbed onto the surface of monomer droplets [136] and at the water/air interface [136]. A dynamic equilibrium between micellular surfactant molecules, monomolecular surfactant molecules and interfacially-adsorbed emulsifier molecules is attained [136]. The bulk of the monomer, typically, exists in the form of monomer droplets of 1-10 μm diameter [136]. A small amount of monomer (ca. 1 weight %) diffuses into the interior of certain micelles [136], however, and so monomer-swollen emulsifier micelles are also found in the system [136]. A low concentration of monomer is also, generally, found in the aqueous phase [136].

Emulsion polymerisation processes were first reported as early as 1912 [146], but it was not until Harkins's paper [147] in 1945 that substantive considerations of the polymerisation mechanism were published. Harkins further developed his observations in 1947 [148], which subsequently lead to his reporting of the first significant qualitative theory of emulsion polymerisation in 1950 [149]. The main features of Harkins's idealised system are shown schematically in figure 1.5.

Figure 1.5 - Representation of an Idealised Emulsion Polymerisation [149]

(A)

(B)

(C)

(D)

(E)

M   represents a monomer molecule;

⌀‿‿‿   represents an emulsifier molecule;

R•   represents a free radical;

P   represents a polymer molecule;

(A) Prior to initiation

(B) Polymerisation Stage 1 - shortly after initiation

(C) Stage 2 - all soap micelles consumed

(D) Stage 3 - monomer droplets consumed

(E) Polymerisation completed

26
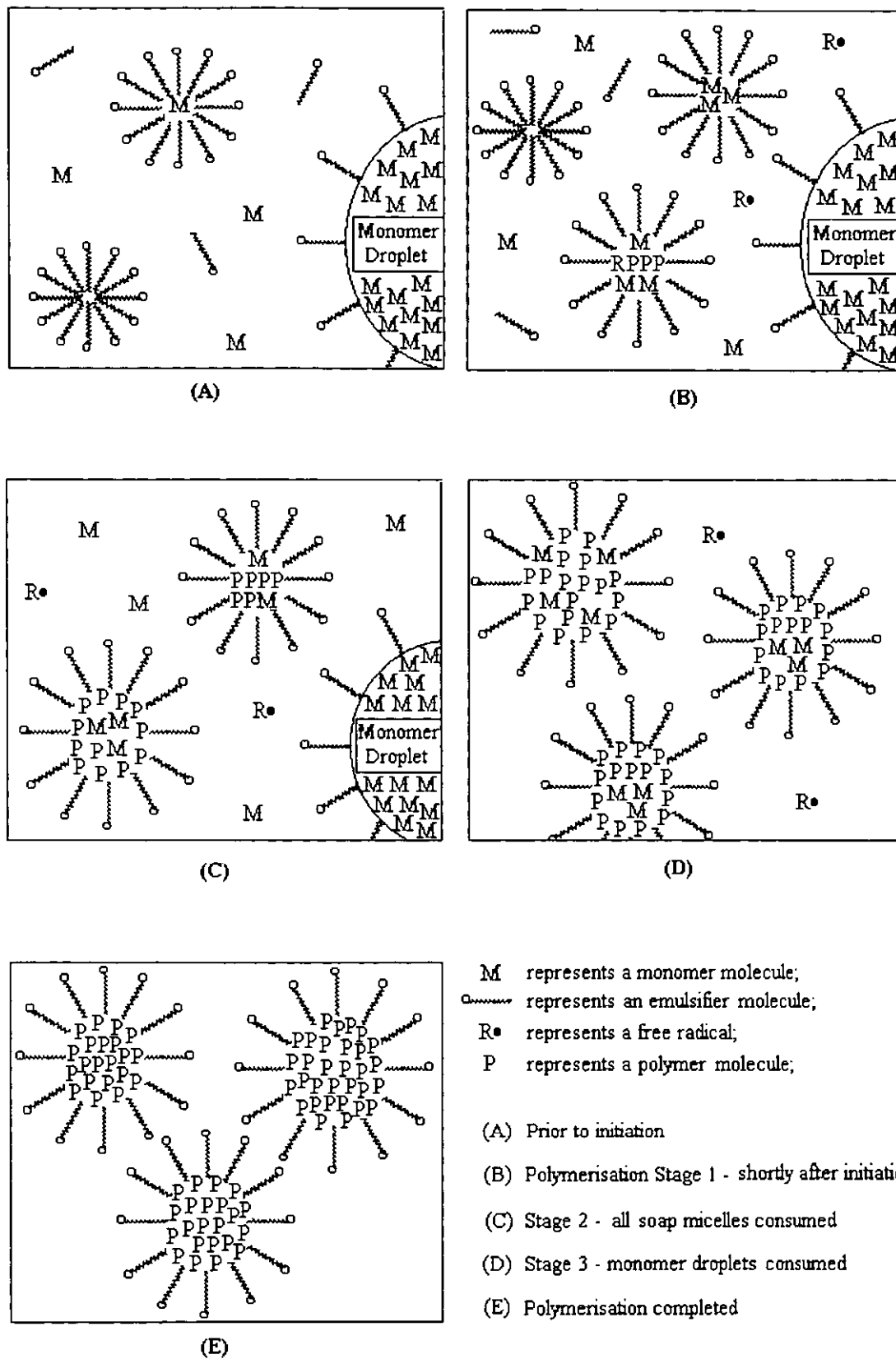
(I) Stage-1; free radicals generated by initiator decomposition diffuse through the continuous phase into the monomer-swollen micelles and particle nucleation occurs [149]. Propagating polymer latex particles swollen with monomer are also present in the system, therefore, after initiation [136, 149]. The number of latex particles in the system increases with time and the rate of polymerisation also increases, during Stage-1 of the polymerisation process.

(II) During the polymerisation, emulsifier is continuously adsorbed onto the surface of the propagating polymer particles, thus preventing flocculation of the latex [136]. This process leads to a reduction in the concentration of surfactant in the aqueous phase, which, in turn, leads to a displacement in the equilibrium between monomolecular surfactant molecules and the remaining, non-activated, soap micelles [136]. The micelles subsequently dissociate and the supply of soap micelles is exhausted after approximately 10-20 weight % monomer conversion [136] (the surfactant concentration is then below its CMC in water). The disappearance of the soap micelles is commonly regarded as an indication that Stage-2 of the polymerisation, where all of the monomer-swollen micelles have been converted into propagating polymer particles [136], has begun. No significant further nucleation is observed, therefore, during Stage-2 of the process, as initiation is considered to solely take place in the monomer-swollen micelles [149]. Monomer droplets are present in the system and monomer molecules constantly diffuse from the droplets into the latex particles - where the monomer is subsequently consumed [149] by the propagating polymer radicals. Before the monomer droplets have disappeared, the concentration of monomer in each particle is constant. The number of polymer particles and the rate of polymerisation are constant [136], therefore, during Stage-2 of the polymerisation.

(III) During Stage-3, after approximately 50 weight % monomer conversion [136], the supply of monomer droplets has been exhausted [136] and monomer-swollen polymer particles are exclusively present in the system. The polymerisation then continues at a steadily decreasing rate until all of the monomer is consumed [136].

(IV) After termination of the polymerisation process, the system contains a colloidal dispersion of electrostatically-stabilised polymer particles.

Harkins's polymerisation mechanism, the micellar nucleation mechanism [149], is, generally, applicable to systems which contain a monomer with low water-solubility (e.g. styrene) [136, 150] and emulsifier (provided that the surfactant is initially present at a concentration above its CMC) [136, 150]. Smith and Ewart [151, 152] attempted to quantify latex particle growth, via the development of a quantitative emulsion polymerisation model which was based on the Harkins polymerisation mechanism. From the basic idealised bulk free radical polymerisation constituent reactions, an expression for the rate of polymerisation can be derived [11] - if the attainment of a steady-state in the free radical concentration is assumed; i.e. if we presume that the rate of initiation, R_i (mol l^{-1} s^{-1}), will be equal to the rate of termination, R_t (mol l^{-1} s^{-1}), for the process. Where the rate of the termination reaction is given by [11]:

$$R_t = -\frac{d[P\bullet]}{dt} = 2k_t[P\bullet]^2 \qquad (1.16)$$

$$\text{i.e. } [P\bullet] = \left(\frac{R_t}{2k_t}\right)^{1/2} \qquad (1.17)$$

k_t is the rate constant (l mol^{-1} s^{-1}) for the termination process and $[P\bullet]$ is the concentration of polymeric free radicals (mol l^{-1}). The rate of polymerisation, R_p (mol l^{-1} s^{-1}), is, therefore, given by [11]:

$$R_p = k_p[P\bullet][M] = \left(\frac{R_t k_p^2}{2k_t}\right)^{1/2} [M] \qquad (1.18)$$

where $[M]$ is the monomer concentration (mol l^{-1}) and k_p is the propagation rate constant (l mol^{-1} s^{-1}).

Emulsion polymerisation processes follow, in general terms, the idealised kinetic behaviour of bulk polymerisations [136]. There are several factors which are unique, however, to emulsion polymerisation systems [136, 142]:

(I)   Each polymerisation locus is isolated from the others in the system.

(II)   The polymerisation loci (monomer-swollen latex particles) are small in volume.

(III)   The particles are isolated from the bulk of the monomer.

(IV)   The viscosity is high inside each latex particle - this effect can lead to an inhibition of radical-diffusion [136].

28

Such phenomena ensure that the kinetics of emulsion polymerisations do deviate from those of bulk polymerisations [136]. According to Smith and Ewart [152], the number of free radicals present in a latex particle, at a given instant, is restricted by the small particle volume, and the number of free radicals that can be accommodated by each latex particle [152] is limited. The Smith-Ewart theory considers all of the possible mechanisms which can potentially lead to a change in the number of free radicals found in a given latex particle (polymerisation locus) [152]. If it is assumed that free radicals are solely generated in the continuous phase of an idealised system containing N isolated reaction loci (each of volume, v and interfacial area, a), the rate of radical entry [152] into a single locus (dn/dt) can be defined by:

$$\frac{dn}{dt} = \frac{\rho}{N} \qquad (1.19)$$

where ρ is the overall rate of entrance into all the N loci.

Once a free radical has entered a locus, it is considered that the radical will propagate - until it is either terminated or it is desorbed from the latex particle. The rate of radical desorption [152] can be defined as:

$$\frac{dn}{dt} = -k_0 \, a \left(\frac{n}{v}\right) \qquad (1.20)$$

where k_0 is the desorption rate constant and n is the number of free radicals in a locus.

If it is assumed that the termination of a free radical can only occur by a mutual radical-radical interaction [152], the rate of termination in a given locus will be:

$$\frac{dn}{dt} = -2 k_t n \frac{(n-1)}{v} \qquad (1.21)$$

where k_t is the termination rate constant and $(n - 1)/v$ is the concentration of free radicals with which any of the n free radicals in a locus can react.

Smith and Ewart considered these three generalised processes for their prediction of the average number of free radicals in the polymerisation loci [152]. It can be shown that the rate of change in the number of latex particles containing the average number of free radicals, can be expressed as [136, 152]:

$$\frac{dN_{\bar{n}}}{dt} = \frac{\rho}{N'}\left[N_{\bar{n}-1} - N_{\bar{n}}\right] + \left(\frac{k_0\,a}{N_A\,v}\right)\left[(\bar{n}+1)N_{\bar{n}+1} - \bar{n}N_{\bar{n}}\right]$$

$$+ \left(\frac{k_t}{N_A\,v}\right)\left[(\bar{n}+2)(\bar{n}+1)N_{\bar{n}+2} - \bar{n}(\bar{n}-1)N_{\bar{n}}\right] = 0 \tag{1.22}$$

where $\bar{n}$ is the average number of free radicals in a latex particle, $N_{\bar{n}}$ is the relative number of latex particles containing $\bar{n}$ free radicals, $(dN_{\bar{n}}/dt)$ is the rate of change in the number of latex particles containing $\bar{n}$ free radicals, N' is the number of particles per unit volume and N_A is the Avogadro constant (mol^{-1}). ρ, k_t, k_0, v and a, have the same significance as defined previously (equations 1.19-1.21).

Smith and Ewart [152] solved the recursion equation (equation 1.22) for three limiting cases, based upon; the average time between successive free radical entries into a particle, t_E; the average time between radical exits from a particle, t_0; and the average time between termination processes, t_t.

Case-1: where $t_0 \ll t_E$ and $\bar{n} \ll 1$.

Case-1 kinetics describe systems where the rate of free radical desorption from the particles is high [136, 152]. On average, therefore, only a small number of particles will have a radical within them, at a given time. This behaviour is uncommon for monomers with low solubilities in water (e.g. styrene) [136], but monomers with appreciable water-solubilities (e.g. methyl methacrylate and vinyl acetate) have been found to follow Case-1 behaviour, under certain reaction conditions [136].

If termination predominates in the aqueous phase, then the rate of polymerisation, R_p, is given by [152]:

$$R_p = k_p[M]\,\alpha\,v\left(\frac{\rho_i}{2k_{tw}}\right)^{1/2} \tag{1.23}$$

where k_p is the propagation rate constant, α is the radical partition coefficient between the polymer particle and aqueous phase, ρ_i is the rate of production of free radicals in the aqueous phase and k_{tw} is the termination rate constant in the aqueous phase [152].

If termination predominately occurs within the polymer particles, the rate equation can be defined as [136, 152]:

$$R_p = k_p [M] \left(\frac{\nu \rho_i}{2 k_0 a} \right)^{1/2}$$

(1.24)

Case-2: where $t_t \ll t_E \ll t_0$ and $\bar{n} = 0.5$.

This scenario applies to systems where desorption of free radicals from the particles is insignificant [136]. Case-2 kinetics describe polymerisation systems where termination within a particle, after a second radical has entered into the particle, is very rapid, when compared to the time interval between the entrance of the two radicals [152]. Consequently, each particle is assumed to contain either one propagating polymer chain or no growing chains [152] (i.e. if the number of latex particles is large, one half of the particles will contain one free radical, whilst the remaining particles will contain no radicals, at a given time). This behaviour appears logical for an idealised emulsion polymerisation, where the presence of a free radical within a latex particle, and subsequent radical termination, are dependent upon the same event - the capture of a free radical by the particle. It follows, therefore, that the probability of a given particle containing or not containing a radical will be equal (i.e. on average, one half of the particles will contain a free radical).

For the Case-2 condition [136, 152], the rate of polymerisation is given by [152]:

$$R_p = k_p [M] \left(\frac{N}{2} \right)$$

(1.25)

where the number of particles per unit volume, N, can be approximated by [152]:

$$N = K \left(\frac{\rho_i}{\mu} \right)^{0.4} (a_s [S])^{0.6}$$

(1.26)

μ is the rate of growth in the volume of a latex particle, a_s is the cross-sectional area of a surfactant molecule, [S] is the surfactant concentration and K is a constant.

Throughout a broad region of the emulsion polymerisation process, the monomer concentration within the particles is constant [136], and, hence, the rate of

polymerisation is dependent only on the number of particles [136, 152] present (at a given temperature). Smith found that the emulsion polymerisation of styrene followed Case-2 kinetic behaviour [153], and this observation has been corroborated by several investigations into styrene emulsion polymerisation [154-156]. Varela De La Rosa *et al.* [154] investigated the batch emulsion polymerisation of styrene (sodium lauryl sulphate emulsifier, potassium persulphate initiator) by direct measurement of the polymerisation rate via the use of an automated reaction calorimeter [154]. A series of emulsion polymerisations were performed with different emulsifier and initiator concentrations [154]. The number of latex particles (N_p) was found to be related to the emulsifier concentration, [S], by [154]:

$$N_p \propto [S]^{0.66} \tag{1.27}$$

and N_p was found to be influenced by the initiator concentration, [I], by [154]:

$$N_p \propto [I]^{0.41} \tag{1.28}$$

Both of these observations are comparable to the theoretical relations predicted by Smith-Ewart Case-2 behaviour [152]. The average number of free radicals per latex particle was calculated for each of these experiments at the maximum polymerisation rate [154]. The classical value of 0.5 for $\bar{n}$ was obtained, which corresponds to Smith-Ewart Case-2 kinetics [152]. Varela De La Rosa *et al.* [154] discovered that the styrene emulsion polymerisation could be described by two distinct stages; Interval-1, where the rate of polymerisation increased up to a maximum and particle nucleation occurred throughout this region, and Interval-3, where monomer droplets were no longer present, and the monomer concentration within the latex particles decreased as a function of time [154]. No Stage-2 (Interval-2 [149]) was observed under the reaction conditions investigated [154], i.e. nucleation was found to occur throughout the polymerisation stage where a free monomer phase was identified [154].

Case-3: where $t_E \ll t_t \ll t_0$ and $\bar{n} \gg 1$.

This relation applies to latices where the rate constant for termination within the particles is small [136, 152]. Case-3 kinetic behaviour is seldom observed for emulsion polymerisation processes [136], although Case-3 kinetics can be followed by

systems which contain large latex particles (if free radical desorption is also insignificant) - the particles are able to accommodate more than one free radical without mutual termination processes occurring instantaneously [155].

For Case-3 kinetic behaviour, the rate of polymerisation, R_p, is given by [152]:

$$R_p = k_p [M] \left(\frac{\rho_i \nu}{2 k_t}\right)^{1/2}$$

(1.29)

Smith-Ewart kinetics are seldomly obeyed for emulsion polymerisations with monomers of appreciable water solubility (e.g. vinyl acetate, methyl methacrylate and acrylonitrile) [136]. The nucleation mechanism is considered to be the dominant factor which influences polymerisation kinetics [136, 142]. The homogeneous nucleation theory [156] considers that electrostatically-charged free radicals (e.g. sulphate radical anions) initially react with monomer in the aqueous phase, to form water-soluble oligomeric radicals [156]. These oligomeric radicals propagate until they reach their critical solubility limit in the aqueous phase, where they subsequently precipitate from solution [156]. The precipitated oligomeric radicals subsequently adsorb surfactant molecules to form spherical, primary, particles [156]. Additional precipitated radicals may then either form new primary particles or they may aggregate with existing particles [156]. The monomer-swollen primary polymer particles then grow by propagation. The primary particles may also flocculate with themselves or with growing particles, to a degree dependent upon the stabilising-efficiency of the surfactant [136, 156]. Consequently, particle growth may take place by both aggregation and propagation, and the number of latex particles is dependent upon the surfactant concentration and its ability to stabilise both the primary particles and the growing latex particles [136, 156].

1.6.2 - SWELLING OF LATEX PARTICLES

The extent of the two, or more, comonomers' partitioning between the latex particles, the monomer droplets, and the aqueous phase in emulsion copolymerisation processes, can have a fundamental influence upon copolymer compositional drift [157, 158] and upon the rate of polymerisation [158]. Additionally, the degree of first-stage polymer particle swelling with second-stage monomer, can also significantly influence the morphology of composite latex particles [159-161]. Consequently, several models for predicting latex particle swelling [162-165] have been developed, in order to try and increase the control of particle structures in multi-component latex systems [165].

Morton *et al.* [162] investigated the saturation swelling of latex particles with solvent. The equilibrium solubility and rate of solution of solvent (styrene, toluene and chlorocyclohexane) was determined [162] for a series of polystyrene latex fractions with varying particle size. It was found that the equilibrium amount of solvent imbibed by the latex particles was proportional to the particle diameter [162], and inversely proportional to the interfacial energy at the particle surface [162]. The molecular weight of the latex polymer was found to have no apparent influence on the equilibrium swelling [162] behaviour, within the molecular weight (M) range investigated (ca. $10^5 \leq M \leq 10^6$ g mol^{-1}). These experimental observations were found to follow theoretical swelling equations determined from thermodynamic analysis [162]. Morton *et al.* [162] predicted that the equilibrium swelling of latex particles, in the presence of free solvent, would be analogous to polymer network swelling [162]. For a linear polymer latex particle, the restraining force (the force which opposes the swelling force) was considered to be the interfacial free energy between the latex particle and the aqueous phase [162]. In the event that the swollen particle is in equilibrium with free solvent [265], then:

$$\Delta G = \Delta G_M + \Delta G_S = 0 \qquad (1.30)$$

where ΔG is the partial molar free energy of the solvent (J mol^{-1}), ΔG_M is the contribution from the free energy of mixing solvent with polymer (the osmotic contribution to ΔG), and ΔG_S is the contribution from the latex particle/water interfacial energy.

Morton *et al.* [162] expressed the partial molar free energy of mixing solvent and polymer in terms of the Flory-Huggins approach [62, 63]:

$$\frac{\Delta G_M}{RT} = \ln(1 - \phi_2) + \phi_2\left(1 - \frac{1}{DP_n}\right) + \chi_{1,2}(\phi_2)^2 \tag{1.31}$$

where ϕ_2 is the equilibrium volume fraction of polymer in the swollen particle, $\chi_{1,2}$ is the polymer-solvent interaction parameter, DP_n is the number average degree of polymerisation, and R and T have their usual significance.

The contribution from ΔG_S to the overall free energy was determined from considerations of the increase in size of the interface as a function of particle size and solvent-type [162]. For spherical particles, the partial molar interfacial free energy component, ΔG_S, can be expressed as [162]:

$$\Delta G_S = \frac{2 V_1 \gamma}{r} \tag{1.32}$$

where V_1 is the molar volume of the solvent (m^3 mol^{-1}), γ is the interfacial energy (J m^{-2}), and r is the latex particle radius (m) at swelling equilibrium.

At equilibrium, it follows [162], therefore, that:

$$\frac{2 V_1 \gamma}{r RT} \approx -[\ln(1 - \phi_2) + \phi_2 + \chi_{1,2}(\phi_2)^2] \tag{1.33}$$

(If the polymer is of high molecular weight).

The swelling equilibrium of a latex particle, for a given polymer/solvent system, would be expected, therefore, to be proportional to its size [162], and to be inversely related to the interfacial energy [162], at constant temperature. Equilibrium swelling of monodisperse polystyrene latices with solvent was performed under isothermal conditions [162]. The swelling of latex particles with different solvents was found to be dependent upon both the $\chi_{1,2}$ parameter and upon the effect of the solvent on the interfacial free energy in the system [162]. Morton *et al.* [162] also considered the effect of monomer swelling on the monomer/polymer ratio in latex particles during batch emulsion polymerisation processes. The latex particles were assumed to be saturated with monomer throughout the stages where a free monomer phase is present [162]. The interfacial energy was considered to increase throughout the

polymerisation, as the size of the particles increases throughout the process and the concentration of soap in the system is constant [162]. Morton *et al.* [162] concluded that the interfacial energy would be proportional to the surface area of the particles (i.e. $\gamma \propto r^2$) and so the expression on the right hand side of equation 1.33 would be proportional to the particle radius. Consequently, over a given period in the polymerisation, where, for example, the conversion had doubled, the radius of the particle would subsequently only increase by approximately 25% [162]. As the function on the right hand side of equation 1.33 increases approximately two to three times more rapidly than ϕ_2, when $\chi_{1,2} \approx 0.5$, the ϕ_2 term would be anticipated to increase by approximately 10% as the particle weight doubled [162]. These observations were considered to signify that, for a given polymerisation, the monomer/polymer ratio within the particles would essentially be constant, provided that a separate monomer phase were present [162] throughout.

Vanzo *et al.* [163] investigated the partial swelling of latex particles with monomer. The vapour pressure of solvent was measured at different swelling ratios [163], thus, circumventing the approach of Morton *et al.* where measurements were recorded solely at the swelling equilibrium for a series of latices with different particle radii. Vanzo *et al.* [163] discovered that their approach also afforded a reliable measurement of equilibrium swelling, given that equilibrium conditions are found when the vapour pressure of the latex system corresponds to the sum of the water and monomer partial vapour pressures [163]. Vapour pressure measurements of monomer solubility were used to estimate the partial molar free energy of the solvent (monomer) by [163]:

$$\Delta G = RT \ln a \qquad (1.34)$$

where ΔG is the partial molar free energy of the solvent and a is the solvent activity.

The monomer vapour was considered to exhibit ideal gas behaviour [163], under the conditions examined, allowing for the activity of the solvent (monomer) to be approximated by p/p^0, the ratio of the vapour pressure at a given volume fraction of polymer in the swollen particle, to the vapour pressure at equilibrium swelling [163]. The partial molar free energy of the solvent, ΔG, was considered to be related to osmotic, ΔG_M, and interfacial, ΔG_S, contributions, as previously discussed by Morton *et al.* (equation 1.30). The osmotic contribution was similarly assumed to follow the

Flory-Huggins relation [62, 63] (equation 1.31) and the interfacial contribution was considered to exhibit Morton-type behaviour (equation 1.32), giving the following relation [163]:

$$\frac{\ln p/p^0 - \ln(1 - \phi_2) - \phi_2}{(\phi_2)^2} \approx \frac{2\,V_1\,\gamma}{RT\,r\,(\phi_2)^2} + \chi_{1,2} \qquad (1.35)$$

Vapour pressure curves were determined for incremental additions of solvent (benzene or vinyl acetate) to poly(vinyl acetate) latex [163]. The point at which the curve reached the equilibrium pressure, corresponding to the presence of a free organic solvent phase, was recorded as an uncorrected solubility value [163]. The solvent solubility in the latex particles was then determined, with corrections applied for the presence of solvent in the vapour and aqueous phases [163]. Accurate measurements of the amount of solvent in the latex particles was thereby determined for each of the vapour pressures [163]. With the knowledge that, at a given point on the corrected vapour pressure curve the amount of solvent within the particles was known, the average volume fraction of solvent within each particle (ϕ_2) was calculated [163]. The vapour pressure (p) and saturated vapour pressure (p^0) measurements recorded, along with the equilibrium volume fraction of polymer (ϕ_2) values recovered, were initially converted into $[\ln(p/p^0) - \ln(1 - \phi_2) - \phi_2]/(\phi_2)^2$ units and these values were subsequently plotted as a function of $1/(\phi_2)^2$ (equation 1.35). Flory polymer-solvent interaction parameters and interfacial tensions were determined from the intercept and gradient of the straight line plots determined for the poly(vinyl acetate)-benzene and poly(vinyl acetate)-vinyl acetate latex systems [163]. Latex dilution was found to increase interfacial tensions in these systems. These observations were attributed to the fact that surfactant was desorbed from the particles on dilution [163]. Correspondingly, latex interfacial tensions were found to decrease with the introduction of additional soap [163]. Increased interfacial tensions were recorded for the benzene latex system, at identical soap contents, reflecting the higher interfacial tension of benzene with water (when compared to vinyl acetate/water) [163].

Aerdts *et al.* [166] investigated the partial and saturation swelling of polybutadiene latex particles, styrene/methyl methacrylate copolymer latex particles and polybutadiene/poly(styrene-*co*-methyl methacrylate) composite latex particles with

monomer [166]. Monodisperse polybutadiene (PBD) microgel latices of different crosslink-density were synthesised by soap-free emulsion polymerisation [166]. Network structures were controlled by the employment of variable chain-transfer agent concentrations and latices were also polymerised to different final conversions [166]. Partial swelling of PBD latices with both styrene and methyl methacrylate was investigated [166] and these experimental observations were compared with a theoretical swelling model [166], developed from a combination of the Vanzo [163] and Flory-Rehner [167] theories (equation 1.36):

$$\ln(1-\phi_2) + \phi_2 + \chi_{1,2}(\phi_2)^2 + \frac{2V_1\gamma\phi_2^{1/3}}{RTr_0} + \frac{\rho(V_1)}{M_c}\{\phi_2^{1/3} - \frac{2\phi_2}{f}\} \approx \ln\left(\frac{[M]_{aq}}{[M]_{aq,\,sat}}\right) \qquad (1.36)$$

where r_0 is the unswollen latex particle radius (m), M_c is the network's average molecular weight between crosslinks (kg mol^{-1}) [167], ρ is the polymer density (kg m^{-3}), $[M]_{aq}$ is the monomer concentration in the aqueous phase (mol l^{-1}), $[M]_{aq,\,sat}$ is the monomer concentration in the aqueous phase at saturation (mol l^{-1}), f is the network functionality [167], V_1 is the molar volume of the solvent (m^3 mol^{-1}), ϕ_2 is the equilibrium volume fraction of polymer in the swollen particle, $\chi_{1,2}$ is the polymer-solvent interaction parameter, and R and T have their usual significance.

The partitioning behaviour of methyl methacrylate was investigated for several PBD latex samples [166]. The PBD latex particle size and microgel crosslink-density were both found to not significantly affect the monomer's partitioning [166]. Styrene/methyl methacrylate (S/MMA) copolymer (S:MMA weight ratios of 1:3 and 1:1) seed latices were swollen with MMA and the composition of the copolymer was also found to have little influence on the partitioning behaviour of methyl methacrylate [166]. The structure of composite latex particles prepared from styrene/MMA copolymerisation in the presence of PBD seed latex [166] was similarly found to not significantly affect the partitioning of methyl methacrylate [166]. Each of these experimental observations [166] was considered to have indicated that the free energy change due to the configurational entropy on partially mixing monomer and polymer [166] (equation 1.31) had dominated the, single monomer, swelling process. Saturation swelling of latex particles with both styrene and methyl methacrylate was performed [166] and these experimental observations were related to a swelling model (equation 1.37), originally developed by Maxwell et al. [164].

38

According to Maxwell [164], the partial molar free energy of each of the two monomers, i and j, is equal in each of the three phases, i.e. the latex particle, monomer droplet and aqueous phases, at equilibrium [164]. The partitioning behaviour of monomer i can then be expressed as [164]:

$$\ln\phi_{pi} + (1-m_{ij})\phi_{pj} + \phi_p + \chi_{ij}(\phi_{pj})^2 + \chi_{pi}(\phi_p)^2$$

$$+ \ \phi_{pj}\phi_p(\chi_{ij} + \chi_{pi} - \chi_{pj}m_{ij}) + \frac{2\,V_{mi}\,\gamma\,\phi_p^{1/3}}{RT\,r_0} \tag{1.37}$$

$$= \ln\phi_{di} + (1-m_{ij})\phi_{dj} + \chi_{ij}(\phi_{dj})^2 = \ln\left(\frac{[M_i]_{aq}}{[M_i]_{aq,\,sat}}\right)$$

where ϕ_i and ϕ_j are the volume fractions of monomer within the latex particles, χ_{ij} is the Flory interaction parameter between the two monomers, χ_{pi} and χ_{pj} are the interaction parameters between each monomer and the polymer, m_{ij} is the ratio of the two monomers' molar volumes, ϕ_{di} and ϕ_{dj} represent the volume fraction of monomer within the monomer droplets, and $[M_i]_{aq}$ and $[M_i]_{aq,sat}$ are the concentrations of monomer i in the aqueous phase, and in the aqueous phase at saturation [164], respectively. The corresponding equation for monomer j can be similarly derived [164].

Methyl methacrylate concentrations in the aqueous phase were observed to proportionately follow the MMA fraction in the droplet phase, for swelling of PBD seed latices in the presence of MMA and styrene monomer [166] - indicating that the monomer partitioning behaviour obeyed Henry's law [58, 166]. Although considerations of both equation 1.37 and the similar equation for monomer j can, in theory, be used to predict monomer partitioning for latex systems containing two monomers, the swelling behaviour can be difficult to predict [164], as interaction parameter values and interfacial tensions are not readily determined experimentally [164]. Maxwell et al. [164, 168] simplified their latex particle swelling theory, by assuming that the monomer volume fractions were equal, that the interaction parameter on mixing two monomers was negligibly small, and that monomer interactions with the same polymer would be equal (i.e. $\chi_{pi} = \chi_{pj}$) [168].

With these assumptions, it follows [168], that:

$$f_{pi} = f_{di}$$
$$f_{pj} = f_{dj}$$

(1.38)

where f_{dx} represents the volume fraction of monomer x in the droplets, and f_{px} represents the volume fraction of monomer in the latex particles [164, 168].

If it is also considered that m_{ij} will be identical to m_{ji} [164], then the molar fraction of monomer in the droplets would also be anticipated to be equal to the molar fraction of monomer within the particles [164]. Maxwell *et al.* [164] also derived relations to predict the actual concentrations of the two monomers in the latex particle phase. For a given seed latex, the concentration of monomers i and j within the particles, C_i and C_j, are related to the monomer fractions in the droplets, f_{di} and f_{dj}, by [164]:

$$C_i = f_{di}[(C_{im} - C_{jm})f_{di} + C_{jm}]$$
$$C_j = f_{dj}[(C_{jm} - C_{im})f_{dj} + C_{im}]$$

(1.39)

where C_{im} and C_{jm} are the saturation concentrations of monomers i and j in the latex particles [164].

For styrene and MMA comonomer swelling within styrene/methyl methacrylate copolymer seed latices (S:MMA weight ratios of 1:3 and 1:1) [166] the monomer fractions in the monomer droplet and latex particle phases were found to be equal (as predicted from equation 1.38 [164]). Similar behaviour was also observed for the swelling of PBD seed latices with these two monomers [166]. The partitioning of monomers within latex samples was, therefore, considered to have been essentially governed by the entropy on mixing of the two monomers [166], as the type of polymer was found to have had no significant influence upon the ratio of the monomers in the polymer and monomer droplet phases, respectively [166]. The absolute monomer swelling value for a given seed latex was found to be dependent, however, upon the polymer type [166] (due to differences in interaction parameters and interfacial tensions). For example, it was observed that the concentration of MMA in the monomer-swollen composite latex particles was higher than the concentrations in swollen PBD particles [166], and the styrene concentration was similarly found to increase, but to a lower extent than with MMA [166]. It was observed that the higher

monomer concentrations within the composite particle phase [166] did not, however, lead to a significant change in the ratio between the two monomer components.

Schoonbrood *et al.* [169] have extended Maxwell's swelling model [164] in order to accurately predict multi-monomer partitioning behaviour within batch emulsion terpolymerisation processes.
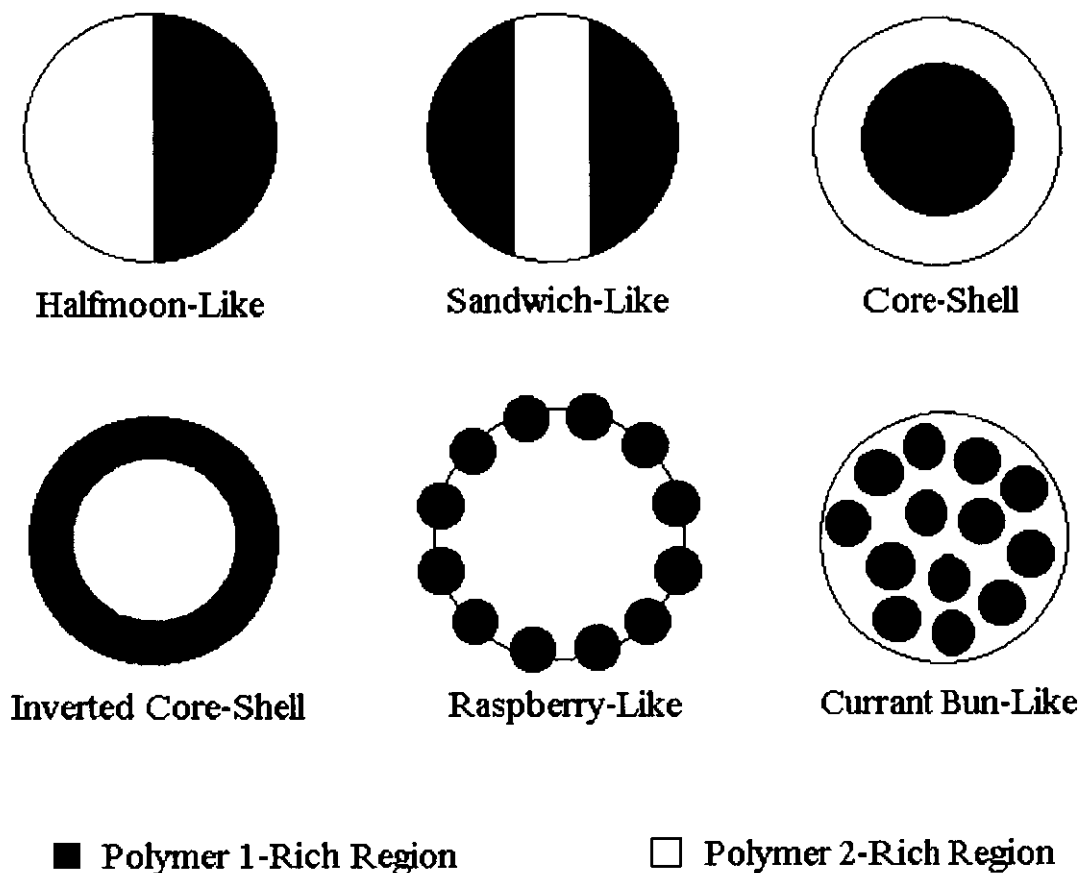
1.6.3 - COMPOSITE LATEX PARTICLES

Composite latex particles are synthesised from sequential emulsion polymerisation, where the second polymer component is synthesised in the immediate presence of a pre-formed, first-stage, polymer latex (seed latex). Under ideal conditions, no further latex particle nucleation is observed during the second polymerisation process [170]. Consequently, the final, composite, latex particles contain two different polymeric components. A significant number of reports into latex particle internal structures (morphologies) have been published [171-186]. Several, reported, particle structures [171, 172] are shown in figure 1.6. It is important to note that these idealised particle structures have been considered to represent particle morphologies found in the latex [171]. The removal of the aqueous phase from the particles, such as during film preparation for analytical characterisation purposes, has the potential to alter the particle's morphology [171]. Similarly, the morphology of a composite latex material often shows characteristics from several of these idealised particle structures [173, 174]. Usually one distinct particle structure cannot be used to fully describe the particle's phase behaviour. The synthesis and characterisation of interpenetrating polymer network (IPN) structured latex particles (section 1.6.4) will be discussed separately from other composite particles.

The physical and mechanical properties of two-stage latex particles are influenced significantly by the particle morphology [175-177]. For example, materials with core-shell latex particle structures can exhibit physical property characteristics which contrast markedly from those of corresponding random copolymer or polymer blend samples [175]. The morphology of a two-component latex particle is understood to be influenced by both the kinetics of the second-stage polymerisation [176] and the thermodynamics of the system [177].

The most significant factors that have been found to influence the final particle morphology, include [178-184]:

(I)   The degree of compatibility (miscibility) between the polymer components.

(II)   The relative hydrophilicities of the two polymers.

(III) The type of initiator employed for each polymerisation.

(IV)   The mode of second-stage monomer addition (e.g. continuous or batchwise).

(V)   The viscosity within the second-stage polymerisation loci (latex particles).

Figure 1.6 - Cross-Sections of Latex Particles - Illustrating Idealised Particle Morphologies [171, 172]

Halfmoon-Like   Sandwich-Like   Core-Shell

Inverted Core-Shell   Raspberry-Like   Currant Bun-Like

■ Polymer 1-Rich Region   ☐ Polymer 2-Rich Region

Berg *et al.* [177] have considered the thermodynamics of two-stage particle formation [177]. In this approach [177], composite latex particle morphologies are considered to solely result from the requirement that the system's interfacial free energy is

minimised. For the three component (polymers i and j, and water) latex system, the free energy can be expressed as [177]:

$$G = \sum \gamma_{ij} A_{ij}$$

(1.40)

where G is the Gibbs free energy (J mol^{-1}), γ_{ij} is the interfacial tension between phases i and j (J m^{-2}), and A $_{ij}$ is the area of the interface between the two phases (m^2 mol^{-1}).

According to this method of analysis [177], each theoretically-possible morphological configuration has a corresponding free energy, and the phase-structure with the lowest free energy is considered to be the most thermodynamically favoured. Although such considerations can predict the most stable phase-structures for two component latex particles, the relative rate of the second-stage polymerisation, and phase separation, processes, has a marked influence upon the final particle morphology [171, 172]. The system's kinetics are significantly dependent upon by the degree of component mobility within the second-stage polymerisation locus (monomer-swollen composite latex particles). A number of factors, including the constituent polymer glass transition temperatures [172], crosslinking [178], and the presence of low molecular weight diluents [179], can influence the degree of polymer mobility. If both of the polymers can readily undergo segmental relaxation processes at the temperature for polymerisation, the energetically-preferred morphology will be attained [172, 179]. If, however, the mobility of one, or both, of the components is significantly hindered, the most thermodynamically favoured phase-structure may not result [176, 178].

Winnik *et al.* [180], Shen *et al.* [181], Okubo *et al.* [172], Beyer *et al.* [182], Wai *et al.* [183], Cho and Lee [171] and Joensson *et al.* [184] have investigated composite polystyrene/poly(methyl methacrylate), PS/PMMA, latex particle structures. Joensson *et al.* [184] polymerised MMA in the presence of monodisperse PS seed latex particles [184], with the thermolysis of lauryl peroxide as second-stage polymerisation initiator. PS latex seed particles were synthesised [184] by soap-free emulsion polymerisation with potassium persulphate as initiator. The influence of the monomer addition process (batchwise or continuous addition) on the morphology of the composite latex particles was investigated [184] by transmission electron microscopy (TEM) analysis. Monomer was allowed to diffuse into the seed latex particles, prior

to initiation of the polymerisation, for batch processes [184], and composite particles were found to contain large (ca. 100 nm), spherical, PMMA domains dispersed in continuous PS matrices [184]. Polymerisation of MMA under starve-fed conditions [184] yielded composite particles with PMMA micro-domains. PMMA inclusions were found to be uniformly distributed throughout the continuous PS phase [184], for composite latex particles prepared from continuous monomer addition processes. A ten-fold decrease in the initiator concentration [184], and, hence, a reduced polymerisation rate [184], for the batch polymerisation process [184], was found to lead to the generation of composite particles containing increased PMMA domain sizes (ca. 500 nm) [184]. The influence of polymerisation locus viscosity on the morphology of composite latex particles was also investigated, by the use of an organic diluent swelling procedure [184]. The temperature for the second-stage polymerisation (60°C) was significantly lower than the constituent polymer glass transition temperatures [184], thus ensuring that second-stage polymerisations had proceeded within highly viscous environments [184]. A composite particle latex was, therefore, synthesised from the starve-fed addition of MMA to a PS seed latex swollen with cyclohexane [184], volume ratio cyclohexane:PS of 3:2 (DSC analysis had determined that the glass transition temperature of the diluent/PS mixture was significantly lower than the polymerisation temperature [184]). The diluent-swollen composite particles' PMMA domains were found to have markedly larger sizes (ca. 500 nm) [184] compared to those of the latex particles prepared from non-plasticised seeds (ca. 10 nm) [184]. The observations that decreased polymerisation locus (latex particle) viscosities [184], and reduced rates of batch second-stage polymerisation [184], had lead to an increase in the second-stage polymer component's domain size, were considered to reflect the importance of the role that macro-radical diffusion (radical transport within the latex particle environment) had played in the development of the particle morphology [184].

Winnik et al. [180] synthesised a series of composite PS/PMMA latex particles by either polymerising MMA in the presence of PS seed latex, or by polymerising styrene in the presence of PMMA seed particles [180]. Seed latex particles were synthesised [180] by soap-free emulsion polymerisation with potassium persulphate as initiator. Second-stage monomers were continuously added, under starve-fed conditions,

throughout the second-stage polymerisation and potassium persulphate thermolysis was used for initiation of polymerisation [180]. Composite latex particle morphologies were investigated [180] by freeze-fracture TEM (FFTEM) analysis. Characterisation of both the PMMA and PS seed latices determined that monodisperse particles with smooth surfaces resulted from first-stage emulsion polymerisation processes [180]. Second-stage polymerisations of styrene were found to generate "raspberry-like" monodisperse composite latex particles with rough surfaces [180], and the degree of surface roughness was found to increase with increasing concentrations of styrene [180]. Second-stage polymerisations of MMA were also found to generate monodisperse latex particles with rough surface topologies [180]. It was observed, however, that the roughness was significantly reduced when compared to particles prepared from second-stage styrene polymerisation [180]. Exterior particle phases of uniform thickness were found to predominately consist of PS [180]. The PS phase-structure was considered to have resulted from the coalescence of small, spherical, PS domains [180], thus, leading to the formation of the PS-rich coating around the PMMA-based particle core. Evidence of limited PS micro-domain phase dispersion within the continuous PMMA-rich particle cores was also observed for several composite material compositions [180]. Composite particles synthesised from the inverse polymerisation process (styrene polymerised in the presence of PMMA seed particles [180]) were considered to comprise of PS-rich particle cores surrounded entirely by balloon-like PMMA shells [180]. The PMMA-rich phase of these materials was found to contain a number of small PS inclusions which decorated only certain areas of the particle surface [180]. The presence of limited PMMA micro-domain phase dispersion within the PS-rich particle core was also observed for a number of composite latex particle compositions [180]. Winnik *et al.* [180] concluded that polymerisation of styrene in the presence of seed PMMA latex particles had not generated the thermodynamically-favoured inverted core-shell particle morphology (PMMA is more hydrophilic than PS [172], suggesting that PMMA, and not PS [180], should have migrated to the particle surface), due to the hydrophilic nature of PS molecules with sulphate end-groups (the highly polar sulphate group is generated from the persulphate decomposition process [143, 144]). The formation of small, spherical, PS occlusions at the particle surface [294] was considered to have arisen from the operation of primary PS latex particle coagulation

[156] processes, during the starve-fed second-stage polymerisation (section 1.6.1). In composite latex systems with MMA as the second-stage monomer [180], electron microscopy analysis also indicated that shell formation had, most probably, resulted from an aggregative polymerisation mechanism [180]. The additional presence of second-stage polymer micro-domain inclusions within particle cores [180] was considered to have resulted from the limited initiation of polymerisation by captured oligomeric radicals within the partially-swollen latex particles [180].

Wai *et al.* [183] characterised composite poly(styrene-*co*-methyl methacrylate)/poly(trideuteromethyl methacrylate) latex particles by small angle neutron scattering [183]. A statistical styrene/methyl methacrylate (weight ratio styrene:MMA of 1:1) copolymer seed latex was prepared by emulsion copolymerisation [183], with sodium lauryl sulphate emulsifier and ammonium persulphate initiator. Trideuteromethyl (methyl-d_3) methacrylate was then introduced to the seed latex (maintained throughout at 70°C) by a starve-fed, continuous, monomer addition process [183]. The intensity of neutron scattering from composite latex particle samples [183] was determined as a function of the radial scattering vector, q (nm^{-1}) [183]:

$$q = \left(\frac{4\pi}{\lambda}\right) \sin\theta \tag{1.41}$$

where λ is the wavelength of the incident beam in vacuo (nm) and 2θ is the scattering angle.

The scattering curve obtained from the composite latex particle sample was found to best fit a hollow-sphere scattering function [183], indicating that scattering was dominated by a neutron containing (methyl-d_3 methacrylate) particle shell [183]. The composite latex particles were, therefore, considered [183] to comprise of poly(trideuteromethyl methacrylate) shells and styrene/MMA copolymer-based particle cores.

Okubo *et al.* [172] indirectly evaluated the morphology of PMMA/PS, PS/PMMA, poly(methyl acrylate)/polystyrene (PMA/PS) and PMA/PMMA (the first-named polymers were the first components synthesised) composite latex particles by soap titration [172]. Polymer seed latices were synthesised by emulsion polymerisation,

46

with potassium persulphate as initiator and sodium dodecyl benzene sulphonate as emulsifier [172]. Second-stage monomers were added to seed latices by one of two methods [172]; batch pre-swelling, where monomer was adsorbed in seed particles for 72 hours before polymerisation [172], or, by a starve-fed, continuous, monomer addition process [172]. The weight ratio of the first and second-formed (composite particle) polymer components was varied between 20:1 and 3:1 [172], for each of the four latex systems investigated. The average area occupied (A_m) by an emulsifier molecule at the composite latex particle surface [172] was determined from soap titration. The A_m value was found to be dependent upon the structure of the seed polymer [172], allowing estimations for composite particle structures to be made from titration techniques [172]. The A_m value for PS, PMMA and PMA seed latex particles was found to increase with polymer polarity [172], indicating that the amount of adsorbed emulsifier had decreased with increasing component hydrophilicity [172]. Polymerisation of styrene, from the continuous monomer addition process, in the presence of PMMA seed latex [172], yielded, in general terms, composite materials containing PS-rich surface layers. At low PS concentrations [172], particles with core-shell morphologies were predicted from titration and particles with inverted core-shell structures [172] were found at intermediate PS concentrations. At the highest PS particle contents [172] significant quantities of PS were found at the particle surface and composite particles with raspberry-like structures were predicted from titration [172]. Composite particles prepared by batch addition of styrene to PMMA seed latex were found to have inverted core-shell structures at low to intermediate PS contents [172], and raspberry-like morphologies were predicted for particles with highest PS concentrations [172]. The contrasting influences of monomer addition on particle morphology [172] was considered to have resulted from differences in particle viscosity during the second-stage polymerisation process [172]. Composite particles prepared from polymerisation of MMA in the presence of PS seed latex [172] were estimated to have core-shell morphologies, from either monomer addition process, with the PMMA component predominating at the particle surface [172]. The relative hydrophilicities of the two polymer components were considered to have dominated the particle morphology [172] in the PS/PMMA system.

Lee and Ishikawa [185] synthesised composite poly(ethyl acrylate-*co*-methacrylic acid)/poly(styrene-*co*-butadiene) latex particles [185]. Hydrophilic seed latices were prepared [304] by emulsion copolymerisation of ethyl acrylate, EA/methacrylic acid, MAA. Composite latices were synthesised by semi-continuous addition of styrene/butadiene (weight ratio styrene:butadiene of 3:2) to poly(ethyl acrylate-*co*-methacrylic acid) seed latex (weight ratio second copolymer:first synthesised copolymer of 4:1) [185]. The influence of component molecular weight on the morphology of composite latex particles was also investigated [185] by polymerising styrene, with and without CCl₄ chain-transfer agent, in the presence of ethyl acrylate/styrene/methacrylic acid terpolymer seed latices (weight ratio EA:styrene:MAA of 5:4:1, prepared both with and without CCl₄ addition). The morphology of poly(ethyl acrylate-*co*-methacrylic acid)/poly(styrene-*co*-butadiene) composite latex particles was investigated by TEM analysis [185]. Osmium tetroxide was used to preferentially-stain [185] the poly(styrene-*co*-butadiene) latex particle component. Electron micrographs indicated that composite latex particles consisted of styrene/butadiene copolymer-rich particle cores [185] and hydrophilic copolymer-rich shells. The presence of the first-formed copolymer component at the particle surface [185] lead the authors to classify the particles as being of inverted core-shell morphology. Composite latex particles of EA/styrene/methacrylic acid terpolymer and polystyrene (weight ratio terpolymer:PS of 1:9) were characterised by potentiometric titration [185]. Hydrophilic seed terpolymer molecules were found to not fully invert [185] in the subsequent emulsion polymerisation of styrene - significant quantities of PS were found to be located at the particle surface. A reduction in the molecular weight of hydrophilic terpolymer, or, polystyrene, or, both of the particle components [185], was found to increase the concentration of hydrophilic component at the particle surface. Lee and Ishikawa [185] concluded that the attainment of an inverted core-shell particle morphology was significantly influenced by both the relative hydrophilicities of the two polymer components and by the ability of polymer molecules to kinetically facilitate phase separation via molecular diffusion [185].

Min *et al.* [186] investigated the structure of P*n*BA/PS core-shell composite latex particles (styrene:*n*BA weight ratio of 1:1). Acrylic seed latices were initially

prepared (with potassium persulphate as initiator and sodium dodecyl benzene sulphonate as emulsifier) by emulsion polymerisation of n-butyl acrylate [186]. Composite latex particles were synthesised by polymerisation of styrene in the presence of PnBA seed latex [186]. The influence of the mode of styrene addition on the structure of core-shell composite latex particles [186] was determined from thin layer chromatography-flame ionisation [187, 188] methods, and from transmission electron microscopy analysis. Three composite latices were synthesised, two from batchwise styrene addition and one with continuous addition of second-stage monomer [186]. The two styrene batch addition processes were performed 75 hours before initiation of polymerisation [186], and immediately prior to initiation, respectively. Thin layer chromatography was used to separate composite latex materials into their three constituent components [186], namely; non-grafted PnBA cores, PS grafted to particle cores, and ungrafted PS shells. Grafting between acrylic polymer-rich particle cores and PS-rich particle shells [186] was observed for each of the composite latices synthesised. The extent of grafting was found to be highest for materials prepared from batchwise styrene addition during the second-stage polymerisation [186], with the pre-swollen latex sample having a lower graft copolymer content than the material prepared from conventional, batchwise, addition of monomer.

1.6.4 - LATEX INTERPENETRATING POLYMER NETWORKS (LIPNs)

IPNs can be synthesised by sequential emulsion polymerisation processes [101, 102, 111-120]. Such latex IPNs are synthesised by the addition of monomer to a microgel latex followed by polymerisation of the monomer within, or on the surface of, these first-formed polymer particles. The morphologies of composite latex particles can be influenced by the thermodynamic compatibility of the two polymeric components [172], the relative hydrophilicity of the two polymers [185], the interfacial tensions in the system [177], the mode of the second-stage polymerisation [172, 184] and the viscosity within the polymer particles [179] (section 1.6.3). A period to allow for microgel swelling with monomer is often employed during latex IPN synthetic routes [116, 118, 166]. Second-stage monomers are practically immiscible with the continuous, aqueous, phase of the latex and the monomer initially constitutes a droplet

phase [136] when the latex/monomer system is agitated (as in latex IPN synthesis). Monomer initially migrates from the droplets to the first-formed polymer network particles [166] (in order to minimise the surface free energy of the monomer phase), but these swelling forces are opposed by the interfacial tension [162] between the first-formed polymer and the aqueous phase, and, consequently, a swelling equilibrium is attained [162] (section 1.6.2). The degree of monomer (with crosslinking agent) partitioning within the first-formed gel particles is considered to have a significant influence on the final morphology of the composite network latex particles [116, 118]. The crosslink-density of the original latex gel particle [166], the presence (or absence) of emulsifier [136], the relative mass of monomer added to the latex [112] (compared to the mass of microgel in the system), the water solubility of the second-stage monomer [136], the swelling temperature [166] and the swelling time [116] can all have an influence on the relative amounts of monomer that are found in each of the three potential phases, i.e. the monomer-swollen microgel particles, the aqueous phase, and the monomer droplet phase [166].

Sperling and co-workers [101, 102] first reported the synthesis of latex IPNs in the early 1970s. Their original research [101] concentrated on latex particles derived from poly(alkyl methacrylates) and poly(alkyl acrylates). Films cast from each latex were extensively characterised by dynamic mechanical analysis. A number of poly(ethyl methacrylate), PEMA/P*n*BA latex IPN systems, with different overall compositions, were investigated [101] and several of these materials were found to exhibit only one, broad, glass transition. The mechanical behaviour of such latex IPNs was considered to have been influenced by the micro-heterogeneous phase morphologies of these systems [101]. Detailed investigations into the synthesis and characterisation of poly(vinyl chloride)/poly(butadiene-*co*-acrylonitrile) latex IPNs [102] have also been reported by Sperling and co-workers.

Narkis *et al.* [111] have investigated the morphology of polystyrene/poly(*n*-butyl acrylate), PS/P*n*BA, sequential IPNs by irradiating frozen latex particles with an electron beam. P*n*BA microgels were synthesised by emulsion copolymerisation [111] of *n*BA with ethylene glycol dimethacrylate, EGDMA. A mixture of styrene and divinylbenzene (DVB) was added dropwise to the latex and quasi-emulsion copolymerisation of styrene/DVB was subsequently initiated [111]. Structured latex

particles (IPNs) were synthesised with approximately 65, 75 and 85 weight % P*n*BA contents [111]. The tensile properties of these materials were compared with those of linear, PS/P*n*BA, latex particles (with P*n*BA synthesised both before and after styrene was polymerised) [111]. Elastomers exhibiting superior tensile strengths, when compared to composite linear (P*n*BA/PS) latex particles, were generated when the elastomer was the first-formed network [111]. Polymerisation of *n*BA (with crosslinking agent) in the presence of PS microgel latex particles lead to the formation of composite materials with inferior tensile properties [111], compared with the IPNs where P*n*BA was the first-formed network. Morphologies of two-stage latex particles were evaluated by cold-stage transmission electron microscopy analysis of flocculated, hydrated, latex particle agglomerates [111]. Exposure of polymer specimens to ionising radiation (e.g. a high energy electron beam) can lead to chain-scission (depolymerisation) and/or crosslinking processes [111, 189, 190]. In the case of acrylic polymers (most notably polymethacrylates) the former process predominates [189], whereas in the case of polystyrene, significant degrees of crosslinking are observed [189]. Mixtures of poly(methyl methacrylate), PMMA, and polystyrene latex particles imbedded within an ice matrix were exposed to ionising radiation (high energy electrons) and the observed behaviour of each of the two types of particle was noted as a function of electron-exposure time [190]. Initially, no significant change in the state of the PS particles was observed on irradiation [190]. After longer times of exposure, cavities began to form around the PS particles and these hollows were found to increase in diameter after longer irradiation times [190]. Eventually, after prolonged exposure to the electron beam, a small decrease in the diameter of the particles was observed. The etching of polystyrene and ice was considered to have resulted from the generation of free radicals in each of the two phases [190]. PS tends to crosslink under free radical attack [191], and, hence, PS is rather stable, whereas the ice was found to have degraded more rapidly [190]. When the distance between the ice surface and the PS particles became large enough, it was considered that mutual interactions between free radicals of the two species were diminished, leading to a decrease in the rate of ice degradation, and that each component had then exclusively followed its own radiolytic behaviour [190]. PMMA particles were observed to undergo rapid depolymerisation after short exposure times, affording a cellular appearance to the particles [317]. Additional irradiation caused further

degradation of the PMMA particles and interparticle fusion between neighbouring particles was also observed [189]. PMMA mostly undergoes chain-scission under the influence of free radical attack [190], and this phenomenon was considered to give rise to the significant loss of mass observed for the PMMA latex particles [189]. Free radicals were considered to have originated from both the ice and PMMA phases [189]. Some of the oligomeric MMA radicals, generated from radiation-induced scission of PMMA, were considered to have diffused into ice cavities that had resulted from free radical attack on the ice phase, and repolymerised, thus filling the ice hollows with oligomeric/polymeric MMA [189]. Such processes were postulated to have occurred concurrently, as the absence of cavities in the ice matrix located around each PMMA particle was noted [189] (this behaviour was in marked contrast to the response of the PS particles). This repolymerisation concept was also considered to have lead to the interparticle fusion that was observed between neighbouring PMMA particles [189]. PnBA/PS latex IPNs were also analysed by cold-stage transmission electron microscopy [111]. Analysis of PnBA elastomer determined that PnBA behaved similarly to PMMA latex particles upon exposure to the electron beam [111]. IPN particles that had been synthesised by copolymerisation of styrene/DVB in the presence of PnBA seed latex (weight ratio of polyacrylate:PS of 3:1) behaved similarly to PnBA latex particles when irradiated [111, 189]. This observation was considered to have arisen from the fact that the two (PnBA and PS) components were significantly mixed, which suggested that a PS rich shell, around a PnBA/PS core, was not present [111]. Comparisons between the behaviour of PnBA particles and the PnBA/PS (mass polyacrylate:PS of 3:1) latex particles were made, after identical electron exposures [111]. The PnBA/PS system exhibited signs of lower mass loss, indicating that interpenetration between the two network phases had occurred [111] (the small, crosslinked, PS micro-domains of such materials were considered to have given the particles additional resistance to radiation exposure). It should be noted that an increase in the PS content of the PnBA/PS network latex particles to 50 weight % lead to the generation of a material that behaved similarly to polystyrene particles during irradiation [111, 189]. This observation was considered to have implied that the particles consisted of shells of polystyrene which covered polyacrylate-rich cores [111], i.e. the extent of mixing between the two components was minimised in this instance. PS/PnBA latex particles (i.e. PS was the network first synthesised),

materials that were found to have inferior tensile properties to the PnBA/PS IPNs, were also irradiated and electron exposure observations determined that the particles consisted of polyacrylate shells surrounding PS cores, i.e. significant phase separation was observed [111]. In summary, Narkis *et al.* [111] determined that PnBA/PS IPNs, materials that behaved as reinforced elastomers, could be synthesised from sequential emulsion copolymerisation processes. Significant phase-mixing was only observed for IPNs where the elastomer was the first synthesised network and where the polystyrene content was in the 25 to 35 weight % range [111]. Impact resistant PS derivatives, IPNs containing PnBA micro-domains, were not synthesised [111].

McDonald *et al.* [112] have reported the synthesis of polyacrylate, PA (terpolymers of nBA/styrene/acrylic acid and allyl methacrylate)/polystyrene semi-I grafted latex IPNs (i.e. linear PS was synthesised). Acrylic microgel particles were synthesised initially, with continuous monomer addition, followed by polymerisation of styrene [112]. Semi-I grafted latex IPN samples were characterised by differential scanning calorimetry, transmission electron microscopy (TEM) and high temperature solid-state ^{13}C NMR spectroscopy. Electron micrographs of IPN films indicated that the elastomer constituted the continuous phase of the matrix and separate, polystyrene, phase domains were observed [112]. Increased polyacrylate crosslink-densities were found to lead to a decrease in the PS domain size, from TEM analysis [112]. ^{13}C NMR peak linewidths for the PA's carbonyl group were recorded at intermittent temperatures between the two, component, glass transition temperatures [112] of the grafted IPN (T_g, PA $\approx 0°C$ and T_g, PS $\approx 100°C$). By heating a polymer sample to a temperature above its T_g, sufficient chain mobility can be induced to average the intermolecular dipole-dipole interactions that cause NMR spectral broadening [112]. For composite IPN particle analysis, it is, therefore, possible to examine the spectrum of the low T_g (rubbery) component phase independently from the glassy polymer phase [112]. NMR peak linewidths are influenced by system relaxation processes which occur after nuclear excitation [192]. Low frequency dipolar interactions, e.g. from polymer backbone rotations, are specifically related to the spin-spin relaxation time (T_2) of the process [193]. Detailed information concerning IPN polymer-chain motions in the solid-state, i.e. molecular motions which are influenced by the morphology of a two-phase polymer system [112], is, therefore, available from ^{13}C NMR peak linewidth analysis [112]. Polyacrylate peak linewidths were found to

broaden as the allyl methacrylate content of the elastomer was increased [112]. These observations were considered to have signified an increase in molecular-mixing between the two polymer components, i.e. line-broadening was ascribed to systems with small polystyrene domain sizes, whereby localised polyacrylate segmental motions within the continuous phase had been influenced by increasing degrees of PS dispersion [112]. It would appear that this line-broadening phenomenon could have also been considered in terms of an increase in grafting between the two components, as the concentration of allyl methacrylate increased [194].

Hourston *et al*. synthesised a series of polyacrylate/polymethacrylate latex IPNs [113-116]. Acrylic elastomer was synthesised first, followed by polymerisation of the methacrylate component [113]. Initially, all IPN materials were synthesised without pre-swelling of the seed latex [113, 114] with monomer. Transmission electron microscopy and dynamic mechanical analysis of compression moulded IPN sheets determined that the degree of phase separation in IPN samples was significantly influenced by the degree of compatibility between the two polymer components [113]. Poly(ethyl acrylate), PEA/poly(*t*-butyl acrylate), P*t*BA, IPNs consisted of two discrete phases, with the low T_g component constituting the continuous phase of the matrix [114]. The IPN showed two well-defined glass transitions and no evidence of significant molecular-mixing between the two network components was observed [114]. PEA/poly(ethyl methacrylate), PEMA, IPNs also showed two-phase structures, but slight inward shifting between the first and second network glass transitions, when compared with their individual glass transition temperatures, was observed [114]. The glass transitional behaviour of the PEA/PEMA system was considered to have arisen from a degree of phase-mixing between the two network components at the molecular level [115]. Additionally, certain PEA microgel latices were swollen (25°C) with either *t*-butyl acrylate (with crosslinker) or ethyl methacrylate (with crosslinker) over 0, 15, 30, 60, 120 and 240 hour swelling times, before initiation of the second-stage copolymerisation [116]. Both PEA/P*t*BA and PEA/PEMA latex IPNs showed increased degrees of mixing between the two network components with increased swelling time, with each material showing two distinct glass transitions [115, 116].

The gas permeability of PEA/PEMA and PEMA/PEA latex IPN films has been reported by Holdsworth and Hourston [117]. Three latex systems were investigated, a PEA/PEMA latex IPN was prepared with the poly(ethyl acrylate) component synthesised initially and the inverse system, a PEMA/PEA latex IPN, was also synthesised from sequential emulsion copolymerisation with tetraethylene glycol dimethacrylate as the crosslinking agent for each system [117]. A latex blend of crosslinked PEA with crosslinked PEMA was also prepared and the weight ratio of the two polymer components was 1:1 for all three systems. Phase-separated materials were synthesised, as determined from dynamic mechanical analysis, and two distinct glass transitions were observed for each of the materials [117]. A degree of mixing, determined from slight inward shifting between the glass transitions of the material when compared with the T_g's of the constituent networks, was observed for all three materials, with the PEMA/PEA latex IPN showing the greatest, and the latex blend showing the lowest, degree of phase-mixing between the two components [117]. The sorption and transport of gases in polymer blends has been used to assess the ability of polymer blend membranes to separate mixtures of gases [195, 196] and gases have also been used as probes to investigate the phase morphology of polymer blends [197, 198]. Permeability coefficients [199] for the three types of membrane were evaluated with CO_2, He, O_2, Ar and N_2 as permeants over a 30°C to 50°C temperature range [117]. The permeabilities for all gases were found to be lowest in the blend membranes and highest in the PEMA/PEA IPN membranes and the gas permeability behaviour was considered to have been significantly influenced by the relative size of the blend phase domains [117].

Liucheng et al. [118] synthesised three-stage latex IPNs of crosslinked PnBA with crosslinked polystyrene and linear poly(methyl methacrylate). An acrylic elastomer seed latex was synthesised initially (nBA copolymerised with ethylene glycol dimethacrylate), followed by copolymerisation of styrene/DVB, and PMMA was the last component to be synthesised [118]. Two distinct glass transitions, corresponding to crosslinked PnBA and PS/PMMA, were observed from dynamic mechanical analysis [118]. The influence of polymerisation initiator on the morphology of the three-stage latex particles was investigated [118]. For the acrylic seed latex preparation, potassium persulphate (KPS) was used as the free radical initiator [118]. Both 2,2'-azobisisobutyronitrile (AIBN) and KPS were investigated as initiators for

second- and third-stage polymerisation processes [118]. Latex IPNs synthesised with AIBN as the initiator in the second and third stages were found to have inverted core-shell morphologies [118], as determined from transmission electron microscopy analysis, with the PS component forming a core which was surrounded by a shell of PnBA and PMMA [118]. These morphologies were attributed to the hydrophobic nature of styrene and AIBN [118]. Materials which were synthesised with persulphate initiator for all three of the polymerisation stages were considered to be of core-shell type morphology [118], where a polystyrene shell component surrounded a PnBA/PMMA core. Surface-anchoring of hydrophilic sulphate fragments from initiator decomposition [145] was considered to have influenced the morphology of these three-stage polymer latex particles [118]. The influence of network crosslink-density, the method of monomer addition (batch or dropwise) during the polymerisation and the polymerisation temperature on the morphology of latex IPNs was also investigated [118]. Each of the materials synthesised exhibited, in general terms, macroscopic phase separation [118], although the extent of phase separation was controlled to a degree by a change in the rate of the polymerisation process [118].

1.7.1 - CROSSLINKED POLYMER MICROSPHERE SYNTHESIS

In addition to macrogel synthesis (section 1.2), polymer networks can be synthesised as discrete, intramolecularly-crosslinked, polymer particles of micron-sized dimensions. Polymer network particles with average diameters of less than 10-20 μm are conventionally classified [200] as crosslinked polymer microspheres. Such network polymer particles are readily synthesised via emulsion [201-204], non-aqueous dispersion (NAD) [205-211], and suspension [212, 213], free radical copolymerisation techniques. In general terms, crosslinked particles prepared from these polymerisation methods differ markedly in terms of particle dimensions. Polymer microspheres prepared from suspension polymerisation techniques typically have 20-50 μm diameters [212], whereas crosslinked polymer particles synthesised from NAD polymerisation techniques often have sizes in the 1-5 μm range [205-208]. Polymer latices recovered from emulsion polymerisation processes typically have particle sizes of the order of 0.1-0.5 μm [201]. Polymer microspheres with

approximately 1-50 μm average particle sizes [210-213] differ from their sub-micron-sized counterparts in that they can not, in general terms, be colloidally-dispersed in organic diluents which are solvents for their linear polymer analogues [214]. Microgels, intramolecularly-crosslinked polymer particles of sub-micron (ca. 0.05-0.25 μm) dimensions [44, 47], are a unique class of polymer networks which have the capacity to be dispersed in organic diluents (sections 1.2 and 1.7.2).

The synthesis of microgels was first described by Staudinger and Husemann [215] during their investigations into the free radical copolymerisation of styrene/divinylbenzene. Soluble polymeric products (microgels) were recovered from styrene/DVB copolymerisations in organic media at divinylbenzene concentrations of less than 8 volume % [215], whereas macro-gelation was observed for systems with increased DVB concentrations [215] (section 1.2). Emulsion copolymerisation of monovinyl/divinyl comonomers has been often considered, in more recent times, to be the most convenient method [201-204] for the synthesis of polymer microgels in high yield. Ding *et al*. [202] utilised soap-free emulsion copolymerisation processes for the synthesis of monodisperse poly(styrene-*co*-divinylbenzene) particles. Several emulsion copolymerisations of styrene/DVB were performed [202] - with the employment of both batchwise and continuous comonomer addition methods. Copolymer conversions were recorded as a function of copolymerisation time [202] by initial removal of aliquots from the reaction vessel at set intervals, followed by gravimetric analysis [202]. Dry copolymer particles recovered from reaction conversion investigations [202] were characterised by differential scanning calorimetry and by an ultrafiltration membrane [216] technique. Batch copolymerisations of styrene/DVB [202] yielded heterogeneously crosslinked copolymer particles. Latex particles were found to have higher crosslink-densities during the early stages of the copolymerisation [202] when compared to crosslink-densities of the final microgel particles. Variation in the network structure of copolymer latex particles was attributed to the preferential consumption of divinylbenzene during the early stages of the reaction [202], leading to a drift in copolymer composition with conversion (section 1.5). The incremental addition of styrene/DVB throughout the emulsion copolymerisation process [202] generated uniformly-crosslinked, monodisperse, poly(styrene-*co*-divinylbenzene) latex particles.

Forget *et al.* [203] synthesised poly(styrene-*co*-divinylbenzene) microgels via a conventional emulsion copolymerisation process (the copolymer particles were generated in the presence of emulsifier). Microgel particles were characterised by gel permeation chromatography (GPC) and dynamic light scattering techniques [203]. The GPC elution behaviour of microgel samples (copolymer particles prepared with 0.10-0.25 mole % DVB contents) [203] was found to significantly differ from the separational-behaviour of dilute polystyrene homopolymer solutions. Comparisons between linear polystyrene and PS microgel separations by GPC were made [203], and the microgel samples were found to have been contaminated with linear polystyrene molecules to an insignificant extent (i.e. copolymer particles were found to, almost exclusively, consist of gel structures). In addition to reports concerning microgel synthesis from conventional emulsion copolymerisation techniques [201-204], Antonietti *et al.* [217] have discussed the synthesis of PS microgel dispersions via free radical microemulsion copolymerisation of styrene/*m*-diisopropenylbenzene.

As briefly mentioned in the previous text, micron-sized crosslinked polymer particles can also be synthesised by non-aqueous dispersion (NAD) polymerisation techniques [205-211]. NAD polymerisations involve the synthesis of a polymer in an organic medium which is a non-solvent for the material [218-219]. In a typical NAD polymerisation process, monomer, stabiliser, organic diluent and free radical initiator form an initially homogeneous solution [219]. On initiation of polymerisation, soluble oligomeric free radicals are generated in solution [219], the free radicals subsequently propagate until they reach a critical chain length, whereby they precipitate from solution, forming nuclei which associate with stabiliser molecules and become stabilised against flocculation [219]. In the early stages of polymerisation the generation of primary particles by homogeneous nucleation [219] may be followed by a rapid decrease in particle number due to aggregation [219]. This causes a decrease in the rate of oligomer consumption by existing particles and renucleation occurs [219], thus leading to the formation of a fresh set of propagating polymer particles. Monomer is subsequently adsorbed from solution by the disperse phase [219] and polymerisation occurs almost exclusively within the growing particles. Stabilisers for NAD polymerisation processes are commonly graft or block copolymers [219, 220], where one of the copolymer's components has an affinity for

the growing polymer and the second component has a high compatibility with the organic diluent [219] (i.e. the polymerisation medium must be a good solvent for at least one of the stabiliser's polymeric components). Adsorption of stabiliser at the polymer particle surface provides colloidal stability for the system [219] - the particles are sterically stabilised [219]. Ober and Lok [205, 206] synthesised monodisperse PS particles by free radical polymerisation of styrene in homogeneous ethanol/water mixtures (with polyacrylic acid as stabiliser). Incorporation of DVB at 0.5 weight % concentrations [205], or less, was found to generate monodisperse crosslinked particle dispersions. At higher (> 0.7 weight % DVB) difunctional comonomer contents, only heterogeneous particle structures could be synthesised - suggesting that intermolecular surface crosslinking between neighbouring particles had occurred [205]. Monodisperse PS particles with high crosslink-densities were subsequently prepared [206] by the addition of ethylenediamine to styrene/glycidyl acrylate copolymer particle dispersions [206]. Tseng *et al.* [207] successfully incorporated 0.3 weight % DVB during copolymerisations of styrene/DVB in ethanol [207]. At DVB contents of 0.6 weight %, or higher [207], particles of heterogeneous structure were synthesised [207]. Monodisperse crosslinked PS particles with 1 weight % divinylbenzene contents were also synthesised [207] - by the addition of small amounts of a compatible co-diluent (an organic liquid which was a solvent for linear polystyrene) to the initial polymerisation charge [207]. Thomson *et al.* [208] synthesised monodisperse, uniformly crosslinked, poly(styrene-*co*-divinylbenzene) particle dispersions in ethanol by NAD polymerisation with poly(N-vinyl-2-pyrrolidone) as stabiliser. Incorporation of DVB at 0.5 weight % concentration (i.e. 99.5 weight % styrene:0.5 weight % DVB) [208] was found to lead to the generation of polydisperse particle size distributions [208]. Monodisperse, uniformly crosslinked, PS microspheres with 1 weight % DVB content were synthesised from a series of continuous divinylbenzene addition experiments [208]. A fixed amount of crosslinker (0.2 weight % DVB) was initially charged to the reaction vessel, along with styrene, free radical initiator, stabiliser and ethanol [208]. After initiation of polymerisation, the system was left for one hour [208] and a DVB (the remaining 0.8 weight % DVB) solution in ethanol was added dropwise to the dispersion over five to nine hour periods (corresponding to DVB delivery rates of approximately 0.1 - 0.2 g/hour) [208]. Li and Stoever [209] synthesised highly crosslinked monodisperse polymer

59

microspheres by dispersion polymerisation of divinylbenzene (DVB of 55 weight % purity, remainder mainly p-ethylvinylbenzene) [209]. Crosslinked particle dispersions in ethanol and acetonitrile [209] were prepared in the presence of poly(N-vinyl-2-pyrrolidone) stabiliser. Monodisperse polymer particles were synthesised from homopolymerisation of divinylbenzene and homopolymerisation of p-methylstyrene [209]. Dilution of DVB with p-methylstyrene, giving effective DVB contents of 5 to 50 weight % [209], was found to exclusively generate coagulum [209]. Li and Stoever [210] also synthesised highly crosslinked monodisperse polymer microspheres by precipitation polymerisation of commercial grade divinylbenzene [210] in acetonitrile. Crosslinked particle dispersions were prepared in the absence of polymeric stabiliser [210] at 2-5 volume % DVB concentrations. A further increase in difunctional monomer concentration was found to generate coagulum only [210]. Li and Stoever [210] postulated that their dilute, stabiliser-free, dispersions of polydivinylbenzene were colloidally stable, as particle aggregation had been prevented by the highly crosslinked, rigid, nature of the particle surfaces [210]. Okubo *et al.* [211, 221-223] have published several reports concerning the synthesis of monodisperse crosslinked polystyrene microspheres. The synthesis of polymer network particles was performed by the utilisation of a two-step experimental procedure [211, 221]. Initially, monodisperse PS microsphere dispersions were synthesised by poly(acrylic acid)-stabilised NAD polymerisation [211] of styrene in ethanol/water mixtures. Styrene, DVB, benzoyl peroxide and poly(vinyl alcohol) were then added to a seed particle dispersion [221-223], followed by dropwise addition of water. Okubo *et al.* [222] determined that the utilisation of optimum rates of water addition (to polymer microsphere dispersions in ethanol [211]) enabled uniformly monomer-swollen polystyrene particle dispersions to be prepared [221]. Rapid addition of water [221] was found to generate mixtures containing both monomer-swollen polymer microspheres and a monomer droplet phase [221]. Okubo *et al.* [360] observed that the process for adsorption of styrene monomer by seed polymer particles was primarily influenced by the separation of monomer from the alcoholic medium, on addition of water [221, 222]. Dynamic swelling [221] of PS microsphere dispersions with divinylbenzene was investigated [221, 222] and structured polymer particles were subsequently synthesised from free radical polymerisation [221-223]. Experimental products [222] were found to consist

primarily of polystyrene/polydivinylbenzene, PS/PDVB, composite particles, with a low concentration (ca. 10 weight % of total polymer content) of small-sized PDVB particles [222]. Polydivinylbenzene contaminant was removed from composite PS/PDVB particle dispersions by high-speed centrifugation [222]. Bromine titration of monodisperse, structured PS/PDVB particle dispersions determined that residual, polymer-bound, vinyl groups were present at the surface of composite particles [222].

Cheng *et al.* [224] synthesised monodisperse composite polystyrene/poly(styrene-*co*-divinylbenzene) microspheres via seeded emulsion polymerisation techniques. Monodisperse PS latices (170 nm average particle diameter) were initially prepared [224] by emulsion polymerisation of styrene, with Aerosol MA (dihexylester of sodium sulphosuccinic acid) emulsification and with potassium persulphate thermolysis for initiation. A monodisperse PS dispersion with 3 μm average particle diameter was also prepared [224] by dispersion polymerisation of styrene in ethanol, with poly(N-vinyl-2-pyrrolidone) as stabiliser and 4,4'-azobis(4-cyanovaleric acid) as free radical initiator. Dispersions of polystyrene particles in ethanol were subsequently converted to aqueous dispersions via distillation [224]. Large particle size (ca. 10 μm diameter) monodisperse composite polystyrene/poly(styrene-*co*-divinylbenzene) latex particles were synthesised via successive seeded emulsion polymerisation of styrene/DVB [224] in the presence of PS microsphere aqueous dispersions. Inert organic diluent was added [224], along with styrene, DVB and free radical initiator [224], to seed latices, prior to initiation of second-stage copolymerisations. Structured polymer microsphere aqueous dispersions were subsequently flocculated [224] and the recovered polystyrene-based composite particles were dried under vacuum. Soxhlet extraction of structured polystyrene/poly(styrene-*co*-divinylbenzene) particles with methylene chloride was then performed [224] - in order to remove soluble polystyrene components from the composite particles. Solvent-treated structured polystyrene microspheres [224] were found to exhibit macroporous behaviour, as determined from scanning electron microscopy, nitrogen adsorption and mercury intrusion porosimetry analysis [224].

1.7.2 - ORGANIC MICROGEL DISPERSIONS

The incorporation of microgel particles within surface coating formulations can yield organic dispersions which exhibit certain superior physical properties [225, 226], when compared to equivalent non-microgel incorporated formulations. The viscometric behaviour of organic microgel dispersions has been widely reported [41, 203, 217, 227, 228], as microgels have been found to significantly influence the rheological characteristics of organic coating formulations [225]. The viscosity behaviour of a microgel dispersion is critically dependent upon the particle crosslink-density [41, 227] and upon the concentration of polymeric solids in the system [227]. Einstein [229-231] derived a theoretical relation for equating the absolute viscosity, η (Pa s), and the volume fraction of particles, ϕ, for an idealised dispersion of hard spheres [229-231]:

$$\eta = \eta_0(1 + 2.5\phi + 4\phi^2 + 5.5\phi^3 + \ldots)$$ (1.42)

where η_0 is the viscosity of the pure diluent (Pa s).

Antonietti and Rosenauer [41], Shashoua and Beaman [227], Forget *et al.* [203], Rodriguez *et al.* [228] and Antonietti, Bremser and Schmidt [217] have characterised organic polystyrene microgel dispersions by dilute solution viscometry. Provided that the flow of a fluid through a capillary is streamlined and lamellar [58], the ratio of the flow-time measured for a dilute solution, t (s), to the flow-time recorded for pure organic diluent, t_0 (s), can be used to determine the viscosity ratio (the relative viscosity, η_{rel}) for the two systems [11]:

$$t / t_0 = \eta_{rel} = \eta / \eta_0$$ (1.43)

The specific viscosity, η_{sp}, can then be evaluated from [11]:

$$\eta_{sp} = (\eta_{rel} - 1)$$ (1.44)

The reduced viscosity, η_{red}, of a polymer solution [11] is defined as:

$$\eta_{red} = (\eta_{sp}/c) \tag{1.45}$$

where c is the solution concentration (g cm^{-3}).

The intrinsic viscosity, $[\eta]$ (cm^3 g^{-1}), is determined from extrapolation of reduced viscosity (η_{red}) curves to infinite dilution [11] (i.e. as $c \to 0$):

$$[\eta] = (\eta_{sp}/c)_{c=0} \tag{1.46}$$

For infinitely crosslinked microgel particles [227], the intrinsic viscosity of organic microgel dispersions would be expected to approach a minimum value [227], the intrinsic viscosity predicted by Einstein [229-231] for dispersions of hard spheres:

$$[\eta] = 2.5/\rho \tag{1.47}$$

where ρ is the solid-state density (g cm^{-3}) of the polymer. (For infinitely crosslinked PS microgels, an intrinsic viscosity of 2.40 cm^3 g^{-1} would be anticipated from theory [227]).

Shashoua and Beaman [227] synthesised a series of poly(styrene-*co*-divinylbenzene) microgels (with divinylbenzene contents varying between 0.10 and 5 mole % DVB on total comonomers) from emulsion copolymerisation processes. Intrinsic viscosities of microgel dispersions were recorded in benzene [227] and $[\eta]$ values were plotted as a function of x^{-1}, where x was the mole fraction of crosslinking agent. A straight line graph, with an intercept of approximately 2.2 cm^3 g^{-1}, was obtained [227] from dilute solution viscometry analysis, indicating that infinitely crosslinked dilute microgel systems should follow Einstein's viscosity relation for dispersions of hard spheres [227]. Antonietti, Bremser and Schmidt [217] and Shashoua and Beaman [227] determined particle sizes of microgel samples in aqueous latices and organic diluents. The ratio of the cubes of particle diameters in water and organic liquid were expressed as a swelling ratio, Q [217, 227] (the volume of the swollen microgel particles divided

by the bulk volume of the microgel). Intrinsic viscosities of microgel dispersions were found to be related to the swelling ratio and polymer bulk-density [217, 227] by:

$$[\eta] = \left(\frac{2.5}{\rho}\right) Q \qquad (1.48)$$

These experimental observations indicated that swelling ratio, Q, for moderately crosslinked microgel particles [217, 227], could be simply estimated from viscometric analysis of dilute microgel dispersions [217, 227]. Shashoua and Beaman [227] comprehensively investigated the rheological behaviour of organic gel particle dispersions as a function of microgel concentration. Absolute microgel dispersion viscosities [227] were found to increase linearly, to a slight extent [227], as microgel concentrations increased from approximately 1 to 5 weight % solids. Low viscosity dispersion behaviour was followed by a sudden transition to high viscosity [227]. The transition was classified in terms of a solution gel point [227], G (g cm^{-3}) - the concentration of solids required to hold all of the dispersant molecules within liquid-swollen microgel particles [227]. Idealised absolute viscosity, η (centipoise, cP), against dispersion solid content, C (weight % microgel), curves [227] are illustrated in figure 1.7. Comparisons between dispersion viscosities for microgel particles synthesised with different crosslinker concentrations [227], indicated that microgels with the highest crosslink-densities showed the highest solution gel points. Shashoua and Beaman [227] also observed that solution gel points recorded for microgel systems of a given crosslink-density were dependent upon the solubility parameter difference between the polymer and organic dispersent [227]. The influence of microgel crosslink-density and the degree of compatibility (solubility parameter-difference) upon solution gel points [227] was considered in terms of macrogel swelling characteristics. For a series of microgel particles with different crosslink-densities, microgels with highly dense network structures would be anticipated to be swollen with a given diluent to the lowest degree (the Flory-Rehner [167] approach for swelling of macrogels) - if microgels are assumed to have similar swelling characteristics to macrogel samples. At a given (microgel dispersion) solids concentration, highly crosslinked microgel particles would have a lower volume fraction of dispersent swelling them, as compared to systems containing swollen microgel particles with loose network structures. The weight fraction of microgel

required to begin to occupy the whole volume of dispersant [227] would, therefore, be correspondingly higher for highly crosslinked microgel particle dispersions (as was observed experimentally [227]). Similarly, maximum swelling of macrogel samples, of a given crosslink-density, is often observed when the solubility parameter (δ) of the organic diluent is equal to the δ value of the polymer network [232]. Microgel particles, of a given crosslink-density, dispersed in "low-swelling" liquids would, therefore, be expected to occupy a smaller volume fraction of dispersant [227], compared to their corresponding "high-swelling" organic diluent systems [227, 232].

Figure 1.7 - Viscosity (η) with Microgel Concentration (C) Curves [227]
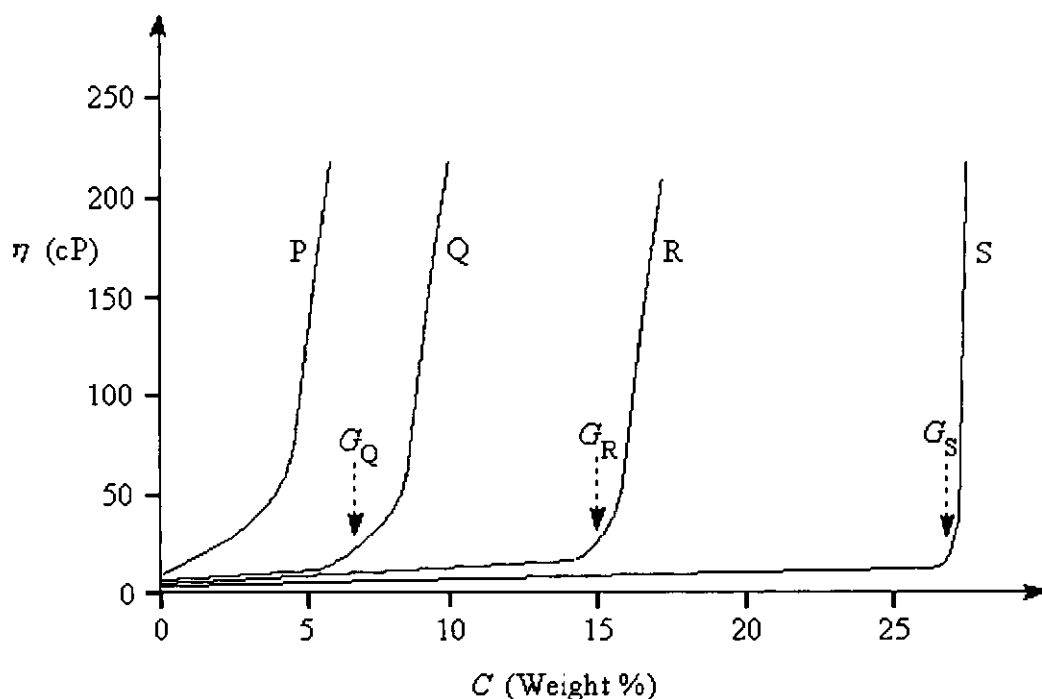
P - Linear Polymer   R - Microgel of Intermediate Crosslink-Density
Q - Lightly Crosslinked Microgel   S - Highly Crosslinked Microgel

Shashoua and Beaman [227] derived an equation to allow for a prediction of the relationship between the solution gel point, G (g cm^{-3}), and the microgel swelling ratio, Q [227] (equation 1.48). It was noted [227] that the term GQ/ρ would define the fraction of the system's total volume which was occupied by swollen microgel particles, at the solution gel point [227]. With the assumption that G would represent the condition where there was hexagonal close packing between swollen spherical

particles [227], it was predicted that solution gel points would be related to swelling ratios [227], from:

$$G = \left(\frac{\pi}{3\sqrt{2}}\right)\frac{\rho}{Q} \qquad (1.49)$$

where ρ is the solid-state density of the polymer (g cm^{-3}).

A comparison between equations 1.47 and 1.49 [227] predicts [227] that G would be related to the intrinsic viscosity, $[\eta]$ (cm^3 g^{-1}), by:

$$G = \left(\frac{2.5\pi}{3\sqrt{2}}\right)\frac{1}{[\eta]} \qquad (1.50)$$

The validity of equation 1.50 was tested [227] by recording G values for microgel dispersions and calculating the theoretical $[\eta]$ term [227]. Intrinsic viscosities predicted from theory (equation 1.50) were compared with values determined from viscometric analysis [227] and a high correlation between the calculated and experimentally-recorded values was observed [227].

Rodriguez and Kaler [233] have investigated the rheological characteristics of monodisperse polystyrene gel particle dispersions in bromoform. The shear viscosity, η (cP), of microgel dispersions (20°C), determined from rotational viscometry analysis [233], was studied as a function of the applied shear stress, τ (Pa), and as a function of microgel concentration, c (g cm^{-3}) [233]. Typical viscosity against shear stress curves determined by Rodriguez and Kaler [233] from viscometric analysis of organic PS microgel dispersions [233] are illustrated in figure 1.8. Rodriguez and Kaler [233] noted that the flow characteristics of their organic microgel dispersions typically followed the viscosity behaviour found in concentrated colloidal dispersions [233]. Newtonian flow was observed in the low shear stress region, whereas, shear-thinning behaviour was followed over an intermediate shear stress range, and Newtonian flow was observed at high shear stresses [233] (as illustrated by curve A in figure 1.8). These organic microgel dispersions [228, 233] (with high particle crosslink-densities) were considered, therefore, to have behaved like model dispersions of hard spheres [233]. Buscall [234, 235] has developed an effective model of the non-Newtonian viscosity characteristics of concentrated microgel

dispersions [234]. This theory has been found to predict satisfactorily [234] the relation between dispersion viscosity and microgel concentration, along with the relation between the viscosity and the applied shear stress [235].

Figure 1.8 - Generalised $\log_{10}\eta$ against $\log_{10}\tau$ Plots Recorded from Rotational Viscometry Analysis [233] of Microgel Dispersions.
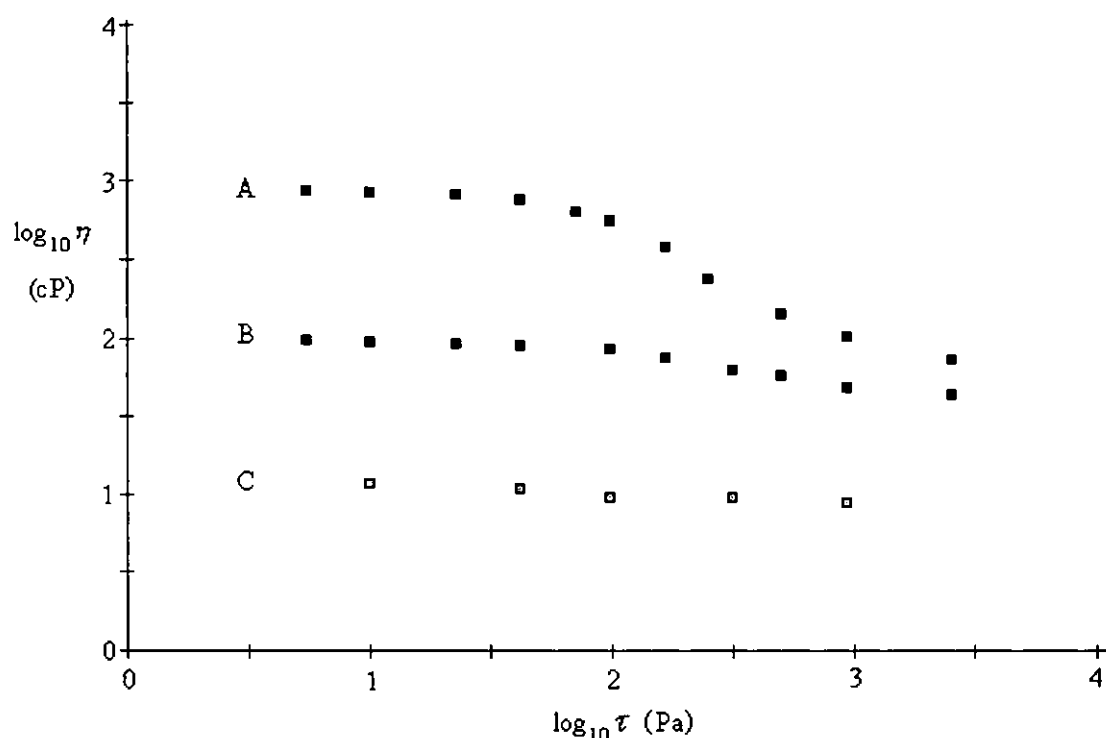
where dispersion A had a microgel concentration of 0.22 g cm^{-3}, system B had a concentration of 0.20 g cm^{-3} and dispersion C had a concentration of 0.14 g cm^{-3} [233].

1.8 - POLYMER-BOUND FREE RADICAL INITIATORS

PS network swelling by monomer/organic liquid mixtures and monomer solubility investigations, performed during this project, evaluated that PS microgel particles dispersed in organic liquid/monomer mixtures could not be exclusively swollen with monomer. These studies predicted that significant quantities of monomer would be present in the continuous phase (a homogeneous organic liquid/monomer/crosslinking agent mixture). Employment of a conventional, continuum-soluble, free radical (FR) initiator for the second-stage polymerisation would not, therefore, have lead to the

generation of IPN microgel dispersions, as acrylic macrogel synthesis would have also occurred. Consequently, it was decided that polymer-bound FR initiator functionalised PS microgel particles should be synthesised. A number of reports [236-246] into the synthesis of polymer-bound free radical initiators, for the preparation of both block and graft copolymers, have been published in the scientific literature. The synthesis of polyesters and polyamides containing main-chain azo linkages from polycondensations of 4,4'-azobis(4-cyanovaleryl chloride), ACVC, with diols [237-240] and diamines [241, 242], has been extensively investigated. Nagai and Ueda synthesised a number of polyamides containing azo linkages [241, 242] by interfacial polycondensation between sebacoyl chloride and hexamethylenediamine in the presence of small quantities of ACVC (mole fraction ACVC, m_{AC}, in copolymer, $0.01 \leq m_{AC} \leq 0.05$). Solutions of these azo-containing polyamides in m-cresol were thermally-decomposed in the presence of styrene [241]. A variety of poly(amide-b-styrene) block copolymers were generated by variation of the polyamide azo content, the molecular weight of the polyamide and the concentration of styrene for the solution copolymerisation [241].

Considerable research interest has also been shown in the synthesis of azo-containing poly(ethylene glycol), PEG, derivatives [237-2400]. Nagai and Ueda synthesised azo-functionalised PEGs from polycondensation of di-hydroxy terminated PEG precursors ($M_n \approx 10,000$ g mol^{-1}) with ACVC [237]. Solutions of polyazoesters in benzene were thermally decomposed in the presence of styrene [237]. A number of poly(PEG-b-styrene) block copolymers were generated by variation of the molecular weight of the PEG precursor and the concentration of styrene for the solution copolymerisation [237]. Hazer synthesised polyazoesters [238] from polycondensations of di-hydroxy terminated PEG precursors with either ACVC or 2,2'-azobisisobutyronitrile, AIBN (via Pinner synthesis) [238]. Azo-macromers [238] were also synthesised by end-capping polyazoesters with methacryloyl chloride. Polyazoester and azo-macromer solutions in chloroform were prepared [238], and polybutadiene, PBD ($M_w = 500,000$ g mol^{-1}), was introduced. Polymer films cast from solution were then heated at 90°C. Grafting reactions of PBD with polyazoesters and azo-macromers yielded PEG/PBD networks. Styrene/PEG block copolymers were also synthesised [238] by bulk copolymerisation of polyazoesters with styrene [238]. Dicke and Heitz synthesised polyazoesters [239] from

tetraethylene glycol and AIBN via a Pinner synthesis. Partial thermal decomposition of the polyazoester was performed in the presence of acrylamide and t-butyl alcohol [239]. Acrylamide/azoester, ACAE, block copolymers ($M_n \approx 200,000$ g mol^{-1}) were recovered and surface tension measurements of copolymer solutions in water [239] determined that the macroinitiators exhibited micellular behaviour, at certain ACAE concentrations. Emulsion polymerisation of vinyl acetate with ACAE emulsifying-initiators generated colloidally-stable poly(vinyl acetate) latices [239].

The synthesis of copolymers containing pendant free radical initiator groups from vinyl, polyaddition, copolymerisation techniques [243-246] has been reported to a lesser extent than the synthesis of main-chain initiator-functionalised copolymers from polycondensation reactions [236-242]. Ajayaghosh synthesised S-acryloyl O-ethyl xanthate, AX (figure 1.9), copolymers with methyl methacrylate (MMA) by AIBN-initiated solution copolymerisation in benzene [243]. Such, AX/MMA, macroinitiators (containing pendant xanthate chromophores) were dissolved in benzene and photolysed in the presence of MMA [243]. Poly(methyl methacrylate) was recovered ($M_n = 40,000$ g mol^{-1}) in 12 weight % yield after 30 minutes of irradiation (wavelength 350 nm). Increasing the photopolymerisation time led to the formation of small quantities of crosslinked AX/MMA copolymer [243]. The rate of MMA polymerisation in benzene was evaluated with both AX/MMA copolymer and S-acetyl O-ethyl xanthate photoinitiators [243]. Rates of MMA polymerisation with macroinitiation were significantly greater than the rates with S-acetyl O-ethyl xanthate initiation [243]. The increase in polymerisation rate for the macroinitiator system was found to result from a reduction in the number of primary radical recombinations, as compared with S-acetyl O-ethyl xanthate-initiated polymerisation [243].

Figure 1.9 - Illustration of the Structure of S-Acryloyl O-Ethyl Xanthate
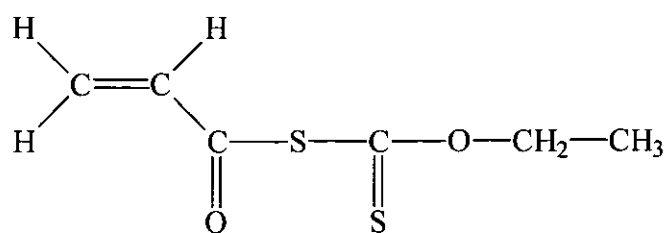
Nuyken and Weidner synthesised *m*-azo-derivatives of styrene (figure 1.10) and these azo-monomers were used for the preparation of pendant azo-functionalised styrene/butadiene latex particles [244, 245]. Substitution of styrene at the meta position ensured that the free radical reactivity of the vinyl bond was not reduced, as evaluated by ^{13}C NMR analysis of styrene and the three *m*-azo-substituted styrenes [245]. Redox emulsion terpolymerisations of styrene/butadiene/*m*-azo-styrene were performed and azo-monomers were incorporated into styrene/butadiene latex particles [244, 245]. The diphenyl derivative (compound 3, figure 1.10) was the only azo-monomer that polymerised ideally (i.e. it did not inhibit polymerisation and generate latex particles in low yield) [245]. A reaction between propagating polymer radicals and azo bonds, leading to the generation of stable, hydrazyl, radicals was considered not to have occurred, to a significant extent, with compound 3 [245]. This phenomenon was attributed to steric hindrance of the β-nitrogen, leading to the less-facile attack of polymer radicals on to azo bonds [245]. Thermal analysis evaluated that the substituent groups of the azo-functionality significantly influenced the decomposition temperature of the azo bonds [245] in styrene/butadiene samples (compound 3 had a temperature giving a ten hour decomposition half-life, $t_{1/2}$ T_{10h}, of 107°C, whereas the $t_{1/2}$ T_{10h} value was 217°C for compound 1). Thermolysis, or photolysis, of azo-functionalised styrene/butadiene latex particles lead to crosslinking of the materials via interactions between free radicals and unsaturated bonds within the terpolymer samples [245].

Figure 1.10 - Illustration of the Structure of *m*-Azo-Styrene Derivatives

Compound	R_1	R_2
1	CH_3	CH_3
2	CH_3	C_6H_5
3	C_6H_5	C_6H_5
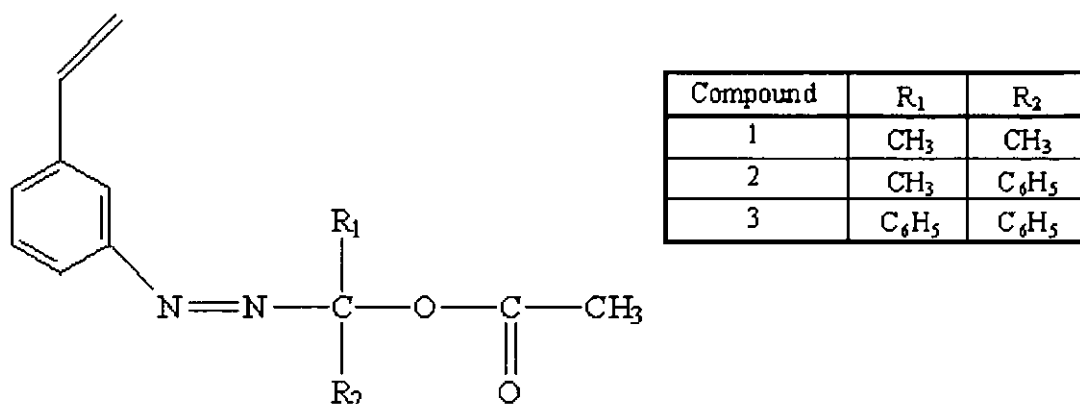
Yamamoto *et al.* [246] synthesised *t*-butylperoxy-2-methacryloyloxyethyl carbonate (PMEC), *t*-butylperoxyisopropyl fumarate (PFPO) and *t*-butylperoxyallyl carbonate (ALPO) peroxide monomers. These peroxides were used to synthesise vinyl graft copolymers [246]. All three materials are commercial products of the NOF Corporation. ALPO and PMEC, along with di-*t*-butylperoxy fumarate (DBPF), were employed in this project as polymer-bound free radical initiators. Detailed descriptions of peroxide monomer synthesis [246] and the copolymerisation behaviour of each peroxide with styrene are discussed in section 2.7 and chapter 7.

CHAPTER 2

EXPERIMENTAL

2.1.1 - REAGENTS USED FOR POLYMERISATION PROCESSES

Polystyrene and poly(n-butyl acrylate) microgels were synthesised by emulsion copolymerisation processes (sections 2.2.1 and 2.3.1, respectively). The corresponding macrogels were synthesised by bulk copolymerisation (sections 2.5.1 and 2.6.1, respectively). The polymerisation reagents are listed below in table 2.1.

Table 2.1 - Polymerisation Reagents

Reagent	Abbreviation	Purity[■]	Additive	Supplier
Styrene		99	15 ppm [†] TBC [‡]	Aldrich
n-Butyl acrylate	nBA	99	50 ppm MEHQ *	Aldrich
Divinylbenzene	DVB	55	1500 ppm TBC	Aldrich
Ethylene glycol dimethacrylate	EGDMA	98	100 ppm MEHQ	Aldrich
Neopentyl glycol diacrylate	NPGDA	95		Aldrich
Sodium lauryl sulphate	SLS	98		Aldrich
Ammonium persulphate	APS	98		Aldrich
2,2'-Azobisisobutyronitrile	AIBN	98		BDH
4,4'-Azobis(4-cyanovaleric acid)	ACVA	75	Water (25 weight %)	Aldrich

[■] Purity (weight %), stated by commercial supplier.

[†] Parts per million.

[‡] p-t-Butylcatechol.

* Hydroquinone monomethyl ether.

All materials were used without further purification, with the exception of styrene and divinylbenzene. These two monomers were each destabilised by washing five times with dilute (10 weight %) sodium hydroxide solution. The destabilised materials were then washed four times with deionised water. Monomers were recovered via

separation and dried over molecular sieve (4Å). The destabilised materials were stored in a refrigerator (5°C) prior to use.

An Elgastat Option 4 purification system was used for the preparation of deionised water for each of the emulsion polymerisations. The water conductivity, κ (S cm^{-1}), was measured by a Jenway (Model 4010) conductivity meter in order to ensure that water of $\kappa \leq 10$ μS cm^{-1} (25°C) was used for each polymerisation.

2.1.2 - VESSELS USED FOR POLYMERISATION PROCESSES

Emulsion polymerisations were performed in a 700 cm^3 straight-walled glass kettle fitted with a five port flange lid (figure 2.1). The joints of the kettle and lid were smeared with silicone oil before the two items were clamped together with a metal clip, thus ensuring that the system was air-tight. The polymerisation vessel was placed in a thermostatically-controlled paraffin oil bath, controllable to within ± 0.5°C. The central port of the lid housed a four-bladed (stainless steel) stirrer which was driven by a variable speed mechanical motor (controllable to within ± 2 rpm). The other (four) ports of the lid were fitted with:

(I)   An inlet for the monomer and emulsifier feeds.

(II)   A water (coil-type) condenser.

(III)   A thermocouple linked to a digital (temperature) display unit.

(IV)   A nitrogen inlet.

A nitrogen purge was introduced to the vessel for 40-60 minute periods before each polymerisation was initiated, in order to ensure complete deoxygenation of the system.

Polystyrene and acrylic macrogels were synthesised from two-stage bulk polymerisations (sections 2.5.1 and 2.6.1, respectively). Initially, a viscous prepolymer/comonomer syrup was synthesised, under nitrogen, by stirring the homogeneous comonomer/initiator solution (60°C) in a sealed straight-walled glass vessel (60°C). The polymerisation vessel was set-up as previously described (section 2.1.2, figure 2.1), with the exception that, on this occasion, the kettle was 250 cm^3 in volume and the comonomer/emulsifier inlet was replaced with a glass stopper.

Figure 2.1 – Vessel used for Emulsion Polymerisation
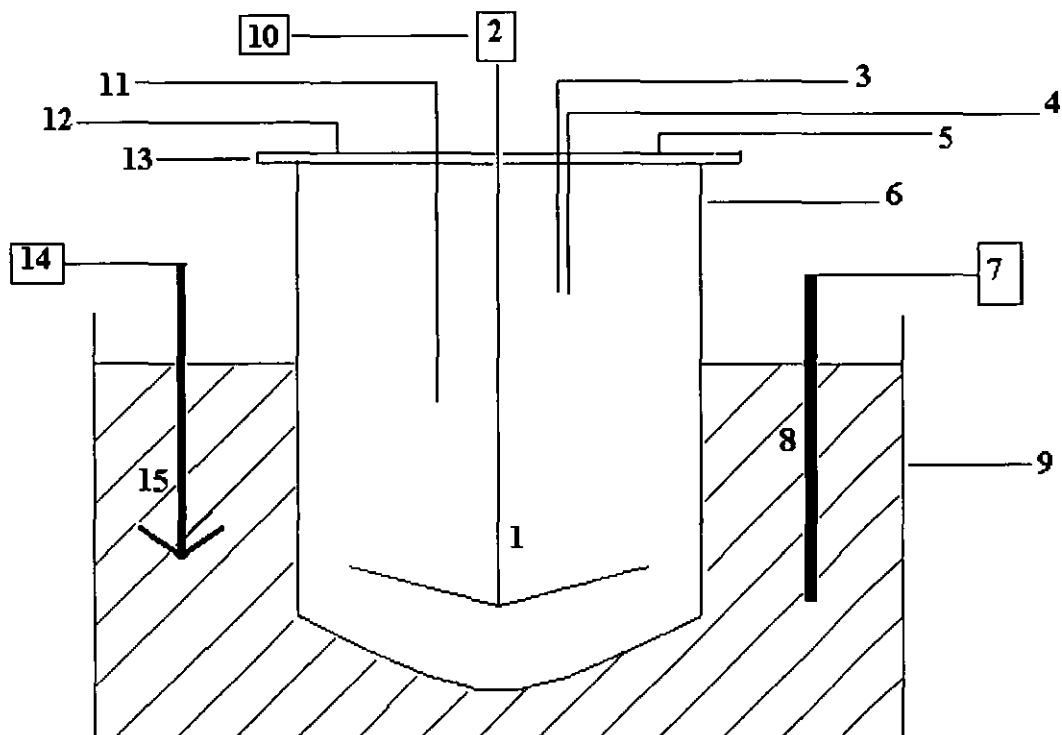
1	Stainless steel stirrer.
2	Mechanical motor.
3	Comonomer inlet tube attached to Watson-Marlow peristaltic pump.
4	Emulsifier inlet tube attached to Watson-Marlow peristaltic pump.
5	Reflux (coil) condenser.
6	Straight-walled glass polymerisation vessel (volume 700 cm^3).
7	Temperature control circuit.
8	Thermocouple.
9	Liquid paraffin oil bath.
10	Optical tachometer.
11	Thermocouple (accurate to ± 0.2°C) linked to digital display unit.
12	Nitrogen inlet tube.
13	Five port flange lid.
14	Mechanical motor.
15	Stainless steel stirrer.

PS macrogels were prepolymerised, under nitrogen, for periods of 15-20 minutes, whereas acrylic prepolymers were heated for 45-90 minutes. The viscous prepolymer/comonomer syrups were then transferred to circular stainless steel moulds. Each mould was fitted with a rubber gasket (diameter 80mm, height 2mm) and six sealing nuts. The moulds were then heated within a constant temperature oven (60°C) for 16-20 hours. Recoveries of PS and acrylic macrogels were performed at temperatures of 140-150°C and 40-70°C, respectively.

2.2.1 - SYNTHESIS OF POLYSTYRENE MICROGELS

Emulsion copolymerisations of styrene/divinylbenzene (0, 1, 5 and 10 weight % DVB) were performed at 75°C with ACVA as initiator. The components for these four emulsion polymerisation processes are given in table 2.2. (Ammonium persulphate-initiated copolymerisations at 90°C proceeded to low yields).

Table 2.2 - Components for Styrene/DVB Copolymerisation

Component	Composition (Weight %)
Styrene/DVB comonomers	20.01
Sodium lauryl sulphate	1.00
4,4'-Azobis(4-cyanovaleric acid)	0.43
Deionised water	78.56

The experimental procedure for the preparation of PS/DVB (5 wt. % DVB) microgel particles via emulsion copolymerisation is outlined below. The three other polystyrene latices were synthesised by similar procedures.

(I) - Initially, 3.60 g SLS and 408.00 g deionised water were added to the 700 cm^3 polymerisation kettle (figure 2.1). The emulsifier/water mixture was heated to 75°C, with stirring (500 rpm), under nitrogen. Once the copolymerisation temperature had been attained, a further 30 minute period was employed to complete deoxygenation of the system.

(II) - Then, 2.60 g ACVA and 11.40 g styrene/0.60 g DVB were introduced, as batches, to the vessel. The system was then left for a fifteen minute period.

(III) - After this period for nucleation, a 102.60 g styrene/5.40 g DVB mixture was introduced, dropwise over a two hour period. Similarly, a 2.40 g SLS/63.00 g deionised water mixture was introduced over this time period.

(IV) - After all of the copolymerisation components had been added, a further one and three quarter hour period of heating at 75°C, with stirring under nitrogen, was employed.

All four latices were subsequently cooled (25°C), filtered through steel mesh (10 μm pore size) and stored in sealed 800 cm³ glass jars.

2.2.2 - CHARACTERISATION OF POLYSTYRENE MICROGELS

The non-volatile components of the emulsions were determined by drying pre-weighed latex samples within a vacuum oven (15 hours at 25°C). Dilute latex samples were analysed by photon correlation spectroscopy (section 2.8.9). Water was evaporated from 50 ml latex samples, housed in glass trays, by standing latices for 5-6 days on a laboratory bench (25°C). The PS samples were then dried in a vacuum oven (130-160 hours, 25°C). Sheets of the four PS samples were subsequently prepared by compression moulding over ten minute periods at 150°C. A semi-positive, stainless steel mould (dimensions: 100 mm x 100 mm x 2 mm) was employed for sheet preparation. Mouldings were performed on an automated Bradley and Turton hydraulic press at a pressure of 40 tonnes. Small bars (ca. 2 x 5 x 20 mm) were cut from sheets that had been heated to 140°C. Such samples were analysed by dynamic mechanical thermal analysis, DMTA (section 2.8.2).

The latices were flocculated by addition to stirred, excess methanol. Polymeric products were recovered via vacuum filtration. Samples were then washed three times with methanol and hot (70°C) water. The polystyrene samples were subsequently dried in a vacuum oven (45-60 hours at 25°C). PS samples were then dispersed in toluene (5 wt. % solids), followed by precipitation into methanol. After material recovery via vacuum filtration, samples were washed with methanol and dried (vacuum oven, 60-80 hours at 25°C). The PS samples were then redispersed, reprecipitated and repeatedly washed with methanol. The recovered materials were

finally dried (25°C) in a vacuum oven (120-150 hours). Purified copolymer samples were analysed by differential scanning calorimetry, DSC (section 2.8.1), diffuse reflectance Fourier transform infrared spectroscopy, DRIFT (section 2.8.6), and by gel permeation chromatography, GPC (section 2.8.3).

Anhydrous ethylbenzene/destabilised styrene (1, 2, 3, 4 and 5 wt. % styrene) mixtures were analysed by Fourier transform infrared (FTIR) spectroscopy (section 2.8.5). Mixtures of these low molecular weight analogues, of a styrene/DVB copolymer containing pendant vinyl groups, were analysed in order to determine the levels of unsaturation within PS microgel particles [247] (comparisons between PS microgel DRIFT spectra and the FTIR spectra of the model compounds were used to estimate the degree of microgel particle unsaturation).

2.2.3 - POLYSTYRENE MICROGEL DISPERSIONS IN ORGANIC MEDIA

Dry samples of polystyrene microgel particles (1, 5 and 10 wt. % DVB) were each added to anhydrous samples of n-butyl acrylate, toluene, tetrahydrofuran (THF), benzyl alcohol and cyclohexanone (5 wt. % solids). Each of the fifteen samples were left to stand, in sealed 400 cm^3 vessels, overnight (25°C). Microgel dispersions were recovered by vacuum filtration and samples were dried by storing over molecular sieve (4Å). The non-volatile component of each dispersion was determined by drying pre-weighed samples in a vacuum oven (8 hours at 70°C). All six of the dispersants were supplied by the Aldrich Chemical Company with sample purities stated to be in the 99-99.8 weight % range. The organic liquids were all stored over molecular sieve (4Å) prior to use.

The rheological behaviour (25°C) of each dispersion (5 wt. % solids) was determined, by testing the samples using a Haake VT500 rheometer (section 2.8.4). Additionally, a PS solution in toluene (5 wt. % solids) was prepared, and this sample was also tested using this rheometer.

2.3.1 - SYNTHESIS OF P*n*BA MICROGELS

Emulsion copolymerisations of *n*-butyl acrylate with 10 weight % divinylbenzene, 10 and 20 weight % ethylene glycol dimethacrylate (EGDMA) and 10 and 20 weight % neopentyl glycol diacrylate (NPGDA) were performed at 90°C with ammonium persulphate (APS) as initiator. A P*n*BA homopolymer latex was also prepared. The components for these six emulsion processes are given in table 2.3.

Table 2.3 - Components for the Synthesis of P*n*BA Microgels

Component	Composition (Weight %)
*n*BA/comonomer mixture	20.02
Sodium lauryl sulphate	1.00
Ammonium persulphate	0.25
Deionised water	78.73

The procedure for the preparation of P*n*BA/DVB (10 wt. % DVB) microgel particles was similar to that listed in section 2.2.1, with the following exceptions.

(I) - The 3.60 g emulsifier/402.00 g water mixture was heated to 90°C.

(II) - Batches of 5.00 g water/0.40 g APS and 10.80 g *n*BA/1.20 g DVB were initially introduced and the system was then left for a forty five minute period.

(III) - A 97.20 g *n*BA/10.80 g DVB mixture was introduced, dropwise over a four hour period. Similarly, a 2.40 g SLS/1.00 g APS/60.00 g deionised water mixture was added over this time period.

(IV) - A 5.00 g water/0.10 g APS charge was added, once all of the comonomers had been introduced to the vessel. A further one hour period of heating at 90°C was then employed to complete the reaction.

The five other acrylic materials were synthesised by similar procedures. All six latices were subsequently cooled (25°C), filtered and stored.

2.3.2 - CHARACTERISATION OF ACRYLIC MICROGELS

The non-volatile component of each emulsion was determined by drying pre-weighed latex samples within a vacuum oven (15 hours at 25°C). Latex samples were analysed by photon correlation spectroscopy (section 2.8.9). Water was evaporated from 50 cm^3 latex samples, housed in glass trays, by standing the samples for 5-6 days on a laboratory bench. The seven acrylic samples were then dried in a vacuum oven (130-180 hours at 25°C). Samples cut from these elastomeric films were analysed by dynamic mechanical thermal analysis and differential scanning calorimetry.

2.3.3 - ACRYLIC MICROGEL DISPERSIONS IN ORGANIC MEDIA

Acrylic microgel dispersions in benzyl alcohol and *n*-butanol were prepared by the addition of latices (20 wt. % solids) to hot (70°C), vigorously stirred organic liquid. Attempts were also made at preparing microgel dispersions in *n*-butyl formate, *n*-butyl propionate, and dimethylformamide (DMF). The vessel employed for this process was a 700 cm^3 glass kettle (figure 2.1). A reflux condenser, nitrogen inlet, digital thermometer, stainless steel stirrer and glass stopper were fitted to the five ports of the vessel lid. All five of the dispersants (each of 98-99 wt. % purity and supplied by Aldrich Chemicals) were stored over molecular sieve (4Å) before use. The quantity of latex sample that was added to the organic liquid was dependent upon the solubility of water in the dispersant [248]. The alcohol/water mixtures prepared were homogeneous (i.e., of one phase). Water was subsequently removed from acrylic dispersions by vacuum distillation [249].

The water content of the *n*-butanol dispersions was estimated by Karl Fischer titration [250]. An automated titration unit was employed and subsequently P*n*BA dispersions were not directly analysed (the possibility of polymer precipitating within the unit, when analysis of liquids that were non-solvents for P*n*BA was to be performed on a later date, was taken into account). Consequently, a blank sample was prepared by the addition of deionised water to the alcohol, in similar volumes to those which had been used for the preparation of microgel dispersions. A distillation procedure, identical to the method employed for microgel dispersion preparation, was then undertaken. The liquid (alcohol) remaining in the distillation flask (after the distillation process had

been stopped because it had appeared, from observations of distillate boiling points, that all of the water had been removed from the alcohol in the flask) was subsequently recovered, and the water content was evaluated by Karl Fischer titration [250]. The water contents of the *n*-butanol and benzyl alcohol dispersions were also estimated by FTIR spectroscopy.

Anhydrous P*n*BA microgel dispersions in *n*-butanol and benzyl alcohol, obtained from distillation procedures, were stored over molecular sieve (4Å). The non-volatile component of each dispersion was determined gravimetrically (under vacuum for 10 hours at 80°C). The rheological behaviour of each dispersion (5 wt. % solids) was determined using a Haake VT500 rheometer (25°C). Additionally, P*n*BA solutions in benzyl alcohol and *n*-butanol (5 wt. % solids) were prepared, and these sample were also tested with this rheometer.

2.4 - SOLUBILITY OF MONOMERS IN ORGANIC LIQUIDS

Once the first-stage microgel particles had been synthesised and dispersed in an organic medium, attempts were to be made at polymerising the second-stage comonomers within the first-formed gel particles. It was considered ideal that the second-stage comonomers should constitute a droplet phase in the chosen monomer/organic liquid mixture. Provided that a free radical initiator which was soluble in the continuous (organic liquid) phase and insoluble in the comonomer (droplet) phase could be found, second-stage polymerisations could then be performed under a modified form of quasi-emulsion conditions.

The phase behaviour of *n*-butyl acrylate and styrene with a number of different organic liquids was determined (25°C). The organic diluents used in these solubility studies are listed in table 2.4. Initially, 50 cm^3 of organic liquid was pipetted into a 250 cm^3 conical flask. The chosen monomer was then added dropwise (for 5 cm^3) from a 10 cm^3 micro-burette. The flask contents were agitated after each addition of monomer and the observed number of liquid phases in each flask was then recorded. Additional monomer was then introduced (in 5 cm^3 portions) until 50 cm^3 had been added. These procedures were then repeated, in order to evaluate the solubility behaviour of the liquids over the whole composition range of the mixtures, with small

volumes of organic liquid being dispensed into flasks containing 50 cm^3 of the monomer.

Table 2.4 - Reagents used for Monomer Solubility Studies

Reagent	Purity (Weight %)	Supplier
n-Butanol	99	Aldrich
Benzyl alcohol	99	Aldrich
Ethanol	90	Aldrich
Methanol	99	Aldrich
Butanone	99	Aldrich
Cyclohexanone	99	Aldrich
N-Methyl formamide	99	Aldrich
Formamide	98	Aldrich
Poly(dimethylsiloxane) [1]		Dow Corning
n-Hexane	95	Aldrich

[1] Number average molecular weight of 2,140 g mol^{-1}.

2.5.1 - SYNTHESIS OF POLYSTYRENE MACROGELS

Polystyrene macrogels (1, 5 and 10 wt. % DVB) were synthesised from bulk copolymerisation with 2,2'-azobisisobutyronitrile (AIBN) employed as initiator. Polystyrene homopolymer was also synthesised by bulk polymerisation. AIBN (1 wt. % on total comonomers) was dissolved in destabilised styrene/DVB mixtures and the systems were then heated to 60°C. Details of the two-stage copolymerisation process are presented in section 2.1.2. Smooth, continuous, PS sheets were recovered after each of the four polymerisation procedures had been completed. The samples were then dried for 60-80 hours within a vacuum oven (40°C).

2.5.2 - CHARACTERISATION OF POLYSTYRENE MACROGELS

Macrogel samples, cut from films that had been heated to 140°C, were analysed by DMTA.

Soxhlet extraction with toluene (12-15 hours) was used to determine the sol-gel ratio [251] for weighed samples (2.0-2.5 g) of each of the three materials containing DVB. Polystyrene macrogel (1, 5 and 10 wt. % DVB) samples (0.20-0.40 g) were weighed into fifteen 7 cm^3 glass vials. Weighed samples of toluene, nBA, THF, cyclohexanone and benzyl alcohol (ca. 5.0 g) were then added to these macrogel samples. The vials were then sealed with a tight-fitting plastic cap. Each system was subsequently left to equilibrate over a 120 hour period (25°C). Swollen macrogels were removed from the glass vessels, placed between two sheets of tissue-paper (to soak-up surplus organic liquid), and then weighed. Polymer network volume fractions, at equilibrium, were calculated for each of the fifteen PS macrogel/organic liquid systems. Tabulated organic liquid [248] and PS [252] density values (25°C) were used to determine component volumes from the masses recorded experimentally.

Equilibrium swelling experiments (25°C), for the three macrogels, were also performed with an anhydrous benzyl alcohol/nBA mixture (10 wt. % nBA). A 120 hour period for equilibration was employed (approximately 10 wt. % solids in each system). This investigation was performed in order to ascertain (estimate) whether monomer (nBA) would preferentially swell the PS network particles of PS microgel dispersions in benzyl alcohol. FTIR spectroscopy analysis of anhydrous benzyl alcohol/nBA mixtures (1, 2, 3, 4, 5, 6, 7, 8, 9 and 10 wt. % nBA) was performed, and FTIR spectra of the liquid mixtures found remaining outside of the macrogel samples (after swelling times had elapsed) were also recorded. Comparisons between FTIR spectra, recorded for both known and unknown (the composition of the liquid mixture found outside of the gel needed to be determined) nBA/benzyl alcohol mixture compositions, enabled predictions of the degree of nBA partitioning within the PS networks to be made.

2.6.1 - SYNTHESIS OF PnBA MACROGELS

Five acrylic macrogels were prepared by bulk copolymerisation (sections 2.1.2 and 2.5.1). PnBA homopolymer was also synthesised. Smooth, continuous polymer sheets were recovered after each of the five polymerisation procedures had been completed. Macrogel samples were dried for 80-100 hours in a vacuum oven (40°C).

2.6.2 - CHARACTERISATION OF ACRYLIC MACROGELS

Acrylic macrogel samples were analysed by dynamic mechanical thermal analysis.

Soxhlet extraction with *n*-butanol (8-10 hours) was used to determine the sol-gel ratio for weighed samples (2.0-3.0 g) of each of the five macrogels. Equilibrium swelling (section 2.5.2) of macrogel samples with *n*-butanol, styrene, and benzyl alcohol was performed (120 hours at 25°C). Tabulated P*n*BA [252] and dispersant [248] density values (25°C) were used for conversion of the experimentally recorded mass data into volume values. The polymer network volume fraction at swelling equilibrium was then calculated for each of the systems.

2.7.1 - SYNTHESIS OF OLEFINIC PEROXIDE MONOMERS

The peroxides, *t*-butylperoxy-2-methacryloyloxyethyl carbonate [246], di-*t*-butylperoxy fumarate (DBPF) and *t*-butylperoxyallyl carbonate (ALPO) [246] were synthesised by the reaction between the required chloroformate/acid chloride and *t*-butylhydroperoxide [246]. The reagents used for peroxide synthesis are listed in table 2.5.

Table 2.5 - Reagents used for Olefinic Peroxide Synthesis

Reagent	Purity (Weight %)	Supplier
MOCF [1]	95	Hodogaya Chemicals
Fumaryl chloride	95	Lancaster Synthesis
Allyl chloroformate	97	Aldrich
t-Butylhydroperoxide [1]	70	Aldrich
Toluene	99	Aldrich
Sodium sulphate	99	Aldrich
Sodium carbonate	99	Aldrich
Potassium hydroxide	99	BDH
Sodium hydroxide	97	Aldrich

[1] 2-methacryloyloxyethyl chloroformate.

[1] 70 weight % solution in water.

The procedure for the synthesis of *t*-butylperoxy-2-methacryloyloxyethyl carbonate (PMEC) [246], a commercially available peroxide monomer from the NOF Corporation [253], is outlined in the following text. Initially, 140 g toluene, 72.25 g *t*-butylhydroperoxide and 92.50 g 2-methacryloyloxyethyl chloroformate were added to a 600 cm³ flask. This reaction vessel was then placed in a water/ice mixture and gentle stirring of the reagents was started. Dropwise addition of 129.25 g dilute potassium hydroxide (20 wt. %) solution was then performed over a 110 minute period. The vessel contents were maintained at 10-15°C throughout this addition process. After the hydroxide addition had been completed, the flask contents were maintained at 10°C for 80 minutes. The reaction vessel was then removed from the water/ice mixture. The flask contents were then added to a 1 litre separating funnel and the materials were left to settle (15 minutes) into two (organic and aqueous) phases. The lower aqueous layer was separated and 400 g deionised water was added to the organic component. After shaking the organic/aqueous liquid mixture for 5 minutes, the materials were left to settle (10 minutes) and the aqueous layer was separated. Addition of 400 g deionised water, followed by separation of the aqueous component, was then performed on two further occasions. Then, 400 g dilute sodium carbonate solution (10 wt. %) was added to the organic component. After shaking of the organic/aqueous liquid mixture for 10 minutes had been completed, the materials were left to settle (15 minutes) and the aqueous layer was separated. Then, three separate additions of 400 g deionised water were made and each addition was followed by removal of the aqueous component. The organic phase was then passed through filter paper containing anhydrous sodium sulphate. The dry, filtered, material was then stored in a sealed 500 cm³ glass jar. The organic product/toluene mixture was placed in a refrigerator, and left overnight. Toluene was removed from the organic liquid mixture by vacuum rotary evaporation at 30°C (1 hour). The recovered material was added to a sealed 250 cm³ glass container, and the vessel was then stored in a refrigerator. The organic product was a clear oil.

The peroxide monomer *t*-butylperoxyallyl carbonate (ALPO) was synthesised by utilising a previously published procedure [246]. Initially, 64.37 g *t*-butylhydroperoxide was stirred with 220 g dilute (10 wt. %) sodium hydroxide solution in an ice bath at 0°C. Then, 61.48 g allyl chloroformate was added dropwise

over 35 minutes. The reagents were maintained at 0°C throughout. The reaction flask was removed from the ice bath, and the reaction products were then left for 50 minutes (25°C). The organic layer was then separated, washed three times with deionised water and dried over anhydrous sodium sulphate. The organic product was a clear oil.

Di-*t*-butylperoxy fumarate (DBPF) was synthesised using similar procedures to those employed for ALPO, with 15.45 g *t*-butylhydroperoxide, 5.14 g sodium hydroxide, 45.01 g deionised water and 7.65 g fumaryl chloride used in the synthesis. The organic product (a white crystalline solid) was heated to 40°C and placed in a refrigerator (5°C) for approximately 2 hours, before recovery.

2.7.2 - CHARACTERISATION OF PEROXIDE MONOMERS

Samples of each of the three organic reaction products were characterised by 100 MHz ^{1}H and 25 MHz ^{13}C NMR spectroscopy (sections 2.8.7 and 2.8.8, respectively), and FTIR spectroscopy. FTIR spectra of 2-methacryloyloxyethyl chloroformate, fumaryl chloride and allyl chloroformate were also recorded.

The purity of each peroxide monomer was estimated by iodimetric titration [254]. The reagents used for these iodide reductions are listed in table 2.6. A 25 cm^3 aliquot of the solution of sodium thiosulphate supplied was pipetted in to a 250 cm^3 volumetric flask. Deionised water was then added to dilute the solution up to the mark. This (0.0101 M) thiosulphate solution was used for each of the titrations. Initially, a solution of iron (III) chloride hexahydrate in acetic acid (0.01 weight % solids) was prepared. Ferric chloride has been found to inhibit certain free radical polymerisations [255] and was, therefore, included for these iodimetric titrations. Samples of each of the three olefinic peroxides (0.05-0.10 g) were dissolved in 50 cm^3 dioxane. Then, 25.0 g of the ferric chloride solution in acetic acid, 0.25 g sodium iodide and 25.0 g deionised water were added to each of the 500 cm^3 flasks. The samples were then left in a wooden cupboard, in the dark, for 12 hour periods. After the materials had been recovered, 25.0 g of deionised water was added.

Table 2.6 – Reagents used for Iodimetric Titration

Reagent	Purity (Weight %)	Supplier
Sodium iodide	99	Aldrich
1,4-Dioxane	99	Aldrich
$FeCl_3.6H_2O$	98	Aldrich
Starch		Aldrich
Acetic acid	99	Aldrich
Sodium thiosulphate [†]	99	Aldrich

[†] Supplied as 0.1008 M aqueous solution.

The reagents were then titrated with the 0.0101 M sodium thiosulphate solution until the mixture became pale yellow. At this stage, 5.0 g of an aqueous starch solution (2 wt. %) was added to the reaction flask. The titration was then continued until the end-point had been reached (the deep blue colour disappeared and the mixture became clear). Three reductions were performed for each of the three peroxide monomers. Additionally, three blank samples (without peroxide) were titrated with thiosulphate.

2.7.3 - COPOLYMERISATION OF PEROXIDES WITH STYRENE

Styrene/ALPO (5 mole % ALPO), styrene/DBPF (2.5 mole % DBPF), and styrene/PMEC (5 mole % PMEC) emulsion copolymerisations were performed over four hour periods at 75°C. A polystyrene latex was prepared under identical conditions (section 2.2.1). The components for these emulsion copolymerisations are given in table 2.7.

Table 2.7 - Components for Peroxide Emulsion Copolymerisation

Component	Composition (Weight %)
Styrene/peroxide comonomers	20.01
Sodium lauryl sulphate (SLS)	1.00
4,4'-Azobis(4-cyanovaleric acid)	0.43
Deionised water	78.56

The experimental procedure for the preparation of styrene/PMEC (5 mole %) copolymer particles was similar to the method listed in section 2.2.1, with the following exceptions:

(I) - Batches of 9.50 g styrene/2.50 g PMEC and 2.60 g ACVA were initially introduced to the vessel.

(II) - A 41.00 g styrene/10.79 g PMEC mixture was introduced, dropwise, to the system, over a one hour period. Once all of the peroxide comonomer had been added, 56.21 g styrene was introduced, dropwise, to the latex over a further one hour period.

The two other copolymer latices were synthesised via similar procedures. Aliquots (ca. 2 cm^3 in volume) were taken from latices at fifteen minute periods throughout these emulsion processes. Each sample's non-volatile component was determined by drying (pre-weighed) latex samples in a vacuum oven (12 hours at 25°C).

2.7.4 - CHARACTERISATION OF PEROXIDE COPOLYMERS

The peroxide copolymers were recovered and purified by similar methods to those listed in section 2.2.2. Samples of the four purified products were analysed by differential scanning calorimetry, gel permeation chromatography, ^{1}H/^{13}C NMR spectroscopy and DRIFT spectroscopy. Ethylbenzene/PMEC, ethylbenzene/DBPF and ethylbenzene/ALPO (1, 2, 3, 4 and 5 mole % peroxide) mixtures were also analysed by FTIR spectroscopy. Mixtures of these low molecular weight analogues of styrene/peroxide copolymer samples were analysed in order to estimate the mole fraction of peroxide within each copolymer (from comparisons between copolymer DRIFT, and model compound FTIR, spectra).

2.7.5 - PS/DVB/PMEC MICROGEL SYNTHESIS

PS/DVB (5 wt. %)/PMEC (0 & 0.25 mole %) emulsion terpolymerisations were performed over six hour periods at 75°C. The components for these emulsion processes are given in table 2.8.

Table 2.8 – Components for Peroxide Microgel Synthesis

Component	Composition (Weight %)
Styrene/DVB/peroxide comonomers	19.99
Sodium lauryl sulphate (SLS)	1.00
4,4'-Azobis(4-cyanovaleric acid)	0.50
Deionised water	78.51

The procedure for the preparation of styrene/DVB (5 weight %)/PMEC (0.25 mole %) microgel particles was similar to that listed in section 2.2.1, with the exception that:

(I) - A batch of 11.40 g styrene/0.60 g DVB/0.35 g PMEC was initially added to the vessel along with 2.60 g initiator. The system was then left for sixty minutes.

(II) - A 28.32 g styrene/1.49 g DVB/0.36 g PMEC mixture was then introduced, dropwise, to the vessel over a sixty minute period.

(III) - After a thirty minute period of heating had been maintained, a 73.57 g styrene/3.87 g DVB mixture was added to the vessel, dropwise, over three hours.

(IV) - A thirty minute period of heating was then maintained.

(V) - A 2.40 g SLS/0.40 g ACVA/63.00 g deionised water mixture was introduced, dropwise, to the system over the six hour duration of the polymerisation.

The other, non-functionalised, microgel latex was synthesised via a similar procedure. Emulsion samples were taken at thirty minute periods throughout these processes and non-volatile components were determined gravimetrically (section 2.2.2).

2.7.6 - CHARACTERISATION OF PEROXIDE MICROGEL PARTICLES

On completion of these emulsion terpolymerisation processes, the latices were cooled (25°C) and filtered (10 μm mesh). The emulsions were then added to the 700 cm^3 polymerisation vessel (figure 2.1), set-up in the manner described previously (section 2.3.3). Latices were subsequently heated to 95°C, with stirring, under nitrogen and the temperature was then maintained for eight hours. The heat treatment was performed in order to decompose any remaining ACVA initiator.

Latex samples were then cooled (25°C) and purified by similar methods to those listed in section 2.2.2. Samples of the two microgels were characterised by DSC.

2.7.7 - PREPARATION OF PEROXIDE MICROGEL DISPERSIONS

Dispersions of the PS/DVB/PMEC (0 and 0.25 mole %) particles in nBA/NPGDA (10 wt. % crosslinker) mixtures (2 wt. % solids) were prepared by addition of 8.0 g of the dried particles to 392.0 g of the comonomers. The systems were gently agitated over a twelve hour period (25°C). Dispersions were subsequently passed through filter paper containing anhydrous sodium sulphate and stored over molecular sieve (4Å). Both of the dispersions were then heated at 110°C, under nitrogen, in a 700 cm^3 polymerisation vessel (set-up as in section 2.3.3). Complete (macro-) gelation of both dispersions occurred after (approximately) five hours of heating. It was not known if polymerisation of the PS/DVB (5 wt.%) dispersion had been initiated by ACVA that was still present in the sample, or, if thermally-induced polymerisation of nBA/NPGDA had occurred. A 400 g anhydrous mixture of nBA/NPGDA (10 wt. % crosslinker) was also heated at 110°C and macro-gelation was similarly found to occur after (approximately) five hours, indicating that the comonomers had copolymerised thermally.

Consequently, 0.20 g hydroquinone monomethyl ether, MEHQ (99 wt. % purity, supplied by Aldrich Chemicals) was added to 400 g of an anhydrous mixture of nBA/NPGDA (10 wt. % crosslinker), and, after the system had been gently agitated for a 2 hour period (25°C), the mixture was heated for 10 hours at 110°C. The non-volatile component of the heat-treated mixture was determined by drying pre-weighed samples under vacuo (20 hours, 70°C). The addition of inhibitor (MEHQ) to the comonomer mixture was found to prevent thermal polymerisation occurring (110°C).

A 400 g dispersion of PS/DVB/PMEC (0.25 mole %) particles (2 wt. % solids) in anhydrous nBA/NPGDA (10 wt. % crosslinker), containing 0.20 g MEHQ, was, therefore, prepared, and the system was heated for 10 hours at 110°C. The copolymerisation yield was determined by gravimetry, as described in the text above.

2.8 - EQUIPMENT USED FOR ANALYTICAL CHARACTERISATION

2.8.1 - DIFFERENTIAL SCANNING CALORIMETRY (DSC)

Differential scanning calorimetry, DSC, is a non-equilibrium calorimetric technique that has found extensive employment in the field of polymer science [256]. For example, glass transition behaviour [257], and, the enthalpy of fusion for semi-crystalline polymers [258], have been investigated by DSC. The DSC apparatus has two distinct cells, (each located in a heating block that can be programmed to give a linear scanning rate) for the sample and reference, respectively [256]. Each cell incorporates a thermocouple, for instantaneous measurement of the temperature of the sample or reference, and a holder for the sample, or reference, pan [256]. A temperature-difference circuit ensures that the temperature variance between the sample and reference is zero. The calorimeter detects the total heat flow into, or from, a sample (relative to a reference) as a function of time or temperature [256]. Consequently, thermodynamic and/or kinetic data can be evaluated for samples that undergo physical or chemical transformations within the selected range of experimental (time and temperature) conditions [259]. There are two general modes of DSC analysis.

(I) Isothermal. The sample and reference are rapidly heated to the required temperature of study. Once the desired temperature has been attained, the power supplied to each of the heaters is adjusted in order to maintain the sample temperature, with time. The difference in power supplied to the two heaters is plotted (y axis) against the time of heating (x axis).

(II) Scanning. The sample and reference are heated at a constant heating rate over a pre-determined temperature range. When the sample undergoes a thermal transition, the power to the two heaters is automatically adjusted in order to retain the temperature of the reference and sample at the same value. This differential power signal is then plotted against the sample temperature.

The DSC method can yield specific heat capacity values that are in excellent agreement with heat capacities evaluated from adiabatic calorimetry [256]. Calibration with a known mass of material with a sharply defined melting point is

required if accurate thermodynamic parameters [259] are to be derived from DSC thermograms. Indium is commonly used as the calibrant (melting point 156.6°C, enthalpy of fusion 28.45 J g^{-1}). When heat flows from the surroundings into the sample (i.e. the sample is undergoing an endothermic transition) at a rate of dQ/dt (J g^{-1} s^{-1}), it is found [260] that:

$$dQ/dt = C_s(dT_s/dt) - C_r(dT_r/dt) - dH_s/dt \qquad (2.1)$$

where Q is the difference in heat supplied to the two (reference, r, and sample, s) cells (J g^{-1}), C is the total heat capacity (J K^{-1} g^{-1}) of the cell (including an empty sample pan for the reference cell and an encapsulated sample for the sample cell), T is the cell temperature (K) and H_s is the enthalpy of the sample (J g^{-1}).

The recorded heat flow, Q_e (at a given temperature, T) when both the reference and sample cells contain an empty sample pan (J g^{-1}) is given by [260]:

$$Q_e = K(\Delta C_e) \qquad (2.2)$$

where K is a constant for the DSC apparatus (K) and ΔC_e is the difference in heat capacity between the two cells (J K^{-1} g^{-1}). Heat flow values, Q_i (at given temperatures, T), are then recorded for two DSC traces with the sample (of mass, m_s) and calibrant, c (of mass, m_c) added to the sample cell [260]:

$$Q_i = K(\Delta C_e + m_i C_i) \qquad (2.3)$$

where m_i is the mass of (g), and C_i is the specific heat capacity (at constant pressure) of (J K^{-1} g^{-1}), component i, respectively.

The specific heat capacity of the sample (J K^{-1} g^{-1}) can be determined from [260]:

$$C_s = \frac{(Q_s - Q_e) \, m_c \, C_c}{(Q_c - Q_e) \, m_s} \qquad (2.4)$$

The enthalpy of a phase transition within the sample (J g^{-1}) can then be evaluated from [259]:

$$H_s = \int C_s \cdot dT \qquad (2.5)$$

A Dupont DSC 910 calorimeter was used for each analysis. The instrument was calibrated with an indium sample. Each polymer sample was run under a nitrogen atmosphere at a heating rate of 10°C per minute. Polystyrene and acrylic polymer samples were typically analysed over 20°C to 240°C and -100°C to 100°C temperature ranges, respectively.

2.8.2 - DYNAMIC MECHANICAL THERMAL ANALYSIS (DMTA)

Dynamic mechanical thermal analysis (DMTA) has been widely employed for the measurement of the glass transition temperature of polymer samples [261]. DMTA is especially useful for estimating the degree of miscibility between the constituent components of polymer blends [262, 263]. During the analysis, a small, sinusoidal, perturbation (strain) is applied to a constrained polymer sample. The resulting stress is measured simultaneously to the strain. Throughout this investigation the applied strain was in the form of a flexural (bending) mode of fixed angular frequency, ω. For linear viscoelastic materials at equilibrium, the applied strain and induced stress both vary sinusoidally with the strain lagging behind the stress (figure 2.2). The strain, ε, at a given instant can be calculated [264] from:

$$\varepsilon = \varepsilon_0 \sin(\omega t) \tag{2.6}$$

where ε_0 is the maximum strain and t is the time.

The induced stress, σ, at any given time [264] can be expressed as:

$$\sigma = \sigma_0 \sin(\omega t + \delta) \tag{2.7}$$

where σ_0 is the maximum stress and δ is the phase angle/phase lag. (For viscous materials, the phase angle is equal to 90°, whereas $\delta = 0$ for perfectly elastic materials. Viscoelastic materials give intermediate δ values [264], as depicted in figure 2.2).

Expansion of the stress, σ, term leads to the following relation:

$$\sigma = \sigma_0 \sin(\omega t) \cos \delta + \sigma_0 \cos(\omega t) \sin \delta \tag{2.8}$$

The stress-strain relationship can, therefore, be defined by a modulus, E', that is in phase with the strain and by a modulus, E", which is 90° out of phase with the strain:

$$\sigma = \varepsilon_0 E' \sin(\omega t) + \varepsilon_0 E'' \cos(\omega t) \tag{2.9}$$

The term E' is referred to as the dynamic storage modulus [264], or alternatively, the real part of the modulus. E" is the dynamic loss modulus, or the imaginary part of the modulus. Thus, E' quantifies the energy stored in the specimen due to the applied strain [264] and E" defines the energy dissipated [264].

Figure 2.2 - The Stress-Strain Relationship
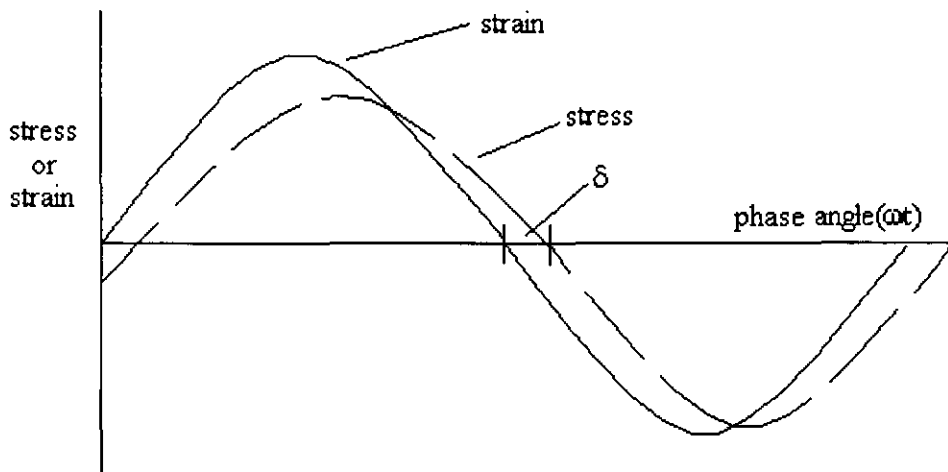
The storage and loss moduli also define a complex modulus, E*, which can be illustrated by a phasor diagram (figure 2.3). Using complex notation for the applied strain and induced stress:

$$\varepsilon = \varepsilon_0 \exp(i\omega t) \quad \text{and} \quad \sigma = \sigma_0 \exp[i(\omega t + \delta)] \tag{2.10}$$

The complex modulus, E*, can, therefore, be defined as:

$$E^* = (\sigma/\varepsilon) \tag{2.11}$$

$$E^* = (\sigma_0/\varepsilon_0)\exp(i\delta) = (\sigma_0/\varepsilon_0)[\cos\delta + i\sin\delta] \tag{2.12}$$

$$\text{i.e.} \quad E^* = E' + iE'' \tag{2.13}$$

The tangent of the phase angle (δ) is related to the dynamic and loss moduli by the following relation:

$$\tan\delta = (E''/E')$$
(2.14)

The tanδ value is named the loss tangent as it represents the ratio of the energy dissipated to the energy stored by the specimen [264] during a cyclic deformation.

Figure 2.3 - Phasor Diagram for Complex Modulus (E*)
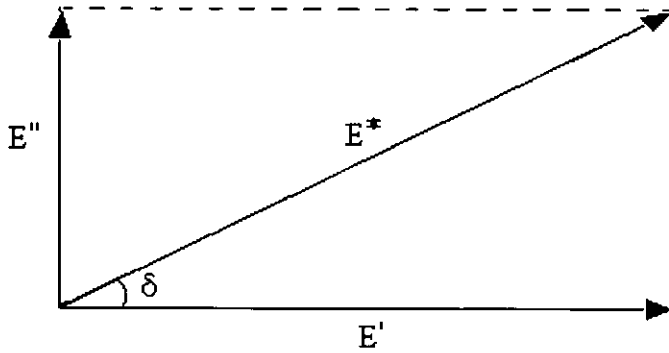
There are two modes of operation for the dynamic mechanical analyser.

(I)   Isothermal. The temperature of the specimen is kept constant and the strain-induced stress is measured over a range of angular frequencies. Such measurements are often recorded at a number of different temperatures (this is a consequence of the impracticality of developing an instrument that can analyse the entire frequency range required to evaluate the complete relaxation spectrum of a polymer sample [264]).

(II)   Fixed frequency. The stress is measured over a broad temperature range and the frequency of the applied strain is kept constant. This method is often used for experimental convenience. Variation of temperature leads to the relaxation processes of interest being brought to within a frequency range [264] that is readily available.

Polymers change from glass-like to rubber-like behaviour [264] as either the temperature is increased or the experimental frequency is decreased. The viscoelastic behaviour of a polymer specimen at one temperature can be related to that at another temperature by a change in frequency (time-scale) alone [264]. This phenomenon is

95

known as time-temperature equivalence and the Williams-Landel-Ferry (WLF) equation [265] describes this effect in mathematical terms:

$$\log a_1 = \frac{C_1(T - T_s)}{C_2 + (T - T_s)} \qquad (2.15)$$

where C_1 and C_2 are constants, T_s is a reference temperature and a_T is the shift factor [265] required for exact displacement of the relaxation spectrum determined at a temperature, T_1, and frequency, f_1, onto the data recorded at a second temperature, T_2.

At low temperatures (and high frequencies), polymers are glassy and specimens subsequently have high storage moduli [264], E' (ca. 10^9 Pascal, Pa), which are relatively independent of temperature. At high temperatures, polymers are rubber-like and of low storage modulus [264], E' (ca. 10^5 Pa). In the intertransitional region, the glass transition (T_g), polymers exhibit viscoelastic behaviour [264] and the storage modulus decreases with increasing temperature. The loss modulus, E", is of low magnitude in the glassy region (ca. 10^6 Pa) and in the region of rubber-like behaviour (ca. 10^4 Pa), since the induced stress and the applied strain are in phase over these regions [264]. The loss modulus increases to a maximum value at the glass transition temperature (ca. 10^7 Pa) [264]. The loss factor (tanδ) has a maximum at the glass transition and is close to zero in both the glassy and rubbery states [264]. Plots of E', E" and tan δ with temperature (at fixed frequency) for a typical amorphous homopolymer are shown in figure 2.4.

A microprocessor-controlled Rheometric Scientific non-resonance forced vibration dynamic mechanical analyser was used throughout this project. All samples were run at a heating rate of 3°C per minute, with a displacement (strain) of 4 (64 μm amplitude) and a fixed frequency of 10 Hertz. Polystyrene and acrylic polymer specimens were typically analysed over 20°C to 200°C and -60°C to 150°C temperature ranges, respectively.

Figure 2.4 - Dynamic Mechanical Data for a Typical Homopolymer

Temperature, T (°C)
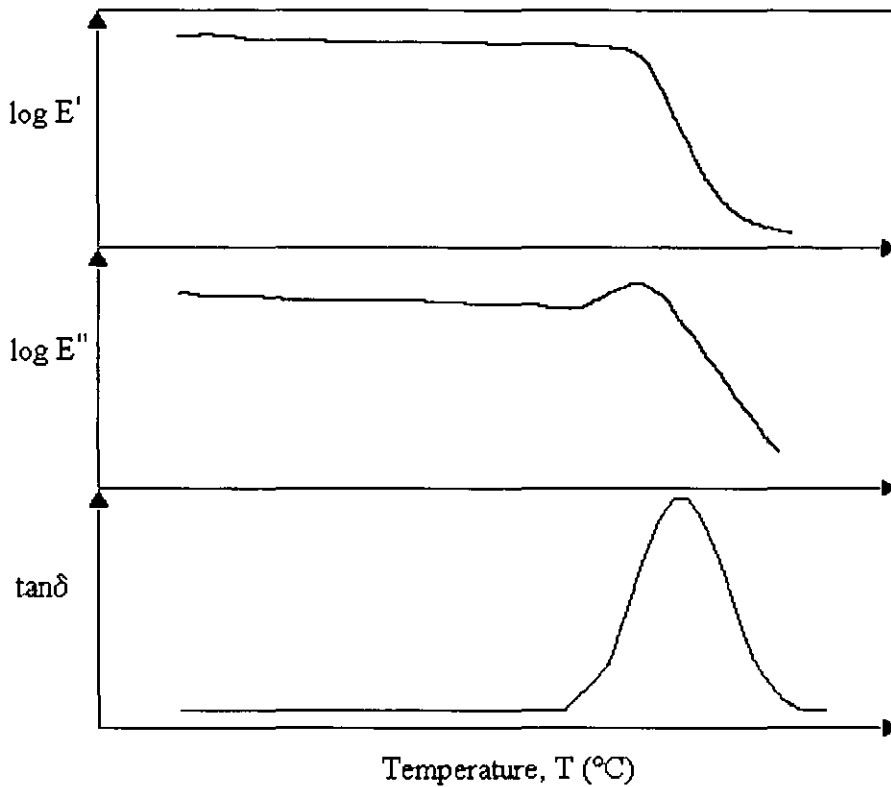
2.8.3 - GEL PERMEATION CHROMATOGRAPHY (GPC)

Classical gel permeation chromatography (GPC) or size exclusion chromatography (SEC) is a non-absolute method for determining average molecular weights and molecular weight distributions of linear polymers. GPC is a fractionation technique in which polymer molecules are separated according to their hydrodynamic volume in solution. Flory predicted [266] that the effective hydrodynamic volume of a linear polymer molecule in solution is proportional to its molecular weight and to the intrinsic viscosity of the solution:

$$V_h = [\eta].M.(1/\Phi) \tag{2.16}$$

where V_h is the equivalent hydrodynamic volume (m^3), M is the molecular weight of the polymer molecule (kg mol^{-1}), Φ is a universal constant (mol^{-1}) and [η] is the intrinsic viscosity [11] of the solution (m^3 kg^{-1}). The intrinsic viscosity of a dilute

polymer solution can be related to the viscosity average molecular weight of the polymer sample, M_V, by use of the Mark-Houwink relation [267]:

$$[\eta] = K(M_V)^a \qquad (2.17)$$

where K (m^3 kg^{-1}) and a ($0.5 \leq a \leq 1.0$, for most linear polymer systems) are constants for a given polymer/solvent system, at constant temperature (extensive listings of K and a values [268] are available). The viscosity average molecular weight (M_V) is given by:

$$M_V = [(\sum M_i^{1+a} N_i) / (\sum M_i N_i)]^{1/a} \qquad (2.18)$$

where N_i is the number of polymer molecules of molecular weight M_i.

During GPC analysis, a dilute polymer solution is introduced into a solvent stream that is flowing through chromatographic columns at a constant flow rate. The columns are packed with beads of a porous gel. Polystyrene gels (styrene/divinylbenzene copolymers) are commonly used as the packing material for the columns [269]. A given polymer molecule can diffuse into the pore structures of the gel to an extent that is dependent on the hydrodynamic volume, V_h (m^3), of the molecule in solution and on the pore size (and size distribution) of the gel [269]. The ability of polymer molecules to penetrate these pore structures is the basis for the separation of molecules of different molecular weight by GPC. High molecular weight polymer molecules enter the smallest fraction of the gels internal structure. Polymer molecules of low molecular weight can penetrate larger fractions of the gel interior and molecules of intermediate hydrodynamic volume partially permeate the pore structure of the gel, to a degree dependent on their molecular weight. Consequently, polymer molecules of the highest molecular weight are eluted from the chromatographic columns first. For a given set of chromatographic columns, there will be a certain fraction of the internal gel structure that can be accessed by a particular solute molecule. The total volume of solvent in the columns (V) is related to the interstitial volume (V_0) and the volume of solvent within the pores (V_i) by:

$$V = V_0 + V_i \qquad (2.19)$$

The size exclusion chromatography coefficient, k_{SEC}, governs the fraction of V_i that can be accessed by a given solute molecule. The retention volume of a given fraction, V_R (cm^3), the volume of solution eluted from the time of injection of the sample to the chromatogram peak, is related to V_i (cm^3), V_0 (cm^3) and k_{SEC} by:

$$V_R = V_0 + k_{SEC} (V_i) = t_R f_V \qquad (2.20)$$

where t_R is the retention time (s) and f_V is the volumetric flow rate (cm^3 s^{-1}).

The retention volume, V_R, is related to the size of a given solute molecule in solution (the hydrodynamic volume, V_h). A typical plot of logV_h against elution volume is shown in figure 2.5. In practice, plots of log molecular weight (log M) versus V_R are plotted, and these graphs exhibit similar behaviour to logV_h against V_R data (as predicted from equations 2.16 and 2.17). Polymer molecules of high molecular weight can be of too large a volume to enter any of the pores and such molecules do not undergo the size exclusion process (depicted by the non-linearity of the curve, at low V_R, in figure 2.5).

Chromatographs contain a solvent delivery system that is capable of delivering a solvent stream of constant (linear) flow rate, a sample injection facility which allows the sample solution to be introduced into the solvent stream without disturbance of the solvent flow, a chromatographic column (or columns) containing beads of a microporous gel, a detector which monitors the output from the column(s) and a recorder which can give continuous output of the data evaluated by the detector. The detector measures the weight concentration of solution that elutes from the column at a given retention volume (retention time). Differential refractometers and ultraviolet (UV) absorption instruments are the commonest examples of GPC detectors [269]. Chromatographs fitted with these detectors require calibration before sample average molecular weights can be determined. Monodisperse polystyrene standards of known molecular weight are most commonly used for analysis of organic solutions. A calibration curve of log molecular weight versus elution volume is initially determined for the set of polymer standards. (A universal calibration [269] is required for determination of average molecular weight values for polydisperse samples of a given polymer if monodisperse standards of the polymer are not available). Calibration curves (e.g. figure 2.5) of this type are essentially linear (provided that the molecular

weight of the polymer is not too high for the pore size of the chosen gel). Polydisperse polystyrene samples can then be run on the GPC and the recorded chromatograms of solute concentration against elution volume are converted into graphs of concentration versus molecular weight by incorporation of the calibration curve data. The number-average (M_n) and weight-average (M_w) molecular weights (along with any other average molecular weight, e.g. the z-average, M_z) of the polydisperse sample can then be determined.

Figure 2.5 - Graph of $\log V_h$ against Retention Volume, V_R, from GPC
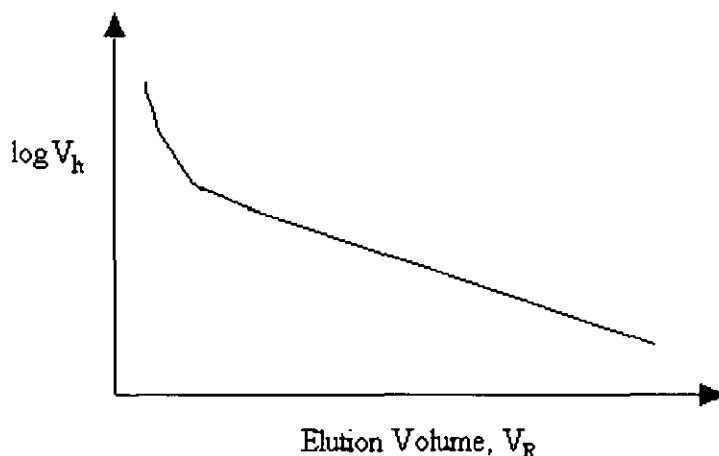
Elution Volume, V_R

The chromatogram (solute concentration versus elution volume data) is usually summed to give the cumulative weight distribution curve which can be normalised to give a total weight value of unity [269]. The derivative of this curve gives the differential weight distribution (equation 2.21) [427], W(M), which is related to the average molecular weights of the sample, as defined by equations 2.22-2.24.

$$W(M) = \frac{dW_v}{dV} \frac{dV}{d(\log M)} \frac{1}{M}$$

(2.21)

where W_v is the weight fraction that has been eluted up to a given volume V, (dW_v/dV) is the height of the chromatogram and $d(\log M)/dV$ is the gradient of the calibration curve at volume V.

$$M_n = \frac{\sum M_i N_i}{\sum N_i} = \frac{1}{\int (1/M).W(M).dM}$$

(2.22)

$$M_w = \frac{\sum M_i^2 N_i}{\sum M_i N_i} = \int M.W(M).dM \qquad (2.23)$$

$$M_z = \frac{\sum M_i^3 N_i}{\sum M_i^2 N_i} = \frac{\int M^2.W(M).dM}{\int W(M).dM} \qquad (2.24)$$

where N_i is the number of eluted polymer molecules of molecular weight M_i.

Chromatograms were recorded at ambient temperatures by an "in-house" constructed chromatograph. The apparatus was fitted with PLGel 2x Mixed Bed-D, PS gel, columns (average pore size of 5μm). Calibration was performed with a mixture of monodisperse polystyrene standards. THF was the eluent employed for sample runs and calibration. Volumetric flow rates of 1.0 cm^3 per minute were employed. Flow rates were monitored by an o-dichlorobenzene marker. A differential refractometer was used to determine the concentration of solute which had eluted from the columns, at a given instant.

2.8.4 - RHEOLOGICAL TESTING OF POLYMER DISPERSIONS

Rotational viscometers measure the shear stress, τ (Pa), versus shear rate, D (s^{-1}), profile of fluid samples. Rheological data (25°C) for microgel dispersions were recorded by a Haake VT500 rheometer. The VT500 consists of a detachable rotor (coaxial sensor) which is connected to a variable speed electric motor via a drive shaft. The coaxial sensor, which fits into a static measuring cup filled with the sample, is programmed to rotate over a designated (linearly increasing) speed range, and the rotor speed (at any instant) is proportional to the shear rate exerted on the sample. The sample's resistance to flow causes movement in a low compliance torsion bar that is mounted between the motor and the drive shaft. The torsion bar deflection is detected by an electronic transducer and the measured torque is proportional to the shear stress induced in the sample. Torque versus rotor speed values are then converted into shear stress versus shear rate data by a microprocessor. The instantaneous viscosity, η (Pa s), of the sample is related to the shear stress (τ) and shear rate (D) by:

$$\eta = (\tau / D) \qquad (2.25)$$

Polystyrene microgel samples were tested with a Haake NV coaxial cylinder sensor (appendix 1) over a shear rate range of 25-2,500 s^{-1}. Certain acrylic dispersions were also tested with the NV sensor. Other, more viscous, acrylic samples were analysed with a Haake MV1 sensor (appendix 1) over a shear rate range of 25-1,000 s^{-1}.

2.8.5 - FOURIER TRANSFORM INFRARED (FTIR) SPECTROSCOPY

Infrared (IR) spectroscopy [270] can be used to characterise molecular vibrations for diatomic and polyatomic molecules. Specific functional groups absorb electromagnetic (EM) radiation of characteristic energies [270] and detailed molecular characterisation can, therefore, result from IR analysis [270]. The frequency, v (Hz), and wavelength, λ (m), of EM radiation are related to the velocity of light, c (m s^{-1}), by:

$$c = v.\lambda \qquad (2.26)$$

The energy of a photon of light, E (J), is given by:

$$E = h.v \qquad (2.27)$$

where h is the Planck constant (J s).

Non-linear and linear polyatomic molecules with N atomic nuclei have 3N-6 and 3N-5 independent modes of molecular vibration [270], respectively. In practice, two general types of vibration are possible within a single bond. It may stretch along its axis or it may bend. A bending vibration requires less energy and occurs at a lower frequency than the corresponding stretching mode [270]. Of the possible, 3N-6, fundamental vibrations for polyatomic molecules, N-1 are stretching, and 2N-5 are bending modes [270]. Simple theories for predicting the vibrational frequency of linear diatomic molecules [270] have been developed. Molecules are considered to consist of two masses (m_1 and m_2) connected by a spring (of zero mass) and vibrations are constrained to displacements of each mass from equilibrium along the molecular axis [270]. If the molecular forces are assumed to be proportional to the displacement of each nucleus from its equilibrium configuration, the displacement of each atom with time, as the molecule undergoes one mode of vibration, can be defined by a sine

or cosine wave [270]. Such vibrations are classified as exhibiting harmonic behaviour. Absorption of IR radiation by a molecule leads to an increase in the vibrational energy of the molecule. Molecules are simultaneously irradiated with a wide range of IR frequencies, but radiation of certain specific frequencies, corresponding to the natural (quantised) vibrational energies of the molecule, is absorbed (or emitted) only. Quantum mechanical theory [270] predicts that harmonic oscillations have energy levels (E_{vib}) that are given by:

$$E_{vib} = (v + \tfrac{1}{2}).h. \nu \qquad (2.28)$$

where ν is the vibrational frequency of the oscillator (Hz), v is an integral quantum number (0, 1, 2, ...) and h is the Planck constant.

The relative populations of the various energy levels are given by the Boltzmann distribution [270]:

$$(n_i / n_0) = \exp[(E_0 - E_i)/kT] \qquad (2.29)$$

where n_0 and n_i are the number of molecules in the zero and ith energy levels, $E_0 - E_i$ is the energy difference between the two energy levels (J), k is the Boltzmann constant (J K^{-1}) and T is the absolute temperature (K). Most molecules are in their ground (v = 0) vibrational level at a temperature of 298K, with a small number in the v = 1 level. Photons with the exact energy required to increase the vibrational quantum number by a value of one are absorbed by a molecule. Since the vast majority of molecules are in the ground state at room temperature, the v = 0 → v = 1 transition, the fundamental transition, dominates the IR absorption spectrum [270].

IR spectra can be plotted in two different modes, either % transmittance (%T) versus radiation wavenumber, $\bar{\nu}$ (cm^{-1}), or absorbance (A) versus wavenumber.

$$\bar{\nu} = \nu/c = 1/\lambda \qquad (2.30)$$

If I_0 is the intensity of radiation (of a given frequency) that impinges on a sample and I is the intensity of the radiation after it has passed through the sample, then the ratio I/I_0 is called the transmittance (T) of the sample and the percentage transmittance (%T) is the original T value multiplied by 100. The absorption of EM radiation by a

sample solution of concentration, c (mol cm^{-3}), in a cell of thickness (pathlength), l (cm), is often given by the Beer-Lambert relation [270]:

$$\log_{10}(I_0/I) = A = \varepsilon.l.c \qquad (2.31)$$

where ε is the molar absorption coefficient (cm^2 mol^{-1}) of the absorbing species at a given frequency, and A is defined as the absorbance of the sample.

The relative intensity of an absorption depends on the effectiveness of the bond in conversion of the absorbed photon energy into molecular vibrational energy [270]. Vibrational modes are infrared active if a change in dipole moment occurs on vibration [270]. The integrated absorbance band intensity, A' (cm mol^{-1}), for a solution is related to the dipole moment change with bond length (inter-nuclear distance) during molecular vibration, $\partial \mu / \partial Q$ (dyne cm^{-1}), and A' values are calculated by integrating the absorption band when spectra are plotted in the absorbance (A) versus wavenumber ($\bar{\nu}$) mode [270, 271].

$$A' = \frac{\pi N_A}{3c^2.(\ln 10)}.(\partial \mu / \partial Q)^2 \qquad (2.32)$$

where N_A is the Avogadro constant (mol^{-1}), A' is the integrated absorptivity (cm mol^{-1}), ln signifies the Napierian logarithm and c is the velocity of light (cm s^{-1}).

Conventional IR spectrophotometers contain a source for infrared radiation, a monochromator, a filter and an infrared detector [270]. IR radiation of a wide range in wavelength is commonly produced by electrically heating a Nernst filament (a source comprised mainly of rare earth metal oxides) [270]. Monochromatic EM radiation is commonly generated by illumination of a diffraction grating with the radiation (comprised of many wavelengths). IR filters are used to limit the wavelength range of the EM radiation, i.e. filters are employed in order to retain only the frequencies required for the excitation of molecular vibrations [270]. Photoconductive cells, thermocouples, and pyroelectric detectors [270] have all been used to measure the intensity of absorbed radiation as a function of wavelength. Fourier transform infrared (FTIR) spectrophotometers utilise a Michelson interferometer in conjunction with an IR detector and a microprocessor [270]. The working of the interferometer is illustrated in figure 2.6. The basic components of the

interferometer are two mirrors, one fixed and the other adjustable (moveable) and a beam splitter which is set at an angle of 45° to the collimated beam. EM radiation from the source is focused on the beam splitter which partially reflects and partially transmits the radiation beam [270]. The beams are each reflected from the mirrors and recombination of the two beams occurs at the beam splitter. Constructive or destructive interference of the two beams results to a degree dependent on the relative position of the non-fixed mirror [270]. As the path difference between the two beams is adjusted, an interferogram of the radiation entering the interferometer is measured by the detector [270]. The interferogram signal reflects the additions (constructive or destructive) of all the interferences of each radiation wavelength [270]. The beam is then passed through the sample and analysed by the detector. Fourier transform analysis calculates the relationship between the intensity of the interferogram with the distance travelled by the mirror, I_x, and with the intensity of the EM radiation at a given frequency, I_v. Calculation of the inverse Fourier transform, by the microprocessor, relates the detected interferogram to the FTIR spectrum of the sample under investigation [270].

$$I_x = \int I_v.\cos(2\pi x v).dv \qquad (2.33)$$

$$I_v = \int I_x.\cos(2\pi x v).dx \qquad (2.34)$$

Figure 2.6 - Diagram of a Michelson Interferometer
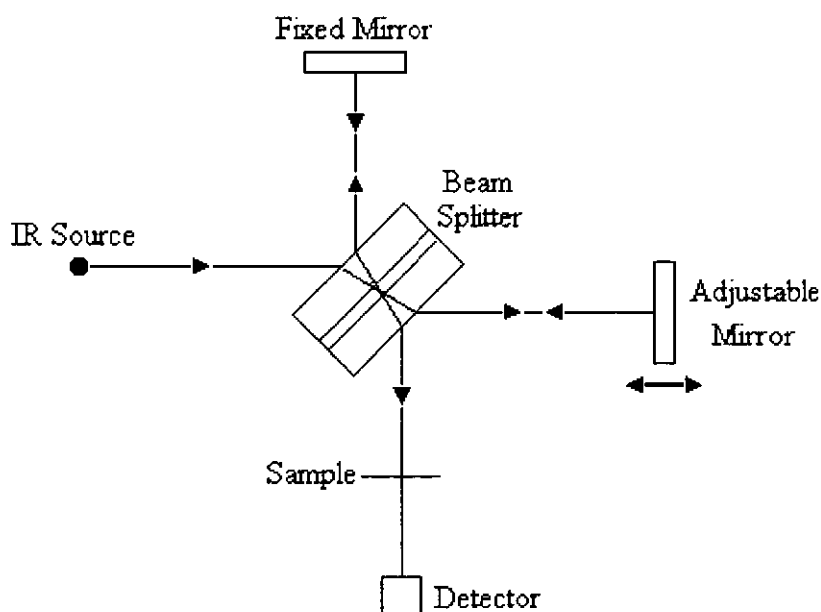
FTIR spectroscopy has certain advantages [270] over the conventional IR technique. Smaller amounts of material can be analysed by FTIR as the intensity of the radiation throughput of the interferometer is significantly greater than the intensities from conventional IR spectrophotometers [270]. The acquisition of data is also more rapid with FTIR spectroscopy, allowing the kinetics of chemical reactions [272] to be evaluated by the technique.

FTIR spectra at Loughborough and Lancaster Universities were recorded on microprocessor-controlled Mattson 3000 and Perkin-Elmer 1720-X spectrophotometers, respectively. All samples were submitted to 16 separate (pulsed) scans and materials were analysed over a 600-4,000 cm^{-1} radiation wavenumber range. Instrument resolutions were fixed at a value of 4 cm^{-1} for all measurements. Each liquid sample was analysed in a liquid (sodium chloride) cell, with the exception of PMEC, DBPF and ALPO samples which were analysed after insertion of one drop (from a 2.5 cm^3 Pasteur pipette) of material between two NaCl plates.

2.8.6 - DIFFUSE REFLECTANCE INFRARED FOURIER TRANSFORM (DRIFT) SPECTROSCOPY

DRIFT spectroscopy [273-276] is an analytical technique that can be applied to the study of polymer surfaces. DRIFT analysis of thin (10 μm) polymer (paint) films on metallic substrates has been reported by Claybourn and Turner [273]. A variety of optical effects were found to be in competition with one another for this particular paint-metal substrate system [273]. The optical interactions that are possible from DRIFT analysis of polymer films on metallic substrates are illustrated in figure 2.7.

A high concentration of scattering centres gives a diffuse reflectance spectrum [274] whereas a low concentration leads to a multipass transmission process, transflectance [274]. Specular reflectance from the sample surface can also occur, but this phenomenon is (generally) only observed [273] if other reflectance processes occur only to a negligible extent [274]. Analysis of a film spread on to a black polymer substrate [274] allowed for elimination of the back-surface reflectance (transflectance)

effect. It can be seen, therefore, that diffuse reflectance FTIR (DRIFT) analysis of polymer surfaces requires careful sample preparation [273-275].

Figure 2.7 - Diagram of Possible Interactions in Reflectance Measurements
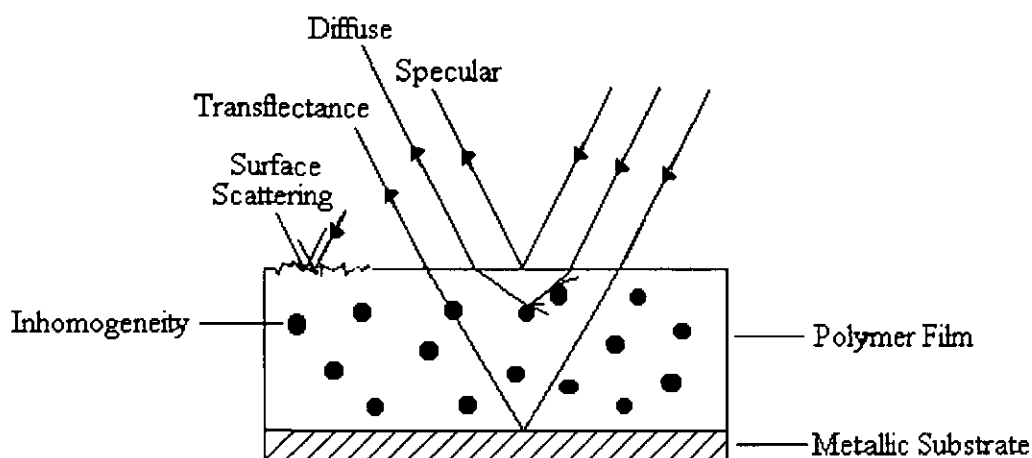
DRIFT measurements were performed with a microprocessor-controlled Mattson 3000 Fourier transform infrared spectrophotometer fitted with a Specac 30° specular reflectance unit. Spectra were recorded for fine dispersions of dry polymer samples (powders) in anhydrous potassium bromide (KBr). Sample powders were lightly pressed into the Specac sample cup using the edge of a micro-spatula and excess powder was scraped-off using the spatula edge. Care was taken to ensure that grooves were absent and that the sample surface was smooth. All samples were submitted to 100 separate (pulsed) scans and materials were analysed over a 600-4,000 cm^{-1} radiation wavenumber range. The instrument resolution was set at a value of 4 cm^{-1} for all measurements.

2.8.7 - ^{1}H NUCLEAR MAGNETIC RESONANCE (NMR) SPECTROSCOPY

Proton (^{1}H) NMR spectroscopy is a powerful analytical technique that has found widespread usage in the fields of chemistry and polymer science. Comprehensive reviews of the NMR characterisation of polymer systems have been written by Fawcett [277, 278]. NMR spectroscopy utilises the phenomenon of nuclear spin (angular momentum) which certain atomic nuclei possess [279]. All nuclei have the properties of mass and electrical charge, however, and a spinning nucleus will,

therefore, generate a magnetic field. The associated nuclear magnetic moment is related to the, parallel, angular momentum (I) vector [279] by:

$$\mu = \frac{\gamma.I.h}{2\pi}$$

(2.35)

where γ is the gyromagnetic ratio (Tesla^{-1} s^{-1}) - a constant for a given nucleus, μ is the magnetic moment (Ampere m^2) and h is Planck's constant (J s).

Application of an external magnetic field leads to an alignment of the nuclear magnetic moments and only certain moment orientations are allowed. Each nucleus of angular momentum, I, has $2I + 1$ possible orientations which are defined by the magnetic quantum number, m_I. The permitted values of the nuclear moment are related to m_I by:

$$m_I = -I, -(I - 1), ..., (I - 1), I$$

(2.36)

If the nuclear moment, I, has a value of one half ($I = \frac{1}{2}$, e.g. ^{1}H), then the possible values of the magnetic quantum number are $+\frac{1}{2}$ and $-\frac{1}{2}$ ($m_I = \pm\frac{1}{2}$). If I is equal to 1 (e.g. ^{2}H), m_I can have values of -1, 0 and +1. In the absence of an applied magnetic field the spin states (m_I) are energetically degenerate. In the case of nuclei with m_I values of $\pm\frac{1}{2}$, the parallel alignment (the α-state) of the spin with the (external) magnetic field is considered to be of lowest energy ($m_I = +\frac{1}{2}$). Conversely, the spin-state that is opposed (antiparallel) to the applied field (the β-state with $m_I = -\frac{1}{2}$) is regarded as being of higher energy. The energy of interaction (E) between the nuclear magnetic moment (equation 2.37) and the applied field is proportional to the nuclear moment and the applied field strength, B_0 (Tesla):

$$E = (-) \frac{\gamma.h.m_I.B_0}{2\pi}$$

(2.37)

The quantum mechanical selection rule for an NMR transition is that the magnetic quantum number can only change by a value of one [279], i.e. $\Delta m_I = \pm 1$. The difference in energy between two spin states (ΔE) is therefore given by:

$$\Delta E = \frac{\gamma.h.B_0}{2\pi}$$

(2.38)

Absorption of electromagnetic (EM) radiation of characteristic frequency (energy) allows for transitions between the lower and higher energy spin states of the nucleus to occur. The frequency, v (Hz), of the radiation required to impart a transition [279] is given by (combining equations 2.27 and 2.38):

$$v = \frac{\gamma.B_0}{2\pi}$$

(2.39)

For a given nucleus, the frequency of the radiation required for a transition between two spin states is, therefore, dependent upon the strength of the applied magnetic field. For NMR spectroscopy, the energies of the radiation required for a transition correspond to the energies of radiation in the radio-frequency region of the EM spectrum [279]. For a nucleus with a spin quantum number of ½ there are two possible transitions. The $\alpha \rightarrow \beta$ transition corresponds to an absorption of radiation whereas the $\beta \rightarrow \alpha$ transition corresponds to induced emission of energy, also known as relaxation [279]. The probability of each transition occurring is identical [279] and, consequently, there would be no net transfer of energy from the applied radiation to the sample if the two energy states were to be equally occupied. The samples are in thermal equilibrium with a Boltzmann distribution of energies [279] (equation 2.29), however, and the largest number of nuclei (N_α) are present in the lowest energy state (the α-state). Application of EM radiation tends to equalise the energy state populations as there are more ($\alpha \rightarrow \beta$) transitions from the more populated lower energy level to the β spin-state [279]. Relaxation processes [279] oppose saturation of populations and restore the Boltzmann distribution via transitions from the higher to the lower ($\beta \rightarrow \alpha$) spin-state (transitions that proceed without the emission of radio-frequency energy). Magnetic energy can be dissipated as thermal energy by excited nuclei through spin-lattice relaxation processes [279] whereby local magnetic fields interact with a given nucleus. For NMR analysis of sample solutions these local fields are predominantly associated with solvent molecules [279]. Spin-lattice relaxations due to dipole-dipole interactions [279] between adjacent nuclei are also found. This second, spin-lattice, process is especially important for ^{13}C NMR spectroscopy where ^{13}C nuclei are relaxed by attached protons (section 2.8.8). A third relaxation process is that of spin-spin relaxation [279] which occurs when two nuclei swap their spins. If the lifetime (Δt) of a particular spin state is very brief there will be an associated

distribution of energies (ΔE) for the process as defined [279] by the Heisenberg uncertainty principle:

$$\Delta t = (h/2\pi.\Delta E) = (1/2\pi.\Delta v)$$
(2.40)

If relaxation is too slow, the nuclear spin state population becomes saturated and the absorption signal disappears [279]. If relaxation is too rapid, line broadening occurs and the NMR signal may disappear into the spectral baseline [279]. Each proton in a particular molecular environment finds itself in a unique magnetic field, and, hence, energy state. When a molecule is placed in an applied field (B_0), orbital currents are induced in the electron clouds of each atom which give rise to (small) local magnetic fields [279]. Such local fields are proportional to B_0, but the field vectors are opposite in direction [279]. Each magnetic nucleus is in effect partially shielded from the applied field by the electrons and requires a slightly higher value of B_0 (or a slightly lower frequency, v) to achieve resonance [279]. The effect of such nuclear screening is to decrease the energy difference (ΔE) between the nuclear energy levels. Non-equivalent protons attached to adjacent carbon atoms in a molecule also interact via slight polarisations in the orbital motion of valence electrons [279]. If two nuclei of spin ½ are so coupled, each will ideally split the other resonance to a doublet since there is an equal probability of each finding the other's spin to be aligned with (+½), or opposed to (-½), the applied magnetic field [279]. In general, if a nucleus of spin ½ has n equivalent neighbouring atoms of spin ½, its resonance will be split into $n + 1$ peaks. Ideally, the relative intensities of the absorption peaks can be predicted from a binomial of the form $(a + b)^n$, where n is the number of equivalent neighbouring atoms. For example, coupling between a single proton with three identical adjacent protons will ideally yield a quartet (relative intensities 1:3:3:1) absorption, whilst the resonance from the group of three equivalent nuclei will be a (1:1) doublet [279]. The strength of the coupling, denoted by the intra-molecular spin-spin coupling constant, J (Hz), is independent of the applied field strength and each J value is determined from the absorption peak-spacing [279].

The difference in absorption frequency between a given proton and the proton of an internal reference material is commonly quoted and these chemical shift parameters are dependent upon the proton's molecular environment [279]. Tetramethylsilane,

TMS, is a suitable internal reference material [279]. The strong singlet absorption from the protons in TMS is conventionally classified as resonating at a frequency, ν (Hz), of zero. The chemical shift, δ (ppm), of a given proton [279] can then be calculated from:

$$\delta\ (ppm) = \frac{[\nu(sample) - \nu(TMS)].10^6\ (Hz.)}{Instrument\ frequency\ (Hz.)} \qquad (2.41)$$

Continuous wave (CW) ^{1}H NMR spectrometers [279] were the first models to be developed, and these instruments contained; an electromagnet that generated a stable homogeneous magnetic field, a radio-frequency (RF) oscillator that provided EM radiation of stable radio-frequency, and a receiver to detect the absorption of energy [279]. The frequency of the radiation was kept constant and the applied magnetic field was swept by passing a small current through the sweep coils of the magnet [279]. The majority of modern NMR spectrometers utilise the Fourier transform (FT) technique (FTNMR) [279]. Samples are subjected to discrete pulses (of μs lifetimes) of radiation that are impinged on to the sample at set intervals [279]. A wide range of radio-frequencies are generated by a pulse of EM radiation, as defined by the Heisenberg uncertainty principal (equation 2.40). Consequently, all nuclei are simultaneously excited by the pulse of radiation and energy is absorbed by the sample [279]. When the radiation is switched off the pulse-induced magnetism decays as the nuclei relax and the thermal Boltzmann distribution of energy state populations is restored [279]. This process is named free induction decay (FID) [279] and the RF detector senses an exponentially decaying signal consisting of superimposed sine waves of variable amplitude and periodicity [279], each corresponding to the resonance frequency of a given nucleus (or set of equivalent nuclei). Fourier transformation of the FID signal interferogram evaluates the individual frequencies that contributed to the pattern of the interferogram [279]. Fourier transform operations allow the NMR absorption information to be plotted as a function of time (the interferogram) or as a function of frequency (chemical shift) [279]. The intensity of an absorption signal is directly proportional to the number of equivalent nuclei of that type in the molecule [279], and the relative number of protons in each molecular environment are obtained from spectral integration [279]. NMR spectra are plotted as graphs of absorption intensity versus chemical shift (δ).

Solution (ca. 10 wt. % solute) ^{1}H NMR spectra were recorded at ambient temperature with $CDCl_3$ as solvent and TMS as an internal reference. 250 MHz and 100 MHz ^{1}H FTNMR spectra were recorded on Jeol FX100 and Bruker spectrometers, respectively. The spectra were typically the result of 30-50 accumulations, recorded over 2 kHz, with a pulse width of 5 µs and an acquisition time of 2 s, with no additional pulse delay. Spectra were sampled using 16 k data points.

2.8.8 - ^{13}C NUCLEAR MAGNETIC RESONANCE (NMR) SPECTROSCOPY

^{13}C NMR spectroscopy analysis was introduced [279, 280] after pulsed ^{1}H FTNMR techniques had been originally developed [280]. Both ^{13}C and ^{1}H nuclei have angular momenta (*I* values) of ½, but the ^{13}C nucleus has a lower gyromagnetic ratio, γ, (0.67 for ^{13}C and 2.67 for ^{1}H) than the proton [279]. Consequently, at the same applied field strength (B_0) there is a smaller energy difference between the two nuclear spin-states (equation 2.38), and a smaller equilibrium population difference is found, therefore, for the ^{13}C nucleus [279]. The ^{13}C isotope is 0.016 times as sensitive [279] to detection as the proton. The ^{13}C nucleus also occurs in lower natural abundance (1.07 atom % of all carbon) than the proton (99.98 atom % of all hydrogen) and so, overall, the ^{13}C nucleus is approximately 6000 times less sensitive than the proton for NMR analysis [279].

One advantage of ^{13}C NMR spectroscopy over ^{1}H NMR is that the range of absorption frequencies (energies) for carbon nuclei varies to a greater extent with their molecular (chemical) environment, as compared with the frequency range observed for the vast majority of proton nuclear transitions [279]. In general terms, ^{13}C nuclei are found to resonate over a chemical shift, δ (relative to TMS), range of 0-200 ppm, whereas proton resonances are, generally, observed over a δ range of 0-10 ppm [279]. Consequently, ^{13}C NMR spectra are often more facile to interpret than ^{1}H NMR spectra because overlapping between absorption signals is less probable [279, 280] in ^{13}C NMR. Spin-decoupling effects also allow for a more facile interpretation of ^{13}C NMR spectra [279], compared with ^{1}H NMR analysis. Spin-spin coupling between adjacent ^{13}C nuclei is not generally observed, due to the low concentration of the ^{13}C isotope in natural abundance spectra. Additionally, ^{13}C NMR spectra are usually

obtained [279], in the first instance, with broad-band decoupling of the protons. By this technique, all of the protons in the sample are subjected to continuous irradiation, which significantly reduces their nuclear spin lifetimes [279]. Consequently, all of the ^{13}C nuclei are decoupled from their neighbouring protons, and, hence, the signal detected from each ^{13}C atom appears as a singlet [279]. Broad-band proton decoupling also enhances an absorption signal by conversion of ^{13}C multiplets into singlet absorptions [279]. For example, the resonance from the ^{13}C nucleus of a methylene ($^{13}CH_2$) group (with an idealised triplet resonance of 1:2:1 intensity ratio, in the absence of proton decoupling) would become, in ideal terms, a singlet of relative intensity 4. In practice, such resonances are often more intense than would have been predicted [279], because broad-band decoupling also affects the relative populations of the thermal spin-state distribution [279]. This is known as the nuclear Overhauser effect (NOE) [280] and the absorption intensities of decoupled ^{13}C NMR spectra normally give non-quantitative data for the relative number of non-equivalent carbon nuclei within the sample (as opposed to ^{1}H NMR where spectral integration gives the relative number of protons in a given local environment) [279].

Solution (ca. 10 wt. % solute) ^{13}C NMR spectra were recorded with $CDCl_3$ as solvent and TMS was used as an internal reference. Proton-decoupled ^{13}C FTNMR spectra were recorded at 25 MHz on a Jeol FX100 spectrometer. The spectra (recorded at ambient temperature) were typically the result of 25-50 k accumulations, recorded over 5 kHz, with a pulse width of 5 μs and an acquisition time of 1 s, with no additional pulse delay. Spectra were sampled using 16 k data points.

2.8.9 - PHOTON CORRELATION SPECTROSCOPY (PCS)

Photon correlation spectroscopy (PCS) is a dynamic light scattering technique [281] that can be used to measure the average particle size (and particle size distribution) of polymer emulsions. The PCS apparatus calculates the particle size from measurement of the sample diffusion coefficient. Random collisions between latex particles and water molecules caused by thermal energy (Brownian motion) lead to random particle movement and subsequent diffusion of the latex particles through the dispersion. For a colloidal dispersion of given viscosity, the rate of diffusion (at constant temperature)

or the diffusion coefficient, D (m^2 s^{-1}), is inversely related to the (average) particle size according to the Stokes-Einstein [282] equation:

$$D = \frac{kT}{3d\pi\eta} \qquad (2.42)$$

where k is the Boltzmann constant (J K^{-1}), T is the temperature (K), d is the equivalent hydrodynamic particle diameter (m), and η is the viscosity of the medium (Pa s).

Photon correlation spectrophotometers are comprised of a monochromatic (laser) light source, an optical system to focus the incident beam, a photomultiplier detector and a microprocessor. Dilute (< 0.2 wt. % solids) latex samples are illuminated by the laser and the scattered light intensity is measured by the (fixed angle) photomultiplier [281]. Scattering of light, at a given instant, leads to an interference pattern. The intensity of light detected by the photomultiplier depends on the interference pattern which, in turn, is dependent on the relative positioning of the polymer particles [281]. As the particles diffuse, their positions relative to one another change causing a constantly fluctuating interference pattern and hence a varying light intensity at the detector [281]. Large particles change positions slowly and cause slow intensity fluctuations at the detector [281], whereas small particles cause rapid fluctuations in intensity [281]. Spectrophotometers measure the fluctuation in the number of scattered light photons and size particles by characterising the timescale of the intensity fluctuations [281]. The timescale of the intensity fluctuation in the light scattered by the diffusing particles is evaluated by computation of the autocorrelation function (G_τ) [281] of the scattered light intensity:

$$G_\tau = < I_t \cdot I_{(t + \tau)} > \qquad (2.43)$$

where I_t is the intensity at time, t, $I_{(t + \tau)}$ is the intensity at time, t + τ, τ is the delay time, and < > represents the time average.

If the autocorrelation function (acf) has a high value, there is a strong correlation between the intensity at any instant compared to that at a time, τ, later, i.e. the particles have diffused only a short distance in the interval between the measurements [281]. Thus, an acf that remains high for a long time interval (τ) indicates that large

particles are in the dispersion [281]. Computation of G_τ for a wide range of delay times allows quantitative measurement of the rapidity of scattered light fluctuations in the sample [281]. This measure of the timescale of fluctuations (the decay time) is directly related to the particle size. If the particles of the dispersion are the same size and shape (monodisperse), the acf of the scattered light intensity is a single decaying exponential [281] (equation 2.44). The measured acf always resembles a decaying exponential [281]. For polydisperse samples the acf is the sum of a number of exponential decays for particles of each size [281]. Mathematical analysis of this composite acf gives the relative proportion of particles of each size in the sample, and, hence, the average particle size and size distribution [281].

$$G_\tau \propto \exp[-2.\Gamma_i(d_i).\tau] \qquad (2.44)$$

where $\Gamma_i(d_i)$ is the decay constant (the inverse of the decay time) for particles of diameter, d_i. The decay constant is related to the diffusion coefficient (D) by [281]:

$$\Gamma_i(d_i) = D.K^2 \qquad (2.45)$$

$$K = 4\pi\sin(\frac{\theta}{2}) \cdot (\frac{n}{\lambda}) \qquad (2.46)$$

where θ is the angle between the transmitted beam and photomultiplier, n is the refractive index of the medium and λ is the laser wavelength in vacuo (m).

Latex samples were analysed by a Malvern Instruments Zetamaster S spectrophotometer at ambient temperature. The samples were illuminated by a 4 mW helium-neon laser light source (wavelength 633 nm). Intensities of scattered radiation were measured at a fixed angle of 90°. One drop (from a 2.5 cm^3 Pasteur pipette) of each latex (20 wt.% solids) was diluted into approximately 5 cm^3 of deionised water. Samples were then transferred to polystyrene cuvettes (5 cm^3 volume). Cuvettes were then placed in to the spectrophotometer's sample holder and each sample was left to stand for a period of at least ten minutes before initiation of the PCS analysis.

CHAPTER 3

POLYSTYRENE MICROGELS

3.1 - PS MICROGELS FROM EMULSION COPOLYMERISATION

Sequential polystyrene/poly(*n*-butyl acrylate) interpenetrating polymer network (IPN) microgel particles were to be investigated within this project. Composite, structured, latex particles (sections 1.6.3 and 1.6.4) can be synthesised from sequential emulsion polymerisation processes. The morphology of composite latex particles has been found to be influenced by many physical parameters (section 1.6.3), although the presence of the aqueous, continuous, phase has been considered to play a fundamental role in the development of particle structure. In general terms, the more hydrophilic polymer component is found as a shell which overcoats a hydrophobic polymer core. Interpenetrating polymer networks (IPNs) are unique kinds of polymer blend which can show significant degrees of molecular mixing between the two, or more, polymer components (section 1.4). The employment of a sequential emulsion polymerisation process for IPN synthesis (section 1.6.4) often yields materials which exhibit significant degrees of phase separation, however. Consequently, sequential IPN microgels were to be synthesised from copolymerisation of second-stage comonomers within organic microgel dispersions within this project. It was anticipated that such composite microgel particles would show increased mixing between the two polymer components, when compared to latex IPNs synthesised from sequential emulsion polymerisation. The experimental procedure for the synthesis of organic sequential IPN microgel dispersions requires the initial synthesis of first-stage polymer microgel particles. These microgels are subsequently dispersed in an organic diluent and second-stage comonomers are then added to the system. Free radical copolymerisation of second-stage comonomers within the first-formed particles would then finally be required for the synthesis of IPN microgels. Emulsion copolymerisation of styrene/divinylbenzene (DVB) has been found by several authors to be a suitable method for synthesising polystyrene microgel particles in high yield [202-204]. Consequently, the PS microgels synthesised in this particular investigation were prepared from emulsion copolymerisation techniques.

A series of four polystyrene latices, prepared with 0 weight % (wt.%), 1 wt.%, 5 wt.% and 10 wt.% DVB, was synthesised using 4,4'-azobis(4-cyanovaleric acid), ACVA, as polymerisation initiator (section 2.2.1). Yields of PS microgels were

determined gravimetrically (section 2.2.2) and latex samples were characterised by photon correlation spectroscopy, PCS (section 2.8.9). Experimental yields and latex particle sizes (25°C) are given in table 3.1.

Table 3.1 - Polystyrene Microgel Yields and Latex Particle Sizes (25°C)

Latex	Yield (Weight %)	Particle Size (nm)
Polystyrene homopolymer	95	54
PS (1 wt.% DVB)	93	50
PS (5 wt.% DVB)	95	51
PS (10 wt.% DVB)	95	48

Latex non-volatile component analysis indicated that each of the polymerisations had proceeded to high conversion (table 3.1). Particle size distribution data obtained from PCS analysis of the PS (5 wt.% DVB) microgel latex is shown in appendix 2. The particle size values listed in table 3.1 are z-average particle diameters (the z-average root-mean-square radius of gyration for the polymer particles [283]). Each microgel latex had an average particle diameter of approximately 50 nm and the distribution of particle sizes within each latex sample was relatively narrow, as illustrated by the size distribution curve (appendix 2).

3.2 - DSC CHARACTERISATION OF PS MICROGEL PARTICLES

Purified, dry, latex particles (section 2.2.2) were analysed by differential scanning calorimetry, DSC (section 2.8.1), over a 20-240°C temperature range. The glass transition temperature (T_g), the temperature at which polymer molecules possess sufficient thermal energy to undergo main-chain segmental relaxation processes [256], can often be obtained from DSC analysis of polymer samples [256, 257]. On heating an amorphous, glassy, polymer specimen to a temperature above its T_g, a small shift in the heat flow curve (section 2.8.1) is observed when the sample temperature passes through the polymer's glass transition [256]. This minor endothermic event (which illustrates that the change in the polymer's specific heat capacity during the transition is of low magnitude [256]) is characteristic of the glass transition [256]. DSC thermograms for polystyrene homopolymer and PS (10 wt.% DVB) microgel samples are shown in figures 3.1 and 3.2, respectively.

Figure 3.1 - DSC Thermogram for Polystyrene Homopolymer
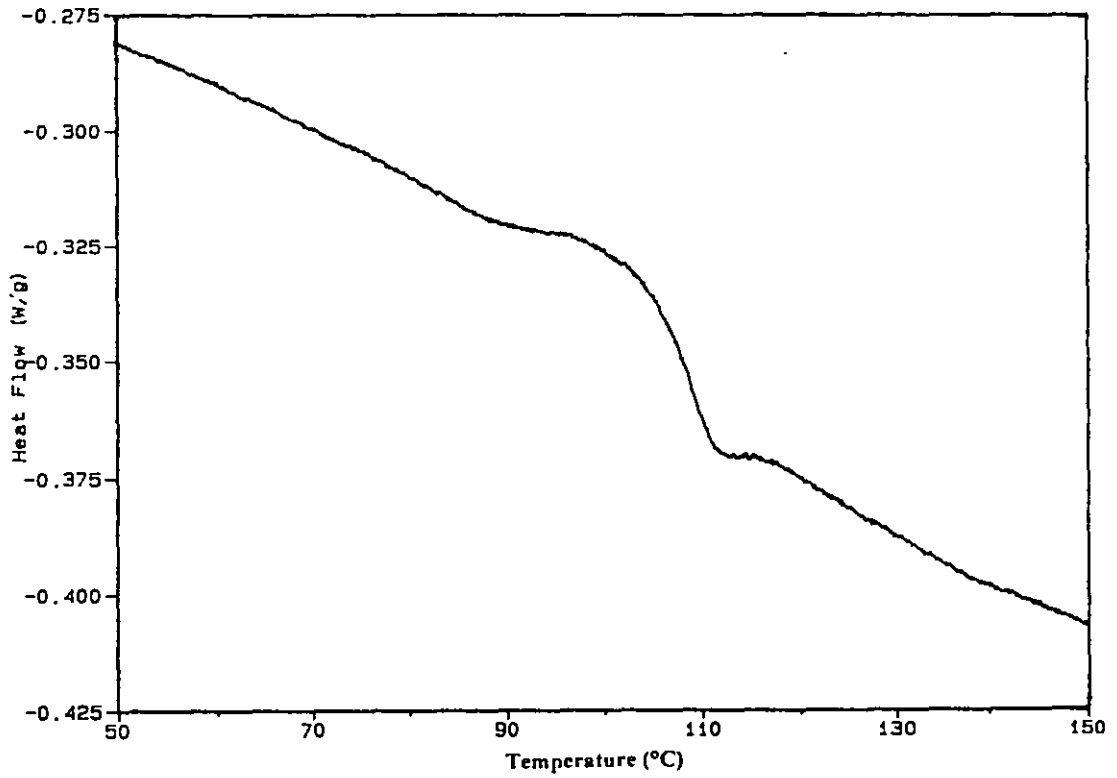
Figure 3.2 - DSC Thermogram for PS (10 wt.% DVB) Microgel
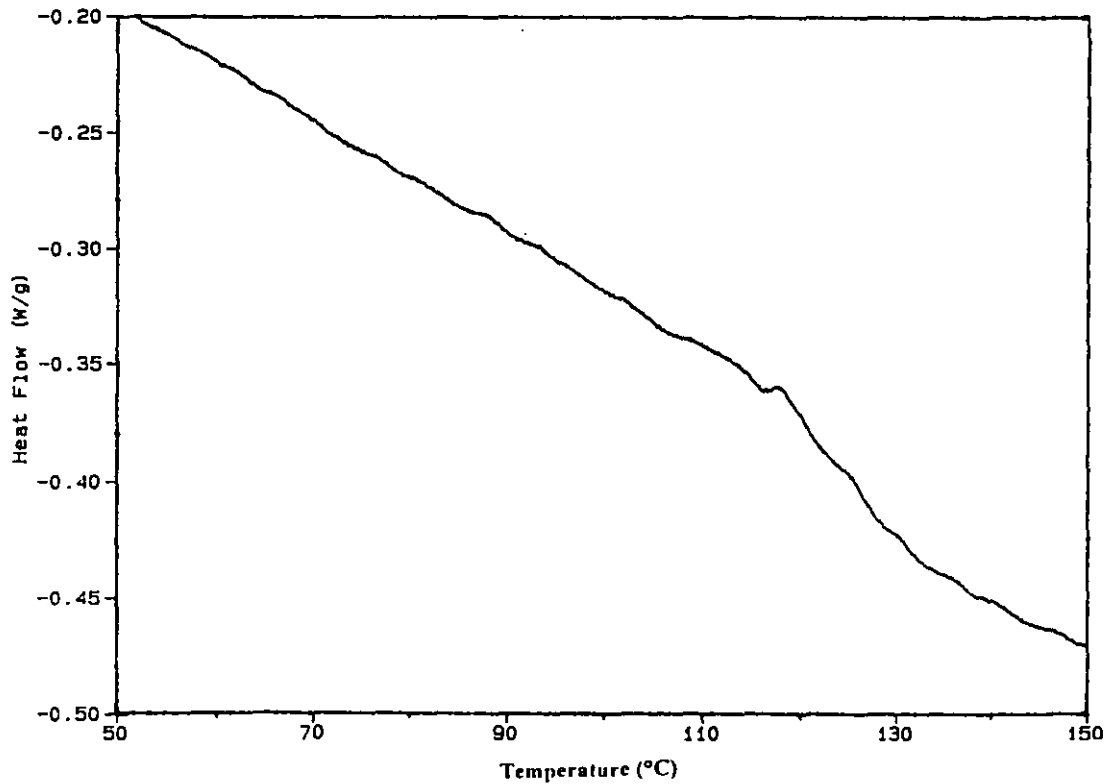
The T_g of each polymer specimen was measured as the temperature at which the heat flow curve exhibited a point of inflection [256]. Glass transition temperatures obtained from DSC analysis of the four polystyrene-based samples are presented in table 3.2.

Table 3.2 - Polystyrene Glass Transition Values from DSC Analysis

Polymer Sample	Glass Transition Temperature, T_g (°C)
Polystyrene homopolymer	104
PS (1 wt.% DVB)	103
PS (5 wt.% DVB)	117
PS (10 wt.% DVB)	126

The glass transition temperature of the PS homopolymer sample is in good agreement with T_g values reported in the literature [257, 284] from DSC analysis of high molecular weight atactic polystyrene. No discernible shift in T_g was observed on copolymerising styrene with 1 weight % divinylbenzene. Endotherms recorded for PS (5 wt.% DVB) and PS (10 wt.% DVB) microgels were observed at higher temperatures than the linear polystyrene transition. This observation would appear to indicate that incorporation of DVB within polystyrene latex particles had lead to the formation of microgel structures [261, 264], as discussed within section 3.3.

3.3 - DMTA CHARACTERISATION OF POLYSTYRENE MICROGELS

Polystyrene sheets, prepared from compression moulding of dried latex samples (section 2.2.2), were characterised by dynamic mechanical thermal analysis (section 2.8.2), DMTA, over a 20-200°C temperature range (measurements were recorded with a heating rate of 3°C per minute - at a fixed frequency of 10 Hz). A coherent sheet suitable for DMTA characterisation could not be obtained via hot-pressing of the PS (10 wt.% DVB) microgel particles. It would appear that this material was too highly crosslinked to allow for substantial polymer sheet integration. Plots of loss tangent (tanδ) versus temperature (section 2.8.2) for the polystyrene, PS (1 wt.% DVB) and PS (5 wt.% DVB) microgel samples are shown in figures 3.3, 3.4 and 3.5, respectively. Glass transition (α-relaxation) parameters (the maximum value of the

loss tangent, tanδ$_{MAX}$, which is found to occur at the glass transition temperature, T$_g$) obtained from DMTA characterisation of the three polystyrene samples are given in table 3.3.

Figure 3.3 - Tanδ with Temperature Curve for Polystyrene
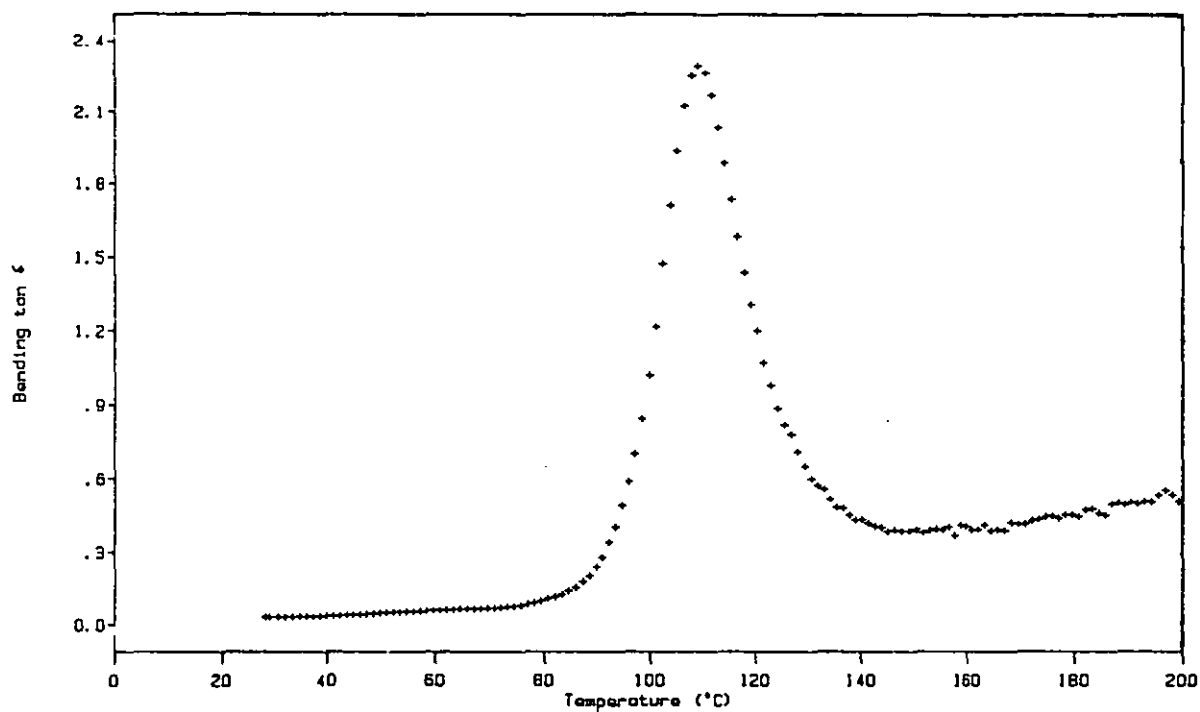
Figure 3.4 - Tanδ with Temperature Curve for PS (1 wt.% DVB) Microgel
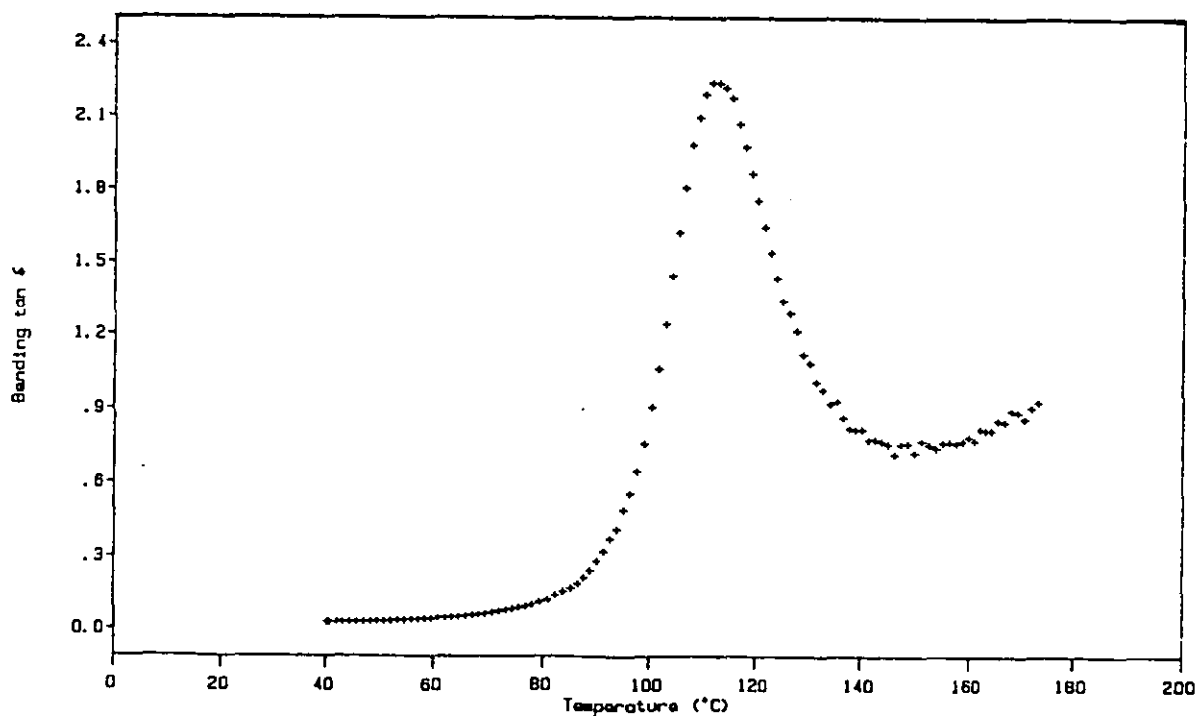
Figure 3.5 - Tanδ with Temperature Curve for PS (5 wt.% DVB) Microgel
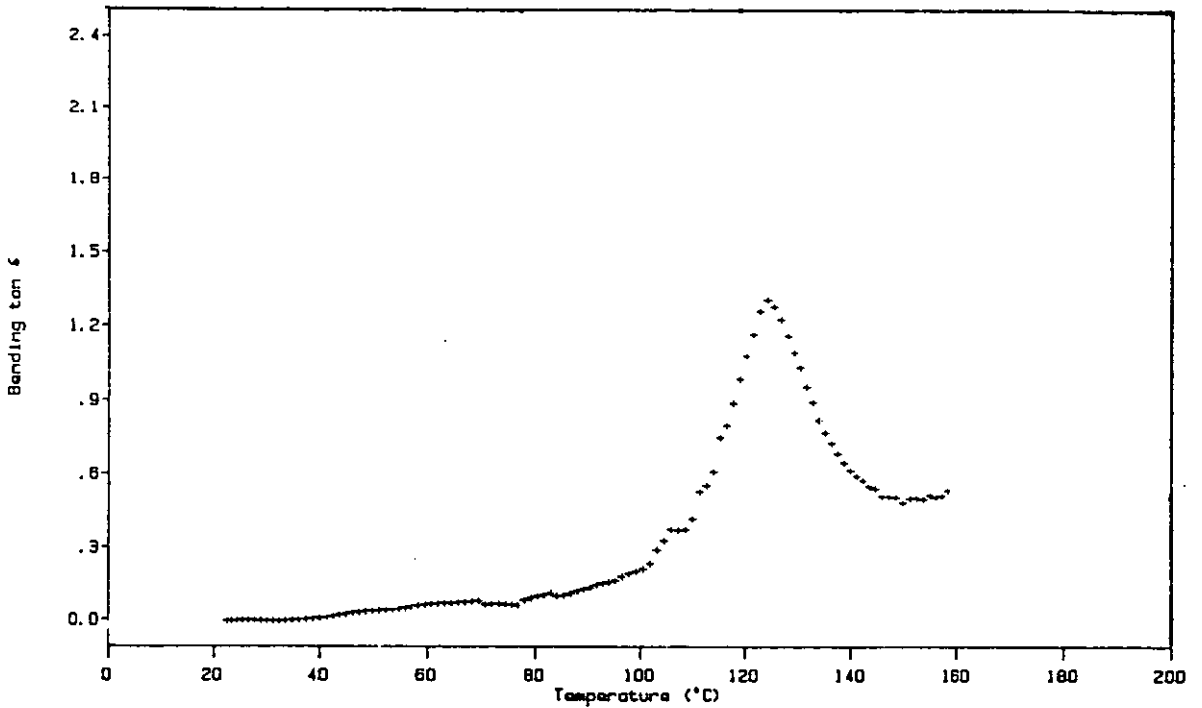
Table 3.3 - Polystyrene Glass Transition Temperatures from DMTA

Sample	$Tan\delta_{MAX}$	T_g (°C) at 10 Hz
Polystyrene	2.3	109
PS (1 wt.% DVB)	2.2	113
PS (5 wt.% DVB)	1.4	123
PS (10 wt.% DVB)		

The increased glass transition temperature recorded for polymer samples from DMTA, when compared to the T_g recorded from DSC (section 3.2), is attributed to time-temperature equivalence phenomena (section 2.8.2) [265]. As can be seen from the contents of table 3.3, DMTA observations indicated that an increase in the concentration of divinylbenzene for the emulsion copolymerisation process had lead to an increase in the material's glass transition temperature. The $tan\delta_{MAX}$ value also decreased in magnitude as the DVB content of the specimen increased.

A shift in the glass transition to a higher temperature is observed on crosslinking a polymer sample [261, 264] (unless the material's crosslink-density is of such a high

value that the glass transition is suppressed completely [261]). This T_g-shift phenomenon is commonly considered [264] to result from free volume effects [285]. The total macroscopic volume of a polymer specimen (v) has been considered [285] to comprise of one volume component, v_0, which represents the actual molecular volume of the polymer molecules (the occupied volume), and a second volume element, v_f, which equates to the volume of sample which is occupied by voids or holes [285], the free volume (i.e. $v_f = v - v_0$). It has been postulated that the occupied volume increases linearly with temperature on heating a glassy polymer specimen to its glass transition temperature [285]. At the glass transition temperature a discontinuity in the polymer's thermal expansivity (α) arises [256]. This process has been considered to promote a sudden expansion in the sample's free volume [264] at T_g, which signifies that molecular relaxations which control the viscoelastic behaviour of a polymer sample commence at T_g [256]. The introduction of intermolecular crosslinks between polymer chains can be considered to reduce the free volume of the system [264], as chemical crosslinks force adjacent chains to become closer together, thereby raising the glass transition temperature of the material [264].

The physical properties of a given polymer network sample depend markedly upon the crosslink-density of the material [261]. The degree of crosslinking for a network is commonly represented by the average molecular weight between crosslinks, M_c (kg mol^{-1}), value [1]. Loosely crosslinked gels have large, and highly crosslinked materials have small M_cs, respectively [1]. Average molecular weights between crosslinks for rubber samples can be determined from stress-strain measurements [286]. Equilibrium swelling of networks with organic diluent is often a convenient method for determining M_c values for macrogel samples [261] (section 5.3). Shashoua and Beaman [227] evaluated M_c values for poly(styrene-*co*-divinylbenzene) microgels prepared from emulsion copolymerisation by determining the light scattering behaviour of benzene-swollen microgel particles [227]. The volume fraction of polymer (ϕ_2) within organic liquid-swollen particles was evaluated from the ratio of the cubes of the (spherical) particle diameters in water and benzene [227]. It was assumed that each microgel particle would follow the theoretical equilibrium swelling behaviour of macrogel samples [227] (the Flory-Rehner [167] approach to network swelling) and M_c values determined for microgel samples were found to be in

excellent agreement with theoretical network M_c's [227] (the M_c value for homogeneous networks where all divinyl units are incorporated within crosslinks [287]).

Nielsen [261] has compared T_g-shift upon crosslinking data and M_c values from physical property measurements, gathered from a series of reports [288-290] detailing macrogel sample characterisation. By averaging all of these experimental results [261], an equation for estimating M_c from the shift in T_g on crosslinking was derived:

$$M_c = A / (T_g - T_{g0}) \tag{3.1}$$

where A is a constant ($A \approx 39$ °C kg mol^{-1}) [261], and T_g (°C) and T_{g0} (°C) are the glass transition temperature of the network polymer and the linear polymer analogue, respectively [261].

Theoretical M_c values (M_c^{calc}) for idealised poly(styrene-co-divinylbenzene) copolymer networks were evaluated [287] from the following relation:

$$M_c^{calc} = m / 2x \tag{3.2}$$

where m is the relative molecular mass (kg mol^{-1}) of the monovinyl comonomer (styrene) and x is the mole fraction of divinyl comonomer (DVB) in the network [287].

Theoretical average molecular weight between crosslinks [287] and M_c values estimated from DMTA T_g-shifts [261] (equation 3.1 and table 3.3) for PS (1 wt.% DVB) and PS (5 wt.% DVB) microgel samples are detailed in table 3.4.

Table 3.4 - Theoretical and Experimental Network M_c Values for PS Microgels

Microgel Sample	M_c^{calc} (kg mol^{-1}) [287]	M_c (kg mol^{-1}) [261]
PS (1 wt.% DVB)	11.8	9.8
PS (5 wt.% DVB)	2.4	2.8

It would appear, from the close agreement between the theoretical and experimental M_c values, that the network structures of these two microgel samples were relatively

homogeneous and that a large proportion of the DVB molecules incorporated had formed crosslinks (if it is assumed that microgel particles behave similarly to macrogels in terms of their T_g-shift on crosslinking behaviour). In addition to the observed increase in microgel glass transition temperature, a reduction in the magnitude of $\tan\delta_{MAX}$ was also observed as the crosslink-density of the network increased (table 3.3). Similar dynamic mechanical behaviour has been reported for many [261, 264] polymer systems on crosslinking. The loss tangent, $\tan\delta$ (section 2.8.2), represents the ratio between the dynamic loss (E") and dynamic storage (E') moduli, i.e. $\tan\delta = (E''/E')$ [264]. The loss modulus quantifies the energy dissipated by the sample during deformation and the storage modulus equates to the energy stored in the specimen [264]. The storage modulus (E') increases, thereby leading to a reduced $\tan\delta_{MAX}$ value, as the crosslink-density of the material increases [218]. This phenomenon is a consequence of the elastic response of lightly crosslinked polymers [1, 264] at temperatures above T_g.

3.4 - GPC CHARACTERISATION OF POLYSTYRENE MICROGELS

Gel permeation chromatograms were recorded for dilute dispersions of the three microgel samples (section 2.8.3). A chromatogram was also recorded for a dilute polystyrene solution. Tetrahydrofuran (THF) was the chromatographic eluent and the gel permeation chromatograph was calibrated with monodisperse polystyrene standards (section 2.8.3). The molecular weight distribution, W(M), versus log M curve (section 2.8.3) for the polystyrene homopolymer sample is shown in figure 3.6.

The elution volume of a polymer fraction incorporating molecules of mass, M, decreases when moving from the left hand side to the right hand side of the log M axis (figure 3.6). Polymer molecules of highest molecular weight elute from the columns first, as they have higher hydrodynamic radii than molecules of low molecular weight (section 2.8.3). As can be seen from the chromatogram for the polystyrene homopolymer sample (figure 3.6), the majority of the polymer molecules have molecular weights in the $4.5 \leq \log M \leq 6.0$ range. Chromatograms for the three polystyrene microgels are shown in figure 3.7.

Figure 3.6 - Polystyrene Molecular Mass Distribution Curve from GPC
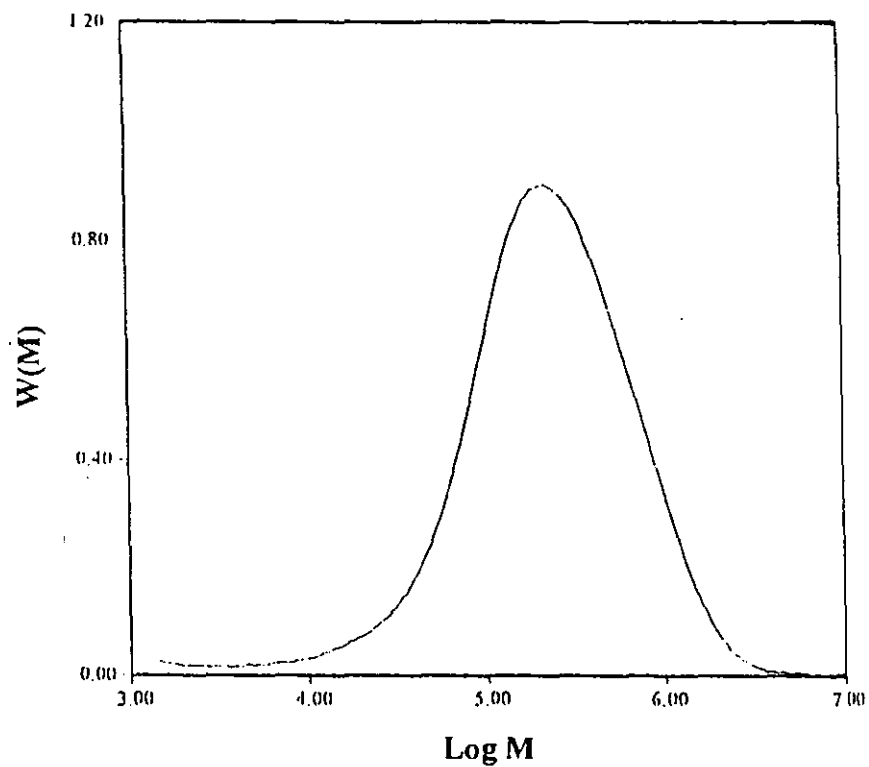
Figure 3.7 - Molecular Mass Distribution Curves for Polystyrene Microgels
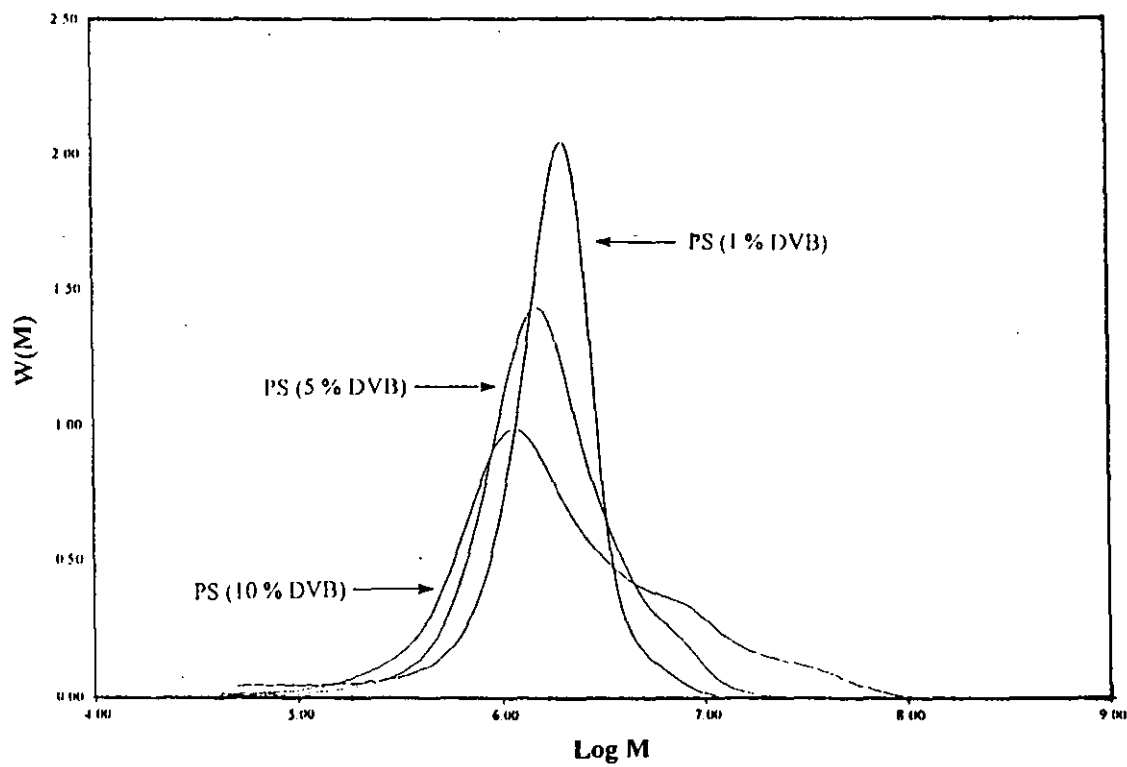
The PS (1 wt.% DVB) microgel particles appear to have a relatively narrow distribution of particle sizes in THF (the majority of the microgel particles elute in the $6.0 \leq \log M \leq 6.5$ range). If it is assumed that the hydrodynamic volumes of the microgel particles were not too large for the microgels to have undergone the size exclusion process (section 2.8.3), these THF-swollen particles can be considered to be relatively monodisperse in terms of particle size, and it would appear, therefore, that the crosslink-densities of the microgel particles were relatively homogeneous. The absence of significant molecular fractions eluting in the $4.5 \leq \log M \leq 6.0$ molecular weight range, suggests that the concentration of soluble (linear) polystyrene component in the PS (1 wt.% DVB) microgel sample was less than 5 weight % of the total polymer content [203]. The chromatogram peak is found to shift to higher elution volumes as the concentration of divinylbenzene in the microgel particles increases (figure 3.7). This behaviour suggests that the crosslink-density of the microgel particles increased as the DVB content increased. Microgels with highly crosslinked structures would be swollen to the lowest extent with organic dispersent [264] and, consequently, the particle sizes of microgel particles with high crosslink-densities would be smaller than the sizes of loosely-crosslinked particles. Polymer molecules are separated according to their hydrodynamic volume in solution by the chromatographic columns (section 2.8.3), with the largest molecules being the first fraction eluted from the chromatograph. The shift in the chromatogram peak to higher elution volumes, as the DVB content of the microgel increases, suggests that highly crosslinked particles are smaller in size than lightly crosslinked particles. The three aqueous microgel latices were all found to contain particles with average diameters of approximately 50 nm (section 3.1). The smaller average size of the highly crosslinked microgel particles, as determined from GPC analysis in THF, would appear, therefore, to have resulted from decreased organic liquid-swelling of these microgels. The chromatographs for the PS (5 wt.% DVB) and PS (10 wt.% DVB) microgel particles exhibited non-Gaussian behaviour at low elution volumes (figure 3.7), the curves tail-off at low elution volume (this effect is most pronounced for the 10 wt.% DVB formulation). This anomalous elution behaviour is attributed to the presence of microgel aggregates within these two (dilute) dispersions. Similar particle-clustering effects have been observed from GPC analysis of poly(styrene-co-divinylbenzene) microgel dispersions in dimethylformamide [203].

3.5 - MICROGEL CHARACTERISATION BY INFRARED SPECTROSCOPY

Polymer networks prepared from free radical copolymerisation of monovinyl/divinyl comonomers, e.g. styrene/divinylbenzene [22-24] and methyl methacrylate/ethylene glycol dimethacrylate [25, 26], are often found to contain unreacted, pendant, vinyl groups [34, 35]. The formation of pendant vinyls has been considered by several authors [34, 35, 39] to result from unequal vinyl group reactivities, where crosslinking (divinyl) comonomers are initially incorporated into polymer chains via the reaction of the first vinyl bond with a macro-radical [34]. The second, pendant, vinyl bond is subsequently considered to be less reactive than the vinyl groups of remaining monovinyl and divinyl comonomer molecules in the system [34, 39]. The network formation process is considered to compete with cyclisation, intramolecular crosslinking, phenomena [24, 33, 34, 39] (whereby pendant vinyls react with free radicals present on the same polymer chain [24, 39]), and preferential consumption effects [34-36, 39, 45] (the favoured incorporation of remaining comonomer molecules, with their more reactive vinyl bonds, into the polymer chain). Malinsky *et al.* [291] determined that the fraction of pendant vinyl groups in poly(styrene-*co*-divinylbenzene) copolymers was lower than expected (as predicted from the relative rates of reaction for all of the vinyl bonds in the system) at low copolymerisation conversions [291], whereas at high conversions the copolymers were found to contain a large excess of these unsaturated bonds. These observations were considered to reflect [291] the preference of pendant vinyl groups to undergo cyclisation reactions at low copolymerisation conversions [291], and it was postulated that at high conversions the mobility of copolymer chains was significantly hindered, whereby the reaction of remaining pendant vinyl groups became diffusion-controlled [291].

Bartholin *et al.* [292] characterised polydivinylbenzene microgels by infrared (IR) spectroscopy. Comparisons between the IR absorptions of polystyrene homopolymer, poly(DVB) microgels and poly(styrene-*co*-divinylbenzene) macrogels were made [292]. IR absorption band assignments were then evaluated for the poly(styrene-*co*-divinylbenzene) networks [292]. Okay *et al.* [45] estimated the pendant vinyl content of *p*-divinylbenzene microgels dispersed in chloroform, after having analysed *p*-isopropylstyrene solutions for IR calibration [45].

It was decided, therefore, that estimations of the pendant vinyl concentration within PS (1 wt.% DVB), PS (5 wt.% DVB) and PS (10 wt.% DVB) microgel particles should be made from IR spectroscopy analysis. The divinylbenzene used for microgel synthesis was of 55 weight % purity (a mixture of *m*- and *p*-divinylbenzenes), the remaining components are comprised mainly of ethylvinylbenzene isomers [209]. The maximum concentration of pendant vinyl groups that could be present, therefore, within the microgel particles prepared, would be of the order of 5.5 weight % of the total polymer content (corresponding to the 10 wt.% DVB microgel particles where each divinylbenzene molecule had been incorporated via the reaction of one vinyl bond only). Analysis of ethylbenzene/styrene mixtures was considered a suitable method for modelling the IR absorption behaviour of poly(styrene-*co*-divinylbenzene) microgels containing pendant vinyl groups. Consequently, mixtures of ethylbenzene/styrene with 1 wt.%, 2 wt. %, . , . , 5 wt.% styrene contents were analysed by Fourier transform infrared (FTIR) spectroscopy (section 2.8.5). The absorbance FTIR spectra of ethylbenzene and styrene are shown in figures 3.8 and 3.9, respectively.

Figure 3.8 - Absorbance FTIR Spectrum of Ethylbenzene
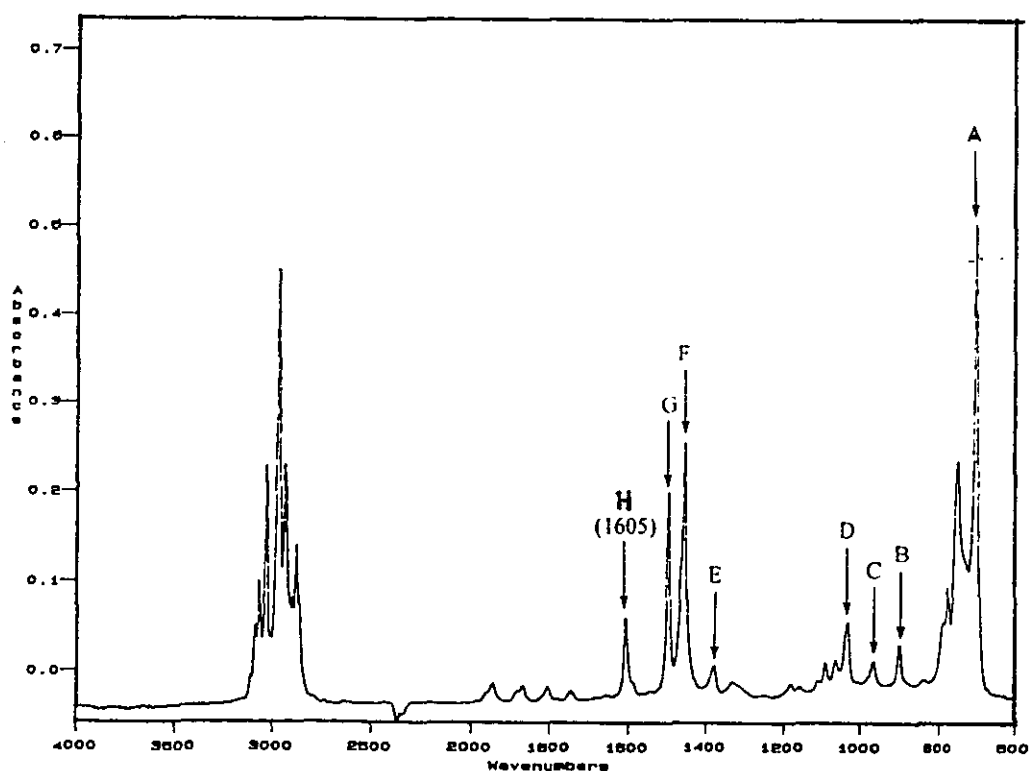
Figure 3.9 - Absorbance FTIR Spectrum of Styrene
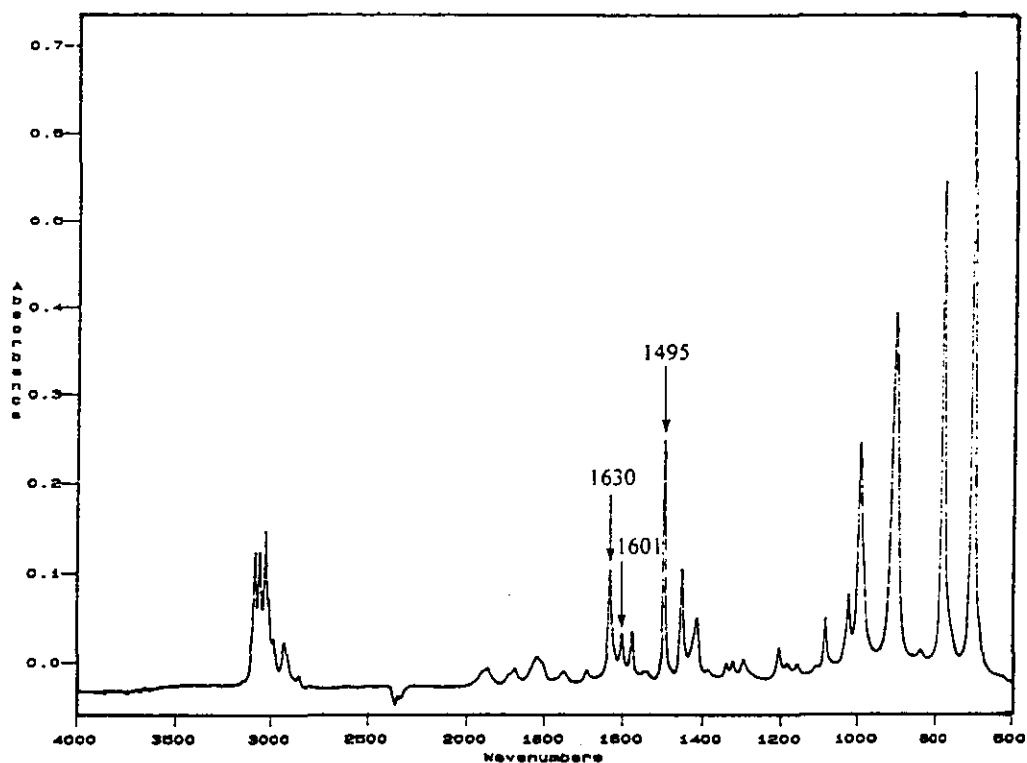
Absorption assignments for several of the ethylbenzene and styrene IR vibration modes [45, 270, 292] are shown in table 3.5.

Table 3.5 - IR Wavenumber ($\bar{\nu}$) Assignments for Specific Molecular Vibrations

Molecular Vibration	$\bar{\nu}$ (cm^{-1}) Ethylbenzene	$\bar{\nu}$ (cm^{-1}) Styrene
Aromatic C-C bond stretch	1497	1495
Aromatic skeletal vibration	1605	1601
Vinyl bond C=C stretch		1630

Several authors [45, 292, 293] have determined that the energy required for carbon-carbon double bond (C=C) stretching vibrations of pendant DVB groups in styrene/DVB copolymers corresponds to a radiation wavenumber of 1630 cm^{-1} (i.e. the vibration occurs at an identical wavenumber to the corresponding vibration in styrene monomer). A vibration from the (monosubstituted) aromatic ring of polymer-bound styrene groups is also commonly observed at 1602 cm^{-1} [292, 293] (i.e. this

vibration occurs at similar frequencies to the corresponding vibrations in ethylbenzene and styrene) during IR characterisation of polystyrene samples. A measurement of the absorbance ratio [270, 294], A_{1630}/A_{1605}, for ethylbenzene/styrene mixtures of known composition could have potentially enabled a determination of pendant vinyl concentrations in styrene/DVB microgels to be made, therefore (where the A_{1630}/A_{1602} ratio determined from IR analysis of microgel particles would have been converted into a pendant vinyl concentration, after referral to the ethylbenzene/styrene IR calibration curve [294]). Expanded regions (covering the 1550-1680 cm^{-1} wavenumber range) of the absorbance FTIR spectra of ethylbenzene, styrene and an ethylbenzene/styrene mixture containing 5 weight % styrene, are shown in figures 3.10, 3.11 and 3.12, respectively.

Figure 3.10 - Expanded Absorbance FTIR Spectrum of Ethylbenzene
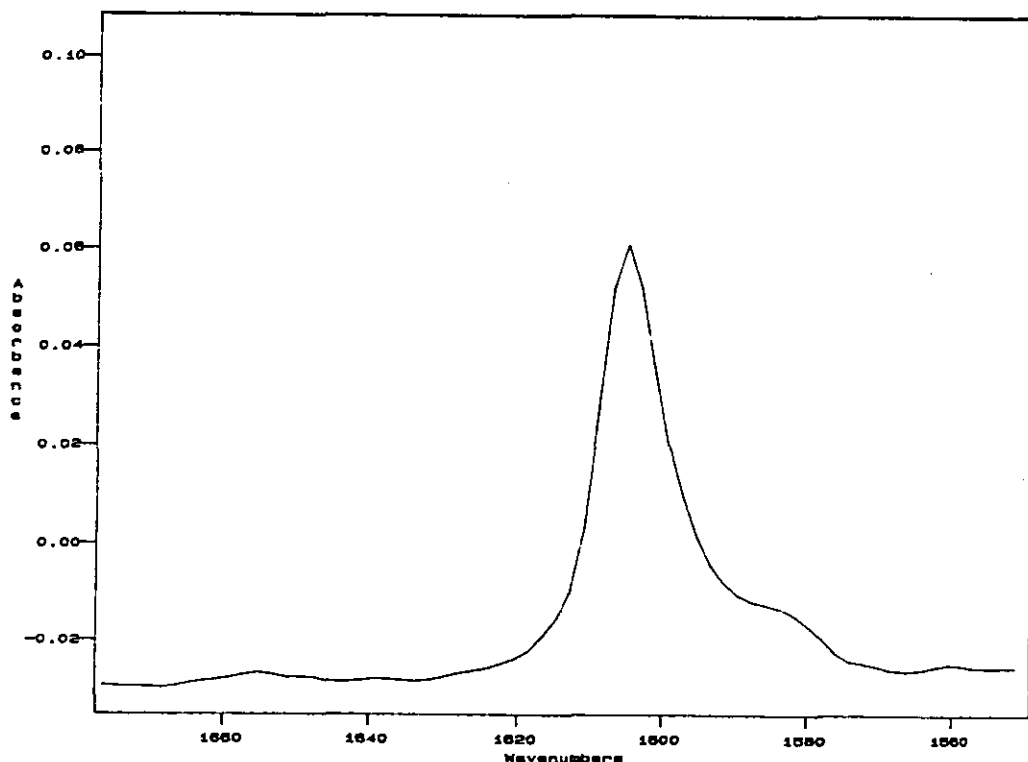
Figure 3.11 - Expanded Absorbance FTIR Spectrum of Styrene
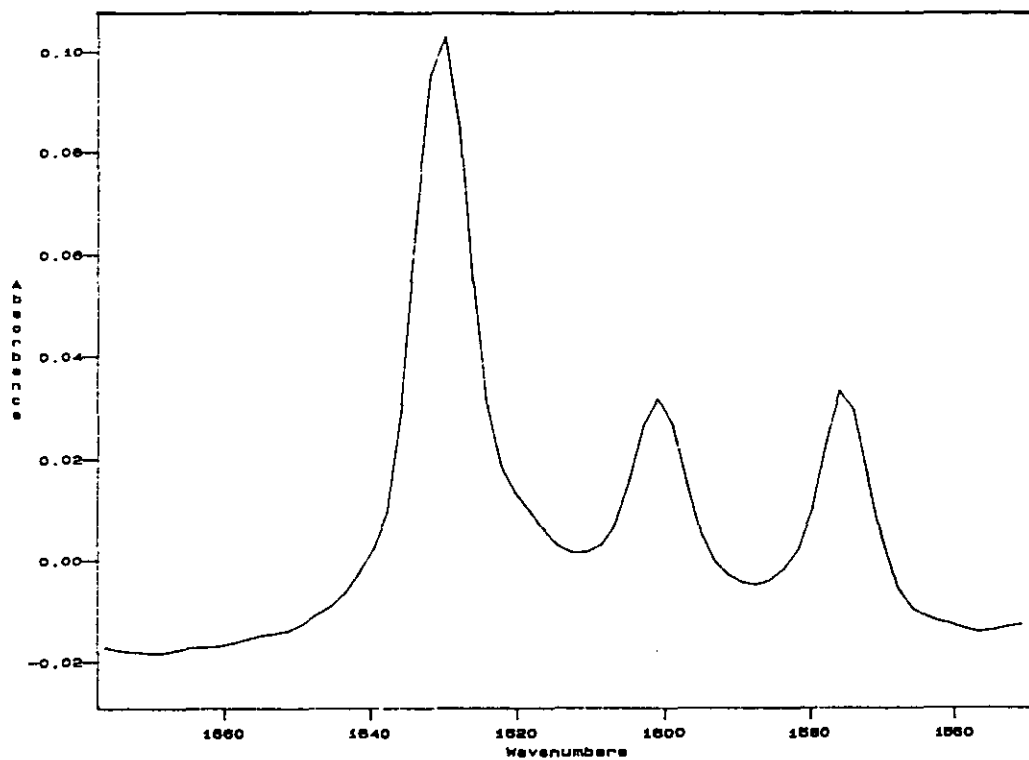
Figure 3.12 - Expanded Absorbance FTIR Spectrum of Ethylbenzene/Styrene Mixture (5 wt.% Styrene)
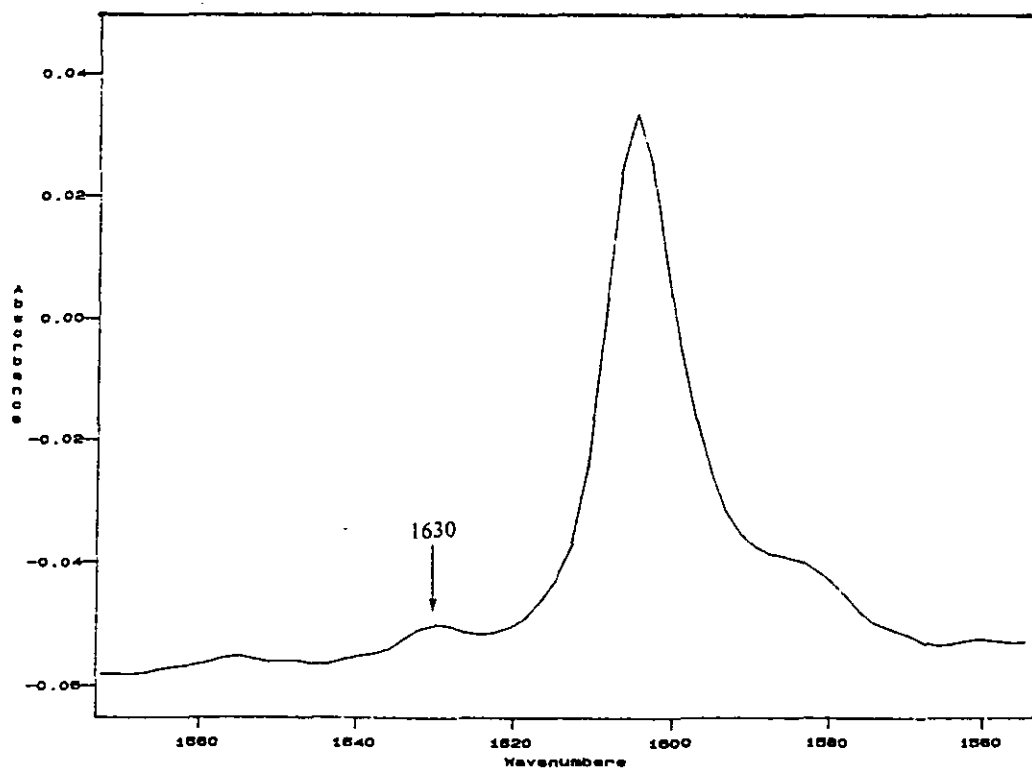
The exceptionally weak absorption from the vinyl bond of styrene in the ethylbenzene/styrene mixture with 5 weight % styrene content (figure 3.12) suggests that IR spectroscopy is not a suitable characterisation method for quantitatively determining the pendant vinyl group concentration within the PS (1 wt.% DVB), PS (5 wt.% DVB), and PS (10 wt.% DVB) microgel particles prepared in this investigation. It should be noted that this conclusion has been made with the assumption that the molar absorptivity (section 2.8.5) of the vinyl bond in styrene is identical to the absorptivity of pendant vinyl bonds (the unsaturated group which results from partial DVB incorporation) in styrene/divinylbenzene microgels. (Batzilla [295] has determined that the absorptivities of the vinyl bonds in *p*-isopropylstyrene and pendant vinyl bonds in styrene/DVB copolymers are of similar magnitude). It is possible that bromine titration [222] experiments could allow for a more accurate estimation of the concentration of residual unsaturated groups within these microgel particles.

Although the unsaturated bond concentration in PS (1 wt.% DVB), PS (5 wt.% DVB) and PS (10 wt.% DVB) microgels could not be quantitatively determined from FTIR analysis, a number of characteristic vibrations from the crosslinking agent (DVB) can be observed [292] from infrared spectroscopy techniques. Samples of polystyrene and the three PS microgels were characterised, therefore, by diffuse reflectance infrared Fourier transform (DRIFT) spectroscopy [296, 297] (section 2.8.6). The DRIFT spectrum recorded for the polystyrene homopolymer sample is shown in figure 3.13.

The FTIR spectrum of ethylbenzene (figure 3.8) and the DRIFT spectrum of polystyrene (figure 3.13) show a number of vibrations which occur at similar vibrational frequencies. The common IR characteristics of these materials are attributed primarily to vibrational modes associated with the monosubstituted aromatic ring of ethylbenzene and polystyrene [270, 292]. Several of the vibrational frequencies determined for the two materials from IR analysis are listed in table 3.6.

Figure 3.13 - DRIFT Spectrum of Polystyrene Homopolymer
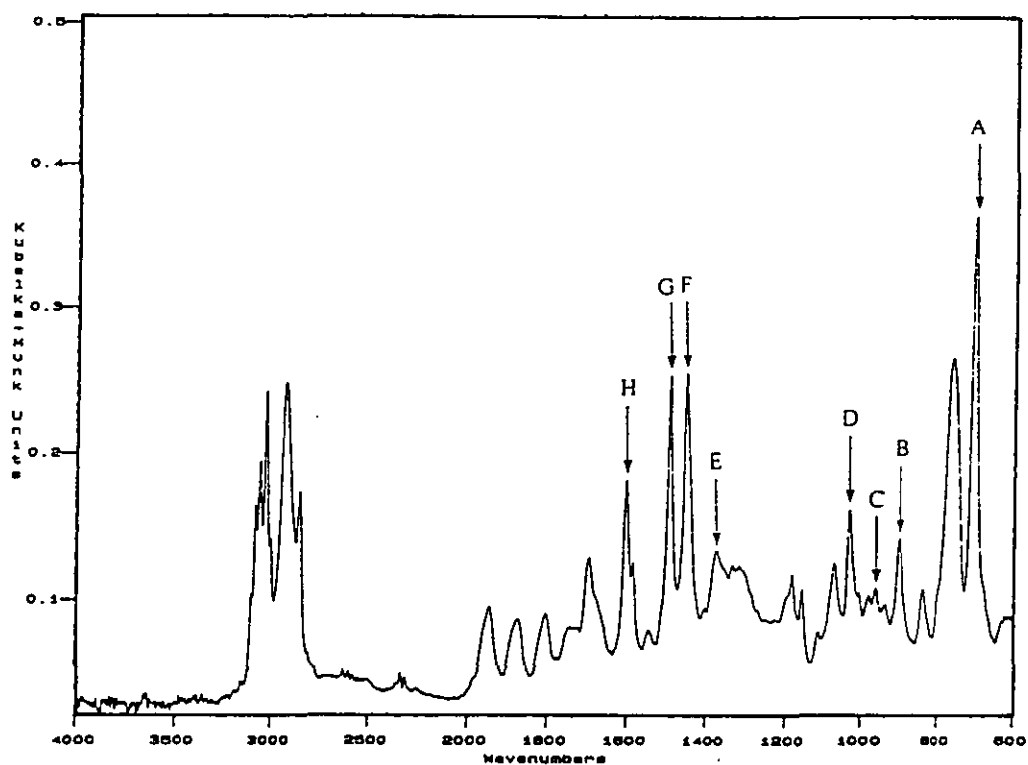
Table 3.6 - Wavenumber ($\bar{\nu}$) Values for Vibrations in PS and Ethylbenzene

Vibration Label	$\bar{\nu}$ (cm^{-1}) Polystyrene	$\bar{\nu}$ (cm^{-1}) Ethylbenzene
A	698	698
B	906	905
C	964	964
D	1028	1030
E	1372	1375
F	1453	1454
G	1493	1497
H	1601	1605

The aromatic C-C stretching frequency of the polystyrene sample (1493 cm^{-1}), determined from DRIFT spectroscopy analysis, is in accordance with the frequency determined for the monosubstituted phenyl ring from FTIR analysis of polystyrene/KBr disks [292]. The frequency determined for the skeletal aromatic ring vibration (1601 cm^{-1}) is also in agreement with published [292, 293] frequency values. The DRIFT spectrum of the PS (10 wt.% DVB) microgel sample is shown in figure 3.14.

Figure 3.14 - DRIFT Spectrum of PS (10 wt.% DVB) Microgel
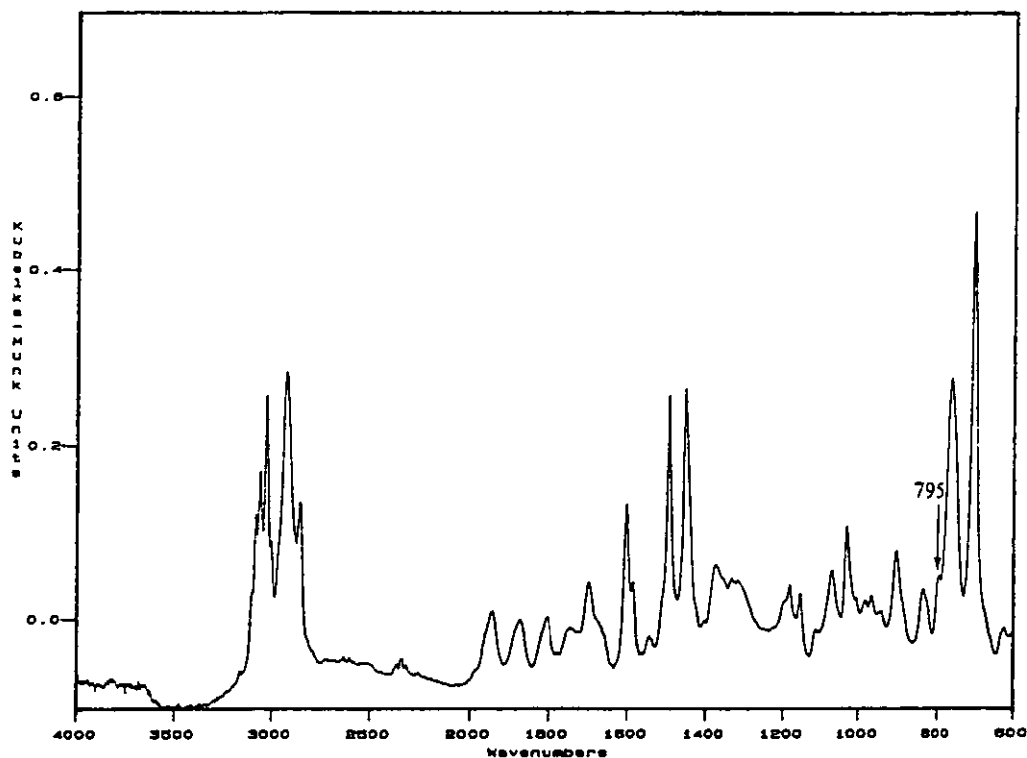
The DRIFT spectrum of the PS (10 wt.% DVB) microgel is identical to the polystyrene DRIFT spectrum (figure 3.13), with the exception that an additional weak resonance is observed at a 795 cm^{-1} radiation wavenumber. The PS (1 wt.% DVB) and PS (5 wt.% DVB) microgels showed no additional IR absorptions when compared to the polystyrene homopolymer sample. Bartholin *et al.* [292] and Malinsky *et al.* [291] have reported that the 795 cm^{-1} vibration corresponds to the out of plane deformation of C-H bonds in the phenyl ring of *m*-disubstituted divinylbenzene molecules in styrene/DVB copolymers [291, 292]. FTIR analysis of poly(DVB) microgels has shown [292] that the out of plane deformation of the phenyl C-H bond in *p*-disubstituted divinylbenzene molecules occurs at a frequency of 1510 cm^{-1}. Vibrations from *p*-disubstituted divinylbenzene groups were not observed from DRIFT spectroscopy analysis of the three microgel formulations. The absence of absorptions from *p*-disubstituted DVB units could possibly have been a consequence of the relatively low concentration of pure DVB isomers within these microgel particles.

3.6 - POLYSTYRENE MICROGEL DISPERSIONS IN ORGANIC MEDIA

Dispersions of the three polystyrene microgel samples were prepared in anhydrous cyclohexanone, toluene, n-butyl acrylate, tetrahydrofuran and benzyl alcohol (section 2.2.3). The fifteen dispersions were all recovered in high yield (ca. 95-98 weight % of the total solids added were dispersed in the organic diluent), with the exception of the PS (10 wt.% DVB)/nBA system, where 35-40 weight % of the polymer particles added, remained as a non-dispersible fraction. Rheological testing of PS (1 wt.% DVB), PS (5 wt.% DVB) and PS (10 wt.% DVB) microgel particle dispersions in THF, toluene (ϕCH_3), nBA, cyclohexanone (CHX) and benzyl alcohol (ϕCH_2OH) was performed at a temperature of 25°C (section 2.8.4). Viscosity measurements were recorded with a Haake NV sensor (appendix 1) over a 25-2500 s^{-1} shear rate range. The viscosity behaviour of a polystyrene solution in toluene (5 wt.% solids) was also examined. Dispersion viscosities, η (centipoise, cP), recorded for the four polystyrene/toluene systems, at a given shear rate, D (s^{-1}), and polymer solids concentration, are given in table 3.7.

Table 3.7 - Polystyrene Microgel Viscosities in Toluene (25°C)

Polymer System	Solids (Weight %)	Shear Rate, D (s^{-1})	η (cP)
Polystyrene	5.3	2,400	17
PS (1 wt.% DVB)	5.0	2,400	5
PS (5 wt.% DVB)	5.0	2,400	2
PS (10 wt.% DVB)	4.8	2,400	2

A comparison between the rheological behaviour of the polystyrene solution and the three microgel dispersions indicated that the viscosities of the organic microgel dispersions were significantly lower than the homopolymer solution viscosity (at the same solid concentration and shear rate). Conformational changes for microgel chains dispersed in organic media are severely limited by the network structure of the microgel particles [203, 214, 227]. Linear polystyrene molecules adopt, on average, a random-coil conformation in solution [11]. At relatively low polymer particle concentrations, microgel dispersions consist of swollen gel particles, surrounded by "free" dispersent molecules [214, 227], however. The presence of such unassociated

liquid molecules, imparts a relatively low viscosity onto organic microgel dispersions [214]. Shashoua and Beaman [227] determined that highly crosslinked, dilute, microgel particle dispersions can follow the Einstein viscosity relation [229-231] for dispersions of hard spheres. Details of reported [227, 233-235] microgel dispersion viscosity characteristics are presented in section 1.7.2.

Dispersion viscosity, η (cP), at a given shear rate and solid content, values, recorded for each of the fifteen microgel dispersions, are given in table 3.8. The viscosities of the five organic dispersants [248] are presented in table 3.9.

Table 3.8 - PS Microgel Dispersion Viscosities (25°C)

Microgel System	Solids (Weight %)	Shear Rate, D (s^{-1})	η (cP)
1% DVB/THF	5.0	2,400	7
5% DVB/THF	5.0	2,400	3
10% DVB/THF	5.5	2,400	2
1% DVB/ϕCH$_3$	5.0	2,400	5
5% DVB/ϕCH$_3$	5.0	2,400	2
10% DVB/ϕCH$_3$	4.8	2,400	2
1% DVB/nBA	5.2	2,400	4
5% DVB/nBA	5.1	2,366	2
10% DVB/nBA	5.5	2,400	2
1% DVB/CHX	5.4	2,400	16
5% DVB/CHX	5.2	2,400	6
10% DVB/CHX	5.4	2,400	3
1% DVB/ϕCH$_2$OH	5.2	2,400	15
5% DVB/ϕCH$_2$OH	5.3	2,400	10
10% DVB/ϕCH$_2$OH	5.0	2,400	9

Table 3.9 - Organic Dispersant Viscosities (25°C) [248]

Organic Liquid	Viscosity, η (cP)
Tetrahydrofuran	0.46
Toluene	0.55
n-Butyl acrylate	0.89
Cyclohexanone	2.20
Benzyl alcohol	5.80

As can be seen from the contents of table 3.8, an increase in the divinylbenzene concentration leads to a reduction in the viscosity of the dispersion. This behaviour

was observed for each of the five dispersant systems. Increasing the divinyl comonomer content of PS microgels leads to an increase in the network's crosslink-density, as determined from microgel characterisation by dynamic mechanical thermal analysis (section 3.3). Rheological characterisation of PS microgel dispersions in benzene [227] has similarly shown that dispersions with highest viscosities contain microgels with the lowest degrees of crosslinking [227] (provided that the dispersions contain similar concentrations of polymer solids). The viscosity characteristics of microgel dispersions are significantly influenced by the network particle's structure, as the level of microgel-swelling with diluent is dependent upon the crosslink-density of the particles [167, 227]. At a given solid concentration, microgel particles with the lowest crosslink-densities are swollen by diluent to the greatest extent [227]. The quantity of free liquid, the liquid found remaining outside of the gel particles, will be correspondingly lower in dispersions which contain loosely-crosslinked particles, when compared to systems containing poorly-swollen, highly-crosslinked, particles (at identical particle concentrations). The presence of an excess of unassociated diluent molecules in the system imparts a low viscosity on the dispersion [214]. The viscosity of each dispersion was comparable, in general terms, to the organic diluent's viscosity. For the levels of microgel crosslinking investigated, and, more significantly, for the low concentration of solids incorporated within these dispersions, it can be concluded that each system was significantly below it's solution gel point (section 1.7.2) [227], the instance where liquid-swollen microgel particles begin to occupy the whole volume of the dispersant.

Swelling of polymer gels with organic liquid is not only influenced by the crosslink-density of the network [11, 232, 298, 299]. The degree of swelling is also significantly influenced, amongst other thermodynamic factors [232, 298], by the difference in solubility parameter between the constituent polymer and swelling agent [11, 232]. For a low molecular weight liquid, the solubility parameter, δ, can be approximated [232] by:

$$\delta = [(\Delta H_{vap} - RT) / V_m]^{1/2} \tag{3.3}$$

where ΔH_{vap} is the liquid's enthalpy of evaporation (J mol^{-1}), V_m is the substance's molar volume (m^3 mol^{-1}), and R and T have their usual significance.

The solubility parameter (δ) values for poly(styrene-*co*-divinylbenzene) [300] and the five organic dispersants [301] are listed in table 3.10.

Table 3.10 - Component Solubility Parameters [300, 301]

Component	Solubility Parameter, δ [J cm^{-3}]$^{1/2}$
Poly(styrene-*co*-divinylbenzene)	18.6
Tetrahydrofuran	18.6
Toluene	18.2
n-Butyl acrylate	18.0
Cyclohexanone	20.3
Benzyl alcohol	24.8

In terms of equilibrium swelling of macrogels [11, 232], the gel is, typically, found to be swollen to the greatest extent when the difference in polymer-diluent solubility parameter is minimised [232] (i.e. when the two δ values are equivalent). Increasing the solubility parameter difference between the network and swelling agent leads to a reduction in the amount of liquid held within the crosslinked polymer component [232]. Shashoua and Beaman [227] determined that polystyrene microgel dispersions in benzene were of higher viscosity than their corresponding dimethylformamide (DMF) dispersions (at similar particle crosslink-density and dispersion solid concentration). This observation was attributed to the decreased solubility parameter difference between the gel particles and dispersant for the PS/benzene microgel system [227]. According to Shashoua and Beaman [227], a larger number of "free" dispersant molecules were available in the DMF dispersion (i.e. fewer liquid molecules were located within the swollen gel particles) - which, thereby, had imparted a markedly decreased viscosity on the dispersion as a whole [227] (at a given concentration of solids in the benzene and DMF dispersions). Reference to the data tabulated in tables 3.8, 3.9 and 3.10, indicates that the microgel dispersions prepared in this particular investigation did not follow such significant viscosity fluctuations when the difference in polymer/liquid solubility parameter was varied. It would appear possible that the three PS microgel systems investigated in this study were

either too highly crosslinked or that the polymer concentration within the dispersions was too dilute, for observations similar to Shashoua and Beaman's [227] to have been recorded in this particular instance. The viscosity of the lightly-crosslinked microgel dispersions in cyclohexanone and benzyl alcohol would appear to contradict these earlier findings [227] in fact. In terms of the benzyl alcohol system, the large difference in incompatibility (solubility parameter difference) between the liquid and polymer could have possibly had a significant influence on the viscosity characteristics of the dispersion [11, 232], rather than the viscosity being almost entirely influenced by the degree of microgel swelling with liquid [214, 227]. These comments are classified in terms of the observation that, in general terms, dissolution of a linear polymer sample is only observed for systems where the difference in liquid/polymer solubility parameter is less than ca. 4 $(J\ cm^{-3})^{1/2}$ [232], in the absence of specific strong intermolecular attractions [11, 232] (such as hydrogen bonding effects) occurring within the system.

In conclusion, the relative ease in synthesising polystyrene microgel dispersions (section 2.2.3), the variety of suitable diluents available for dispersion preparation, and the relatively low viscosities of these organic microgel systems (at a concentration of 5 weight % solids), indicated that the polymerisation of nBA within PS particles could be investigated as a route for the potential synthesis of organic PS/PnBA IPN microgel dispersions.

CHAPTER 4

ACRYLIC MICROGELS

4.1 - CHARACTERISATION OF P*n*BA MICROGELS

The compatibility between the two polymer components [98-100], the relative masses of the two component networks [99, 125, 126], the crosslink-density of the first- [103] and second-formed [104, 105] networks and the order of network synthesis [99, 100, 123, 125], can have marked influences upon the morphology of sequential interpenetrating polymer network (macrogel) samples (section 1.4). Sequential IPN microgel dispersions were to be synthesised within this investigation from copolymerisation of second-stage comonomers within the first-formed particles of an organic microgel dispersion. It was anticipated that the order of network synthesis could significantly influence the IPN particle morphology, and hence, the physical properties of the IPN. Acrylic, poly(*n*-butyl acrylate)-based, microgels were synthesised, therefore, in order to determine the suitability of organic P*n*BA microgel dispersions as precursors for the synthesis of sequential P*n*BA/PS IPN microgel dispersions.

Emulsion copolymerisations of *n*BA with 10 wt.% DVB, 10 wt.%, 20 wt.% ethylene glycol dimethacrylate (EGDMA) and 10 wt.%, 20 wt.% neopentyl glycol diacrylate (NPGDA) were performed with ammonium persulphate as initiator (90°C), as detailed previously (section 2.3.1) A P*n*BA homopolymer latex was also synthesised. Copolymerisation yields were determined gravimetrically (section 2.3.2) and latex samples were characterised by photon correlation spectroscopy, PCS (section 2.8.9). Experimental yields and latex particle sizes (25°C) are given in table 4.1.

Table 4.1 - Copolymerisation Yields and Final Latex Particle Sizes (25°C)

Latex	Yield (Weight %)	Particle Size (nm)
P*n*BA homopolymer	99	43
P*n*BA (10 wt.% NPGDA)	99	42
P*n*BA (20 wt.% NPGDA)	96	45
P*n*BA (10 wt.% EGDMA)	98	46
P*n*BA (20 wt.% EGDMA)	99	46
P*n*BA (10 wt.% DVB)	98	45

It would appear, from latex non-volatile component analysis, that each copolymerisation had proceeded to high conversion. Particle size distribution data obtained from PCS analysis of the PnBA (20 wt.% EGDMA) microgel latex is shown in appendix 3. The particle sizes listed in table 4.1 are z-average particle diameters (section 3.2). It can be seen, from the contents of table 4.1, that each microgel latex had an average particle diameter of approximately 45 nm.

4.2 - DSC CHARACTERISATION OF PnBA MICROGELS

Dried films, cast from acrylic latices (section 2.3.2), were analysed by DSC at a heating rate of 10°C per minute (section 2.8.1). DSC thermograms for PnBA homopolymer and PnBA (10 wt.% EGDMA) microgel samples are shown in figures 4.1 and 4.2, respectively. The α-relaxation (glass transition) temperatures evaluated for each material (section 3.3) are given in table 4.2.

Figure 4.1 - DSC Thermogram for Poly(n-butyl acrylate) Homopolymer
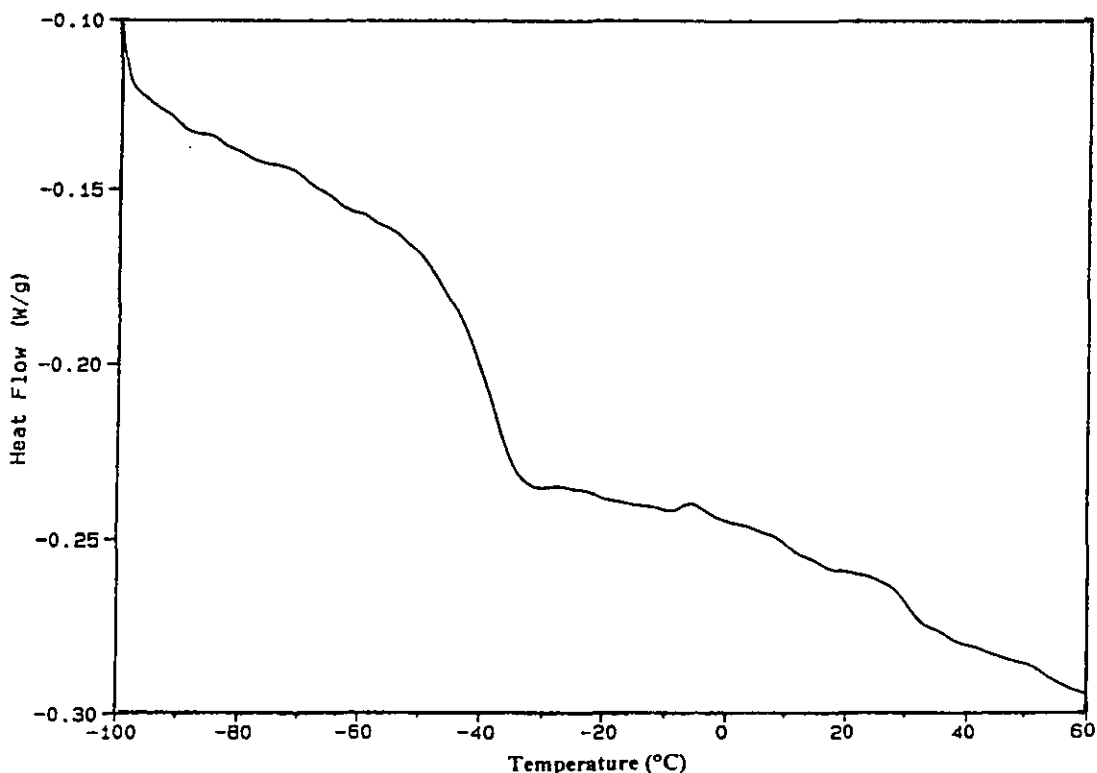
Figure 4.2 - DSC Thermogram for PnBA (10 wt.% EGDMA) Microgel
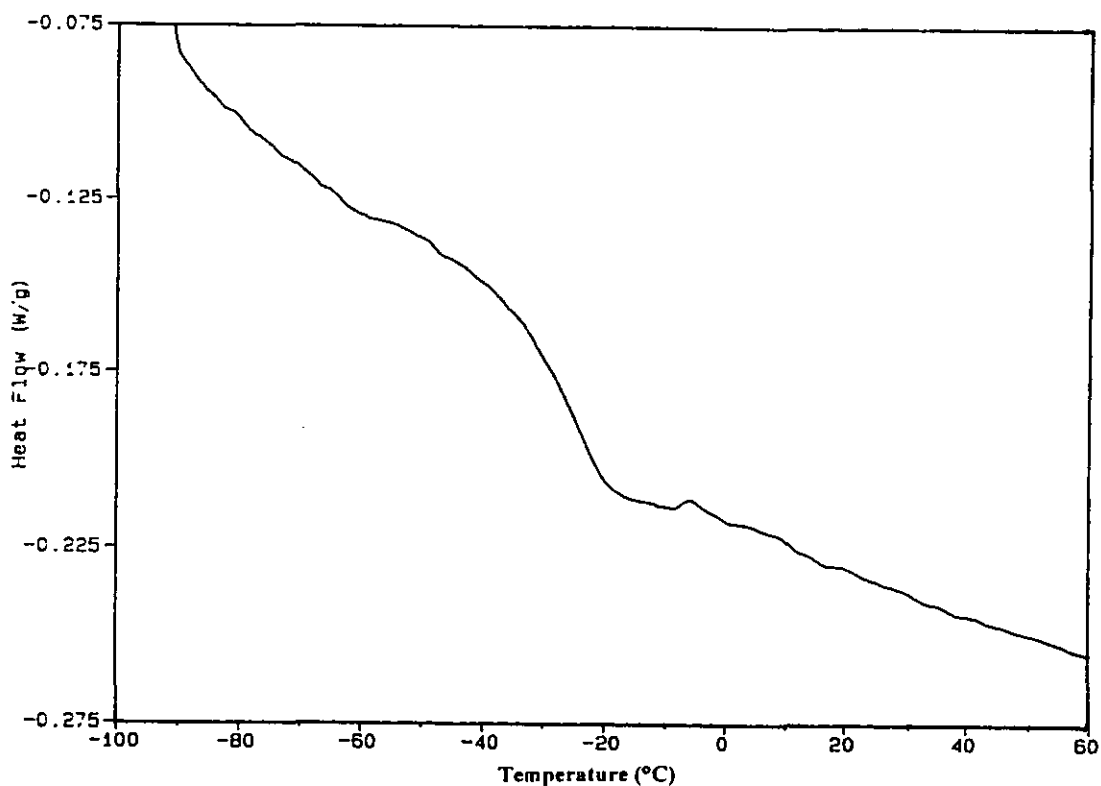
Table 4.2 - PnBA Microgel Glass Transition Temperatures from DSC Analysis

Polymer Sample	Glass Transition Temperature, T_g (°C)
Poly(n-butyl acrylate)	-45
PnBA (10 wt.% NPGDA)	-32
PnBA (20 wt.% NPGDA)	-23
PnBA (10 wt.% EGDMA)	-30
PnBA (20 wt.% EGDMA)	-12
PnBA (10 wt.% DVB)	-31

The glass transition temperature evaluated for the PnBA homopolymer sample is approximately 10°C higher than the T_g value reported in the literature (T_g = -54°C) [302] for poly(n-butyl acrylate). The DSC characteristics of the glass transition are influenced by the thermal history [256, 257] of the polymer sample. Additionally, glass transition temperatures are influenced by polymer molecular weights [11, 261, 264], the degree of crosslinking for the sample [11, 261], and by plasticising agents [11, 303]. Non-equivalent molecular weights [11], or thermal histories [257], for the PnBA sample prepared in this study and for the material previously analysed [302],

could possibly have lead to the T_g-differences observed between the two homopolymer samples. The glass transition temperature recorded for each of the five PnBA microgel samples (table 4.2) was higher than the homopolymer's T_g value, indicating that the incorporation of divinyl comonomers within acrylic latex particles had lead to the formation of crosslinked particle structures [261, 264] (section 3.2). The PnBA (10 wt.% DVB), PnBA (10 wt.% EGDMA) and PnBA (10 wt.% NPGDA) microgel samples would appear to be of comparable glass transition temperature (table 4.2). Incorporation of 20 weight % NPGDA and 20 weight % EGDMA within two of the microgel formulations, lead to a further increase in T_g, indicating that these two microgel samples had the highest particle crosslink-densities [261].

4.3 - CHARACTERISATION OF ACRYLIC MICROGELS BY DMTA

Dried acrylic polymer films, formed after the evaporation of water from latex samples (section 2.2.2), were characterised by dynamic mechanical thermal analysis, DMTA, over a -60°C to 150°C temperature range (section 2.8.2). Plots of loss tangent (tanδ) versus temperature (sections 2.8.2 and 3.3) for the poly(n-butyl acrylate), PnBA (10 wt.% NPGDA), PnBA (20 wt.% NPGDA) and PS (20 wt.% EGDMA) microgel samples are shown in figures 4.3, 4.4, 4.5 and 4.6, respectively. Glass transition, α-relaxation, parameters (section 3.3) obtained from DMTA characterisation of the six acrylic polymer samples are given in table 4.3.

Table 4.3 - Acrylic Polymer Glass Transition Temperatures from DMTA

Sample	Tanδ_{MAX}	T_g (°C) at 10 Hz
PnBA homopolymer	2.0	-18
PnBA (10 wt.% NPGDA)	1.4	- 8
PnBA (20 wt.% NPGDA)	1.1	2
PnBA (10 wt.% EGDMA)	1.3	0
PnBA (20 wt.% EGDMA)	1.0	23
PnBA (10 wt.% DVB)	1.4	1

Figure 4.3 - Tanδ with Temperature Curve for P*n*BA Homopolymer
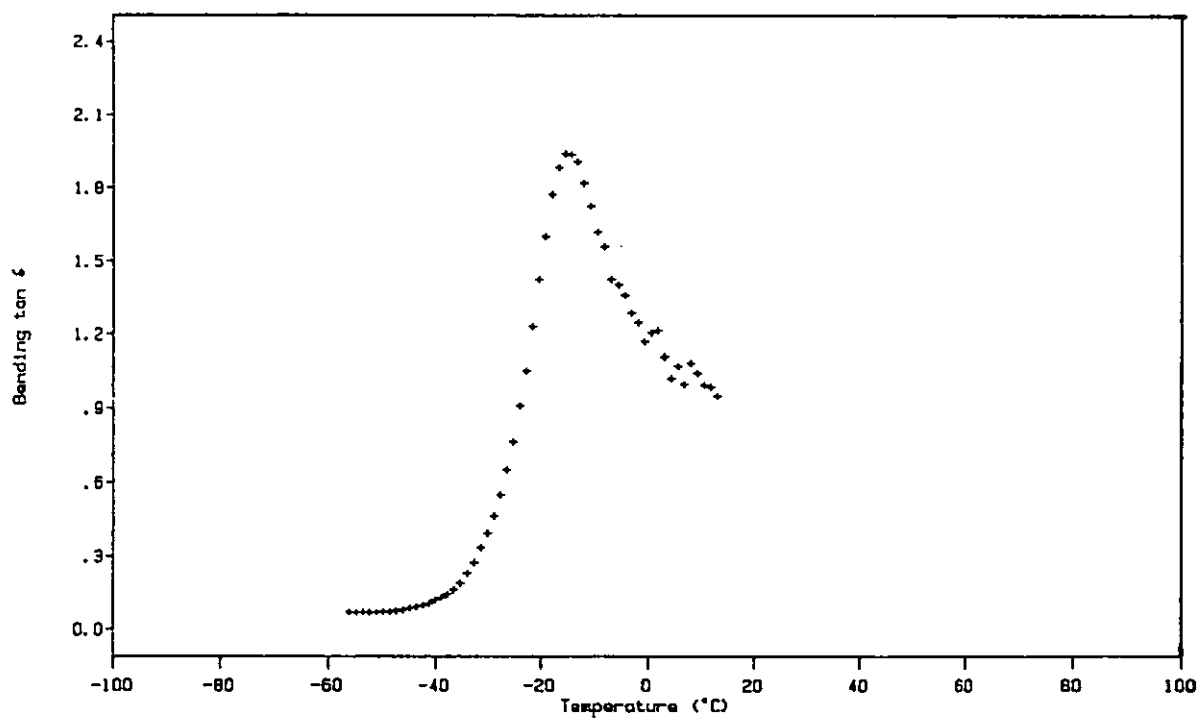
Figure 4.4 - Tanδ with Temperature Curve for P*n*BA(10 wt.% NPGDA) Microgel
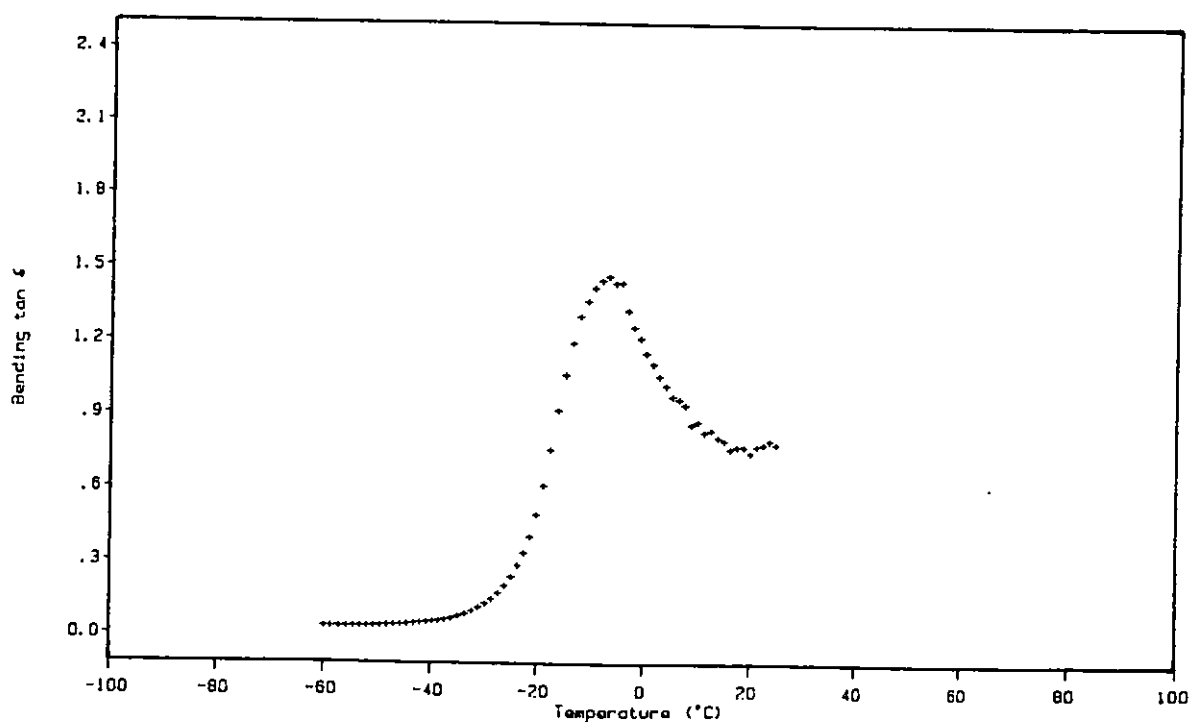
Figure 4.5 - Tanδ with Temperature Curve for P*n*BA(20 wt.% NPGDA) Microgel
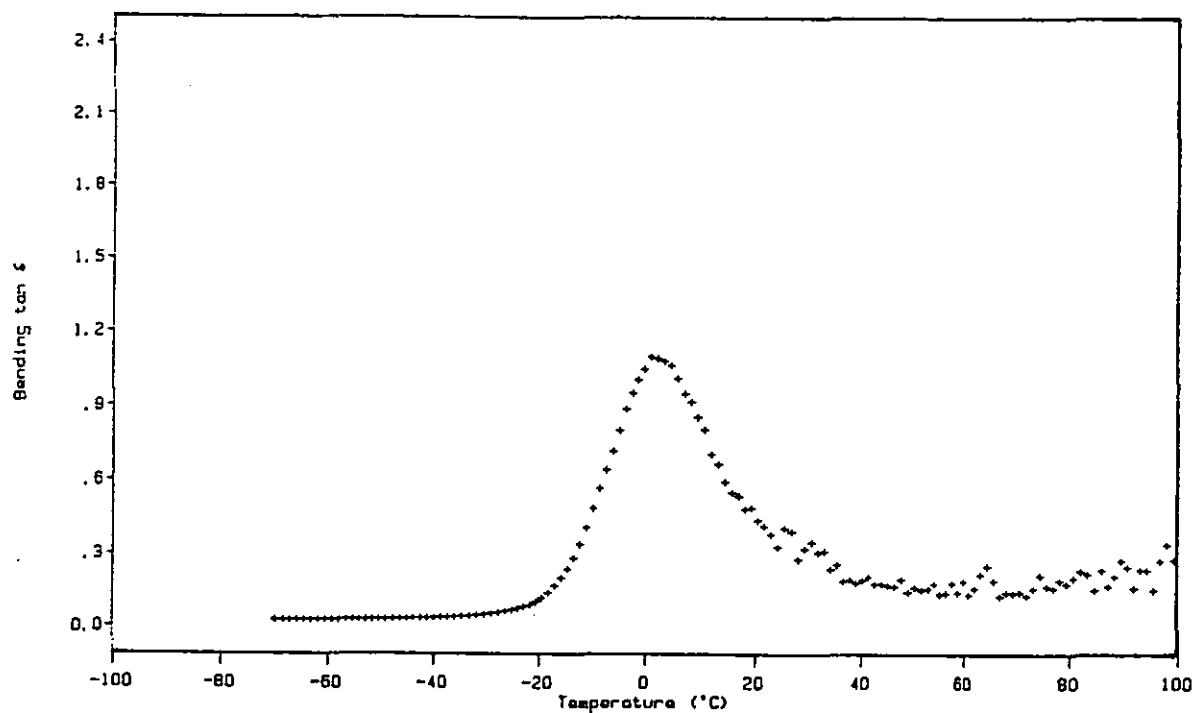
Figure 4.6 - Tanδ with Temperature Curve for P*n*BA (20 wt.% EGDMA) Microgel
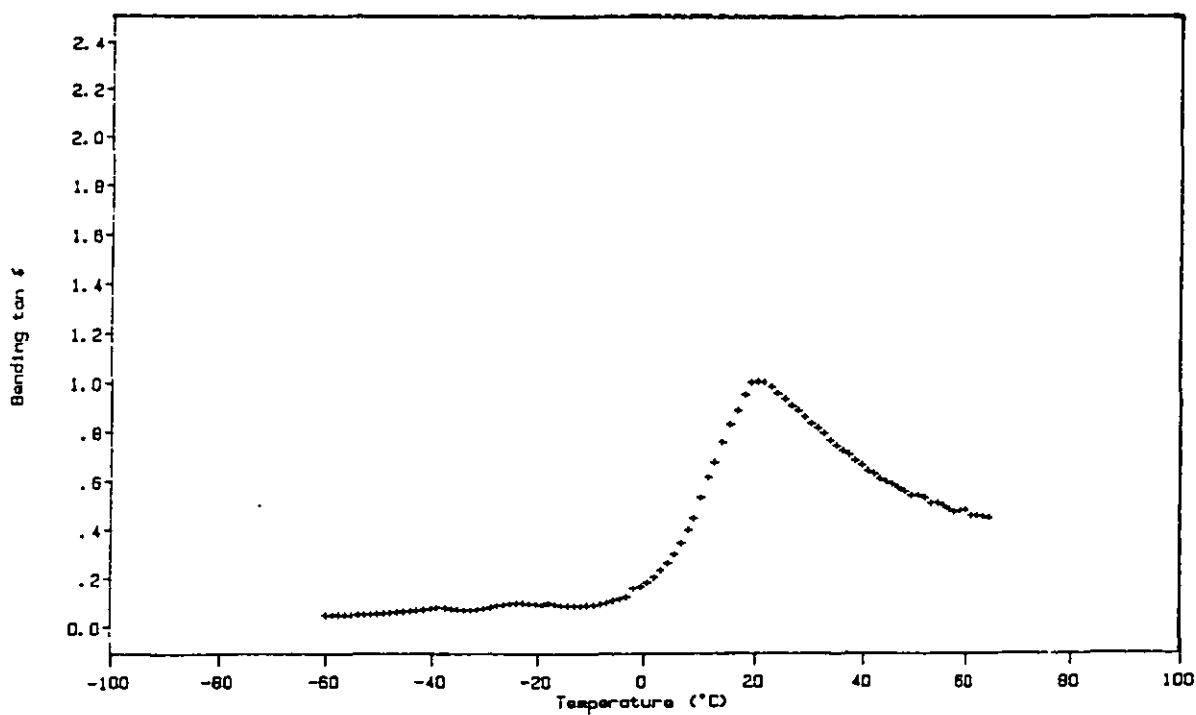
As can be seen from table 4.3, DMTA observations indicate that the incorporation of a divinyl comonomer within the latex particle formulation leads to an increase in the material's glass transition temperature (when compared to the T_g of the PnBA homopolymer sample). The $\tan\delta_{MAX}$ value (table 4.3) also decreases in magnitude as the concentration of the divinyl moiety within the particles increases. These observations are in accordance with the glass transition behaviour determined for polystyrene microgels from DMTA analysis (section 3.3). Shifts in glass transition temperature values are observed on crosslinking polymer samples [11, 261] (section 3.3). Nielsen [261] compared T_g-shift upon crosslinking data with average molecular weight between crosslink (M_c) values determined from macrogel sample, physical property, characterisations [261, 288-290]. By averaging all of these experimental results [261], a relation for the estimation of M_cs from the shift in T_g on crosslinking was derived [261] (equation 3.1, section 3.3). Theoretical average molecular weight between crosslinks [287] (equation 3.2, section 3.3) and M_c values estimated from DMTA T_g-shifts [261] (equation 3.1) for acrylic microgel samples (table 4.3) are detailed in table 4.4.

Table 4.4 - Theoretical and Experimental Network M_c Values for PnBA Microgels

Microgel Sample	M_c^{calc} (kg mol^{-1}) [287]	M_c (kg mol^{-1}) [261]
PnBA (10 wt.% NPGDA)	0.8	3.9
PnBA (20 wt.% NPGDA)	0.4	2.0
PnBA (10 wt.% EGDMA)	1.0	2.2
PnBA (20 wt.% EGDMA)	0.5	1.0
PnBA (10 wt.% DVB)	1.2	2.1

Network average molecular weight between crosslink values estimated from glass transitional shifts [261] are higher than theoretical M_c values (the average molecular weight between crosslink value for a homogeneous network where all divinyl units have been incorporated as chemical crosslinks [287]). The crosslink-densities of the microgel particles are lower, therefore, than would be anticipated for their corresponding perfect network analogues (section 1.1). Shifts in glass transition temperature values, from DMTA analysis, for polystyrene microgel particles (section 3.3) were comparable to those anticipated from considerations of network T_g-shift with crosslinking relations [261] (equation 3.1). The increase in glass

transition temperature on crosslinking, for each of the five acrylic microgel samples, was lower than would be anticipated [261] for ideal network samples, where divinyl comonomers are exclusively consumed within crosslinks. Additionally, statistical linear copolymer samples are found to have glass transition temperatures which are intermediate between the two corresponding homopolymer T_g values [256, 305, 306].

The extent of the glass transition temperature shift on copolymerisation is dependent upon the relative concentration (weight fraction) of the two comonomer components [256, 305]:

$$1 / T_g = (w_1 / T_{g1}) + (w_2 / T_{g2})$$ (4.1)

where w_i is the weight fraction of component i, T_{gi} is the glass transition temperature of homopolymer i and T_g is the glass transition temperature of the copolymer [305].

Copolymerisation effects on T_g were not considered for poly(styrene-*co*-divinylbenzene) microgels, as both of the constituent comonomers are of similar molecular structure. Copolymerisation of *n*BA with, for example, methyl methacrylate, would generate polymeric materials with increased glass transition temperatures, when compared to P*n*BA homopolymer (T_g P*n*BA ≈ -50°C, whereas T_g PMMA ≈ 100°C [307]). Copolymerisation of *n*BA with EGDMA, or DVB, would increase the glass transition temperature of the polymeric material, even if the divinyl comonomer was exclusively incorporated within the copolymer main-chain via the addition/reaction of only one of its double bonds (i.e. T_gs for acrylic materials synthesised from *n*BA with either EGDMA or DVB would be higher than the T_g of P*n*BA homopolymer, even if divinyl comonomer incorporation had not lead to crosslinking of the material). The coupling of this copolymerisation effect on T_g, with the observation that T_g shifts observed for acrylic microgels from DMTA characterisation were lower than would be predicted for the effect of crosslinking alone [261] (equation 3.1), suggests that the crosslink-density of the P*n*BA (10 wt.% DVB), P*n*BA (10 wt.% EGDMA) and P*n*BA (20 wt.% EGDMA) microgels was significantly lower than would be anticipated if the divinyl comonomers had been

incorporated perfectly (i.e. for ideal network synthesis). It is interesting to note that the discrepancy between the M_c value from the glass transition temperature shift [261] and the M_c value for a perfect network [287] is greatest for the two NPGDA microgel samples, where the copolymerisation influence on T_g [305] is anticipated to be the lowest of the three crosslinking agents investigated. Detailed characterisation of rubbery microgel particles appears to have received little attention in the scientific literature, considerations of these anomalous T_g shifts can only be cautionary in nature. It is possible that divinyl comonomer incorporation within acrylic microgel formulations had not only lead to crosslinking of the sample, the presence of these divinyl moieties could have additionally contributed to the formation of extensive chain branching [5, 11, 31, 261]. Branched polymer materials have lower T_gs than their linear polymer analogues [11]. Chain-branching is often considered to increase the free volume (section 3.3) of the polymer sample [11, 264, 284]. Such an approach for detailing the glass transition behaviour of branched polymers [11, 284] considers that the ends of a polymer chain have a significant associated free volume [284]. Branched materials have a greater number of chain ends when compared to their linear polymer analogues, and, subsequently, the increased free volume within branched polymer samples [11, 284] is considered to impart a lower T_g on the material. Lovell *et al.* [304] reported the presence of extensive chain-branching within P*n*BA-based materials synthesised from emulsion polymerisation processes (samples were prepared with ammonium persulphate as free radical initiator at 75°C) [304]. Branches were considered [304] to have resulted from the initial abstraction of hydrogen atoms from tertiary C-H bonds in polymer-bound *n*BA repeat units [304]. Propagation from the resulting polymeric radicals (by the addition of *n*BA monomer) was considered [304] to have subsequently followed the hydrogen abstraction process [304], leading to the formation of chain branches. The apparent readiness of the tertiary hydrogen in polymer-bound *n*BA repeat units to undergo abstraction [304] reactions, coupled with the copolymerisation proceeding at a temperature (section 2.3.1) considerably greater than the acrylic material's glass transition [302], could possibly have lead to the consumption of considerable concentrations of crosslinking agent via short-chain branching processes (section 1.2) [11, 32, 33], within these acrylic microgel systems. The observation that the shift in T_g on crosslinking PS microgels (section 3.3) [261]

was comparable to the T_g-shift anticipated for "ideal" network synthesis (sections 1.2 and 3.3), whereas acrylic microgels appeared to be less highly crosslinked than their ideal network analogues, could also have resulted from either greater copolymer compositional drift (section 1.5) occurring within the acrylic copolymerisation process or from extensive intramolecular cyclisation (section 1.2) reactions occurring within the PnBA-based microgel systems.

4.4.1 - ACRYLIC MICROGEL DISPERSIONS IN ORGANIC MEDIA

Polystyrene microgel particles, recovered from flocculation (the particles were precipitated from the addition of emulsion to excess methanol) of aqueous latices (section 2.2.2), were initially dried under vacuum. Dry polystyrene powders were subsequently added to organic liquid (toluene, nBA, THF, benzyl alcohol or cyclohexanone) and microgel dispersions were recovered in high yield after standing the systems for approximately fifteen hours at ambient temperature (section 2.2.3 and section 3.6). Polymers recovered from the addition of acrylic microgel latices to methanol were rubbery and dispersions could not be recovered from the addition of precipitated microgel to organic diluent (even under conditions of vigorous agitation at high temperature). The dispersibility-difference observed between the polystyrene and PnBA microgels, is considered to have resulted from the two microgel systems' contrasting glass transition behaviour. PS microgels were significantly below their glass transition temperature [284] during latex flocculation at 25°C. The recovered powdery material can be considered to have comprised of discrete, glassy, polymer spheres. Acrylic microgels were above their T_g [302] during latex flocculation, however. It would appear possible that extensive chain-entanglements between adjacent rubbery microgel particles could have occurred on precipitation of acrylic latices, whereby such rubbery particle agglomerates could not be subsequently "untangled" when added to organic liquid. Consequently, organic acrylic microgel dispersions were prepared via vacuum distillation procedures (section 2.3.3) [249]. Acrylic latex was added to hot (ca. 70°C), vigorously stirred, organic liquid, at a concentration where the diluent/water mixture was of one phase (section 2.3.3). Colloidal acrylic dispersions in homogeneous organic liquid/water mixtures were initially recovered from such processes, and aqueous components were subsequently

removed via vacuum distillation. Attempts to prepare acrylic dispersions in dimethylformamide, n-butyl propionate and n-butyl formate proved unsuccessful. Polymeric materials were precipitated from these liquids, suggesting that each diluent was incompatible with the acrylic microgel formulations investigated [214, 232]. Apart from the necessity for the organic diluent to be a solvent for the microgel's linear polymer analogue [214], the diluent was required to be of higher boiling point than water. Additionally, the higher the affinity the liquid had with water, the more facile it became to prepare an organic microgel dispersion (higher quantities of aqueous latex could be added to the liquid for the generation of dispersions in homogeneous diluent/water mixtures, prior to distillation). Dispersions of the five crosslinked PnBA samples were subsequently prepared in anhydrous n-butanol and benzyl alcohol. Additionally, the PnBA (20 wt.% EGDMA) microgel formulation was precipitated on addition to n-butanol.

4.4.2 - ESTIMATION OF MICROGEL DISPERSION WATER CONTENTS

Colloidal microgel particle dispersions in alcohol/water mixtures were prepared by the addition of aqueous acrylic microgel latex to organic diluent (section 2.3.3). Vacuum distillation processes [249] were subsequently performed, in order to try to remove all of the aqueous component from these dispersions. A control distillation was performed with an n-butanol/water mixture which had been prepared from similar procedures employed for the preparation of acrylic microgel dispersions in n-butanol (section 2.3.3). The liquid recovered, after termination of the distillation process, was titrated with Karl Fischer reagent [250]. The Karl Fischer reagent is composed of iodine, sulphur dioxide, methanol and pyridine [250]. Each of these components enters into the basic reaction with water molecules, if water is present in the system under analysis [250]. The overall process involves the two-step reaction [250]:

$$C_5H_5N.I_2 + C_5H_5N.SO_2 + C_5H_5N + H_2O \longrightarrow 2\ C_5H_5N.HI + C_5H_5N.SO_3 \qquad (4.2)$$

$$C_5H_5N.SO_3 + CH_3OH \longrightarrow C_5H_5N(H)SO_4CH_3 \qquad (4.3)$$
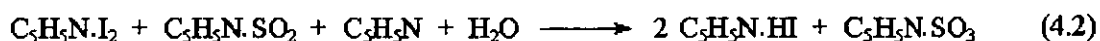
In the course of the reaction of water with the reagent, the reduction of iodine to iodide ion (HI) is monitored [250] to determine the water content. The titration end-point can be detected visually or electrometrically [250]. Electrometric methods were utilised during this investigation with the employment of a Baird and Tatlock AF3 instrument. The water content of the n-butanol (nBuOH) sample was found to be less than 0.05 weight % of the distillate's composition, i.e. this control experiment suggested that the acrylic microgel dispersions prepared would, most probably, have been anhydrous.

The water content of PnBA microgel dispersions in benzyl alcohol and n-butanol was also estimated from FTIR spectroscopy (section 2.3.3). Comparisons between the intensities of absorption for the H-Ô-H bending frequency of water molecules (1654 cm^{-1} in nBuOH/water and 1639 cm^{-1} in benzyl alcohol/water) in alcohol/water (0, 0.5, 1.0, 2.0, 3.0, 4.0 and 5.0 wt.% water content) mixtures were initially made. (The wavenumber for the H-Ô-H bending frequency in alcohol/water mixtures is shifted from the value of 1640 cm^{-1} for water [58], as a consequence of hydrogen bonding effects [270]). %Transmittance FTIR spectra recorded for samples of n-butanol, an nBuOH/water (2 wt.% H$_2$O) mixture, benzyl alcohol, and a benzyl alcohol/water mixture (5 wt.% H$_2$O) are shown in appendices 4, 5, 6 and 7, respectively. Vibrations from water molecules (1654 cm^{-1}/1639 cm^{-1}) were detected at a water concentration of 0.5 weight %, in the calibration experiments. No discernible absorptions from H$_2$O molecules were observed in samples taken from organic microgel dispersions, however. Transmittance FTIR spectra recorded for PnBA (10 wt.% DVB) dispersions in n-butanol and benzyl alcohol are shown in appendices 8 and 9, respectively. The apparent absence of absorptions from water in both of the samples, indicated that the water content of the dispersions was significantly less than 0.5 % by weight. An additional IR absorption, located at a radiation wavenumber of 1737 cm^{-1}, was observed for microgel dispersions, when compared to FTIR spectra recorded for anhydrous organic liquid. This absorption peak corresponds to the stretching frequency of the C=O carbonyl bond of polymer-bound nBA repeat units [308].

4.4.3 - RHEOLOGICAL CHARACTERISATION OF DISPERSIONS

Rheological characterisation of PnBA (10 wt.% NPGDA), PnBA (20 wt.% NPGDA), PnBA (10 wt.% EGDMA), PnBA (20 wt.% EGDMA) and PnBA (10 wt.% DVB) microgel particle dispersions (5 wt.% solids content) in n-butanol (nBuOH) and benzyl alcohol (ϕCH$_2$OH) was performed at a temperature of 25°C (section 2.8.4). Viscosity measurements for the n-butanol dispersions were recorded with a Haake NV sensor (appendix 1), whereas viscosities of benzyl alcohol dispersions and poly(n-butyl acrylate) homopolymer solutions in nBuOH and benzyl alcohol were recorded with a Haake MV1 sensor (appendix 1). Each polymer/organic liquid system was tested over a 25-1000 s^{-1} shear rate range. Dispersion viscosities, η (centipoise, cP), recorded for the five PnBA/nBuOH systems, at a given shear rate, D (s^{-1}), and polymer solids concentration, are given in table 4.5.

Table 4.5 - Acrylic Microgel Viscosities in n-Butanol (25°C)

Polymer System	Solids (Weight %)	Shear Rate, D (s^{-1})	Viscosity, η (cP)
PnBA	5.2	728	56
PnBA (10 NPGDA)	5.2	756	12
PnBA (20 NPGDA)	4.6	756	10
PnBA (10 EGDMA)	5.2	756	19
PnBA (10 DVB)	5.0	756	10

Dispersion viscosities recorded for the six PnBA/benzyl alcohol systems, at a given shear rate, and solids concentration, are given in table 4.6.

Table 4.6 - Acrylic Microgel Viscosities in Benzyl Alcohol (25°C)

Polymer System	Solids (Weight %)	Shear Rate, D (s^{-1})	Viscosity, η (cP)
PnBA	5.5	721	161
PnBA (10 NPGDA)	4.5	725	79
PnBA (20 NPGDA)	5.2	721	89
PnBA (10 EGDMA)	4.9	721	80
PnBA (20 EGDMA)	4.7	725	96
PnBA (10 DVB)	5.3	721	44

The viscosities of the two organic diluents employed for the preparation of acrylic microgel dispersions are given in table 4.7 [248].

Table 4.7 - Organic Dispersant Viscosities [248] (25°C)

Organic Diluent	Viscosity, η (cP)
n-Butanol	2.56
Benzyl alcohol	5.80

Acrylic microgels behave similarly to polystyrene gel particles in terms of their viscosity behaviour. The viscosity of the microgel dispersion is significantly lower than the corresponding homopolymer solution viscosity. This viscosity reduction for microgel systems can be considered to result from the restricted mobility of polymer-chain sections [214, 218, 227] (section 3.6) within microgel particles (the number of possible conformational changes that can be adopted by segments of the polymer chain are reduced for microgels, when compared to their linear polymer analogues). The n-butanol dispersion viscosities do not appear to be significantly influenced by the crosslink-density (section 3.3) of the microgel particles, at the 5 weight % solids dispersion concentration employed. The viscosities of the acrylic microgel dispersions in nBuOH are also comparable to the viscosity of the pure organic diluent (table 4.7). It would appear that these acrylic microgel dispersions could all have been at concentrations below their solution gel points [227] (section 1.7.2), the instance were liquid-swollen microgel particles begin to occupy the whole volume of the dispersant. Sufficient quantities of free liquid molecules (liquid which is not found within the swollen microgel particles) could be present in each of these systems, imparting a relatively low viscosity onto the dispersion as a whole (section 3.6) [214, 227]. Shear stress, τ (Pa), versus shear rate, D (s^{-1}), curves (25°C) for PnBA solution, and PnBA (10 wt.% NPGDA) microgel, formulations in n-butanol are presented in figures 4.7 and 4.8, respectively. Shear stress against shear rate curves for PnBA solution and PnBA (10 wt.% NPGDA) microgel formulations in benzyl alcohol (25°C), are shown in figures 4.9 and 4.10, respectively.

Figure 4.7 - Shear Stress-Shear Rate Curve for P*n*BA Solution in *n*-Butanol
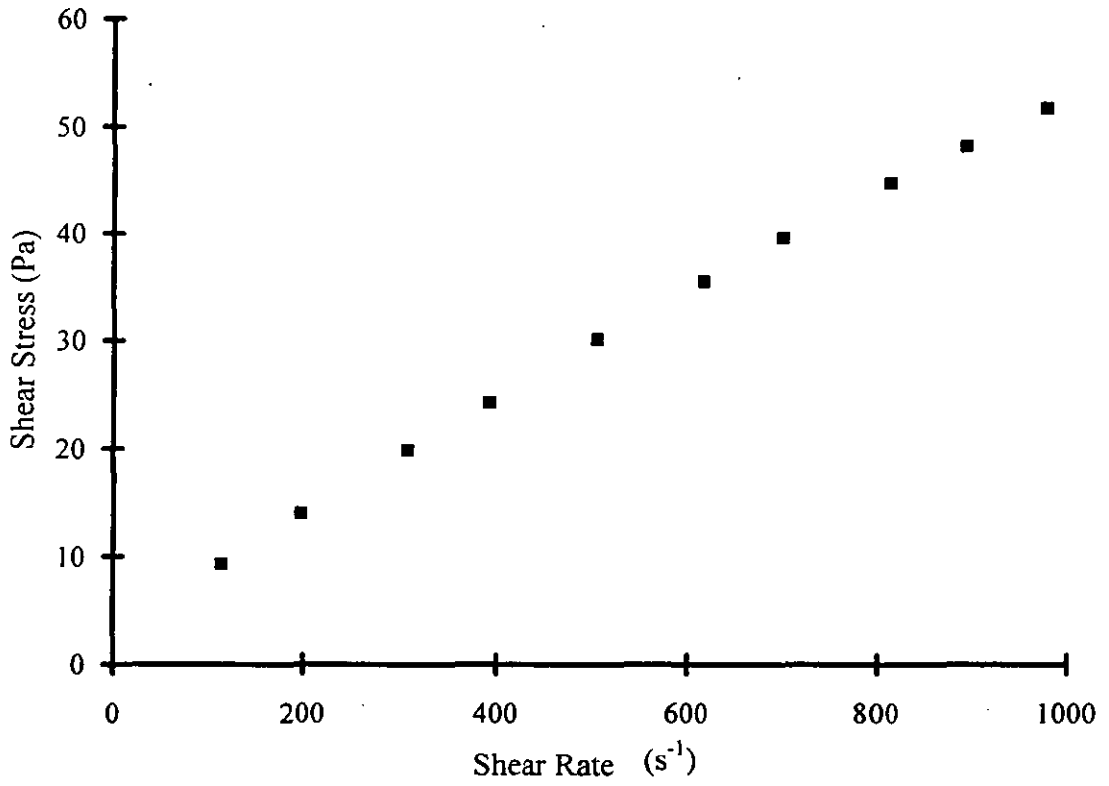
Figure 4.8 - Shear Stress-Shear Rate Curve for P*n*BA (10 % NPGDA)

Microgel Dispersion in *n*-Butanol
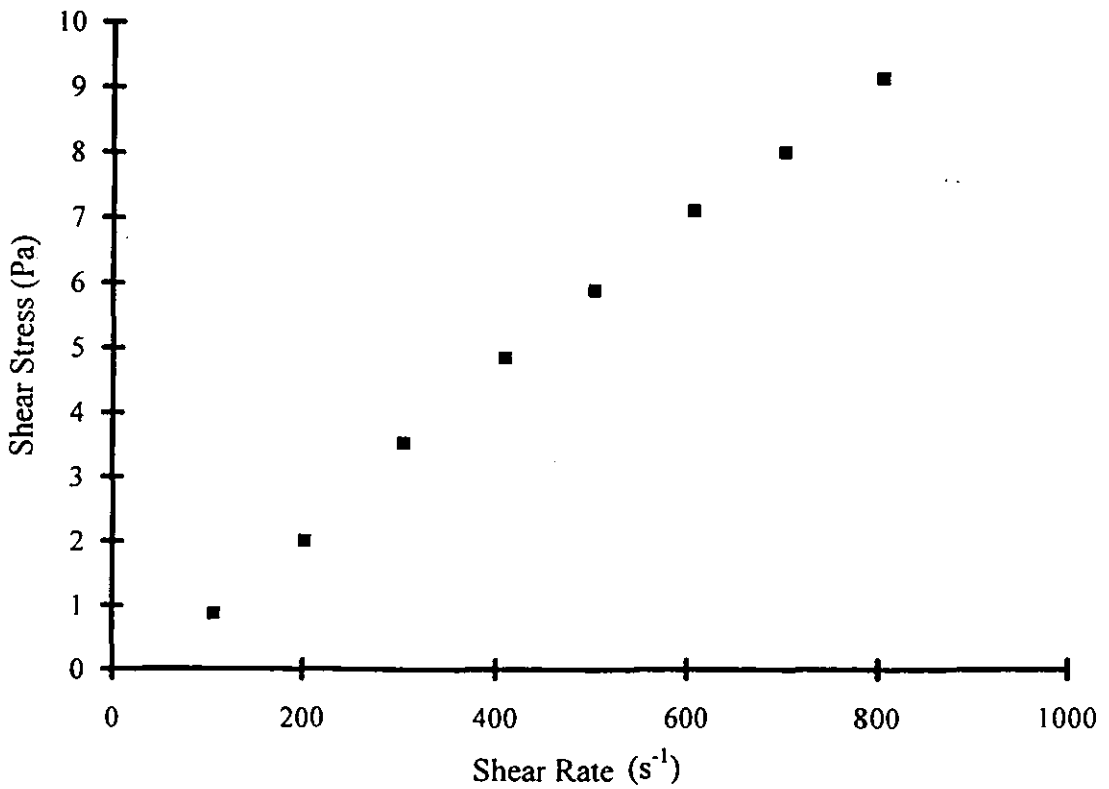
Figure 4.9 - Shear Stress-Shear Rate Curve for P*n*BA Solution in Benzyl Alcohol
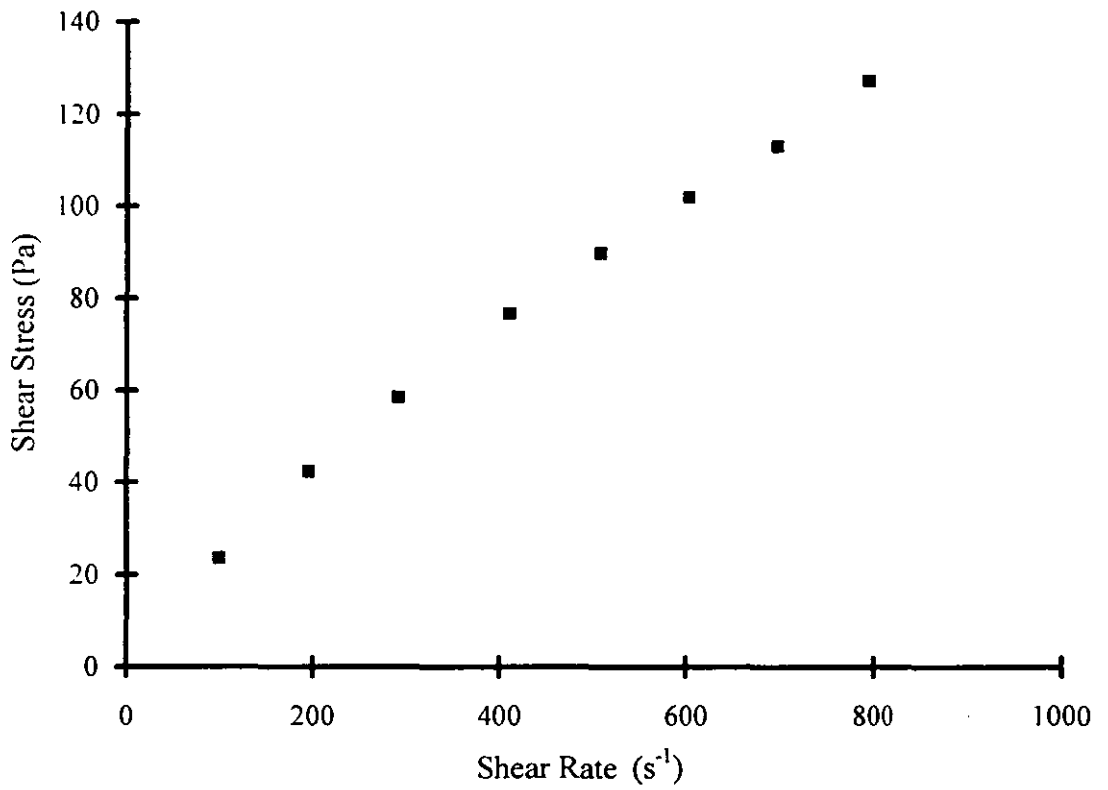
Figure 4.10 - Shear Stress-Shear Rate Curve for P*n*BA (10 wt.% NPGDA)
Microgel Dispersion in Benzyl Alcohol
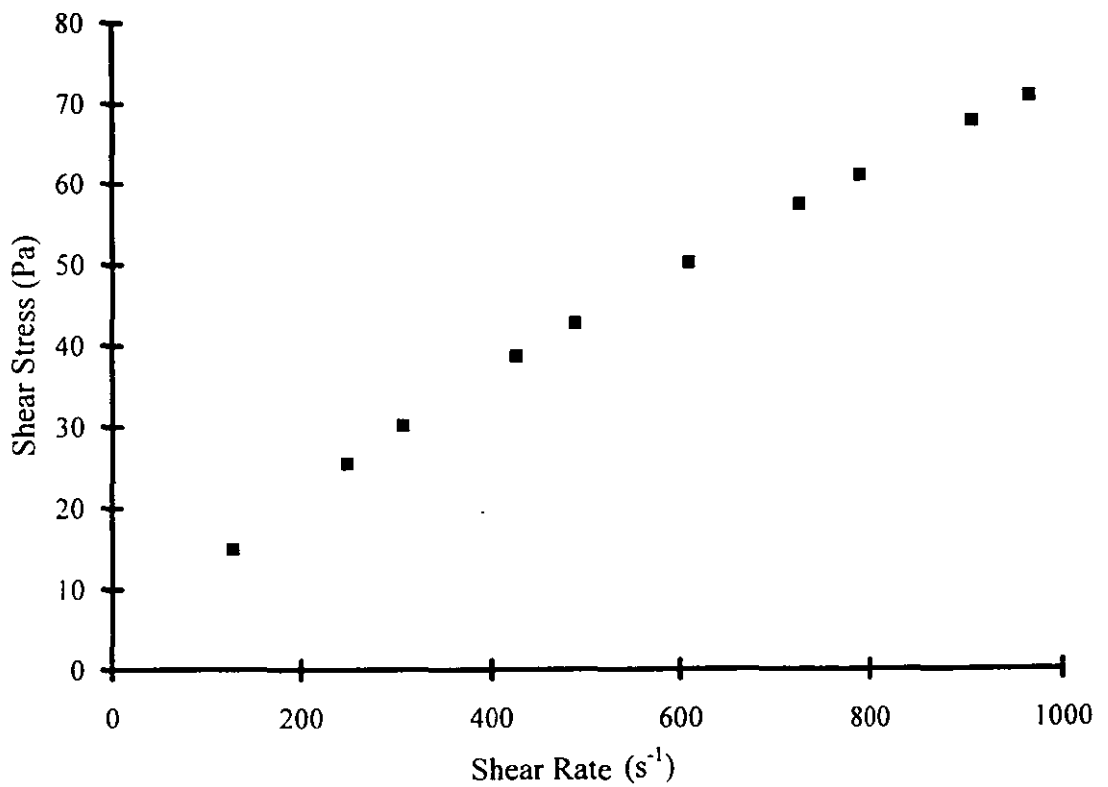
Microgel dispersions show shear-thinning (pseudoplastic) behaviour over the 25-1000 s^{-1} shear rate range [233, 309], as can be seen from the decrease in the gradient of the shear stress-shear rate curve ($\eta = \tau/D$) [309] as the shear rate increases. This behaviour is commonly observed from rheological characterisation of colloidal dispersions (section 1.7.2) [233-235]. The viscosities of the benzyl alcohol dispersions (table 4.6) appear to follow no set pattern of behaviour, in terms of the relation between the particle's crosslink-density (table 4.3) and the dispersion viscosity. Furthermore, for any given microgel formulation, the viscosity of the benzyl alcohol dispersion was significantly higher than the corresponding n-butanol formulation. The solubility parameters of poly(n-butyl acrylate) and n-butanol [301] are listed in table 4.8.

Table 4.8 - Component Solubility Parameters [301]

Component	Solubility Parameter, δ [J cm^{-3}]$^{1/2}$
PnBA	18.0
n-Butyl alcohol	23.3

If microgel dispersion viscosities could be purely considered in terms of particle-swelling with organic diluent effects (section 3.6) [214, 227], it would be apparent that benzyl alcohol had swollen the gel particles to a greater extent than had n-butanol (for each of the four microgels which had been dispersed in both of the organic diluents). The exceptionally high viscosity of the poly(n-butyl acrylate) solution in benzyl alcohol ($\eta = 161$ cP), compared to the n-butanol solution ($\eta = 56$ cP), suggests that there could have been other thermodynamic factors which significantly influenced the viscosity behaviour of acrylic microgel dispersions in benzyl alcohol. A similar, but significantly less marked, viscosity increase was also observed for polystyrene microgel dispersions in benzyl alcohol (section 3.6). It would appear possible that benzyl alcohol is a "special case" as a dispersant for PS and PnBA. The exceptionally large differences between the polymer (PS or PnBA) and benzyl alcohol solubility parameter (section 3.6 and table 4.8) [232] could have had a critical influence on the viscosity of the dispersion in these two instances. The high viscosity of the acrylic benzyl alcohol microgel dispersions ($\eta \approx 80$ cP) at 5 weight % solid concentrations,

compared to organic polystyrene dispersion viscosities (section 3.6), rendered acrylic microgel synthetic processes unsuitable for the preparation of first-stage microgel dispersion precursors for IPN microgel synthesis (n-butanol is a non-solvent for polystyrene, copolymerisation of styrene/DVB within acrylic dispersions in nBuOH would, most probably, have lead to precipitation of the IPN particles). Consequently, it was decided that initial investigations into IPN microgel synthesis should involve copolymerisation of acrylic comonomer within organic polystyrene microgel dispersions.

4.5 - SOLUBILITY OF nBA AND STYRENE WITH ORGANIC LIQUIDS

Polystyrene (chapter 3), or poly(n-butyl acrylate), microgel dispersion preparation, was merely the first completed element, of several separate processes required, within the IPN microgel synthetic pathway. Second-stage comonomers were then to be added to the first-stage microgel dispersion. Comonomer addition was to be subsequently followed by free radical copolymerisation of these second-stage components within the first-formed microgel particles. The partitioning behaviour of comonomer within the first-stage gel particles was of critical importance for the synthesis of IPN particles. Exclusive sorption of comonomer molecules within the first-formed microgel particles would have suggested that second-stage copolymerisations could be initiated by continuum-soluble free radical initiator. Partial swelling of microgel with comonomer, with the remaining comonomer molecules constituting a droplet phase (under mechanical agitation), could have also potentially allowed, via the employment of a modified quasi-emulsion copolymerisation process [222, 223], for IPN microgel synthesis (provided that a free radical initiator which was soluble in the organic dispersant, but insoluble in the comonomer droplet phase, could have been found). The presence of large quantities of comonomer within the continuous phase, a homogeneous organic diluent/comonomer mixture, would have been most undesirable for IPN microgel synthesis. The employment of a continuum-soluble free radical initiator within such a system would, most probably, have lead either to the synthesis of acrylic microgel particle contaminants (section 1.2), or, to the generation of acrylic macrogel (the

nature of the acrylic copolymer synthesised would be dependent upon the concentration of comonomer within the system, as detailed in section 1.2). Consequently, the solubility behaviour of styrene and n-butyl acrylate monomers (25°C) within a variety of different organic diluents was determined (section 2.5.1). The solubility parameters (section 3.6) of several of the liquids employed within these investigations are detailed in table 4.9. Additional component solubility parameter values are listed in tables 3.10 and 4.8.

Table 4.9 - Solubility Parameters of Liquids used for Monomer Solubility Studies

Organic Diluent	Solubility Parameter, δ (J cm^{-3})$^{1/2}$ [301]
Poly(dimethylsiloxane)	10.0 - 12.1
n-Hexane	14.9
Butanone	19.0
Styrene	19.0
Ethanol	26.0
Methanol	29.7
N-Methyl formamide	32.9
Formamide	39.3
Water	47.9

The solubility parameter of a given material can be considered [11, 232] to reflect the relative extent of attraction between the substance's molecules. For example, liquids which exhibit strong hydrogen bonding have high solubility parameters (e.g. water and formamide [301]). Non-polar materials, e.g. methane and n-hexane, have relatively low δ values, however [232, 301]. Two substances are mutually-soluble if the Gibbs free energy of mixing [58] is negative (section 1.3). For mixtures of low molecular weight liquids, the entropy of mixing is generally positive (and, of low magnitude) [58] (section 1.3). Consequently, for a given liquid pair, solubility of the components can be considered to occur [11, 58, 232] only below a limiting, positive, value of the enthalpy of mixing. For highly endothermic mixing processes, phase separation results, therefore, on mixing the two liquid components [58, 232].

Hildebrand [310] derived a relation for prediction of the enthalpy on mixing two dissimilar materials:

$$\Delta h_m = \phi_1 \phi_2 (\delta_1 - \delta_2)^2 \qquad (4.4)$$

where Δh_m is the enthalpy of mixing per unit volume (J m^{-3}), ϕ_i is the volume fraction and δ_i is the solubility parameter [(J m^{-3})$^{1/2}$] of component i, respectively [310].

The Hildebrand method [310] for estimation of enthalpies of mixing predicts that two phase systems are observed, therefore, on mixing two materials where the difference in component solubility parameter is large [58, 232] (section 1.3). Styrene and n-butyl acrylate monomers both have low water solubilities (< ca. 0.5 g l^{-1} at 25°C) [248]. This observation can be considered to result [310] from the large differences in solubility parameter between water and the two monomers. Okubo et $al.$ [221-223] have investigated the swelling of monodisperse polystyrene microsphere dispersions in ethanol/water mixtures with divinylbenzene. The preparation of composite PS/poly(DVB) particles [222, 223] was found to compete with additional poly(DVB) synthesis [223], unless the alcohol/water medium was of sufficient polarity [232], and optimum monomer addition conditions were employed (section 1.7.1) [232, 233].

Formamide was the only organic liquid examined which was (practically) immiscible with both nBA and styrene. Each of the other organic liquid/monomer systems were found to be of one-phase over all mixture compositions (25°C). Formamide has a high boiling point [248] and the material also has undesirable toxicity effects. Additionally, formamide has been found to react with organic peroxides [248]. Consequently, none of the organic liquids examined was considered suitable for attempts at IPN microgel synthesis from second-stage, modified, quasi-emulsion copolymerisation processes [222, 223].

CHAPTER 5

POLYSTYRENE MACROGELS

5.1 - SOL-GEL RATIOS FOR POLYSTYRENE MACROGELS

The preparation of organic acrylic microgel dispersions was found to be limited to systems where the organic liquid was a solvent for linear P*n*BA, where the liquid was higher-boiling than water, and where the affinity between water and the organic diluent was high (section 4.4.1). Acrylic dispersions were finally prepared in *n*-butanol (*n*BuOH) and benzyl alcohol, only (section 4.4.1). Copolymerisation of styrene/divinylbenzene within acrylic microgel dispersions in *n*-butanol would, most probably, have lead to precipitation of IPN microgel particles, as *n*BuOH is a non-solvent for linear polystyrene [214, 311]. Additionally, acrylic microgel dispersions in benzyl alcohol were of high viscosity at low dispersion solid concentrations (section 4.4.3). Low viscosity organic polystyrene microgel dispersions were prepared in a variety of organic dispersants, however (section 3.6). Consequently, IPN microgel synthesis was considered to be potentially more facile, if copolymerisation of acrylic comonomers within organic PS microgel dispersion techniques were to be utilised. Ideally, the introduction of second-stage comonomers within organic PS microgel dispersions would have lead to exclusive adsorption of comonomers within first-stage microgel particles. IPN microgel synthesis could have then been attempted with the employment of a continuum-soluble free radical initiator. The partitioning behaviour of *n*BA monomer within polystyrene gel/organic liquid systems was, therefore, of critical importance for determining the ideal synthetic route for IPN microgel preparation. Preferential sorption of solvent by linear polymer molecules in dilute binary liquid mixtures [312-316] has been considered to be governed by several factors [312-314]. Temperature [315], chemical structure of the (linear) polymer chain [313, 315], the nature of the two solvents [313, 314], and binary mixture composition [312, 313], are the major parameters that have been considered [312-316] in the analysis of preferential sorption. For a polymer solution in a thermodynamically good solvent [11], it is possible to vary the solvency of the medium by introducing controlled quantities of a second, theta, solvent [313]. The coefficient of selective adsorption [312, 313] of one of the two solvent components can be subsequently determined from sedimentation phenomena [317], differential refractometry analysis [318, 319], or, densitometry [320-322] techniques (amongst other [323-326] analytical characterisation methods). Preferential monomer (*n*BA)

swelling of PS microgel particles dispersed in organic diluent could potentially be determined from centrifugation techniques [227]. Second-stage monomer would be initially added to an organic polystyrene microgel dispersion, and, after sufficient time had passed for equilibration to be attained within the system, swollen microgel particles could be sedimented by high speed centrifugation [227]. Analytical characterisation of the supernatant could potentially allow for a determination of the relative quantities of monomer imbibed within the particles, and the monomer composition within the homogeneous (two-component) liquid mixture (the continuous phase for second-stage copolymerisations). An estimation of PS microgel particle swelling with monomer, within organic microgel dispersion systems, was made from equilibrium swelling of PS macrogel samples with a benzyl alcohol/nBA mixture (10 wt.% nBA) within this particular investigation. Benzyl alcohol was chosen as the inert organic diluent as a consequence of the large solubility parameter difference [232] between the material and polystyrene (section 3.3), when compared to the solubility parameter difference between polystyrene and nBA monomer (section 3.3).

Polystyrene macrogel samples were prepared from bulk free radical copolymerisation processes (sections 2.1.2 and 2.5.1). Soxhlet extraction with toluene (section 2.5.2) was performed on polymer samples taken from the recovered, PS (1 wt.% DVB), PS (5 wt.% DVB) and PS (10 wt.% DVB), macrogel sheets (section 2.5.1). The quantity of soluble polymer component (the sol component [327]) which is extracted from a given macrogel sample, can give an indication of the efficiency of intermolecular crosslinking within the macrogel system [327]. The sol content of each PS macrogel sample was evaluated from:

$$\text{Sol} = \{(m_1 - m_2) / m_1\} \times 100\,\% \qquad (5.1)$$

where m_1 is the original mass of the macrogel sample (g), prior to extraction, and m_2 is the final sample mass (g) after extraction with toluene.

Sol components determined for the three macrogel samples are detailed in table 5.1.

Table 5.1 - Sol Components of Polystyrene Macrogel Samples

Macrogel System	Sol Content (Weight %)
PS (1 wt. % DVB)	1.24
PS (5 wt. % DVB)	0.58
PS (10 wt. % DVB)	0.31

Consideration of the sol data presented in table 5.1 signifies that the gel component of each material was high (> 98.7 weight % of the total system solids, for each of the three formulations investigated). Increasing the concentration of crosslinking agent lead to a decrease in the fraction of soluble (linear and/or branched polymer) component present within these materials. It would appear that the incorporation of divinylbenzene had, therefore, lead to extensive intermolecular crosslinking [327] of these PS-based materials.

5.2 - DMTA CHARACTERISATION OF POLYSTYRENE MACROGELS

Macrogel samples recovered from bulk copolymerisation processes (section 2.5.2) were analysed by dynamic mechanical thermal analysis, DMTA (section 2.8.2). Plots of loss tangent versus temperature (sections 2.8.2 and 3.3) for the PS (1 wt.% DVB), PS (5 wt.% DVB) and PS (10 wt.% DVB) macrogel samples are shown in figures 5.1, 5.2, and 5.3, respectively. The glass transition (α-relaxation) parameters (section 3.3), obtained from DMTA characterisation of the four polystyrene-based materials, are listed in table 5.2.

Table 5.2 - Polystyrene Macrogel Glass Transition Data from DMTA

Sample	$Tan\delta_{MAX}$	T_g (°C) at 10 Hz
Polystyrene	2.7	109
PS (1 wt.% DVB)	1.8	117
PS (5 wt.% DVB)	1.6	122
PS (10 wt.% DVB)	1.5	131

Figure 5.1 - Tanδ with Temperature Curve for PS (1 wt.% DVB) Macrogel
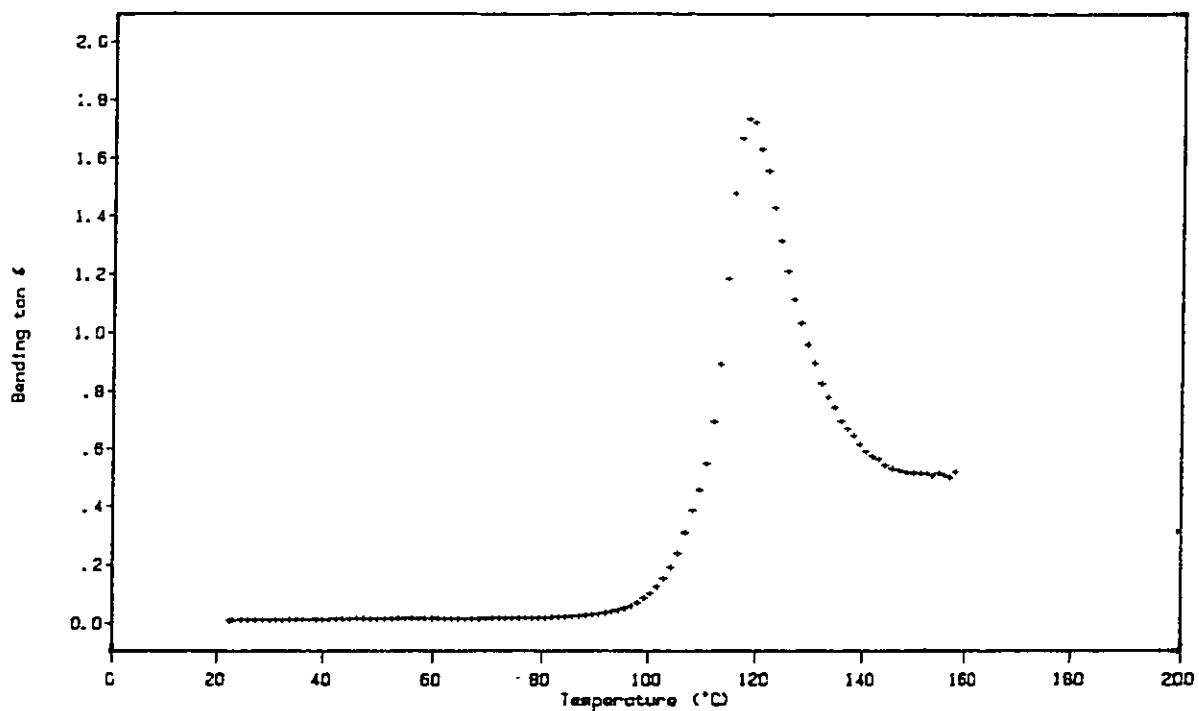
Figure 5.2 - Tanδ with Temperature Curve for PS (5 wt.% DVB) Macrogel
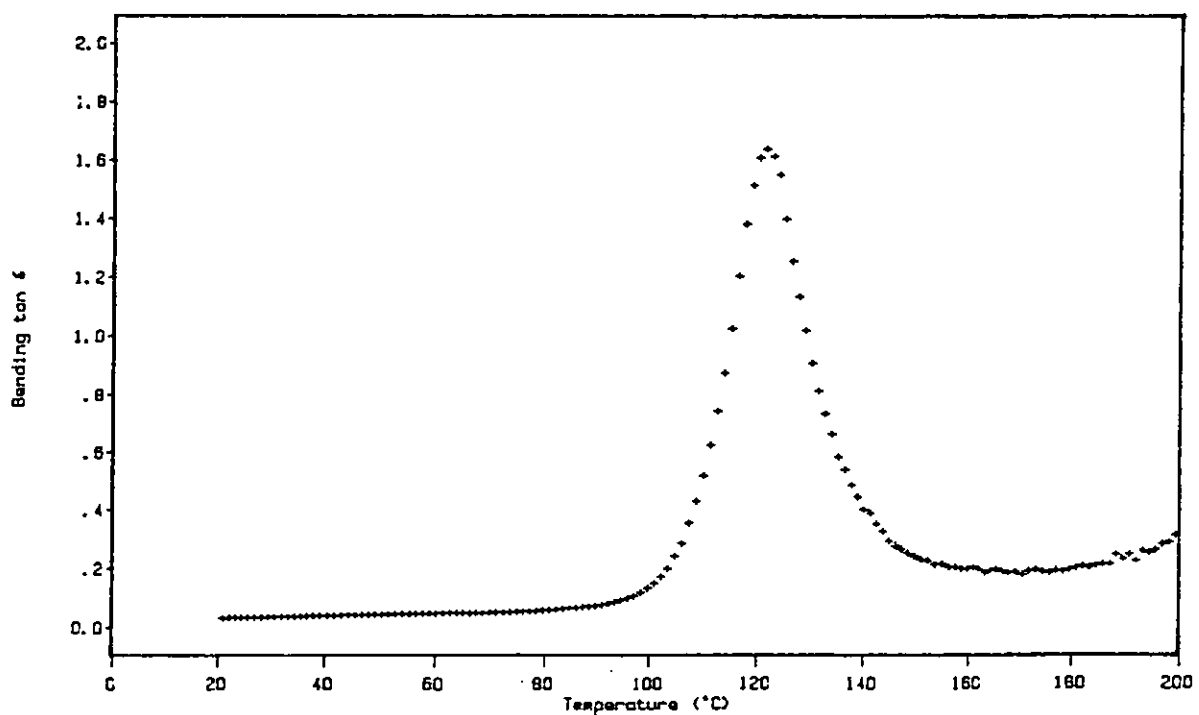
Figure 5.3 - Tanδ with Temperature Curve for PS (10 wt.% DVB) Macrogel
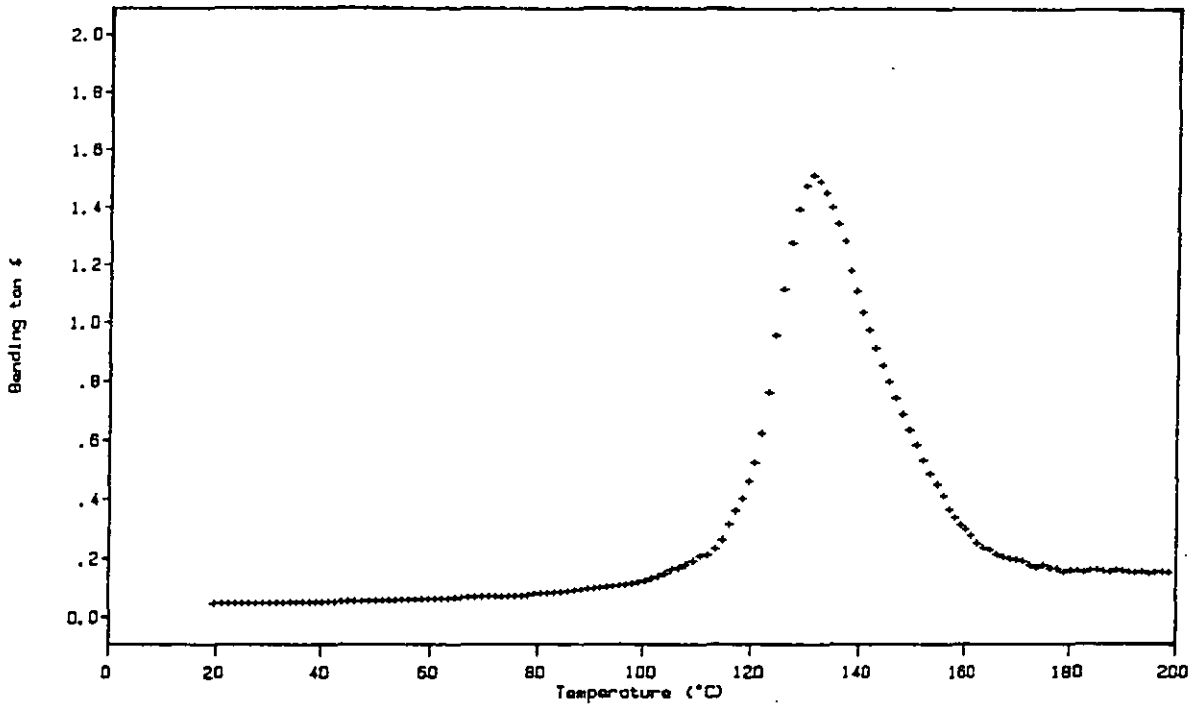
DMTA observations indicate that the incorporation of increasing concentrations of DVB within the copolymerisation formulation leads to an increase in the macrogel's glass transition temperature (when compared to the T_g of the polystyrene homopolymer sample). The $tan\delta_{MAX}$ value (table 5.2) also decreases in magnitude as the concentration of the divinyl moiety within the macrogel formulation increases. These observations are in accordance with the glass transition behaviour determined for polystyrene microgels from DMTA analysis (section 3.3). Shifts in glass transition temperature values are observed on crosslinking polymer samples [261, 264] (section 3.3). Estimations of macrogel average molecular weight between crosslink (M_c) values were made from insertion of macrogel T_g-shifts (table 5.2) into the Nielson [261] relation (equation 3.1, section 3.3). Theoretical average molecular weight between crosslinks [287] (equation 3.2, section 3.3), M_c^{calc}, and M_c values estimated from T_g-shifts [261], for the three polystyrene macrogel samples prepared, are detailed in table 5.3.

Table 5.3 - Theoretical and Experimental Network M_c Values for PS Macrogels

Macrogel Sample	M_c^{calc} (kg mol^{-1}) [287]	M_c (kg mol^{-1}) [261]
PS (1 wt.% DVB)	11.8	4.9
PS (5 wt.% DVB)	2.4	3.0
PS (10 wt.% DVB)	1.2	1.8

The PS (5 wt.% DVB) and PS (10 wt.% DVB) macrogel M_c values from DMTA characterisation [261] are comparable to the theoretical [287] average molecular weight between crosslink values for homogeneous network samples. The T_g-shift observed for the PS (1 wt.% DVB) macrogel formulation is higher than the value anticipated [287] for its corresponding perfect network analogue (section 1.2), when determined by the Nielson [261] approach. The crosslink-density of this particular macrogel is apparently higher, therefore, than would be anticipated for the corresponding "ideal" network sample (section 1.2). It would appear, therefore, that the Nielson relation [261] does not apply to this particular material. PS macrogel glass transition temperatures were found to be higher than the corresponding microgel T_g values (section 3.3). Such observations could suggest that either the macrogel structures were less homogeneous than microgel network structures (section 1.2), or, that a greater number of divinyl moieties had been incorporated within chemical crosslinks under bulk polymerisation conditions. Microgels were synthesised from emulsion copolymerisation processes with semi-continuous comonomer addition (section 2.2.1). Macrogels were synthesised from bulk copolymerisation (section 2.5.1), however. Compositional drift in the network structure during the course of the copolymerisation process [34-36, 39] would be anticipated, therefore, to have been potentially more marked for the macrogel formulation (section 1.5). Microgel molecular weights are significantly lower [41] than the molecular weights of macrogel molecules, materials which have been considered [45] to comprise of intermolecularly crosslinked microgel aggregates. The increased glass transition temperatures observed for the PS macrogel samples (sections 3.3 and 5.2) could have potentially resulted from the operation of one, or more, of these contrasting synthetic characteristics, as detailed above, which can be exhibited by these two non-equivalent modes of copolymerisation (sections 1.2, 1.5 and 3.3).

5.3 - EQUILIBRIUM SWELLING OF POLYSTYRENE MACROGELS

Macrogels, in contrast to microgel particles, can not be dispersed in organic diluents. The addition of organic liquid to a macrogel sample can, however, lead to extensive swelling of the gel with liquid [167, 299, 328]. The non-equivalent behaviour between macrogel and microgel formulations results from the differences in molecular size (molecular weight) observed between the two types of material [41, 45]. Microgels prepared from free radical solution copolymerisation of styrene and divinylbenzene [41] have been found to be limited to molecular weights below 10^8 g mol^{-1}. The molecular weight of a macrogel molecule is, theoretically [11, 31], infinite, however. Macrogel samples can absorb several times their own weight of organic liquid [167, 328], to a degree dependent upon the crosslink-density [167, 299] of the network. In the resulting, swollen, gel, interactions between swelling agent and segments of the network polymer overcome the attraction between adjacent segments of the polymer chain [329]. As a result, the network becomes swollen up to a point where its osmotic pressure (free energy of dilution) is balanced by the network's strain and by its loss of entropy [329].

Equilibrium swelling (section 2.5.5) of polystyrene macrogel samples was performed with anhydrous tetrahydrofuran (THF), cyclohexanone (CHX), n-butyl acrylate (nBA), toluene (ϕCH$_3$) and benzyl alcohol (ϕCH$_2$OH). Recorded macrogel and liquid-swollen macrogel masses were subsequently converted into the two respective component's mass values. Polystyrene network volume fractions (ϕ_2) at equilibrium were then evaluated from [330]:

$$\phi_2 = (m_2 / \rho_2) / \{ (m_1 / \rho_1) + (m_2 / \rho_2) \} \qquad (5.2)$$

where m_2 is the mass of polymer network at equilibrium, m_1 is the mass of swelling agent at equilibrium, ρ_2 is the bulk density of the macrogel and ρ_1 is the density of the swelling agent.

Table 5.4 - PS Macrogel ϕ_2 Values from Equilibrium Swelling (25°C)

Macrogel/Swelling Agent System	Polymer Volume Fraction, ϕ_2 (25°C)
PS (1 wt.% DVB)/THF	0.165
PS (5 wt.% DVB)/THF	0.229
PS (10 wt.% DVB)/THF	0.284
PS (1 wt.% DVB)/ϕCH$_3$	0.178
PS (5 wt.% DVB)/ϕCH$_3$	0.243
PS (10 wt.% DVB)/ϕCH$_3$	0.297
PS (1 wt.% DVB)/nBA	0.241
PS (5 wt.% DVB)/nBA	0.383
PS (10 wt.% DVB)/nBA	0.528
PS (1 wt.% DVB)/CHX	0.192
PS (5 wt.% DVB)/CHX	0.273
PS (10 wt.% DVB)/CHX	0.546
PS (1 wt.% DVB)/ϕCH$_2$OH	0.354
PS (5 wt.% DVB)/ϕCH$_2$OH	0.579
PS (10 wt.% DVB)/ϕCH$_2$OH	0.740

(where the ϕ symbol of ϕCH$_3$ and ϕCH$_2$OH represents the phenyl, C$_6$H$_5$, group).

Published poly(styrene-*co*-divinylbenzene) [331] and organic liquid [248] densities were used for determination of polymer volume fractions (equation 5.2). The solubility parameters for poly(styrene-*co*-divinylbenzene) [300] and for each of the organic dispersants [301] are listed in table 3.10.

For any given swelling agent, the ϕ_2 value increases as the macrogel's divinylbenzene content increases (table 5.4). These findings suggest that the higher the concentration of DVB comonomer within the bulk copolymerisation formulation, the higher the crosslink-density of the resulting macrogel [167]. PS (1 wt.% DVB) macrogels were swollen to the highest extent, by each of the five swelling agents investigated (table 5.4). For THF, toluene, cyclohexanone and benzyl alcohol swelling data, the ϕ_2 value increases as the solubility parameter difference between polystyrene and the liquid increases [232, 300, 301]. The highest levels of liquid swelling, for a given macrogel sample, are found with THF, and the lowest degrees of swelling are found with benzyl alcohol. These observations are consistent with the method of Hildebrand [310] (section 4.5) which predicts that the enthalpy on mixing two dissimilar materials, in the absence of specific thermodynamic interactions [232, 310] occurring

within the system, becomes less endothermic as the solubility parameter difference between the two materials is minimised [310] (section 4.5). According to this approach [232, 310], therefore, the Gibbs free energy [58, 232] on mixing two dissimilar materials should become increasingly less positive, as the solubility parameter of the first component approaches that of the second material within such a system [232, 310]. The level of macrogel swelling with n-butyl acrylate would appear, however, to be significantly lower than the degree of network swelling anticipated from solubility parameter considerations [232] alone. The average molecular weight between crosslinks, M_c value, for affine networks [167], from equilibrium swelling investigations, can be estimated [167, 328] from the Flory-Rehner [167] equation:

$$\ln(1 - \phi_2) + \phi_2 + \chi_{1,2}(\phi_2)^2 + \frac{\rho\,(V_1)\phi_2^{1/3}}{M_c} - \frac{2\phi_2}{f} = 0 \qquad (5.3)$$

where ϕ_2 is the volume fraction of network polymer at swelling equilibrium [167], $\chi_{1,2}$ is the polymer-solvent interaction parameter [167], ρ is the bulk density (kg m^{-3}) of the macrogel, V_1 is the molar volume of the swelling agent (m^3 mol^{-1}), f is the network functionality [167], and M_c (kg mol^{-1}) is the average molecular weight between crosslinks for the network sample [167].

Theoretical M_c values [287], corresponding to average molecular weights of idealised network structures (sections 1.2 and 3.3), were calculated for the three PS networks synthesised. Additionally, M_c values were evaluated from PS macrogel/toluene equilibrium swelling (25°C) experiments [167] (section 2.5.2). The parameters inserted into the Flory-Rehner equation [167] for the three PS/toluene systems, were; $\chi_{1,2} = 0.44$ [332], $\rho = 1050$ (kg m^{-3}) [331], $V_1 = 1.06 \times 10^{-4}$ (m^3 mol^{-1}) and $f = 4$ [333]. Theoretical and experimentally-determined M_c values are shown in table 5.5.

Table 5.5 - Macrogel Average Molecular Weight Between Crosslink Values

Macrogel System	M_c^{calc} (kg mol^{-1}) [287]	M_c (kg mol^{-1}) [167]
PS (1 wt.% DVB)	11.8	12.9
PS (5 wt.% DVB)	2.4	5.9
PS (10 wt.% DVB)	1.2	3.5

In general terms, the crosslink-densities (from equilibrium swelling investigations) of the three polystyrene macrogel samples [167] appear to be of comparable magnitude to their idealised values [287]. The two highly crosslinked materials, i.e. the PS (5 wt.% DVB) and PS (10 wt.% DVB) macrogel samples, do, however, appear to be, on average, less highly crosslinked than would be anticipated for the corresponding "idealised" network samples [287]. Each network was synthesised via bulk free radical copolymerisation (section 2.5.1), the preferential consumption of divinylbenzene during the early stages of the copolymerisation process (sections 1.2 and 1.5) has been commonly observed [34-36, 39] under such synthetic conditions. The homogeneity of the network structure would, therefore, be anticipated to diminish [36, 39, 45] within systems containing high concentrations of crosslinking agent, under bulk copolymerisation conditions (section 1.5). The M_c value recorded for the PS (1 wt.% DVB) macrogel, from equilibrium swelling [167] (section 2.5.2), appears to closely mirror the crosslink-density anticipated for its corresponding perfect network analogue [287]. The drift in copolymer compositional structure [34-36, 134, 135] (section 1.5) would be anticipated to be the lowest for this particular material [34, 35], therefore, out of the three polystyrene macrogel formulations investigated. Significant discrepancies between crosslink-densities evaluated from DMTA macrogel T_g-shifts [261] (table 5.3 and section 3.3) and from equilibrium swelling [167] (table 5.5) investigations are also apparent. The empirical nature of the Nielson relation [261] (equation 3.1, section 3.3) could possibly have been the underlying factor for this particular observation.

5.4 - PS MACROGEL SWELLING WITH BENZYL ALCOHOL/nBA

PS macrogels were synthesised in order to estimate the equilibrium swelling behaviour of PS networks with benzyl alcohol/n-butyl acrylate mixtures. If nBA was found to partition solely within PS networks, second-stage copolymerisations of acrylic comonomers within PS gel particles dispersed in benzyl alcohol could have been justifiably attempted with the employment of continuum-soluble initiator. The three polystyrene macrogel samples prepared were swollen with a benzyl alcohol/nBA mixture (10 wt.% nBA) with ca. 10 wt.% solids content employed for each swelling experiment (120 hours at 25°C), as discussed previously (section 2.5.2). The masses of macrogel, benzyl alcohol and nBA initially added to each vessel were recorded (table 5.6). After the period for equilibration (section 2.5.2), swollen macrogels were recovered, and their masses were then determined (table 5.6). Compositions of benzyl alcohol/nBA mixtures which remained outside of gel components were determined from FTIR spectroscopy [270, 294] (sections 2.5.2 and 2.8.5). FTIR spectra of benzyl alcohol/nBA mixtures (1, 2, 3, 4, 5, 6, 7, 8, 9 and 10 wt.% nBA) were also recorded (section 2.5.2), for IR calibration purposes [45, 294]. An absorbance ratio (A_{1728}/A_{698}) [294] for the benzyl alcohol absorption at 698 cm^{-1} (figure 5.4) and the carbonyl (C=O) stretching absorption (nBA) at 1728 cm^{-1} wavenumber [270] (figure 5.5) was determined for each of the ten FTIR calibration spectra (section 2.5.2). The absorbance FTIR spectrum for a benzyl alcohol/nBA (5 wt.% nBA) mixture is shown in figure 5.6, and the FTIR absorbance ratios (A_{1728}/A_{698}) determined for the ten calibrant mixtures are given in table 5.7.

Table 5.6 - Polystyrene Macrogel and Benzyl Alcohol/nBA (10 wt.% nBA) Masses Recorded for Three-Component Equilibrium Swelling Studies

Macrogel	Initial Gel Mass (g)	Mass Liquid Added (g)	Final Gel Mass (g)
PS (1 wt.% DVB)	0.42	4.20	1.21
PS (5 wt.% DVB)	0.35	3.50	0.58
PS (10 wt.% DVB)	0.24	2.40	0.36

Figure 5.4 - Absorbance FTIR Spectrum of Benzyl Alcohol
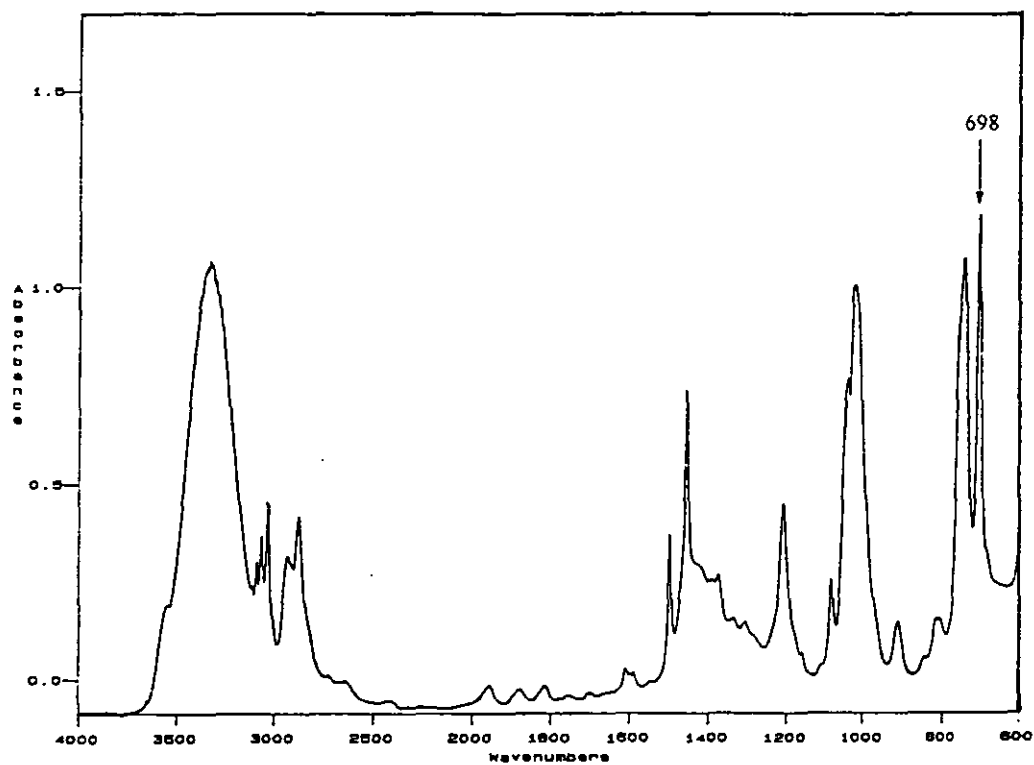
Figure 5.5 - Absorbance FTIR Spectrum of *n*-Butyl Acrylate

174
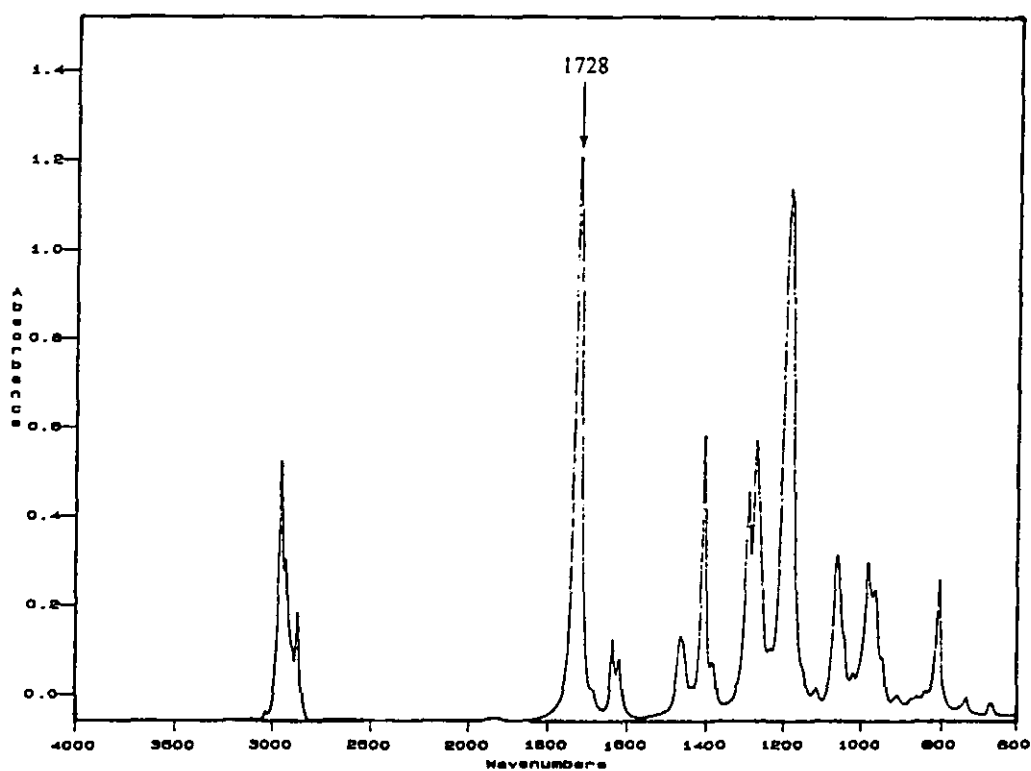
Figure 5.6 - Absorbance FTIR Spectrum of Benzyl Alcohol/nBA (5 wt.% nBA)
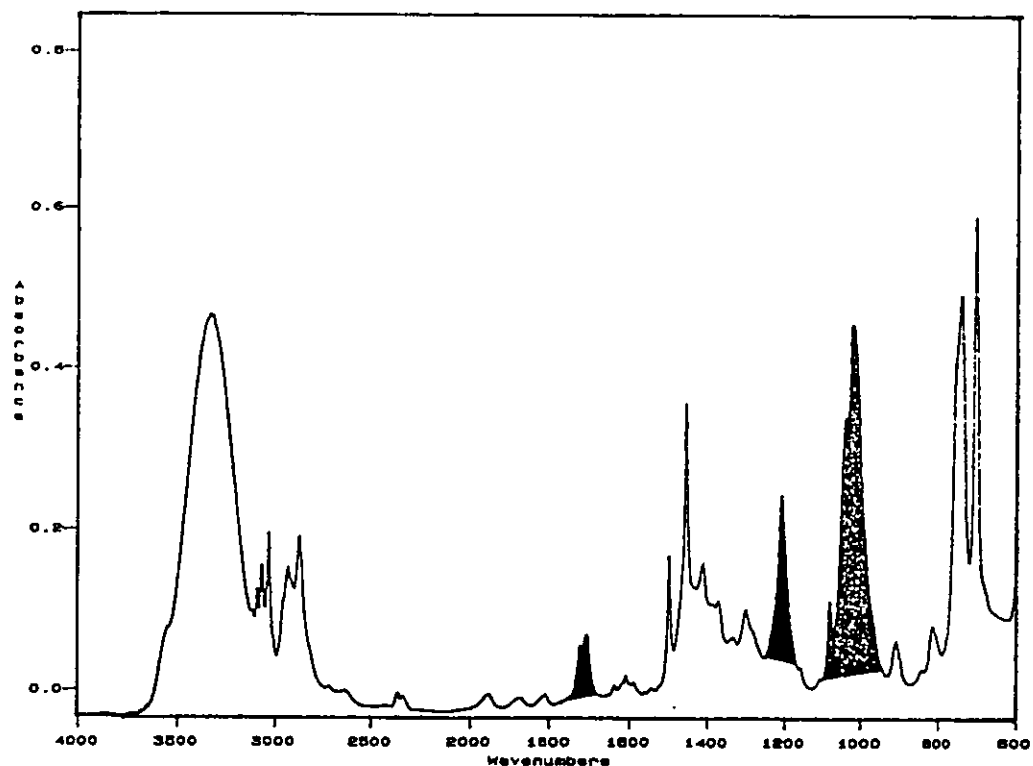
Table 5.7 - FTIR Absorbance Ratios for Benzyl Alcohol/nBA Calibrants

nBA Content (Weight %)	IR Absorbance Ratio (A_{1728}/A_{698})
1.0	0.03
2.0	0.06
3.0	0.11
4.0	0.14
5.0	0.18
6.0	0.22
7.0	0.24
8.0	0.28
9.0	0.32
10.0	0.37

The absorbance FTIR spectrum recorded for the swelling agent recovered after equilibrium swelling of the PS (5 wt.% DVB) macrogel sample (section 2.5.2) is shown in figure 5.7. FTIR absorbance ratios [270, 294] for the three liquid mixtures found to remain outside of PS networks after equilibrium swelling were recorded (section 2.5.2). These absorbance ratios are displayed in table 5.8.

Figure 5.7 - Absorbance FTIR Spectrum of the Swelling Agent Recovered from the PS (5 wt.% DVB) Macrogel System
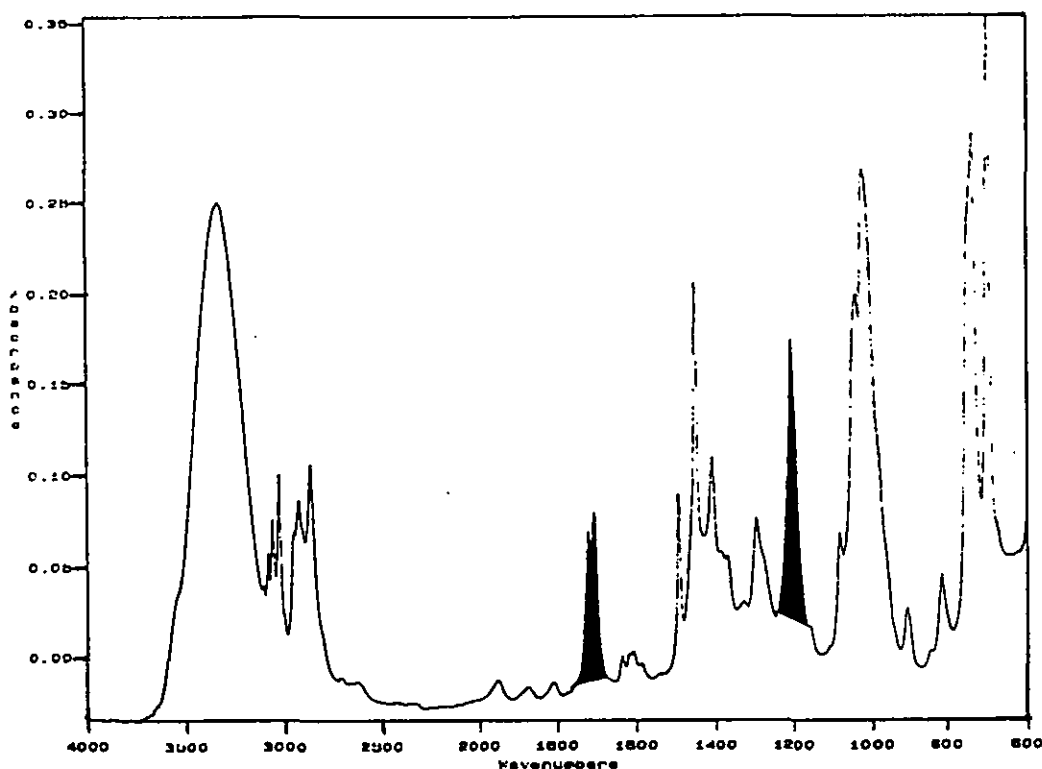
Table 5.8 - Absorbance Ratio for Liquid Mixture Found to Remain Outside of Gel

Macrogel Sample	IR Absorbance Ratio (A_{1728}/A_{698})
PS (1 wt.% DVB)	0.35
PS (5 wt.% DVB)	0.35
PS (10 wt.% DVB)	0.36

The concentration of nBA found within the liquid mixture recovered after equilibrium swelling (section 2.5.2) would appear to be, ostensibly, identical to the initial concentration of acrylic monomer in the nBA/benzyl alcohol swelling agent (as signified from the data represented in tables 5.7 and 5.8). It can be concluded from these equilibrium swelling experiments that nBA had not preferentially swollen these PS networks, under the experimental conditions utilised (section 2.5.2). The use of continuum-soluble initiator for copolymerisation of second-stage, acrylic, comonomers within PS microgel dispersions in benzyl alcohol, would, therefore, most probably have lead to the generation of acrylic macrogel (acrylic microgel contaminants could have also possibly resulted from such a procedure, the nature of

the acrylic gel component recovered would have been dependent upon the volume fraction of second-stage crosslinking agent within the system, as discussed in section 1.2). The apparent absence of an organic diluent/monomer system suitable for second-stage polymerisations under a modified form of quasi-emulsion conditions (section 4.5) [222, 223], and the apparent non-preferential sorption of monomer in the PS/nBA/benzyl alcohol system (a mixture where the solubility parameter of the polymer network and monomer were comparable in magnitude whereas the inert organic diluent was anticipated to have been significantly less compatible with the gel [232, 310]), lead to an investigation into the synthesis of PS microgel particles functionalised with second-stage polymerisation initiator fragments (chapter 7). These techniques were investigated in order to try and minimise the extent of second-stage polymerisation within the continuum, under conditions where polymerisation of a second network within the particles of a first-stage organic microgel dispersion was to be attempted, i.e. for experimental investigations into the synthesis of IPN microgel dispersions.

CHAPTER 6

ACRYLIC MACROGELS

As can be seen from table 6.1, Soxhlet extraction procedures indicated that the gel component of each material was high (> 98.2 weight % of the total system solids, for each of the five formulations investigated). Increasing the concentration of crosslinker for both the NPGDA and EGDMA systems yielded materials with decreased soluble-component (linear and/or branched polymer) fractions. It would appear that the incorporation of divinyl comonomer had, therefore, led to extensive intermolecular crosslinking of these PnBA-based materials [327].

6.2 - DMTA CHARACTERISATION OF PnBA MACROGEL SAMPLES

Macrogel samples recovered from bulk copolymerisation processes (section 2.6.1) were analysed by dynamic mechanical thermal analysis (section 2.8.2), DMTA (measurements were recorded at a 3°C per minute heating rate at a fixed frequency of 10 Hz). Plots of loss tangent (tanδ) versus temperature (sections 2.8.2 and 3.3) for the poly(n-butyl acrylate) homopolymer, and PnBA (10 wt.% NPGDA), PnBA (20 wt.% NPGDA) and PnBA (20 wt.% EGDMA) microgel samples, are shown in figures 6.1, 6.2, 6.3 and 6.4, respectively. Glass transitional parameters (section 3.3) obtained from DMTA characterisation of the six acrylic materials are listed in table 6.2.

Figure 6.1 - Tanδ with Temperature Curve for PnBA Homopolymer
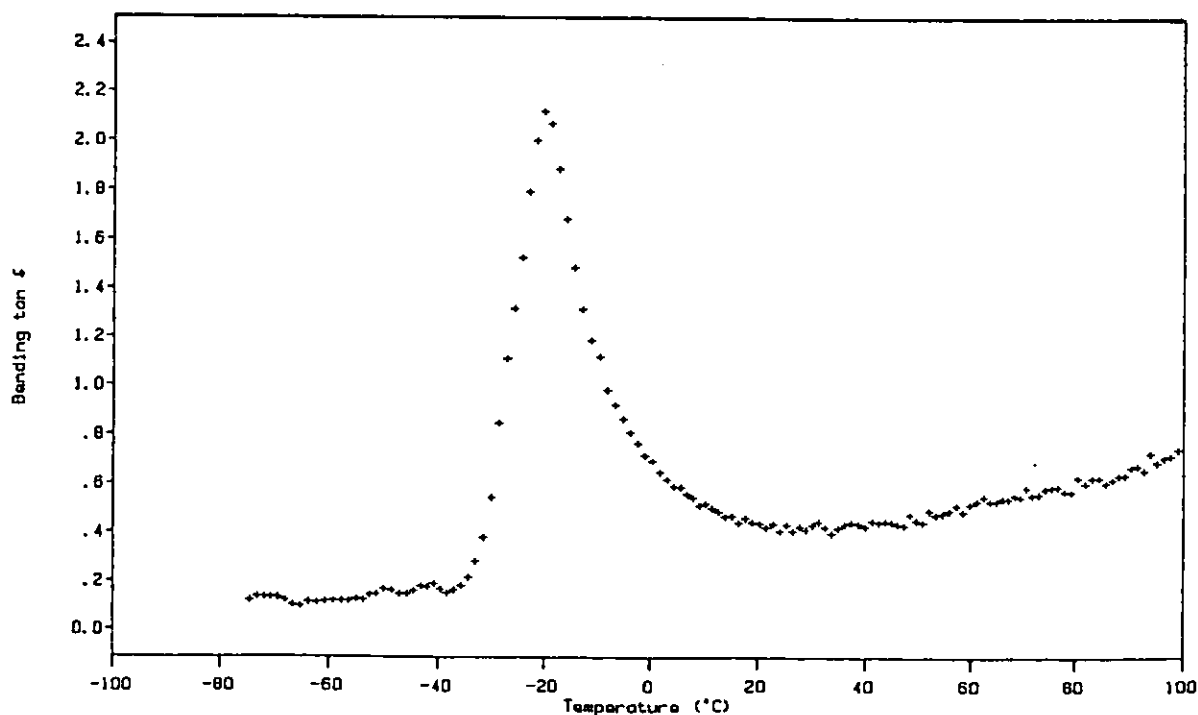
Figure 6.2 - Tanδ with Temperature Curve for P*n*BA (10 wt.% NPGDA) Macrogel
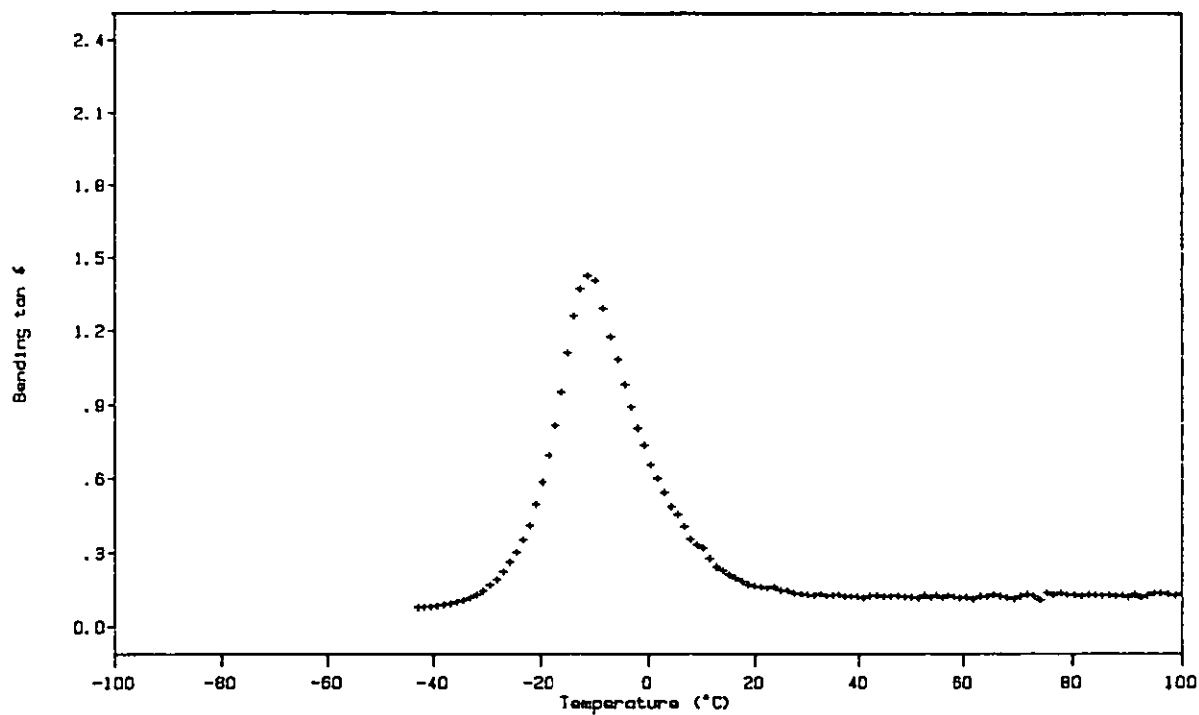
Figure 6.3 - Tanδ with Temperature Curve for P*n*BA (20 wt.% NPGDA) Macrogel
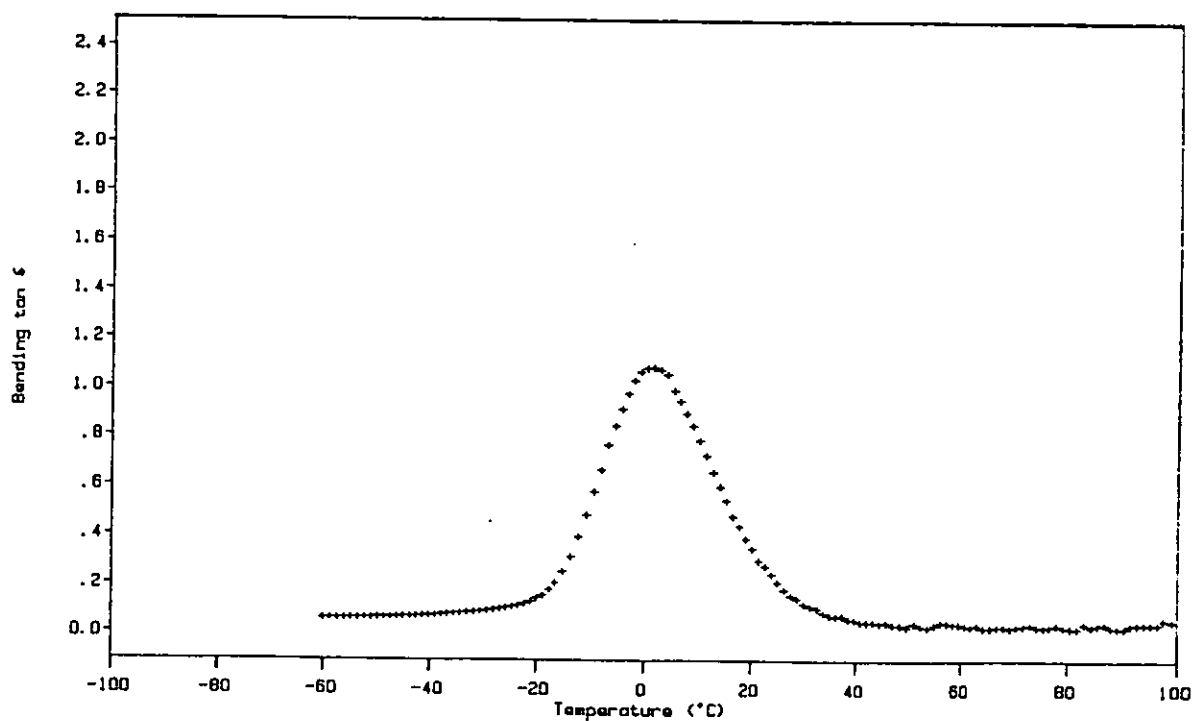
Figure 6.4 - Tanδ with Temperature Curve for P*n*BA (20 wt.% EGDMA) Macrogel
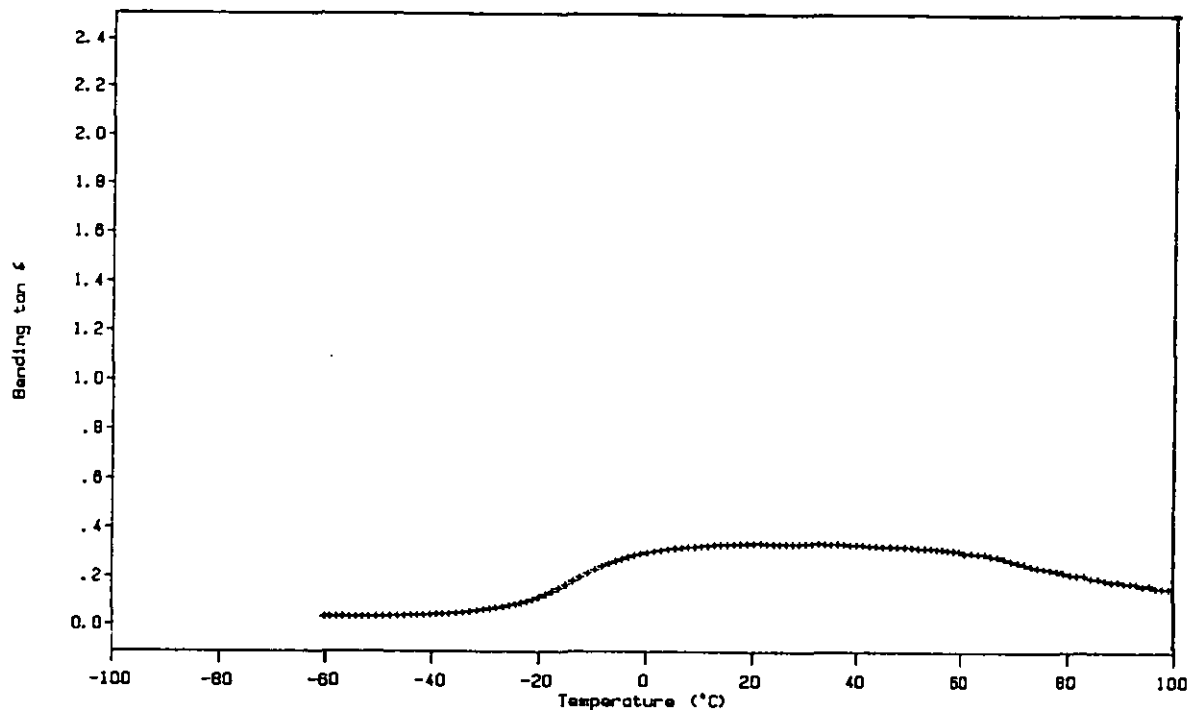
Table 6.2 - Acrylic Polymer Glass Transition (T_g) Data from DMTA

Sample	Tanδ$_{MAX}$	T_g(°C) at 10 Hz
P*n*BA homopolymer	2.1	-20
P*n*BA (10 wt.% NPGDA)	1.4	-11
P*n*BA (20 wt.% NPGDA)	1.1	2
P*n*BA (10 wt.% EGDMA)	0.8	- 6
P*n*BA (20 wt.% EGDMA)	0.3	
P*n*BA (10 wt.% DVB)	0.8	- 7

In general terms, the rheological behaviour of each acrylic macrogel sample (table 6.2) mirrors the DMTA characteristics of its corresponding microgel formulation (section 4.3). The one notable exception to this observation is the P*n*BA (20 wt.% EGDMA) system (figures 4.6 and 6.4). It would appear possible that either an "imperfect" network (section 1.2) had resulted from copolymerisation of *n*BA with 20 weight % ethylene glycol dimethacrylate under bulk, free radical, copolymerisation conditions [11, 35] or that this macrogel was sufficiently highly crosslinked for the material's glass transition to be suppressed completely [261].

Incorporation of EGDMA within the acrylic formulation (figure 6.4), at a level of 20 weight %, was, therefore, considered unsuitable for the synthesis of sequential polystyrene/PnBA IPN microgels, as the generation of an elastomeric network was required from the second-stage polymerisation process.

As can be seen from the contents of table 6.2, DMTA characterisation indicates that the incorporation of a divinyl comonomer within each acrylic formulation leads to an increase in the glass transition temperature for the resulting macrogel (when compared to the T_g of the PnBA homopolymer sample). The $tan\delta_{MAX}$ value (table 6.2) also decreases in magnitude as the concentration of the divinyl moiety within the formulation increases. These observations are in accordance with the glass transition behaviour determined for acrylic microgels from DMTA analysis (section 4.3). A shift in the glass transition to a higher temperature is observed on crosslinking a polymer sample [11, 261] (sections 3.3, 4.3 and 5.2). Nielson [261] developed an estimation for the degree of network crosslinking from a measurement in the T_g-shift on crosslinking (equation 3.1, section 3.3). Acrylic macrogel theoretical average molecular weight between crosslinks [287] (sections 1.2 and 3.3) and M_c values estimated from DMTA characterisation [261] (table 6.2) are detailed in table 6.3.

Table 6.3 - Theoretical and Experimental Network M_c Values for PnBA Macrogels

Macrogel Sample	M_c^{calc} (kg mol^{-1}) [287]	M_c (kg mol^{-1}) [261]
PnBA (10 wt.% NPGDA)	0.8	4.3
PnBA (20 wt.% NPGDA)	0.4	1.8
PnBA (10 wt.% EGDMA)	1.0	2.8
PnBA (20 wt.% EGDMA)	0.5	
PnBA (10 wt.% DVB)	1.2	3.0

Network average molecular weight between crosslink values estimated from glass transitional shifts [261] are significantly higher than theoretical M_c values (the average molecular weight between crosslinks for the corresponding homogeneous network where all divinyl units are incorporated as chemical crosslinks [287]). The increase in glass transition temperature on crosslinking [261] (section 3.3), for each of the five acrylic macrogel samples was, therefore, appreciably lower than would have been anticipated for the corresponding "ideal" network sample [287] (section 1.2). Similar deviations from the Nielson approach [261] were observed from DMTA

characterisation of acrylic microgel samples (section 4.3). It can be concluded that either acrylic gel glass transitions do not adhere to the Nielson [261] estimation for T_g-shift/crosslink relations or that the level of crosslinking within the acrylic copolymers synthesised was significantly diminished, when compared to the theoretical maximum degree of crosslinking for each of the formulations [287] (sections 1.2, 3.3 and 4.3). If it is assumed that, generally, the Nielson approach [261] affords a fair estimation for crosslink-densities from T_g measurement, there are several potential causes for a possible diminution in the degree of crosslinking encountered within acrylic macrogel formulations. The tertiary hydrogen in polymer-bound nBA repeat units has been found to abstract readily [304] during the polymerisation process. The possibility for hydrogen abstraction via free radical attack [11, 304] on copolymer molecules, coupled with the "high" copolymerisation temperature (when compared to the copolymer's glass transition temperature [11, 302], as signified by the data within table 6.2), could have potentially lead to the consumption of considerable concentrations of crosslinking agent via branching processes (section 1.2) [11, 32, 33], within each acrylic macrogel formulation. It would also appear possible that propagating branched polymer radicals could have reacted with pendant vinyl bonds within the same polymer chain, thereby leading to the consumption of divinyl moieties via intramolecular cyclisation reactions (section 1.2). Additionally, reduced pendant vinyl bond reactivity effects [34, 35] could have potentially operated within each acrylic copolymerisation process, whereby unreacted pendant vinyl bonds could have remained within acrylic polymer chains on completion of each copolymerisation process.

6.3 - EQUILIBRIUM SWELLING OF ACRYLIC MACROGELS

Equilibrium swelling of acrylic macrogel samples (25°C) was performed with anhydrous styrene (ϕC_2H_3), n-butanol (nBuOH) and benzyl alcohol (ϕCH_2OH), as detailed previously (section 2.6.2). The solubility parameter (δ) values for PnBA and for the three organic swelling agents [301] are listed in tables 3.10, 4.8 and 4.9. Experimentally recorded macrogel and liquid-swollen macrogel masses (section 2.6.2) were converted into component volumes by utilisation of published PnBA [334] and

organic liquid [248] density values. Acrylic macrogel volume fractions (ϕ_2) at equilibrium (table 6.4) were subsequently evaluated (equation 5.2, section 5.3).

Table 6.4 - Acrylic Macrogel ϕ_2 Values from Equilibrium Swelling (25°C)

Macrogel/Liquid System	Network Volume Fraction, ϕ_2 (25°C)
PnBA (10 wt.% NPGDA)/ϕC$_2$H$_3$	0.304
PnBA (20 wt.% NPGDA)/ϕC$_2$H$_3$	0.336
PnBA (10 wt.% EGDMA)/ϕC$_2$H$_3$	0.245
PnBA (20 wt.% EGDMA)/ϕC$_2$H$_3$	0.372
PnBA (10 wt.% DVB)/ϕC$_2$H$_3$	0.278
PnBA (10 wt.% NPGDA)/nBuOH	0.509
PnBA (20 wt.% NPGDA)/nBuOH	0.531
PnBA (10 wt.% EGDMA)/nBuOH	0.466
PnBA (20 wt.% EGDMA)/nBuOH	0.532
PnBA (10 wt.% DVB)/nBuOH	0.477
PnBA (10 wt.% NPGDA)/ϕCH$_2$OH	0.369
PnBA (20 wt.% NPGDA)/ϕCH$_2$OH	0.435
PnBA (10 wt.% EGDMA)/ϕCH$_2$OH	0.341
PnBA (20 wt.% EGDMA)/ϕCH$_2$OH	0.466
PnBA (10 wt.% DVB)/ϕCH$_2$OH	0.343

The results from equilibrium swelling of the two EGDMA and two NPGDA macrogel samples suggest that, for any given swelling agent, the ϕ_2 value increases as the concentration of divinyl comonomer within the macrogel formulation increases (table 6.4). These findings suggest that for these four materials the higher the level of divinyl comonomer incorporated within the bulk copolymerisation process, the higher was the crosslink-density for the resulting macrogel sample [167]. Comparable network volume fractions at equilibrium (table 6.4) were determined from swelling of the PnBA (10 wt.% NPGDA), PnBA (10 wt.% EGDMA) and PnBA (10 wt.% DVB) macrogel samples with each of the three swelling agents investigated. This observation is considered to signify that these macrogel samples were of comparable crosslink-density [167] (a similar conclusion was also apparent from an investigation into the dynamic mechanical behaviour of each of these three materials, as illustrated by the contents of table 6.2). The PnBA (20 wt.% NPGDA) macrogel was swollen the least by each of the three swelling agents investigated (table 6.4), when compared to the three other macrogel formulations which exhibited discernible glass transitions (section 6.2). Such findings would appear to suggest that this particular network had

the highest crosslink-density of the four "classical" network samples synthesised (section 6.2). In general terms, the highest levels of liquid swelling, for any given macrogel sample, were found with styrene, and the lowest degrees of swelling were found with n-butanol (table 6.4). These observations appear to be inconsistent with the method of Hildebrand [310] (section 4.5) which would predict that the Gibbs free energy [58, 232] on mixing the two dissimilar materials within each swelling system, should have become increasingly less positive, as the solubility parameter of the swelling agent approached that of the network polymer [232, 310] (table 6.4), in the absence of specific thermodynamic interactions [232] occurring within the system. The specific reason for the apparently "low" swelling characteristic of each acrylic macrogel/n-butanol formulation is not immediately obvious to the author. It is possible that a similar phenomenon was also observed for acrylic microgel formulations (section 4.4.3). The viscosity of microgel dispersions in n-butanol were significantly lower than their corresponding benzyl alcohol dispersions, at comparable solid concentrations (section 4.4.3). This experimental observation could have been a possible consequence of increased microgel particle swelling with benzyl alcohol [227] effects (sections 1.7.2, 3.6 and 4.4.3).

An estimation of the polymer-solvent interaction parameter $(\chi_{1,2})$ [167] for the acrylic macrogel/styrene system was determined from the Watson-Bristow [335] approach:

$$\chi_{1,2} = \beta + \frac{V_1}{RT}(\delta_1 - \delta_2)^2$$

(6.1)

where β is the lattice constant [335] ($\beta = 0.34$), V_1 is the molar volume (m^3 mol^{-1}) and δ_1 is the solubility parameter (J $m^{-3})^{1/2}$ of the swelling agent, δ_2 is the solubility parameter of the polymer (J $m^{-3})^{1/2}$, and R and T have their usual significance.

Average molecular weight between crosslink (M_c) values for the five acrylic macrogel/styrene systems were determined from the insertion of polymer network volume fractions (table 6.4) into the Flory-Rehner [167] equation (section 5.3), with $\chi_{1,2} = 0.39$ [335], $f = 4$ [333], $\rho = 1040$ kg m^{-3} [334] and $V_1 = 1.15$ x 10^{-4} m^3 mol^{-1}.

The solubility parameter of each network polymer [335] was considered to be identical to the δ value of P*n*BA homopolymer (table 4.8). Theoretical [287] and experimental [167, 335] M_c values for each acrylic network are shown in table 6.5.

Table 6.5 - Experimental [167, 335] and Theoretical Acrylic Network M_c Values

Macrogel	M_c^{calc} (kg mol^{-1}) [287]	M_c (kg mol^{-1})
P*n*BA (10 wt.% NPGDA)	0.8	2.8
P*n*BA (20 wt.% NPGDA)	0.4	2.1
P*n*BA (10 wt.% EGDMA)	1.0	4.8
P*n*BA (20 wt.% EGDMA)	0.5	1.6
P*n*BA (10 wt.% DVB)	1.2	3.5

In general terms, the crosslink-densities (from equilibrium swelling investigations) of the five acrylic macrogel formulations [167] appear to be markedly lower than their idealised values [287] (table 6.5). These findings mirror those previously concluded from dynamic mechanical characterisation of these materials [261] (section 6.2). Definitive comments about the apparent deviation in structure of these five acrylic macrogels, when compared to their idealised [287] network analogues, would appear to be unsubstantiated, however, since the methods of Nielson [261], Flory and Rehner [167] and Watson and Bristow [335] are, at best, estimations for physical characterisation [167, 261, 335, 336] only. If it is assumed that the apparent diminution in crosslink-density for acrylic macrogel samples, when compared to their idealised [287] network analogues (section 1.2), predicted from both dynamic mechanical analysis [261] (section 6.2) and equilibrium swelling [167, 335] observations, is "real", then there are several possible reasons for the observance of this effect. Chain branching [5, 11, 31, 261], reduced pendant vinyl bond reactivities [34, 35] and short-chain cyclisation processes [11, 32, 33] are the major phenomena which could potentially have decreased the level of crosslinking within each acrylic macrogel system, as discussed previously in section 6.2.

In terms of suitability for second-stage batchwise copolymerisation of acrylic comonomers within PS microgel formulations, the difunctional comonomer, neopentyl glycol diacrylate (NPGDA) would appear to be a suitable crosslinking agent for the second-formed, acrylic network component. Both the P*n*BA (10 wt.%

NPGDA) and P*n*BA (20 wt.% NPGDA) macrogel samples showed near-identical glass transitional behaviour (section 6.2) to their corresponding microgel samples (section 4.3), materials prepared from emulsion copolymerisation with semi-continuous comonomer addition (section 2.3.1). Compositional drift within the network structure [34-36, 39] (sections 1.2 and 1.5) would appear to have been minimised, therefore, during batchwise copolymerisation of *n*BA/NPGDA.

CHAPTER 7

POLYMER-BOUND

FREE RADICAL

INITIATORS

7.1.1 - OLEFINIC PEROXIDE YIELD AND PURITY VALUES

During this project, an investigation into the equilibrium swelling of polystyrene macrogel with a benzyl alcohol/n-butyl acrylate mixture (section 5.4) was performed. FTIR analysis determined that PS networks were not preferentially swollen with acrylic monomer. It was considered that the employment of a conventional, continuum-soluble, free radical source as an initiator for copolymerisations of nBA/difunctional comonomer mixtures within organic PS microgel dispersions would not, therefore, have generated organic IPN particle dispersions. Acrylic macrogel would, most probably, be the major product of such a synthetic process (if the concentration of divinyl comonomer was sufficiently high for macro-gelation to occur). Additionally, the solubility behaviour of nBA and styrene monomers (25°C) with a number of organic liquids was determined (sections 2.4 and 4.5). The miscibility of both monomers with each of these diluents, over the entire composition range, ensured that organic IPN microgel dispersions could not be synthesised under a modified form of quasi-emulsion second-stage polymerisation conditions [232, 233].

Consequently, it was decided that the synthesis of polymer-bound (second-stage) free radical initiator molecules, located toward the centre of PS/DVB microgel particles, would be attempted, in order to try and minimise the degree of polymerisation within the continuum. Such a synthetic procedure was anticipated to have required a "seed and feed" emulsion terpolymerisation technique. A styrene/DVB/initiating comonomer seed (e.g. 20 weight % of the total comonomer content) would initially be terpolymerised to completion. The remaining (styrene/DVB) feed would then be copolymerised under starve-fed conditions [337]. Ideally, the initiating comonomer would be more hydrophobic than crosslinked polystyrene [172, 180, 181], if free radical sources were to be located toward the centre of PS microgel particles. Particle nucleation (leading to the generation of both functionalised and non-functionalised microgel initiator particles) during the feed stage would have been most undesirable. It was anticipated that such renucleation could have been avoided, however, provided that optimum emulsion copolymerisation conditions were employed [181, 184].

Generation of free radicals at the centre of PS microgel particles dispersed in organic liquid/acrylic comonomer mixtures would also not lead to the synthesis of pure IPN particle dispersions. Chain-transfer to monomer [11] and propagation [11] processes would almost certainly ensure that free radicals would be found at the surface of PS microgel particles. Propagation of acrylic comonomer molecules in the continuous phase, leading to the generation of macrogel (or, possibly, acrylic microgel, if the comonomer concentration was lower than the volume fraction of comonomers required for macro-gelation), would then, most probably, occur rapidly. Additionally, thermal homolytic bond-scission processes [11, 338] (caused by, for example, thermal decomposition of pendant, polymer-bound, initiator groups) for free radical production would generate both polymer-bound and low molecular weight (i.e. "mobile") free radical fragments [338]. Such, low molecular weight, free radicals would have the capacity to diffuse from the microgel particle interior environment and initiate acrylic copolymerisation in the continuum. A high concentration of polymer-bound chain-transfer agent or free radical inhibitor moieties at the PS microgel particle surface would also, therefore, be required, if polymerisation within the continuum were to be minimised, and if IPN particle synthesis was, consequently, to be maximised.

The olefinic peroxides, t-butylperoxy-2-methacryloyloxyethyl carbonate (Tradename, Peromer MEC, abbreviated to PMEC, hereafter) [246], t-butylperoxyisopropyl fumarate (BPIPF) [246] and t-butylperoxyallyl carbonate (ALPO) [246] are commercial products of the NOF Corporation. Poly(methyl methacrylate) and poly(vinyl acetate) derivatives containing pendant peroxide functionalities have been previously synthesised [246] from suspension copolymerisation techniques. These macro-initiator systems were used for the synthesis of poly(methyl methacrylate-g-styrene) and poly(vinyl acetate-g-styrene) graft copolymers [246]. Grafting between the two network components of an IPN is not necessarily desirable, if materials with enhanced physical properties [98, 99] are to result. The concentration of polymeric peroxide fragments required to initiate acrylic copolymerisations was anticipated to be low (ca. 0.1-0.5 mole %), however, thus ensuring that few graft-sites would originate from macro-initiator decomposition. Significant quantities of PS homopolymer were also synthesised [246] during the thermal decomposition of methyl

methacrylate/peroxide and vinyl acetate/peroxide copolymers [246] in the presence of styrene monomer. Homopolymer synthesis was considered to have arisen [246] from (low molecular weight) *t*-butoxyl free radical initiation of polymerisation, as this (*t*-butoxyl) radical is generated during the thermal decomposition of peroxide-containing copolymers [246]. The *t*-butoxyl free radical has been extensively employed as a polymerisation initiator [339].

The peroxide monomers, *t*-butylperoxy-2-methacryloyloxyethyl carbonate (PMEC) [246], di-*t*-butylperoxy fumarate (DBPF) and *t*-butylperoxyallyl carbonate (ALPO) [246] were synthesised during this investigation (section 2.7.1). The molecular structures of PMEC, DBPF and ALPO are illustrated in figures 7.1, 7.2 and 7.3, respectively.

Figure 7.1 - *t*-Butylperoxy-2-Methacryloyloxyethyl Carbonate (PMEC)
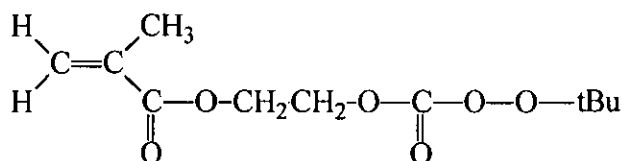
Figure 7.2 - Di-*t*-Butylperoxy Fumarate (DBPF)
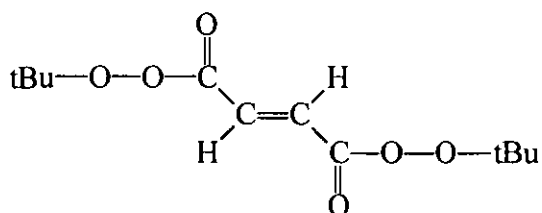
Figure 7.3 - *t*-Butylperoxyallyl Carbonate (ALPO)

192
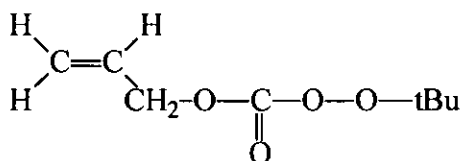
The peroxide monomer *t*-butylperoxy-2-methacryloyloxyethyl carbonate (PMEC) [246] was synthesised from the reaction between 2-methacryloyloxyethyl chloroformate and *t*-butylhydroperoxide (section 2.7.1) under modified experimental conditions [253] to those originally developed by Davies and Hunter [340] for the synthesis of peroxy carbonates from alkyl chloroformates. The synthesis of *t*-butylperoxyallyl carbonate (ALPO) from the reaction of allyl chloroformate with *t*-butylhydroperoxide (*t*-BuOOH) was performed under similar conditions to those reported previously [246]. The peroxy ester di-*t*-butylperoxy fumarate, DBPF (a crystalline solid, melting point 27-29°C), was synthesised from the reaction of fumaryl chloride with *t*-BuOOH under modified synthetic conditions [246] to those reported by Milas and Surgenor [341] for the synthesis of peroxy esters from alkyl acid chlorides.

The products recovered from the reaction between *t*-BuOOH and chloroformate, or acid chloride, were reduced with sodium iodide (section 2.7.1) [254], under acidic conditions. The stoichiometry of the reaction between organic peroxide and iodide ion [254] is depicted by equation 7.1, and the stoichiometry of the reaction between thiosulphate ion and iodine is depicted by equation 7.2.

$$2\,H^+ + R\!-\!O\!-\!O\!-\!R' + 2\,I^- \longrightarrow R'\!-\!OH + R\!-\!OH + I_2 \quad (7.1)$$

where R and R' represent alkyl groups.

$$I_2 + 2\,S_2O_3^{2-} \longrightarrow 2\,I^- + S_4O_6^{2-} \quad (7.2)$$
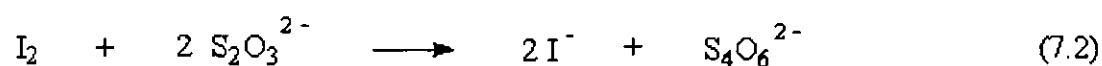
The number of moles of peroxide in each sample was determined from:

$$\text{Peroxide Content, P (moles)} = \frac{(A - B) \times 0.0101}{2000} \quad (7.3)$$

where A is the thiosulphate titre (cm^3) for the sample and B is the titre average (cm^3) for the blank samples (section 2.7.1).

The purities of both ALPO and PMEC were evaluated from:

$$\text{Purity (Weight \%)} = \frac{P \times M \times 100\%}{M_s} \quad (7.4)$$

where M_s is the sample mass (g) and M is the molecular mass of the peroxide monomer (g mol^{-1}).

The purity of the DBPF sample was evaluated from:

$$\text{Purity (Weight \%)} = \frac{P \times M \times 100\%}{2M_s} \tag{7.5}$$

The factor of two is included (in the denominator of equation 7.5) due to the difunctionality of DBPF. The peroxide yield and purity values are given in table 7.1.

Table 7.1 - Peroxide Purity and Experimental Yield Values

Peroxide	Yield (Weight %)	Purity (Weight %)
PMEC	89	96
DBPF	66	99
ALPO	55	95

Iodide-reduction analysis determined that peroxides of high purity were synthesised from the reaction between t-butylhydroperoxide and chloroformate/acid chloride. It would appear, from the moderate yield values of these (pure) organic peroxides, that water-soluble contaminants had also been synthesised from these experimental techniques (additional reaction products are considered to have been soluble in the aqueous phase, because organic material impurities with low water solubilities would not have been removed by the aqueous work-up/separation technique performed for each peroxide synthesis. Consequently, a significant diminution in the purity of the peroxide sample would be anticipated, if, non-water-soluble, organic, by-products had also been synthesised). It would appear possible that chloroformate/acid chloride molecules had also reacted with hydroxide ions (or water), to generate the, corresponding, carboxylic acids. The presence of excess sodium (or potassium) ions in the reaction system (section 2.7.1) would be expected to give the salts of these acids, and, in general terms, the alkali metal salts of carboxylic acids have high water-solubilities [342]. Additionally, hydroxide ion attack on peroxide molecules [341] could have potentially lead to partial hydrolysis of the reaction product. It would appear possible that molecules of t-butylhydroperoxide and carboxylic acid salt recovered from hydrolysis could have also been separated during the aqueous work-up process.

7.1.2 - $^1H/^{13}C$ NMR CHARACTERISATION OF OLEFINIC PEROXIDES

A sample of the product recovered from the reaction of *t*-butylhydroperoxide with 2-methacryloyloxyethyl chloroformate was analysed by 100 MHz ^1H NMR spectroscopy. The ^1H NMR spectrum of this material is shown in figure 7.4. Proton resonance characteristics predicted [279] to be observed from ^1H NMR analysis of *t*-butylperoxy-2-methacryloyloxyethyl carbonate (PMEC) are listed in table 7.2 (the, predicted, peak multiplicities are considered to arise from first-order proton coupling [279]). The resonances observed from ^1H NMR characterisation of the reaction product are detailed in table 7.3.

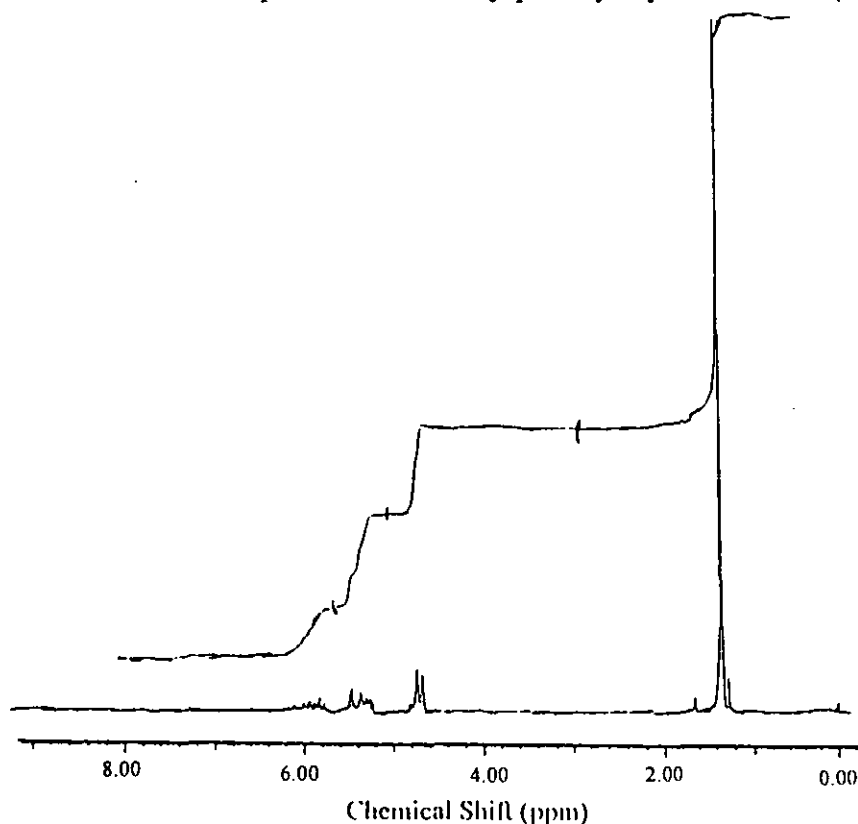### Figure 7.4 - ^1H NMR Spectrum of PMEC
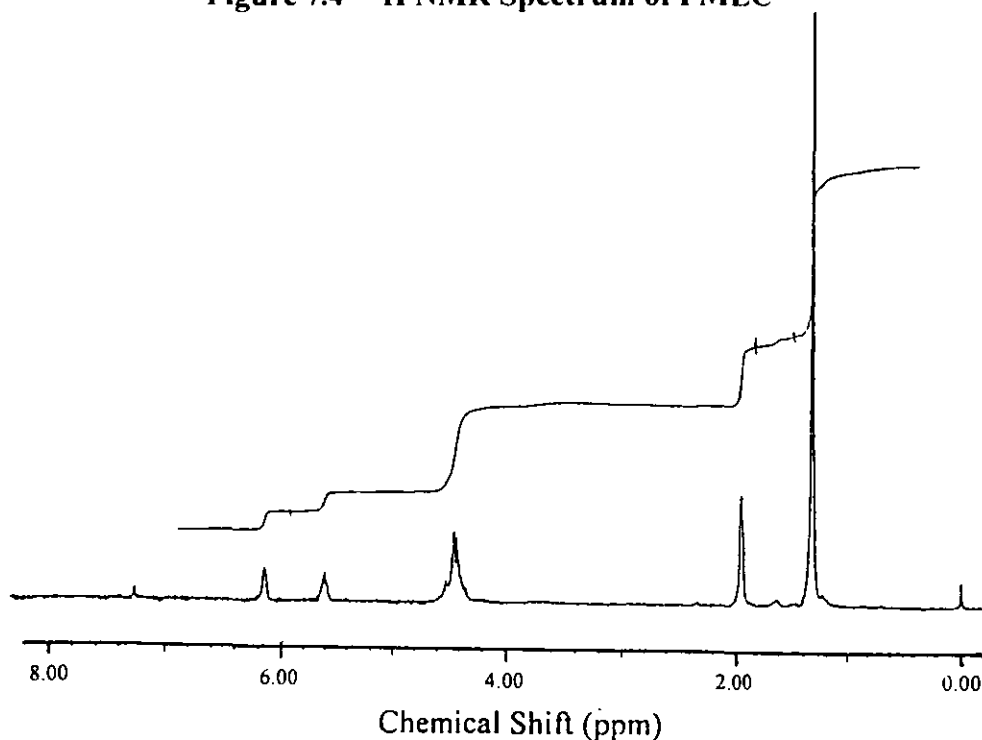
Chemical Shift (ppm)

Table 7.2 - ^1H Resonances Predicted for NMR Spectrum of PMEC

Proton Type	Chemical Shift [1]	Signal Multiplicity	Relative Intensity
Methyl	1.0-2.0	Singlet	9
α-Methyl	1.0-2.0	Singlet	3
Methylene	2.0-4.0	Two Triplets	4
Vinyl	4.5-6.0	Two Doublets	2

[1] Parts per million (ppm) relative to tetramethylsilane (TMS).

195

Table 7.3 - Absorptions Observed from ^{1}H NMR Analysis of PMEC

Proton Type	Chemical Shift	Signal Multiplicity	Relative Intensity
Methyl (*t*-Butyl)	1.35	Singlet	9
α-Methyl	1.95	Singlet	3
Methylene	4.40	Multiplet	4
Vinyl	5.90	Two Doublets	2

Inspection of the ^{1}H NMR chemical shift, signal multiplicity and peak integral values, inferred that *t*-butylperoxy-2-methacryloyloxyethyl carbonate (PMEC) had been synthesised from the reaction between the chloroformate and *t*-BuOOH. A sample of PMEC was also characterised by 25 MHz ^{13}C NMR spectroscopy (figure 7.5). Predicted proton absorptions [280] for PMEC are listed in table 7.4 and resonances observed from ^{13}C NMR analysis of this material are detailed in table 7.5.

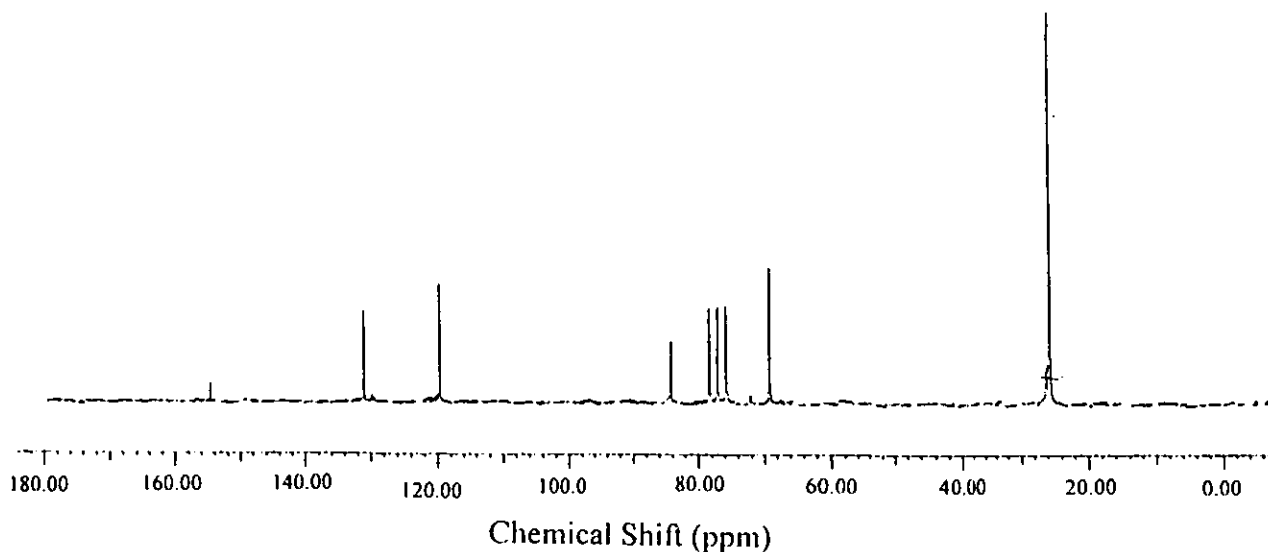**Figure 7.5 - ^{13}C NMR Spectrum of PMEC**
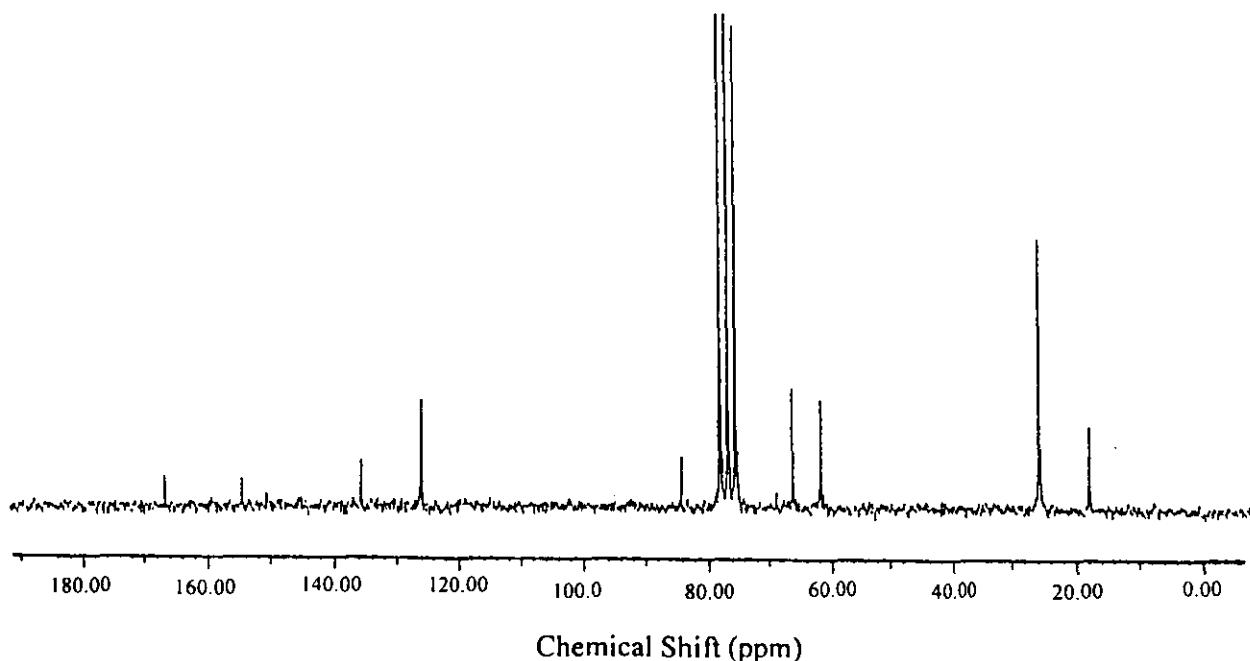
Chemical Shift (ppm)

Table 7.4 - ^{13}C Resonances Predicted for NMR Spectrum of PMEC

Type of Carbon Atom	Chemical Shift (ppm, relative to TMS)
α-Methyl	20-40
Methyl	20-40
Methylene	60-80
Methylene	60-80
Tertiary	80-100
Vinyl	120-140
Vinyl	120-140
Carbonyl (peroxy carbonate)	160-180
Carbonyl (peroxy ester)	160-180

Table 7.5 - Resonances Observed from ^{13}C NMR Analysis of PMEC

Type of Carbon Atom	Chemical Shift (ppm, relative to TMS)
α-Methyl	18
Methyl	26
Methylene	62
Methylene	66
Tertiary	84
Vinyl (with geminal protons)	126
Vinyl (non-proton substituted)	136
Carbonyl (peroxy carbonate)	154
Carbonyl (vinyl ester)	167

Inspection of the ^{13}C NMR spectrum of the reaction product determined that the olefinic peroxide, t-butylperoxy-2-methacryloyloxyethyl carbonate (PMEC) had been synthesised. The signal from the methyl carbons of the t-butyl group is the most intense ^{13}C NMR absorption. This phenomenon is attributed to the fact that broadband proton decoupling, a technique that was employed for ^{13}C NMR analysis of PMEC, affects the relative populations of the thermal spin-state distributions [279] - the nuclear Overhauser effect [280].

A sample of the product recovered from the reaction of fumaryl chloride with t-BuOOH was also characterised by 100 MHz ^{1}H NMR spectroscopy (figure 7.6). Predicted proton absorptions [279, 280] for DBPF monomer are listed in table 7.6 and resonances observed from ^{1}H NMR analysis of this material are detailed in table 7.7.

Table 7.6 - ^{1}H Resonances Predicted for NMR Spectrum of DBPF

Proton Type	Chemical Shift ^{1}	Signal Multiplicity	Relative Intensity
Methyl	1.0-2.0	Singlet	9
Olefinic	4.5-6.0	Singlet	1

^{1} Parts per million (ppm) relative to tetramethylsilane (TMS).

Figure 7.6 - ^{1}H NMR Spectrum of Di-*t*-Butylperoxy Fumarate (DBPF)
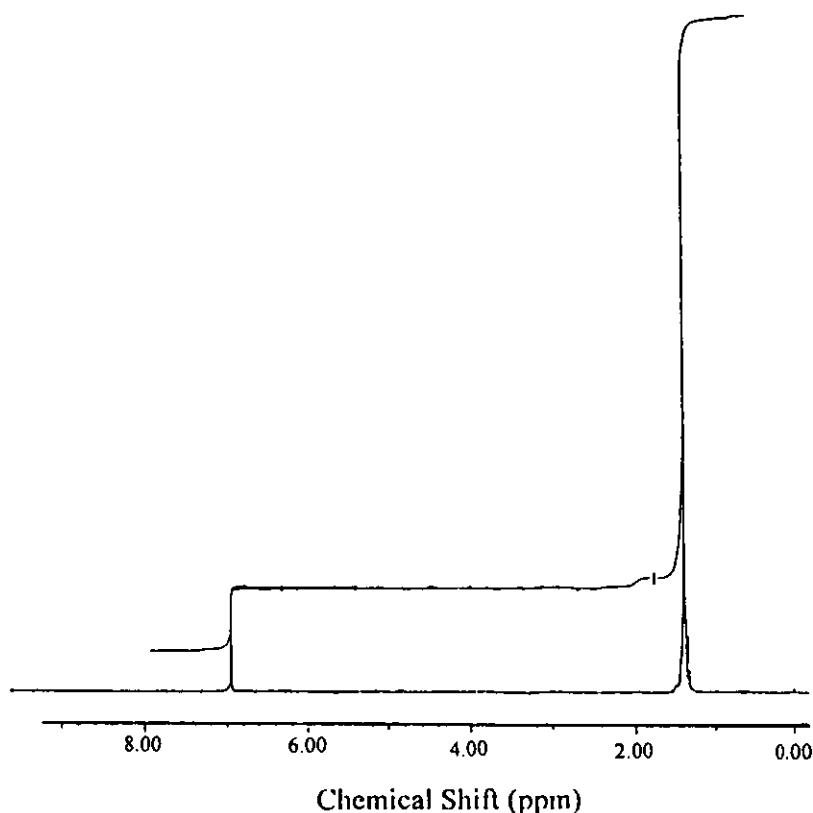
Chemical Shift (ppm)

Table 7.7 - Absorptions Observed from ^{1}H NMR Analysis of DBPF

Proton Type	Chemical Shift	Signal Multiplicity	Relative Intensity
Methyl (*t*-Butyl)	1.35	Singlet	9
Olefinic	6.90	Singlet	1

The high chemical shift for the olefinic proton is attributed to the de-shielding effect of both the carbon-carbon double bond and the carbonyl group [279]. Analysis of the chemical shift, signal multiplicity and ^{1}H NMR peak integral values inferred that di-*t*-butylperoxy fumarate (DBPF) had been synthesised from the reaction between the

acid chloride and *t*-BuOOH. A sample of DBPF was also analysed by 25 MHz ^{13}C NMR spectroscopy (figure 7.7). Carbon resonances predicted [280] to be observed from analysis of DBPF are listed in table 7.8. The absorptions observed from ^{13}C NMR characterisation of this material are detailed in table 7.9.

Figure 7.7 - ^{13}C NMR Spectrum of Di-*t*-Butylperoxy Fumarate (DBPF)
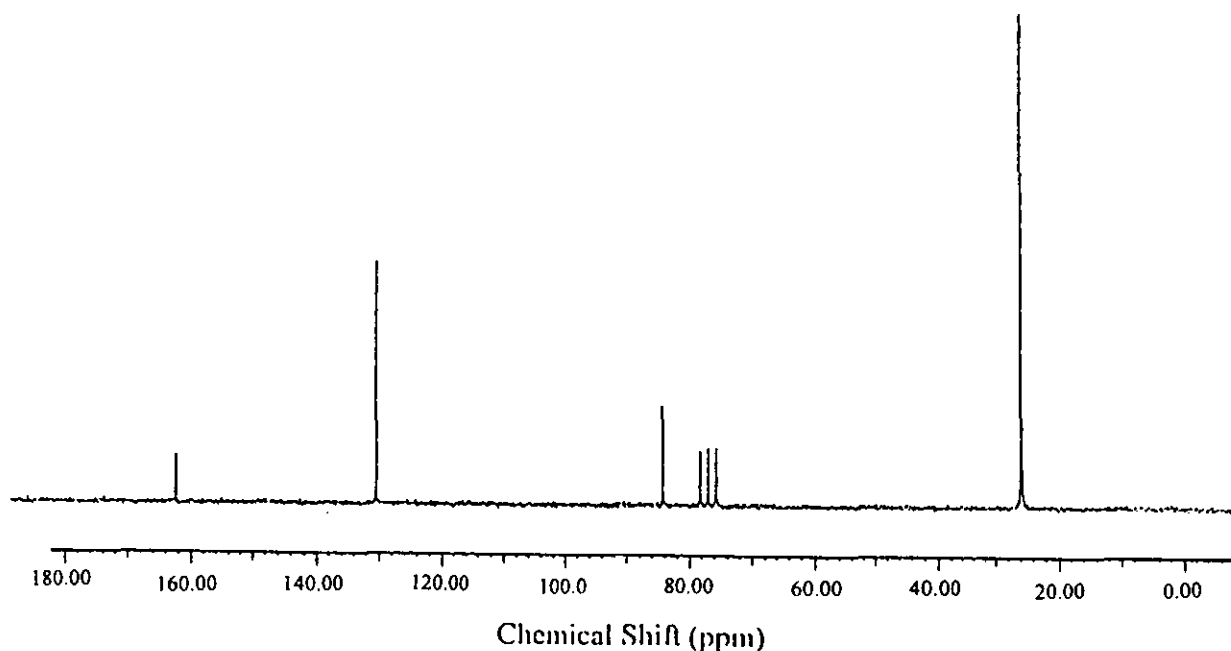
Chemical Shift (ppm)

Table 7.8 - ^{13}C Resonances Predicted for NMR Spectrum of DBPF

Type of Carbon Atom	Chemical Shift (ppm, relative to TMS)
Methyl	20-40
Tertiary	80-100
Olefinic	120-140
Carbonyl	160-180

Table 7.9 - Resonances Observed from ^{13}C NMR Analysis of DBPF

Type of Carbon Atom	Chemical Shift (ppm, relative to TMS)
Methyl	26
Tertiary	84
Olefinic	130
Carbonyl	162

The methyl and tertiary carbons of DBPF were found to resonate at identical chemical shifts to those in PMEC (this observation is to be expected. since both of the materials contain the *t*-butylperoxy group). Close inspection of the 25 MHz ^{13}C NMR spectrum of the organic product recovered from the reaction between fumaryl chloride and *t*-butylhydroperoxide indicated that di-*t*-butylperoxy fumarate had been synthesised.

A sample of the product recovered from the reaction between allyl chloroformate with *t*-BuOOH was analysed by 100 MHz ^{1}H NMR spectroscopy (figure 7.8). Resonances predicted [279] to be observed for pure ALPO from ^{1}H NMR characterisation are listed in table 7.10. Absorptions observed from ^{1}H NMR analysis of this material are detailed in table 7.11.

Figure 7.8 - ^{1}H NMR Spectrum of *t*-Butylperoxyallyl Carbonate (ALPO)

Table 7.10 - ^{1}H Resonances Predicted for NMR Spectrum of ALPO

Proton Type	Chemical Shift	Signal Multiplicity	Relative Intensity
Methyl	1.0-2.0	Singlet	9
Allyl	2.0-4.0	Doublet	2
Vinyl	4.5-6.0	Multiplet	3

200

Table 7.11 - Absorptions Observed from ¹H NMR Analysis of ALPO

Proton Type	Chemical Shift	Signal Multiplicity	Relative Intensity
Methyl	1.35	Singlet	9
Allyl	4.70	Multiplet	2
Vinyl	5.95	Multiplet	3

Referral to the chemical shift, signal multiplicity and ¹H NMR peak integral values for the reaction product lead to the prediction that *t*-butylperoxyallyl carbonate had been synthesised. A sample of ALPO was also analysed by 25 MHz ¹³C NMR spectroscopy (figure 7.9). ¹³C resonances predicted [280] to be observed for ALPO, from ¹³C NMR characterisation, are listed in table 7.12. Absorptions observed from ¹³C NMR analysis of this material are detailed in table 7.13.

Figure 7.9 - ¹³C NMR Spectrum of *t*-Butylperoxyallyl Carbonate (ALPO)

Chemical Shift (ppm)

Table 7.12 - ^{13}C Resonances Predicted for NMR Spectrum of ALPO

Type of Carbon Atom	Chemical Shift (ppm, relative to TMS)
Methyl	20-40
Allyl	60-80
Tertiary	80-100
Vinyl	120-140
Vinyl	120-140
Carbonyl	160-180

Table 7.13 - Resonances Observed from ^{13}C NMR Analysis of ALPO

Type of Carbon Atom	Chemical Shift (ppm, relative to TMS)
Methyl	26
Allyl	69
Tertiary	84
Vinyl ($H_2C=$)	120
Vinyl (mono-proton substituted)	131
Carbonyl	154

Analysis of the 25 MHz ^{13}C NMR spectrum of the organic product recovered from the reaction between allyl chloroformate and t-BuOOH, determined that the olefinic peroxide, t-butylperoxyallyl carbonate (ALPO), had been synthesised. The (peroxy carbonate) carbonyl carbon of ALPO was found to resonate at an identical chemical shift to that of the peroxy carbonate carbonyl group in PMEC. This observation would appear to indicate that both materials contained the methylene carbonate peroxide group.

7.1.3 - FTIR CHARACTERISATION OF OLEFINIC PEROXIDES

Transmittance FTIR spectra of 2-methacryloyloxyethyl chloroformate (MOCF), fumaryl chloride, allyl chloroformate, PMEC, DBPF and ALPO were recorded. Wavenumber, $\bar{v}$ (cm^{-1}), and peak assignment data [270] from the FTIR spectra of MOCF (figure 7.10) and PMEC (figure 7.11) are given in figures 7.12 and 7.13, respectively.
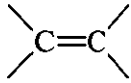
Figure 7.10 - FTIR Spectrum of MOCF
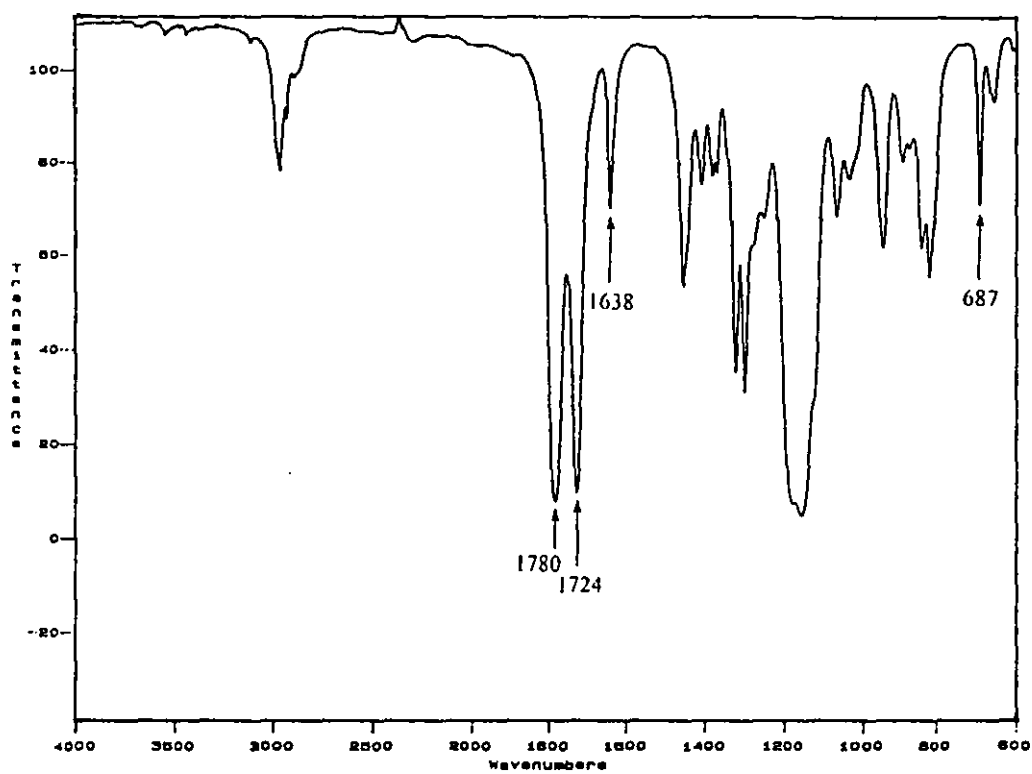
Figure 7.11 - FTIR Spectrum of PMEC
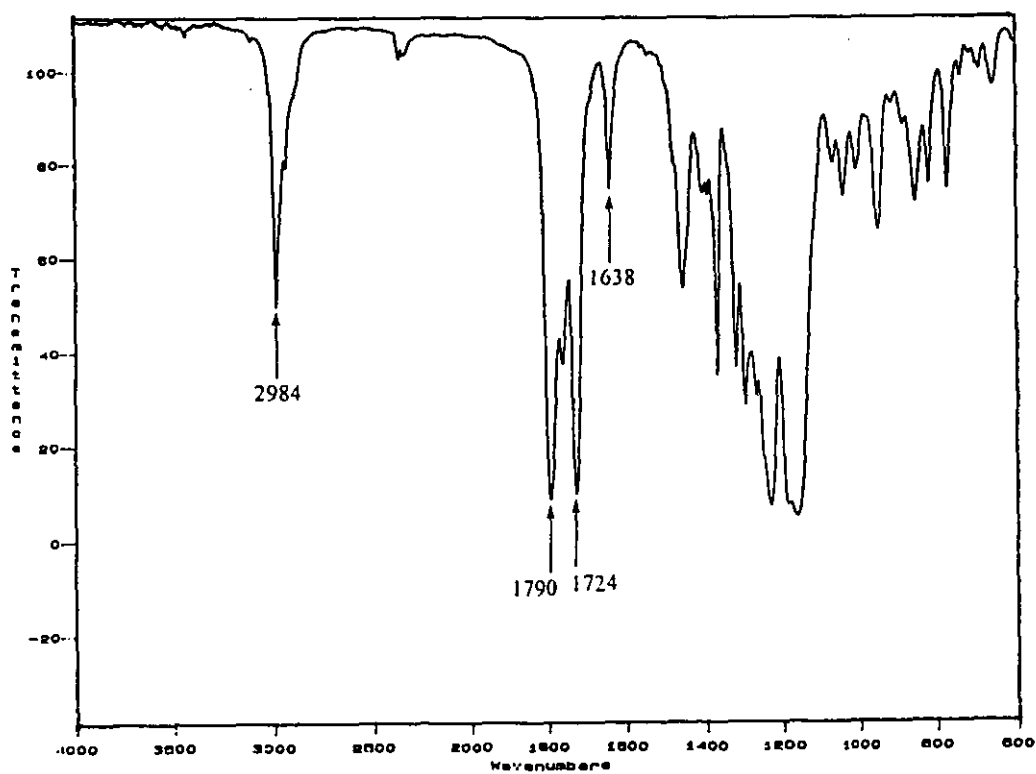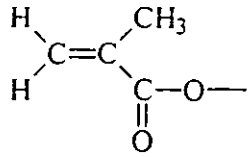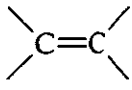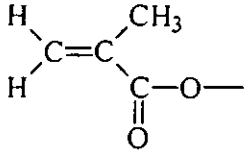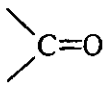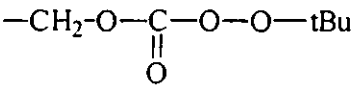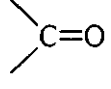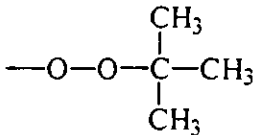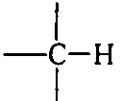
Figure 7.12 - IR Wavenumber ($\bar{\nu}$) and Peak Assignment Data for MOCF

$\bar{\nu}$ (cm^{-1})	Molecular Environment	Vibration

687

$$-CH_2-O-\underset{\underset{O}{\|}}{C}-Cl$$

—C—Cl (stretch)

1638

H, CH$_3$ C=C, H, C—O— (with C=O)

>C=C< (stretch

1724

H, CH$_3$ C=C, H, C—O— (with C=O)

>C=O (stretch

1780

$$-CH_2-O-\underset{\underset{O}{\|}}{C}-Cl$$

>C=O (stretch

A moderately strong absorption, corresponding to the C-Cl stretching frequency [270], was observed at a radiation wavenumber of 687 cm^{-1}. A moderately strong absorption, corresponding to the stretching frequency of the C=C double bond [270] was also observed (1638 cm^{-1}). Two carbonyl stretching frequencies are observed [270]. The absorption from the chlorine-substituted carbonyl has a higher wavenumber than the vinyl ester carbonyl absorption ($\bar{\nu}$ = 1780 and 1724 cm^{-1}, respectively).

The product from the MOCF/t-BuOOH reaction does not show an IR absorption from the C-Cl bond of the chloroformate (figure 7.11). Absorptions from stretching of the C=C double bond (1638 cm^{-1}) [270] and stretching of the vinyl ester carbonyl group (1724 cm^{-1}) occur at identical frequencies to those in the chloroformate. The peroxycarbonate carbonyl group shows a characteristic doublet (1759 cm^{-1}, 1790 cm^{-1}) [343]. A strong absorption, corresponding to the C-H stretching frequency of the (t-butyl) methyl groups, was also observed, at a radiation wavenumber of 2984 cm^{-1}.

Figure 7.13 - IR Wavenumber ($\bar{\nu}$) and Peak Assignment Data for PMEC

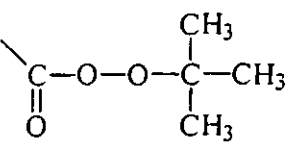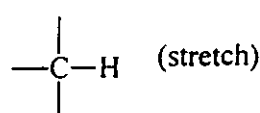| $\bar{\nu}$ (cm^{-1})	Molecular Environment	Vibration
1638	H,C=C(CH$_3$)—C(=O)—O—	C=C (stretch)
1724	H,C=C(CH$_3$)—C(=O)—O—	C=O (stretch)
1790, 1759	—CH$_2$—O—C(=O)—O—O—tBu	C=O (stretch)
2984	—O—O—C(CH$_3$)$_2$—CH$_3$	C—H (stretch)

Wavenumber and peak assignments [270] for the IR absorptions of fumaryl chloride (figure 7.14) and DBPF (figure 7.16) are given in figures 7.15 and 7.17, respectively.

Figure 7.14 - FTIR Spectrum of Fumaryl Chloride

Figure 7.14 - FTIR Spectrum of Fumaryl Chloride
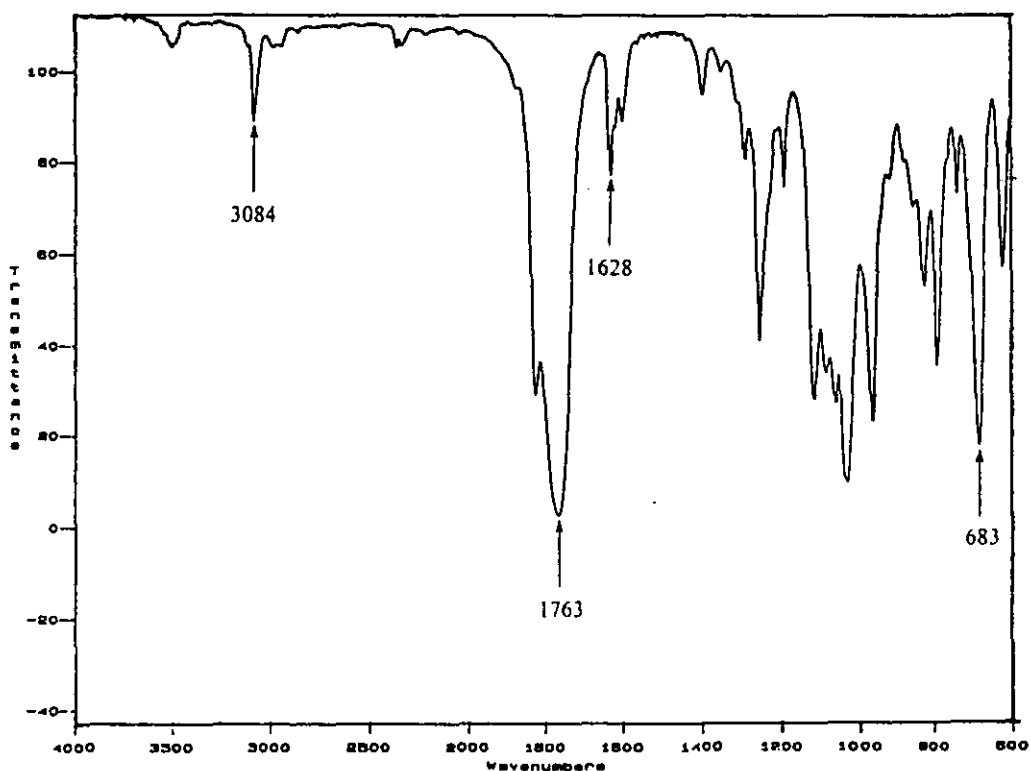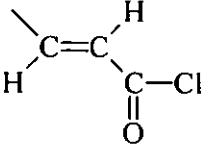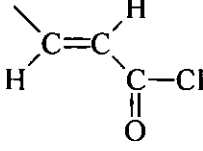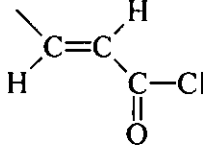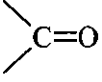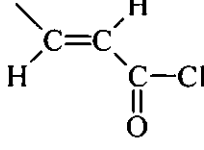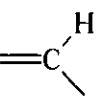
Figure 7.15 - IR Wavenumber ($\bar{\nu}$) and Peak Assignments for Fumaryl Chloride

$\bar{\nu}$ (cm^{-1})	Molecular Environment	Vibration
683	(structure)	—C—Cl (stretch)
1628	(structure)	C=C (stretch)
1763	(structure)	C=O (stretch
3084	(structure)	=C—H (stretch)

A strong absorption, corresponding to the C-Cl stretching frequency [270], was observed at a wavenumber of 683 cm^{-1}. An absorption corresponding to stretching of the C=C double bond [270] was also found ($\bar{\nu}$ = 1628 cm^{-1}). One carbonyl (C=O) stretching mode is observed ($\bar{\nu}$ = 1763 cm^{-1}). The absorptions in the 2700-3100 cm^{-1} wavenumber region (which correspond to the stretching frequencies of C-H bonds [270]) are of interest. A single absorption was observed ($\bar{\nu}$ = 3084 cm^{-1}). This frequency corresponds to the stretching vibrational energy of the olefinic C-H bond [270].

The IR spectrum of the product from the reaction of fumaryl chloride with t-BuOOH does not show an absorption from the C-Cl bond of the acid chloride (figure 7.16). An absorption from stretching of the C=C double bond was observed ($\bar{\nu}$ = 1644 cm^{-1}) [270]. The peroxy ester carbonyl group shows a single absorption at 1763 cm^{-1}. Additionally, a strong absorption was observed at a wavenumber of 2984 cm^{-1}. This frequency corresponds to the stretching vibrational energy of the C-H bond in the (t-butyl) methyl groups.

Figure 7.16 - FTIR Spectrum of DBPF

Figure 7.16 - FTIR Spectrum of DBPF
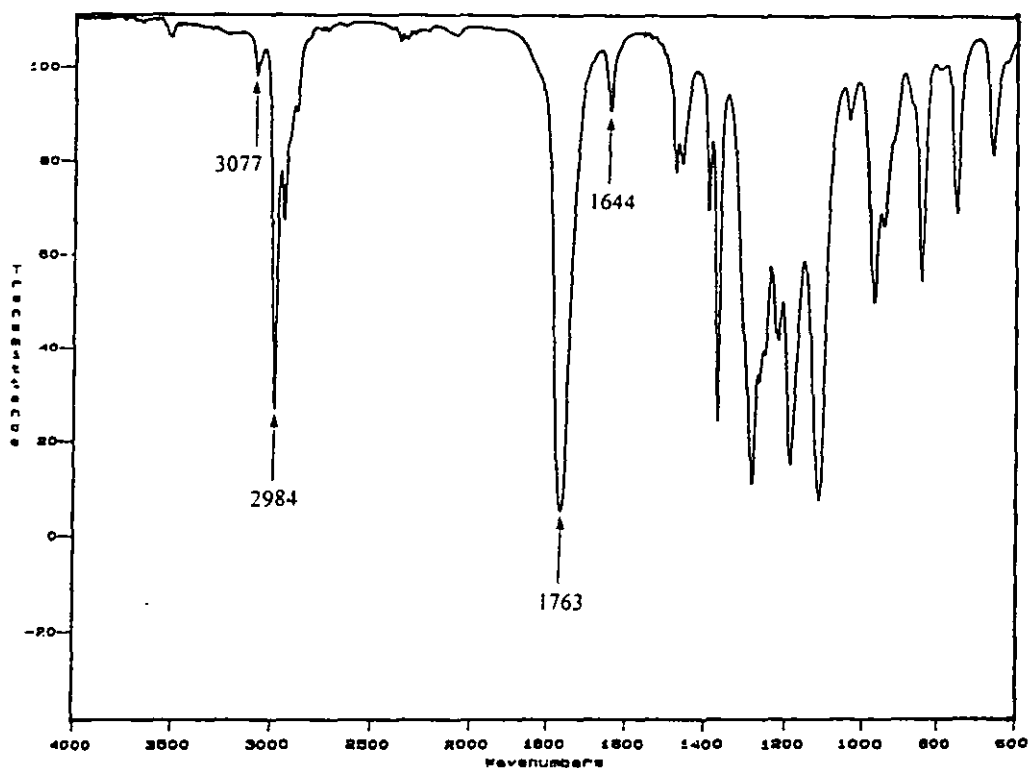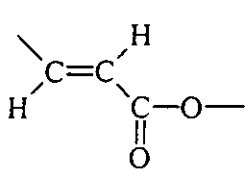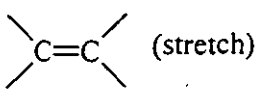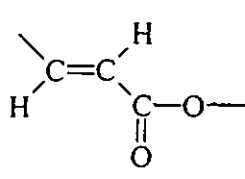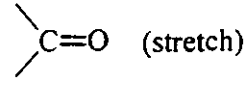
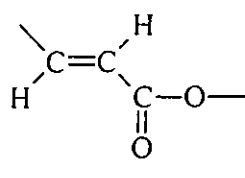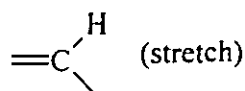## Figure 7.17 - IR Wavenumber ($\bar{\nu}$) and Peak Assignment Data for DBPF

$\bar{\nu}$ (cm^{-1})	Molecular Environment	Vibration
1644		$>\!C\!=\!C\!<$ (stretch)
1763		$>\!C\!=\!O$ (stretch)
2984		$-\!C\!-\!H$ (stretch)
3077		$=\!C\!<^{H}$ (stretch)

207

Wavenumber and peak assignments [270] for the IR absorptions of allyl chloroformate (figure 7.18) and ALPO (figure 7.20) are given in figures 7.19 and 7.21, respectively.

Figure 7.18 - FTIR Spectrum of Allyl Chloroformate
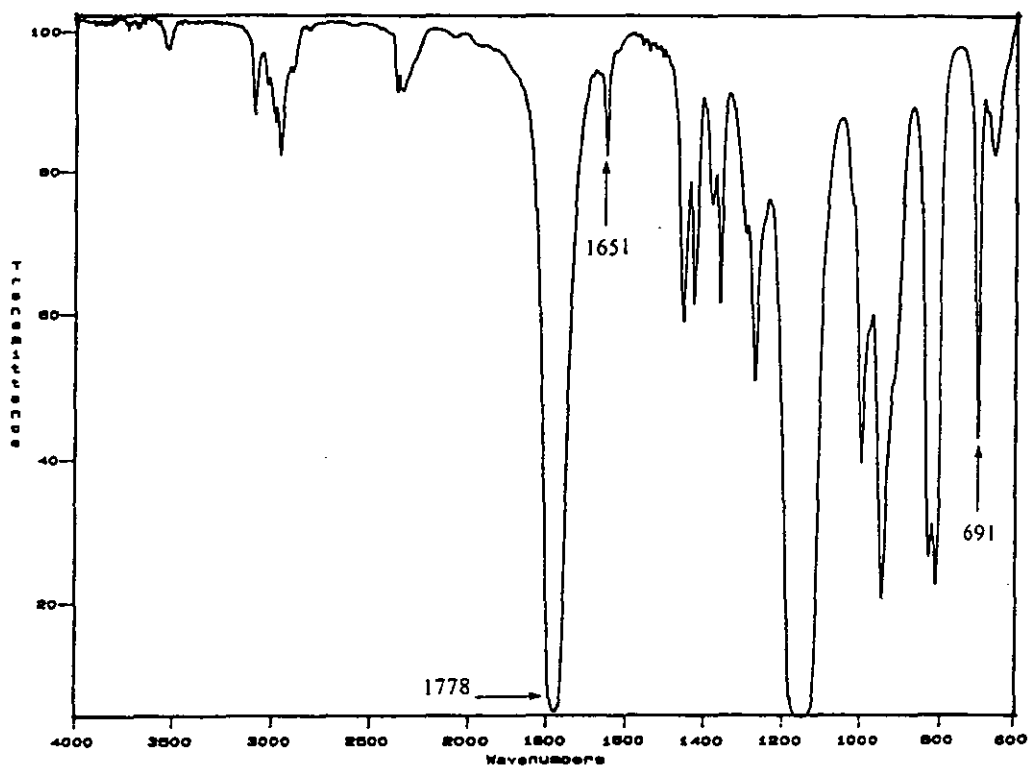
Figure 7.19 - IR Wavenumber and Peak Assignments for Allyl Chloroformate

$\bar{\nu}$ (cm^{-1})	Molecular Environment.	Vibration
691	$-CH_2-O-\underset{\underset{O}{\|\|}}{C}-Cl$	$-C-Cl$ (stretch)
1651	$\underset{H}{\overset{H}{}}C=C\overset{H}{\underset{CH_2-O-\underset{\underset{O}{\|\|}}{C}-}{}}$	$C=C$ (stretch)
1778	$-CH_2-O-\underset{\underset{O}{\|\|}}{C}-Cl$	$C=O$ (stretch)

208

Moderately strong absorptions, corresponding to the C-Cl stretching frequency [270] (691 cm^{-1}) and to the stretching frequency of the C=C double bond (1651 cm^{-1}) [270] were observed in the FTIR spectrum of allyl chloroformate. The absorption from the carbonyl group [270] was observed at an IR radiation wavenumber of 1778 cm^{-1}.

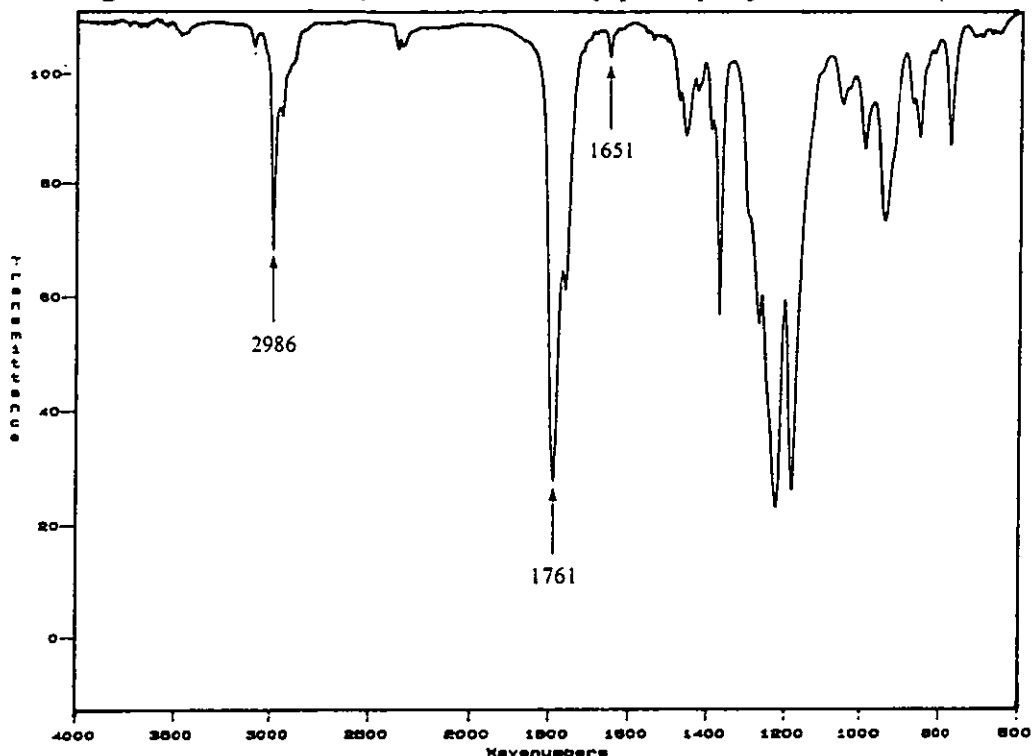**Figure 7.20 - FTIR Spectrum of *t*-Butylperoxyallyl Carbonate (ALPO)**

Figure 7.21 - IR Wavenumbers ($\bar{\nu}$) and Peak Assignments for ALPO

$\bar{\nu}$ (cm^{-1})	Molecular Environment	Vibration
1651	$\begin{array}{c} H \\ \end{array}$ H H C=C H CH$_2$-O—	C=C (stretch)
1761,1790	—C—O—O—C—CH$_3$ ‖ O CH$_3$ CH$_3$	C=O (stretch)
2986	—C—O—O—C—CH$_3$ ‖ O CH$_3$ CH$_3$	—C—H (stretch)

The FTIR spectrum of the product from the reaction between allyl chloroformate and *t*-butylhydroperoxide does not show an absorption from the C-Cl bond of the chloroformate. The absorption from stretching of the C=C double bond (1651 cm^{-1}) occurs at an identical wavenumber to that of the chloroformate. The peroxycarbonate carbonyl group shows a characteristic doublet [343] (1761 cm^{-1}, 1790 cm^{-1}). The absorption at 1790 cm^{-1} occurs at an identical wavenumber to the corresponding vibration in PMEC. Additionally, a strong absorption was observed at a radiation wavenumber of 2986 cm^{-1}, corresponding to the C-H stretching frequency of the (*t*-butyl) methyl groups [270].

7.2 - STYRENE/PEROXIDE EMULSION COPOLYMERISATION

It was decided that, in order to try to minimise the synthesis of P*n*BA macrogel (when attempting to copolymerise acrylic comonomers within PS microgel dispersions in organic media), pendant second-stage (peroxide) free radical initiator molecules were to be "built-in" toward the centre of PS/DVB microgel particles (section 7.1.1). Ideal copolymerisation of peroxide monomer with styrene, to completion, would be required in order for this synthetic procedure to be viable. The suitability of each peroxide monomer for the synthesis of initiator-functionalised PS microgel particles was determined from emulsion copolymerisation (section 2.7.3) of styrene/PMEC (5 mole % PMEC), styrene/DBPF (2.5 mole % DBPF) and styrene/ALPO (5 mole % ALPO). A polystyrene latex was prepared under identical reaction conditions (section 2.2.1).

Samples were periodically taken from latices throughout these emulsion polymerisation processes. The non-volatile component of each aliquot was determined by drying (pre-weighed) latex samples within a vacuum oven (twelve hours at 25°C). Copolymer conversion versus reaction time data were determined from these non-volatile component values. It was assumed that the materials remaining after the period of sample drying were emulsifier, initiator and copolymer materials only. Both DBPF and PMEC have high vapour pressures. If DBPF or PMEC (monomeric) molecules were present in these latex samples, the copolymer conversion data recorded would be higher than the actual conversion for the emulsion

copolymerisation (DBPF and PMEC monomer molecules would not have evaporated under the drying conditions employed). Conversion versus reaction time data for the four latices are given in table 7.14. The copolymer conversion versus copolymerisation time data are also shown, in figure 7.22.

Table 7.14 - Peroxide Copolymer Conversion Versus Reaction Time Data

	Emulsion Copolymerisation Conversion (Weight %)			
Time (Minutes)	Polystyrene	Styrene/PMEC	Styrene/DBPF	Styrene/ALPO
15	05	08	05	01
30	13	13	13	06
45	22	22	19	14
60	30	30	30	20
75	45	40	42	29
90	52	53	49	38
105	67	61	57	43
120	80	74	66	51
150	91	95	73	63
240	95	98	78	77

The conversion versus time data for the styrene/PMEC (5 mole %) copolymerisation followed the same behaviour as the polystyrene emulsion system. This copolymerisation (styrene/PMEC) proceeded to very high yield. These findings suggest that PMEC did not significantly affect the emulsion polymerisation behaviour of styrene. Comonomer reactivity ratios (section 1.5) for copolymerisation of styrene (M_1) with PMEC (M_2) have been previously evaluated $(r_1 = 0.45$ and $r_2 = 0.49)$ [253]. Each of the two generalised types of macro-radical adds, therefore, a molecule of the other comonomer at approximately twice the rate of incorporation of its own monomer. For ideal copolymerisation (i.e. when the comonomer units within each copolymer chain are randomly incorporated), each of the two (generalised) types of macro-radical show an identical preference for the addition of one comonomer over the other (i.e. $k_{11}/k_{12} = k_{21}/k_{22}$) [11]. An ideal copolymerisation has a comonomer reactivity ratio product $(r_1.r_2)$ of unity (section 1.5), therefore. Consideration of the comonomer reactivity ratios for the styrene/PMEC system indicates that both comonomers should have been consumed at similar rates throughout the

copolymerisation. High molecular weight comonomer blocks of each of the two components [11] should not, therefore, have been readily generated in this instance.

Figure 7.22 - Graph of Copolymerisation Yield Versus Copolymerisation Time
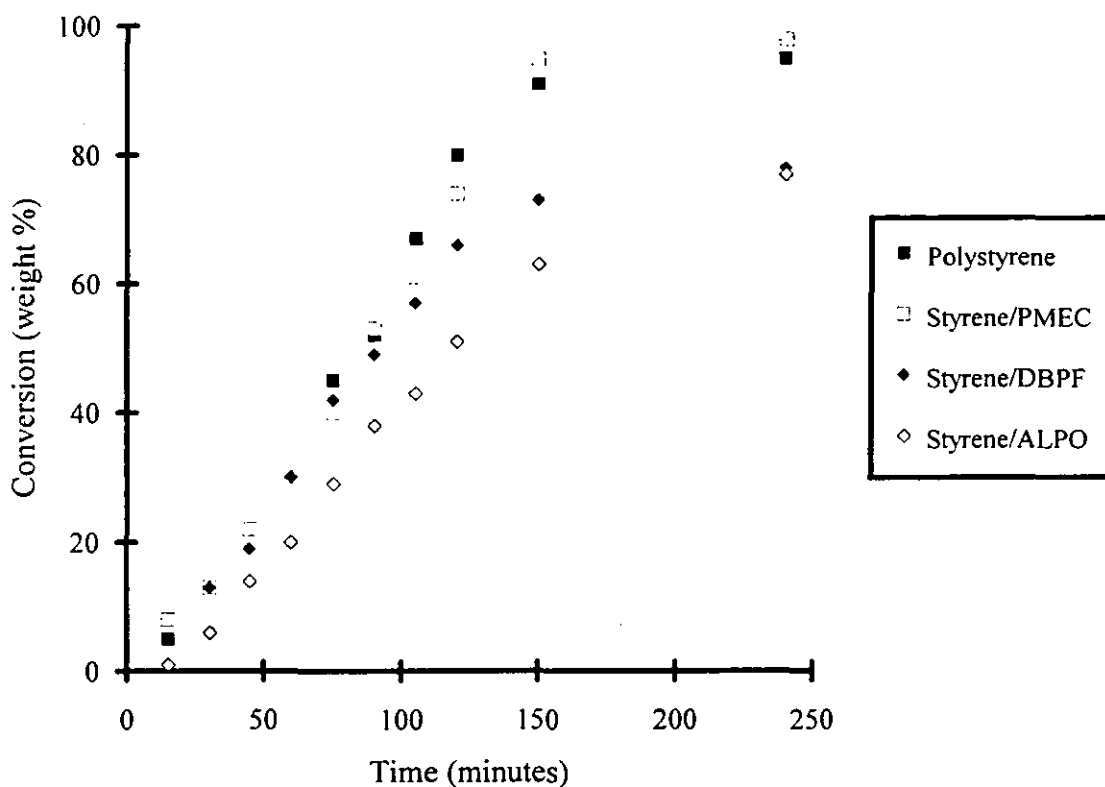
The styrene/ALPO (5 mole %) emulsion copolymerisation was retarded in comparison with the PS emulsion polymerisation and the copolymerisation product was recovered in low yield. Polymerisations of allylic monomers tend to proceed to low degrees of conversion [344-346]. Abstraction of an allylic proton by another free radical, thus leading to the generation of resonance-stabilised monomer radicals, is considered to occur in such systems [334, 335]. These radicals are considered to be inefficient at reinitiating polymerisation [335]. This degradative hydrogen transfer process imparts retardation upon polymerisation and leads to low polymerisation yields (polymers of low molecular weight are often recovered [335, 336]). Low conversion, bulk (free radical), copolymerisations of styrene (m_1)/allyl acetate (m_2) have been reported by Heatley *et al.* [347]. Comonomer reactivity ratios ($r_1 = 66$ and $r_2 = 0.02$) were determined from ^1H NMR analysis of comonomer sequence distributions [347]. Copolymers with high allyl acetate contents were not recovered [347], due to the large difference in the rate of styrene and allyl acetate consumption. Incorporation of high

(i.e. > 90 mole %) allyl acetate concentrations within the feed was also found to lead to low copolymerisation conversion and only low molecular weight materials were recovered [347]. Comonomer reactivity ratios for the styrene (m_1)/ALPO (m_2) system ($r_1 = 31$ and $r_2 = 0.02$) have been determined [253]. These values are similar to the reported styrene/allyl acetate copolymerisation data [347]. The relatively poor conversion and retardation of the styrene/ALPO (5 mole %) emulsion copolymerisation (section 2.7.3) is attributed to the degradative transfer [334, 335] to allylic monomer process. ALPO was, therefore, discounted as a potential source for the synthesis of structured polymer-bound free radical initiator groups (section 7.1.1).

The styrene/DBPF (2.5 mole %) copolymerisation was retarded in comparison with the polystyrene emulsion process and the copolymerisation proceeded to low conversion. Homopolymerisation of a 1,2-disubstituted ethylene derivative is, generally, an unfavourable process [348]. Propagation rate constants are, typically, low in such systems [348], as propagation is sterically hindered [348, 349]. Dialkyl fumarates, especially those bearing bulky (e.g. isopropyl and/or t-butyl) groups, can homopolymerise [349-351], however, and high molecular weight polymers are often recovered [350, 351]. The lifetimes of propagating polymer radicals can be as long as 150-200 seconds [350] during such polymerisation processes, compared with average lifetimes of approximately 1 second for free radical polymerisation of acrylic esters [350]. This significant increase in radical lifetime is a consequence of the exceptionally low bimolecular termination rate constant found in these systems [348, 350]. Comonomer reactivity ratios for the styrene (m_1)/t-butylperoxyisopropyl fumarate [12] (m_2), BPIPF, system ($r_1 = 1.08$ and $r_2 = 0.01$) have been determined [253]. The replacement of the alkyl (isopropyl) ester group of BPIPF with a t-butoxyl substituent (DBPF) will influence the copolymerisation characteristics of the material (i.e. the r_1 and r_2 values for styrene/DBPF would be different to those for the styrene/BPIPF system) [11]. It would appear, however, that styrene would be consumed more readily than DBPF during the early stages of copolymerisation (as is the case for styrene/BPIPF) [253], and that peroxide groups would, therefore, be non-ideally incorporated within copolymer samples.
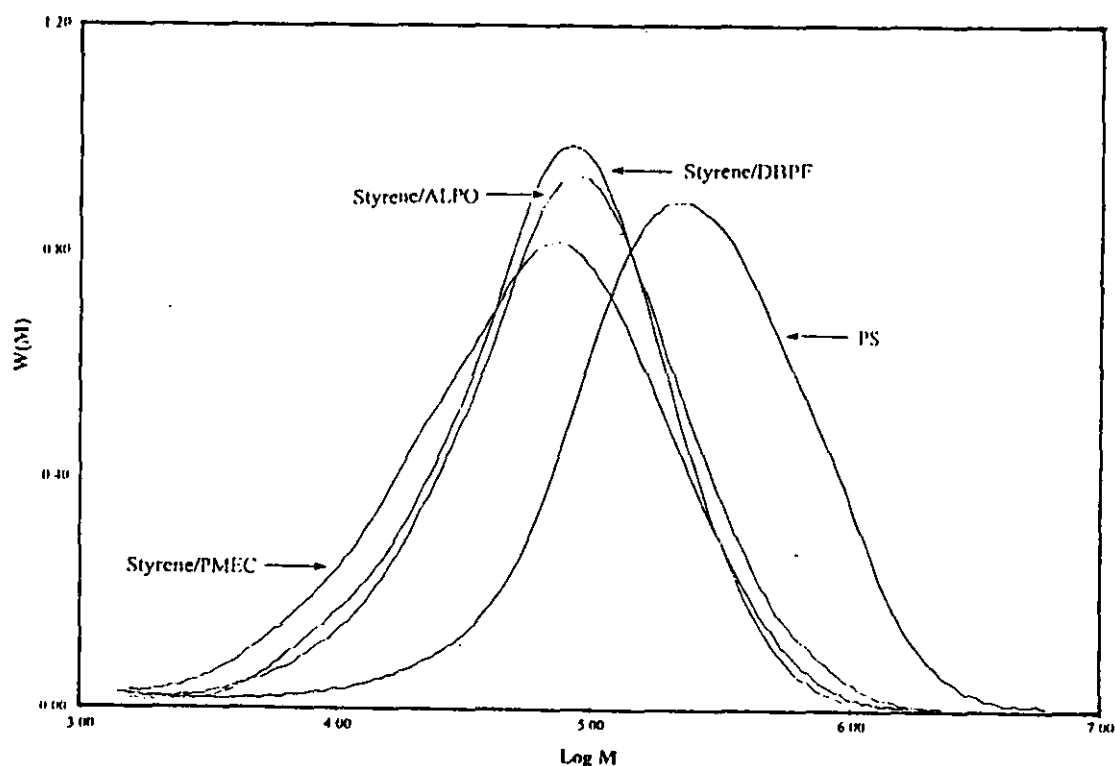
7.3.1 - STYRENE/PEROXIDE COPOLYMER MOLECULAR WEIGHTS

Samples from all four latices were rigorously purified (in order to remove any unreacted monomer from copolymer samples) by employing the procedures detailed previously (sections 2.2.2 and 2.7.4). Purified polymeric materials were analysed by gel permeation chromatography, GPC (section 2.8.3). Number-average molecular weight (M_n), weight-average molecular weight (M_w), the average molecular weight at the chromatogram peak (M_p), and sample polydispersity, D (M_w/M_n), values for each of the four samples are shown in table 7.15. Molecular mass distribution, W(M), versus log M (section 2.8.3) curves for these samples are shown in figure 7.23.

Table 7.15 - Molecular Weights for Styrene/Peroxide Copolymers from GPC

Sample	M_n (g mol^{-1})	M_w (g mol^{-1})	M_p (g mol^{-1})	D (M_w/M_n)
Polystyrene	84,000	363,000	223,000	4.3
Styrene/PMEC	28,000	104,000	72,000	3.8
Styrene/DBPF	38,000	105,000	84,000	2.8
Styrene/ALPO	37,000	131,000	84,000	3.5

Figure 7.23 - Copolymer Molecular Mass Distribution Curves from GPC

The chromatographic data show that high molecular weight peroxide copolymers were recovered from each copolymerisation process. Peroxide comonomer incorporation (5 mole % PMEC, 2.5 mole % DBPF and 5 mole % ALPO) lead, however, to a reduction in the molecular weight of each polystyrene-based sample. The mole fraction of peroxide comonomer in styrene/DVB/peroxide microgel particles was to be in the 0.10-0.50 mole % range. It was anticipated that the influence of peroxide comonomer upon the molecular weight of PS/DVB microgel would be significantly reduced at such, low, peroxide concentrations. For this particular investigation, the most important aspect of styrene/peroxide copolymerisation was considered to be the degree of peroxide incorporation within copolymer latex particles. All of the added peroxide would need to be incorporated within PS/DVB/peroxide microgel "seed" particles (before a styrene/DVB feed was copolymerised over the particles), if, centrally peroxide-functionalised microgels were to be synthesised (section 7.1.1). Estimations of the peroxide content of each of the three peroxide copolymer samples were made from DSC analysis (section 7.3.2), ^{1}H/^{13}C NMR spectroscopy (section 7.3.3) and diffuse reflectance Fourier transform infrared (DRIFT) spectroscopy (section 7.3.4).

7.3.2 - DSC CHARACTERISATION OF PEROXIDE COPOLYMERS

Purified samples of each copolymer were analysed by differential scanning calorimetry, DSC (section 2.8.1). DSC thermograms for the styrene/PMEC, styrene/DBPF, styrene/ALPO and PS samples are shown in figures 7.24, 7.25, 7.26 and 7.27, respectively.

DSC analysis indicated that each of the three copolymers show exothermic behaviour at temperatures above 120°C. An exotherm was not observed from the PS sample. The magnitude of each exotherm, the temperature at which (significant) decomposition began (Onset T) and the temperature at the exotherm maximum (Maxima T) for the three copolymers are given in table 7.16.

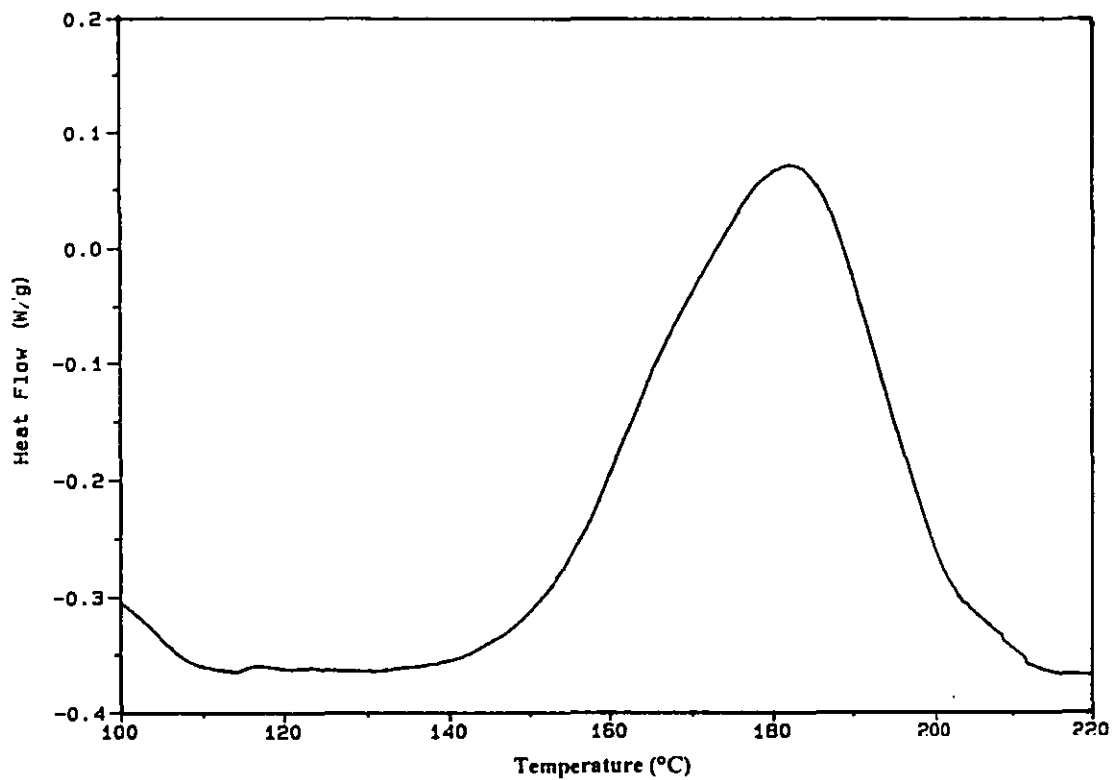# Figure 7.24 - DSC Thermogram for Styrene/PMEC Copolymer

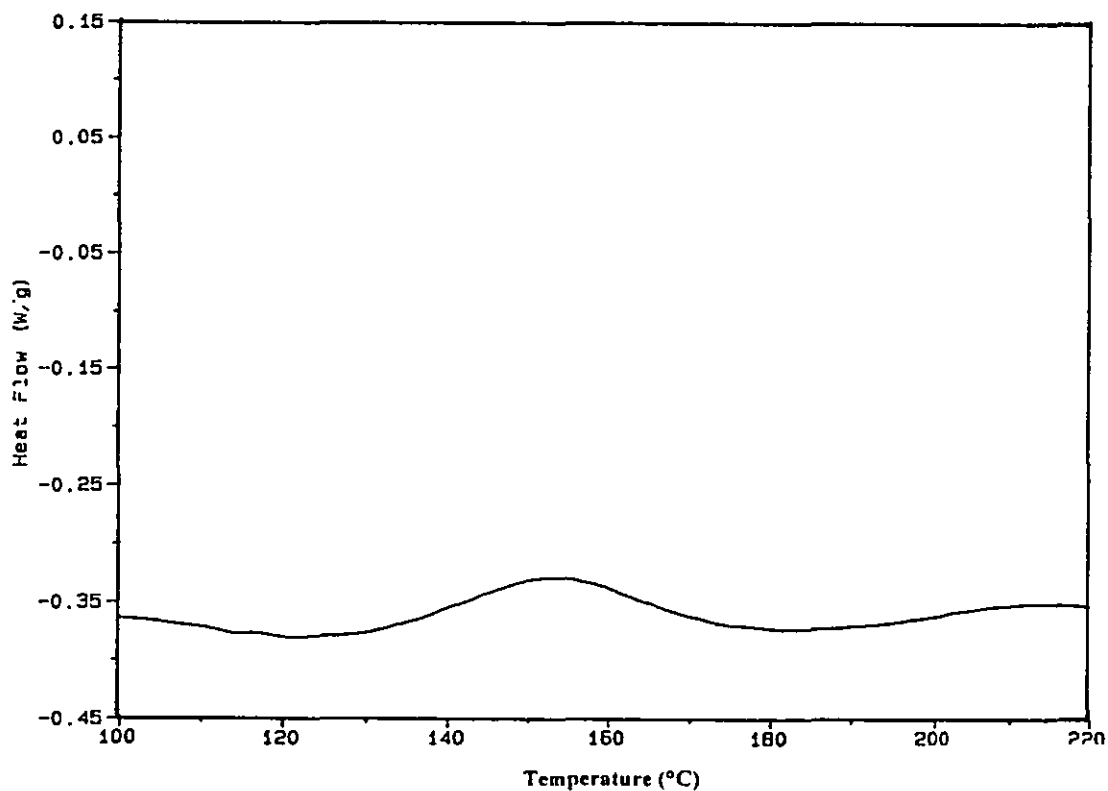# Figure 7.25 - DSC Thermogram for Styrene/DBPF Copolymer

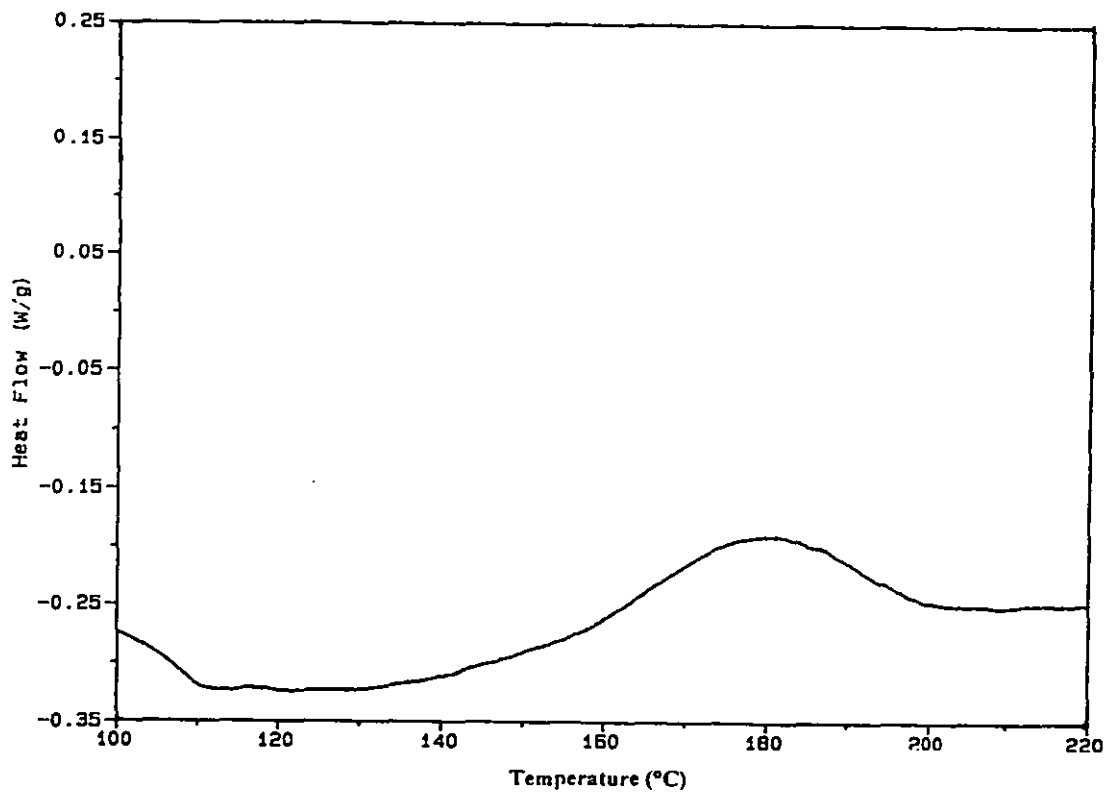Figure 7.26 - DSC Thermogram for Styrene/ALPO Copolymer
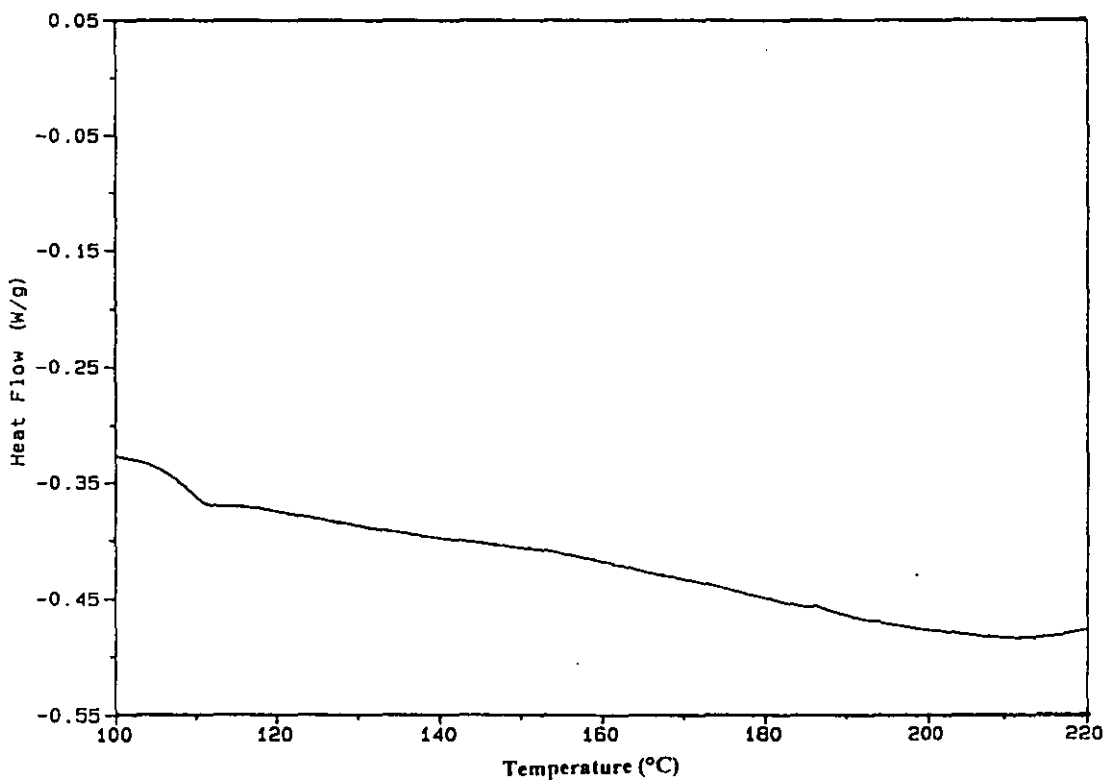

Figure 7.27 - DSC Thermogram for Polystyrene

Table 7.16 - Exotherm Magnitude & Temperature (T) at Onset & Maxima Data

Sample	Magnitude (J g^{-1})	Onset T(°C)	Maxima T(°C)
Styrene/PMEC	80.4	135.9	181.9
Styrene/DBPF	7.1	122.1	152.9
Styrene/ALPO	15.3	130.8	178.3

The exotherms are considered to arise from the thermal decomposition of *t*-butylperoxy bonds [352, 353]. The styrene/PMEC copolymer yielded the largest exotherm of the three copolymers and the styrene/DBPF copolymer generated the smallest exotherm. All three copolymerisations were performed with 5 mole % peroxide concentrations in the comonomer feed. It can be concluded, if we assume that the amount of heat evolved (from a given mass of sample) was proportional to the number of *t*-butylperoxy bonds in the copolymer [352], that the styrene/PMEC sample had the largest peroxide content of the three copolymers (if it is also assumed that the enthalpy of each decomposition process is of the same magnitude [352]). This observation suggests that PMEC had copolymerised more efficiently with styrene than did both DBPF and ALPO (the styrene/DBPF and styrene/ALPO copolymers appear to have significantly lower peroxide concentrations).

Barrett [352] determined the rate of thermal decomposition of 2,2'-azobisisobutyronitrile (AIBN), benzoyl peroxide and di-isopropylperoxy dicarbonate solutions in di-*n*-butylphthalate from differential scanning calorimetry analysis. The dissociation rate constant, k_d, data for AIBN evaluated from DSC [352] analysis was compared with published rate constant values determined from conventional analytical techniques [352, 354, 355]. Excellent agreement between the rate constant values, obtained from DSC and conventional analytical methods, was observed [352]. This calorimetric technique has also been used to determine the thermal dissociation behaviour of pendant azo groups in styrene/butadiene/*m*-azostyrene terpolymer samples [245]. With this procedure, the rate of heat evolution, dH/dt (J s^{-1}), with respect to time, t (s), or temperature, T (K), was determined from the DSC decomposition exotherm [352] (the DSC heating rate, K s^{-1}, was considered to be constant). Barrett concluded [352] that the total exotherm area (relative to the DSC baseline), A (J), corresponded to the heat of reaction, ΔH, and that an area, a (J),

corresponded to the heat evolved up to a given time, t (s). An assumption was then made for this DSC kinetic method [352], namely that the amount of heat evolved (up to a given time, t) was proportional to the number of moles (n) of reagent that had decomposed, i.e.:

$$a / A = n / n_0 \qquad (7.6)$$

and

$$-\left(\frac{dn}{dt}\right) = -\left(\frac{n}{A}\right) \cdot \left(\frac{dH}{dt}\right) \qquad (7.7)$$

where n_0 is the number of moles of reactant that were present initially.

For a first-order decomposition process (e.g. the thermolytic scission of free radical initiator molecules [338]), the rate constant for the reaction, k_d (s^{-1}), at a given temperature, T (K), was determined from [352]:

$$k_d = \frac{(dH / dt)}{(A - a)} \qquad (7.8)$$

The temperature of the system was increased, at a pre-determined (constant) heating rate, throughout the DSC analysis (section 2.8.1). Consequently, a set of rate constant values can be determined from a single DSC trace [352], as values of dH/dt and the area under the thermogram are recorded with temperature. The influence of temperature, T (K), on the rate constant, k (s^{-1}), of a first order reaction can often be estimated from the Arrhenius relation (equation 7.9) [58].

$$k = A \cdot \exp(- E_A / RT) \qquad (7.9)$$

or

$$\ln k = \ln A - (E_A / RT) \qquad (7.10)$$

where A is the pre-exponential (frequency) factor (s^{-1}), E_A is the activation energy of the reaction (J mol^{-1}), R is the gas constant (J mol^{-1} K^{-1}) and ln signifies the Napierian logarithm. Hence, the activation energy (and frequency factor) of a first order Arrhenius-type reaction can be readily determined from a plot of ln k versus $1/T$ (K^{-1}).

The dissociation rate constants for decomposition of *t*-butylperoxy bonds in the styrene/PMEC and styrene/DBPF copolymers were determined as a function of temperature (table 7.17) from DSC analysis [352]. Rate constant versus temperature data for the styrene/ALPO copolymer could not be determined, because of the non-linearity of the DSC baseline for this sample [352] (figure 7.26). It would appear, because of the presence of the *t*-butylperoxy carbonate fragment in both the styrene/ALPO and styrene/PMEC copolymer samples, that the thermal decomposition of polymer-bound ALPO groups should closely follow the dissociation behaviour of PMEC fragments in the styrene/PMEC copolymer (the dissociation rate constant as a function of temperature behaviour of a vinyl acetate/ALPO copolymer sample has been found to closely mirror the thermal decomposition behaviour of a methyl methacrylate/PMEC copolymer sample [253]). The observed similarities (in terms of the onset, maxima, and end temperatures of the two exotherms) between the styrene/PMEC (figure 7.24) and styrene/ALPO (figure 7.26) thermograms would also suggest that these peroxide dissociations are of comparable rate constant-temperature behaviour [352].

Table 7.17 - Styrene/Peroxide Copolymer Decomposition Rate Constant with Temperature Data from DSC Analysis

	Peroxide Dissociation Rate Constant, k_d (s^{-1}), from DSC	
Temperature, T (°C)	Styrene/PMEC	Styrene/DBPF
140		3.70×10^{-3}
145		6.55×10^{-3}
150		1.07×10^{-2}
155		1.62×10^{-2}
160	2.24×10^{-3}	2.31×10^{-2}
165	3.64×10^{-3}	3.28×10^{-2}
170	5.35×10^{-3}	5.24×10^{-2}
175	7.66×10^{-3}	
180	1.13×10^{-2}	
185	1.65×10^{-2}	
190	2.38×10^{-2}	

The rate constant, k_d (s^{-1}), at a given temperature, T (°C), data for the styrene/PMEC and styrene/DBPF copolymer thermal decompositions were converted into ln k_d values. Graphs of ln k_d versus 1/T (K^{-1}) for the styrene/PMEC (appendix 10) and

styrene/DBPF (appendix 11) samples were plotted, and both sets of data were found to give linear (ln k with 1/T) relations. The thermal dissociation of these polymer-bound *t*-butylperoxy bonds would, therefore, appear to follow a first-order (Arrhenius) decomposition process [58]. The activation energy, E_A, and frequency factor, A, values for the dissociation of peroxide bonds in styrene/PMEC and styrene/DBPF samples (table 7.18) were determined from the gradient and intercept (equation 7.10) of the ln k versus 1/T graphs (appendices 10 and 11, respectively).

Table 7.18 - Dissociation Activation Energies and Frequency Factors from Peroxide Copolymer Thermal Decomposition Values (DSC)

Copolymer Sample	Activation Energy, E_A (kJ mol^{-1})	Frequency Factor, A (s^{-1})
Styrene/PMEC	127	5.4×10^{12}
Styrene/DBPF	125	2.4×10^{13}

The activation energies of *t*-butylperoxy bond decompositions in styrene/PMEC and styrene/DBPF copolymers, from DSC analysis [352], are of similar magnitude to the energies of activation for decomposition of conventional free radical (acyl peroxide and peroxy carbonate) initiator molecules [352]. The rate constant, k (s^{-1}), of a reaction that follows first-order kinetics (such as for the thermal decomposition of free radical initiators [11, 58]) is related to the half-life, $t_{1/2}$ (s), of the reaction by:

$$t_{1/2} = (\ln 2) / k \qquad (7.11)$$

Provided that the energy of activation (E_A) and the frequency factor (A) of a (Arrhenius) first-order reaction are known, the temperature (T) required to give a specific half-life for the reaction can be determined. For example, the temperature giving a ten hour reaction half-life, $t_{1/2}$ T_{10h} (K), is related to the rate constant, k (s^{-1}), of the process, by:

$$k = 0.693 / 36000 \text{ s} = 1.925 \times 10^{-5} \text{ s}^{-1} \qquad (7.12)$$

and k is then simply related to the temperature, T (K), of the system in accordance with the Arrhenius relation [58] (equation 7.9).

The temperatures giving a ten hour, $t_{1/2}$ T_{10h} (°C), a four hour, $t_{1/2}$ T_{4h} (°C), and a 1 hour, $t_{1/2}$ T_{1h} (°C), decomposition half-life for the dissociation of peroxide bonds in the styrene/PMEC and styrene/DBPF copolymer samples (as determined from DSC analysis) are detailed in table 7.19.

Table 7.19 - Thermal Decomposition Reaction Half-life with Temperature Relations for Peroxide Copolymers (DSC)

Sample	$t_{1/2}$ T_{10h} (°C)	$t_{1/2}$ T_{4h} (°C)	$t_{1/2}$ T_{1h} (°C)
Styrene/PMEC	108	117	131
Styrene/DBPF	86	94	107

The temperatures giving a ten hour dissociation half-life, $t_{1/2}$ T_{10h} (°C), for the decomposition of peroxide bonds in t-butylperoxy-2-methacryloyloxyethyl carbonate (PMEC), t-butylperoxyisopropyl fumarate (BPIPF), t-butylperoxyallyl carbonate (ALPO), and methyl methacrylate/PMEC, vinyl acetate/BPIPF and vinyl acetate/ALPO copolymer samples [246] are given in table 7.20.

**Table 7.20 - Peroxide Decomposition Half-life Values [246]**

Peroxide Sample	Ten hour Dissociation Half-life Temperature, $t_{1/2}$ T_{10h} (°C)
PMEC	104
Methyl methacrylate/PMEC copolymer	104
BPIPF [1]	107
Vinyl acetate/BPIPF copolymer	80
ALPO	97
Vinyl acetate/ALPO copolymer	105

[1] It is anticipated that the thermal decomposition behaviour of di-t-butylperoxy fumarate (DBPF) monomer is comparable to that of BPIPF monomer.

The temperatures giving a ten hour half-life for the decomposition of t-butylperoxy bonds in styrene/PMEC and styrene/DBPF copolymers are similar to the values determined for methyl methacrylate/PMEC and vinyl acetate/BPIPF copolymer samples [246]. The thermolytic behaviour of the t-butylperoxy group in PMEC monomer [246, 352] does not appear to be significantly influenced by the

222

copolymerisation processes, either upon copolymerisation with styrene or from copolymerisation of PMEC with vinyl acetate [246]. The temperatures required for thermal cleavage of the *t*-butylperoxy bond in DBPF monomer (the decomposition temperature behaviour of DBPF is assumed to be comparable with that of BPIPF) would appear to be markedly higher than those required for decomposition of the DBPF group in the styrene/DBPF copolymer sample (similar behaviour has been observed from copolymerisation of BPIPF with vinyl acetate [246]). The thermal decomposition of an alkyl-substituted *t*-butylperoxy ester derivative (figure 7.28) proceeds via one of two possible mechanisms [338]. The mechanism of thermolysis, which is followed by a given *t*-butylperoxy ester derivative, is governed, predominantly, by the structure of the (alkyl chain) substituent [338].

Figure 7.28 - Mechanism of Thermolytic Decomposition for Alkyl-Substituted
***t*-Butylperoxy Ester Derivatives**
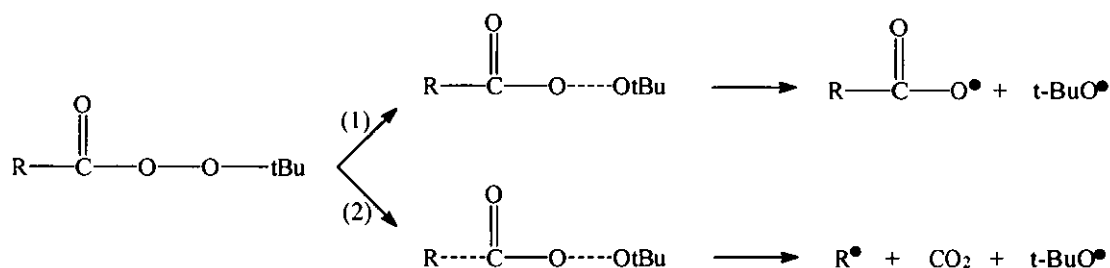
where *R* denotes an alkyl group.

Mechanism 1 (figure 7.28) involves homolysis of the O-O single bond, whereas mechanism 2 proceeds via a two bond, concerted, homolytic decomposition [338]. Alkyl-substituted *t*-butylperoxy ester derivatives which undergo the concerted homolysis mechanism, involving simultaneous scission of O-O and C-C single bonds, decompose at significantly faster rates [338] than *t*-butylperoxy ester derivatives which decompose via the one-bond homolysis mechanism (table 7.21). The significantly lower half-lives and activation energies for the concerted mechanism of thermolysis (table 7.21) reflects the influence that the alkyl radical (R•) stability has on the decomposition mechanism [383]. It is possible that the (apparent) increase in decomposition rate for polymer-bound DBPF fragments, compared with DBPF

monomer, could be due to a change in the homolysis mechanism from one bond (DBPF) to a two bond, concerted process (for the copolymer). Alternatively, both of the systems could decompose thermally via the concerted (two bond) mechanism, with the increased stability of the polymer-bound (tertiary) radical (compared with the secondary monomer radical) influencing the rate of peroxide decomposition [338].

**Table 7.21 - Kinetic Parameters for the Thermolysis of *t*-Butylperoxy Esters [338]**

R in RCO_3-tBu	$t_{1/2}$ at 60°C (s)	E_A (kJ mol^{-1})	Mechanism
Phenyl (Ph)	1.8×10^6	142	O-O Homolysis
t-Bu	1.8×10^4	128	Concerted
Ph_3C	60	101	Concerted

DSC analysis of styrene/PMEC, styrene/DBPF and styrene/ALPO copolymer samples determined that PMEC had been incorporated to a significantly greater extent than both DBPF and ALPO. Emulsion terpolymerisation of styrene/DVB/PMEC would, therefore, appear to be the most-suitable method for the preparation of centrally-functionalised PS/peroxide microgels. Such functionalised PS microgel particles were to be subsequently dispersed in *n*BA/NPGDA mixtures, and synthesis of IPN microgel dispersions was then to be attempted by thermally decomposing the peroxide bonds of the PS network particles. The dissociation rate constant for the thermal decomposition of free radical initiator molecules is, generally, required to be of the order of 10^{-4}-10^{-5} s^{-1} [11], if initiation of polymerisation is to be satisfactorily achieved (at the required decomposition temperature). The temperature, T, required for initiation of *n*BA/NPGDA copolymerisation (from the thermolysis of PS/PMEC microgel particles) would, therefore, appear to be in the 110°C $\leq$ T $\leq$ 125°C range.

7.3.3 - ^{1}H/^{13}C NMR CHARACTERISATION OF PEROXIDE COPOLYMERS

DSC analysis of styrene/peroxide copolymer samples determined that PMEC had been incorporated to a significantly greater extent than both DBPF and ALPO during the emulsion copolymerisation process (section 7.3.2). The mole fraction of peroxide in each of the three copolymers could not be determined from these calorimetric results.

(It is possible that a determination of the dissociation enthalpies of PMEC, DBPF and ALPO homopolymer samples could enable the peroxide content of copolymers to be estimated from DSC thermograms, however). ^{1}H NMR spectroscopy [277, 356-358] and FTIR spectroscopy [294, 359, 360] techniques can, under certain circumstances, be employed to quantitatively determine the composition of copolymer samples. Samples of PS and styrene/PMEC, styrene/DBPF and styrene/ALPO copolymers were analysed by 250 MHz ^{1}H and 25 MHz ^{13}C NMR spectroscopy (sections 2.8.7 and 2.8.8, respectively). The ^{1}H NMR spectrum of the PS sample is shown in figure 7.29.
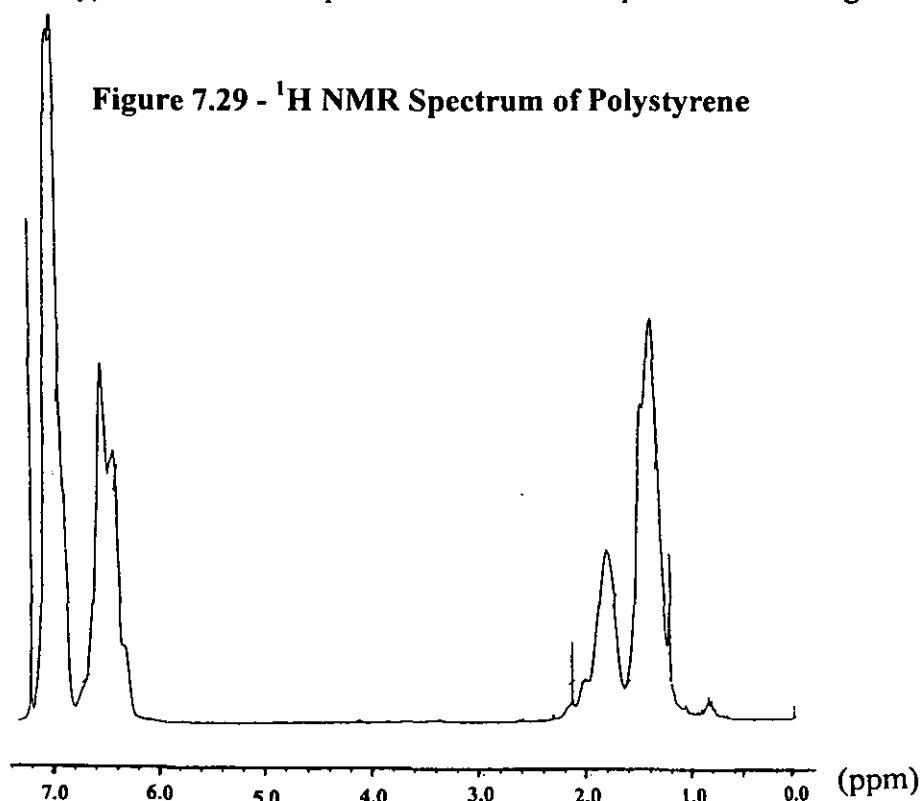
Figure 7.29 - ^{1}H NMR Spectrum of Polystyrene

| | 7.0 | 6.0 | 5.0 | 4.0 | 3.0 | 2.0 | 1.0 | 0.0 | (ppm) |

The 250 MHz ^{1}H NMR spectrum of the polystyrene sample exhibits the characteristic resonances observed from ^{1}H NMR analysis of high molecular weight, atactic PS samples [361, 362]. Resonances from aromatic protons are observed over a 6.3-6.8 ppm chemical shift range, corresponding to absorptions from *ortho* protons, and over a 6.8-7.2 ppm range, corresponding to resonances from *meta-para* proton environments [361]. Absorptions from β-methylene, backbone, protons are observed over the 1.3-1.7 ppm range, and α-proton (methine) resonances are found over the 1.7-2.1 ppm chemical shift region [361]. The singlet absorption situated at 7.25 ppm is attributed to non-deuterated solvent ($CHCl_3$). The 250 MHz ^{1}H NMR spectra recorded for the styrene/PMEC, styrene/DBPF and styrene/ALPO copolymer samples are shown in figures 7.30, 7.31 and 7.32, respectively.

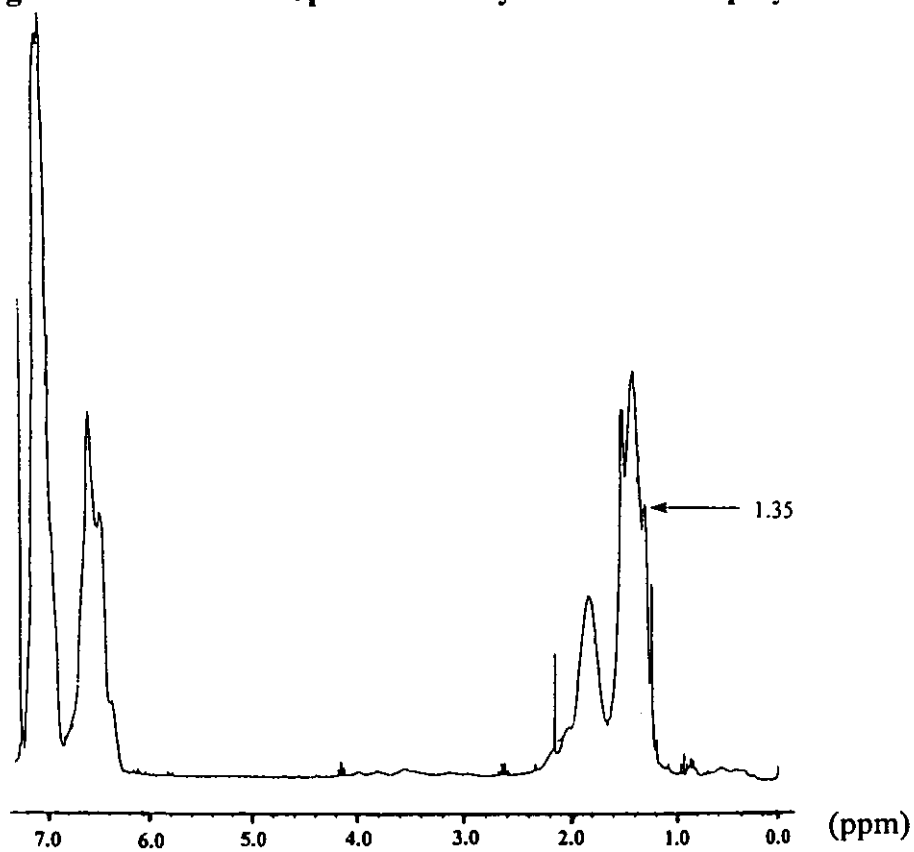**Figure 7.30 - ^{1}H NMR Spectrum of Styrene/PMEC Copolymer**

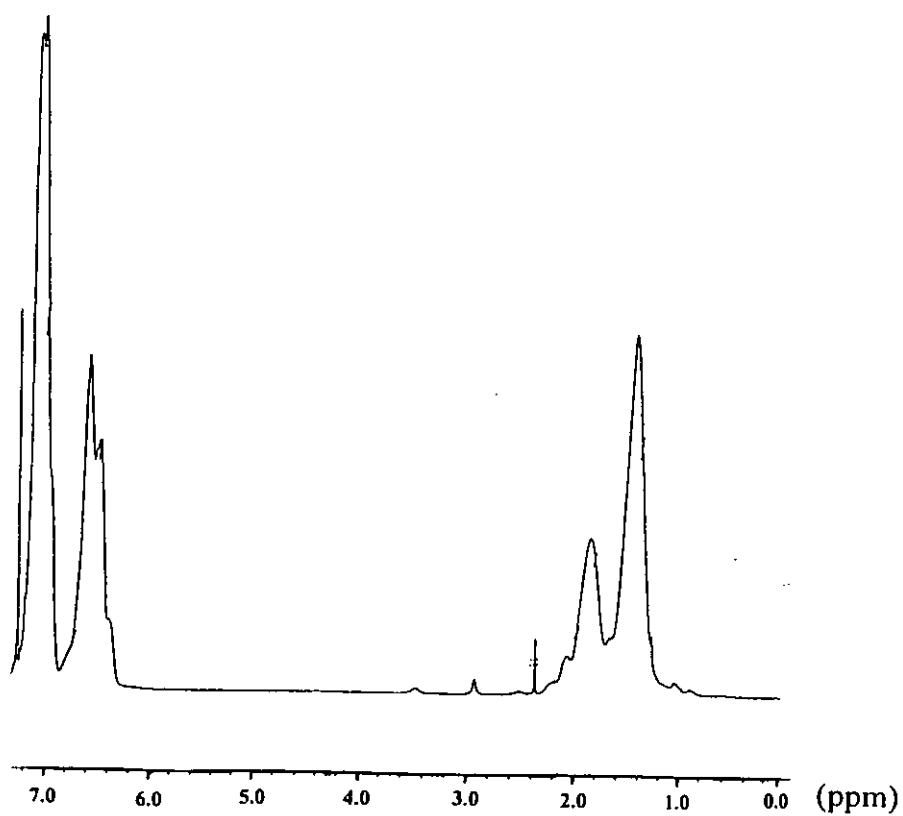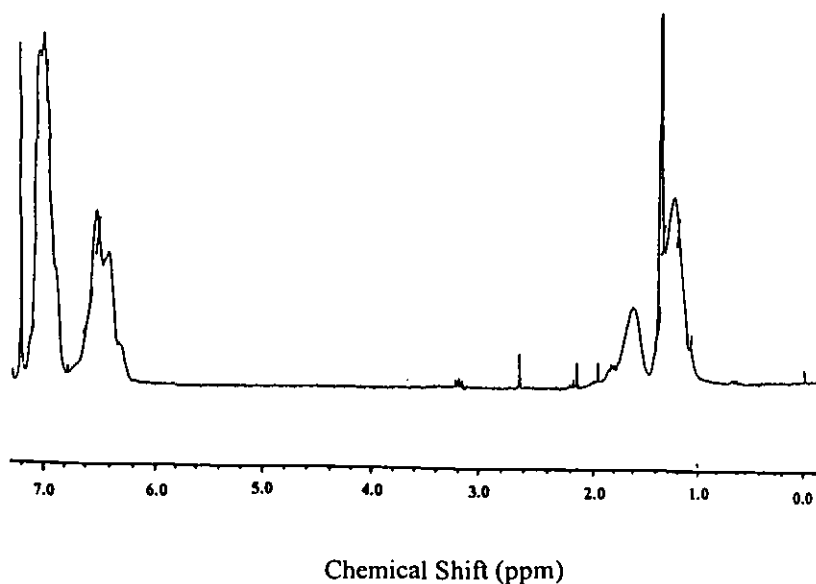**Figure 7.31 - ^{1}H NMR Spectrum of Styrene/DBPF Copolymer**

Figure 7.32 - ^{1}H NMR Spectrum of Styrene/ALPO Copolymer

Chemical Shift (ppm)

The 250 MHz ^{1}H NMR spectrum of the styrene/PMEC copolymer exhibits an additional ^{1}H resonance (a singlet, situated at a chemical shift of 1.35 ppm), corresponding to absorption from the methyl protons of the *t*-butyl group in PMEC (section 7.1.2), when compared with the ^{1}H NMR spectrum of the polystyrene sample (figure 7.29). In principal, the mole fraction of each comonomer in a copolymer sample can be determined from ^{1}H NMR peak integral information [280, 356, 361]. For example, the mole fraction of methyl methacrylate (MMA) in styrene/MMA copolymers can be determined from comparison between the peak integrals for the methoxyl proton resonances (MMA) with those from the aromatic proton resonances (styrene) [356]. In practice, however, many copolymer systems do not readily yield quantitative mole fraction values [279, 361]. Suitable resonances from both comonomer repeat units can not always be found. Overlapping between proton absorptions from each of the components is often observed [279]. Unfortunately, this appears to be the case for the styrene/PMEC copolymer system. The methyl resonances from PMEC's *t*-butyl group are found to overlap with the β-methylene absorptions from main-chain styrene groups. The methyl resonance is insufficiently resolved for accurate peak integration. It is possible that the PMEC methyl resonance

227

could be resolved from the methylene absorptions of styrene groups at higher magnetic field strengths (e.g. 400 MHz or 600 MHz ^{1}H NMR) [280]. No other ^{1}H resonances from PMEC groups are readily distinguishable from the spectral baseline. The 250 MHz ^{1}H NMR spectra of the styrene/DBPF copolymer (figure 7.31) and styrene/ALPO copolymer (figure 7.32) show close resemblance to the absorption characteristics of the atactic polystyrene sample (figure 7.29). Resonances from DBPF and ALPO groups are not apparent (section 7.1.2). This observation suggests that the mole fractions of peroxide groups in these two copolymer samples were significantly lower than the peroxide content of the styrene/PMEC copolymer [279]. Each of the copolymers was synthesised with 5 mole % peroxide comonomer in the copolymerisation feed (section 2.7.3). It would appear, therefore, from ^{1}H NMR analysis, that ALPO and DBPF had both inefficiently copolymerised with styrene.

The 25 MHz ^{13}C NMR spectra recorded for the polystyrene, styrene/PMEC, styrene/DBPF and styrene/ALPO samples are shown in figures 7.33, 7.34, 7.35 and 7.36, respectively.
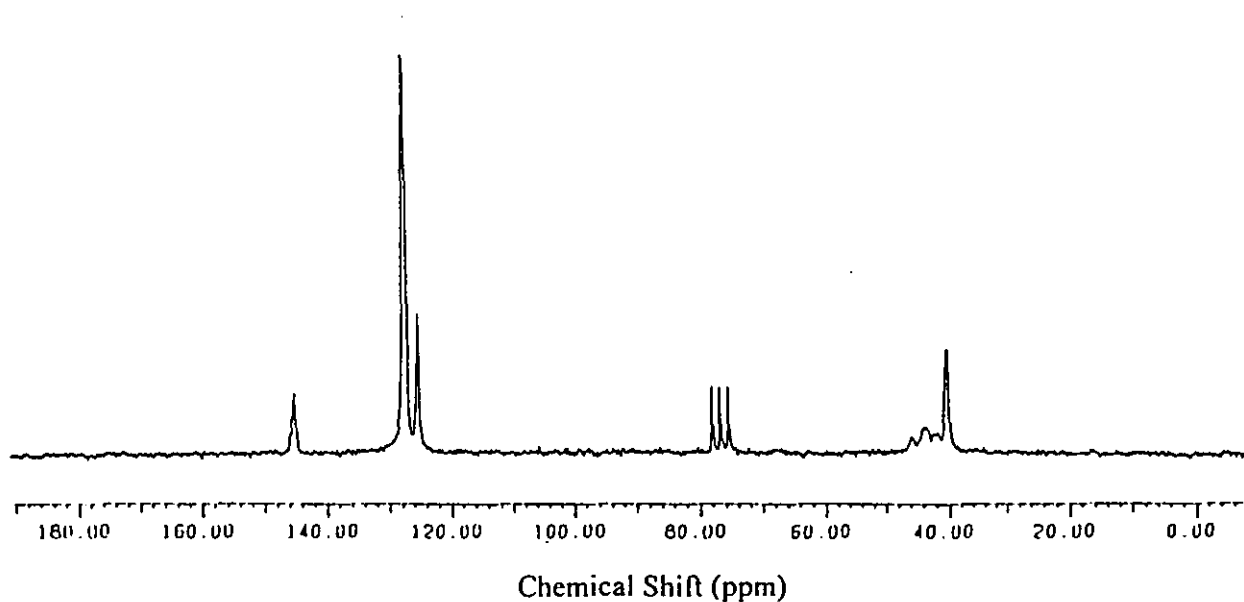
Figure 7.33 - ^{13}C NMR Spectrum of Polystyrene

Chemical Shift (ppm)

Figure 7.34 - ^{13}C NMR Spectrum of Styrene/PMEC Copolymer

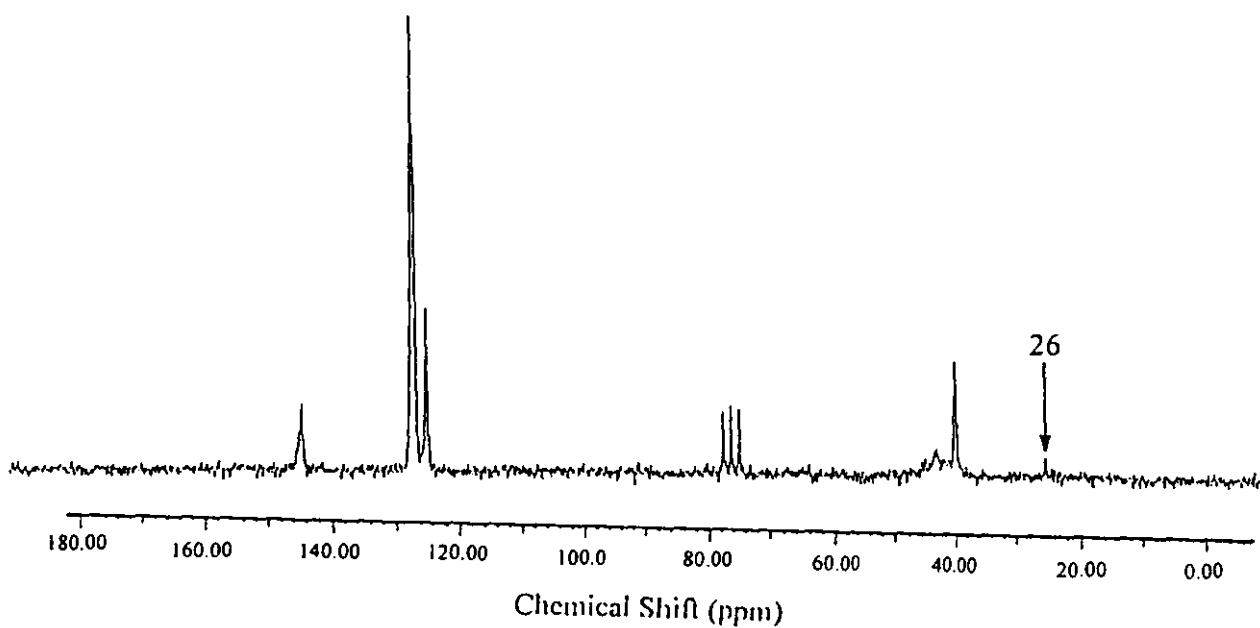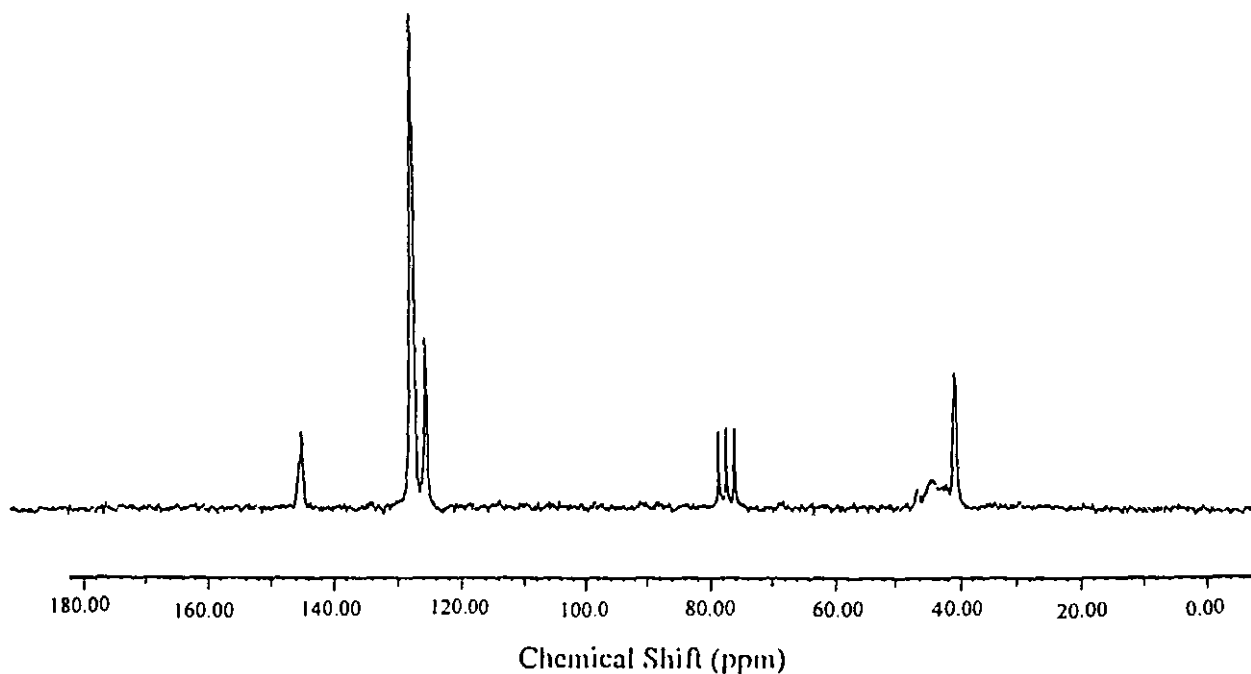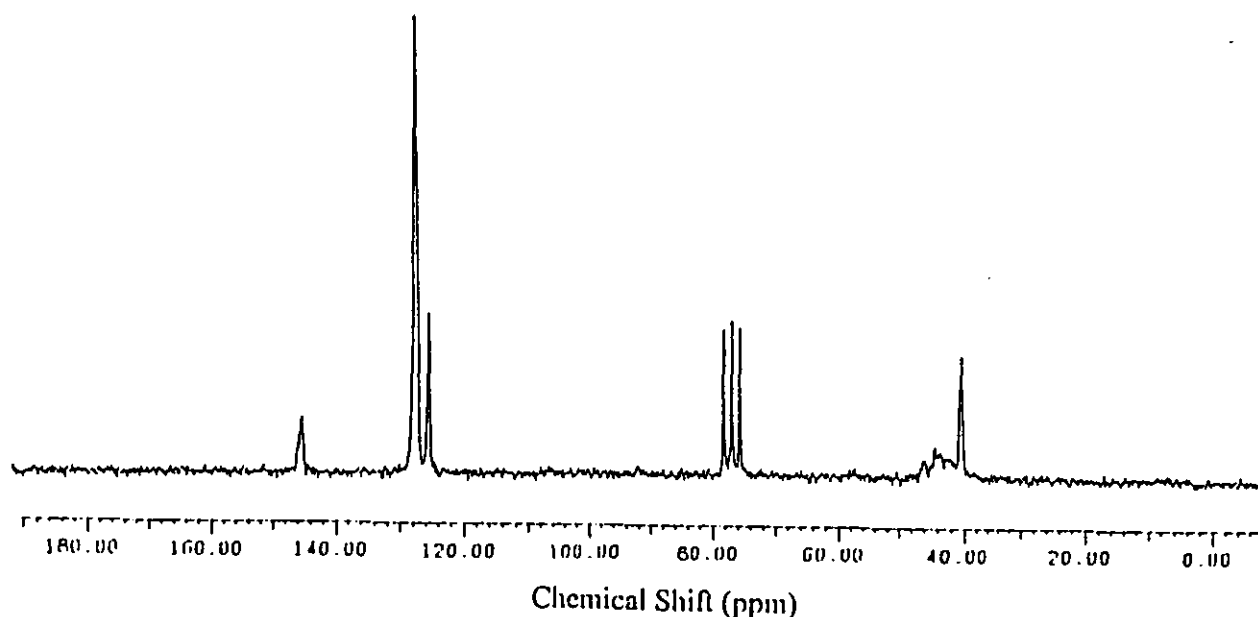**Figure 7.35 - ^{13}C NMR Spectrum of Styrene/DBPF Copolymer**

Figure 7.36 - ^{13}C NMR Spectrum of Styrene/ALPO Copolymer

Chemical Shift (ppm)

The 25 MHz ^{13}C NMR spectrum of the polystyrene sample exhibits the characteristic resonances observed from ^{13}C NMR analysis of high molecular weight, atactic PS samples [363, 364]. The resonance from *para* aromatic protons is centred at 125 ppm [363]. Absorptions from *ortho-meta* aromatic proton environments are located at a chemical shift of 128 ppm [363]. The tertiary aromatic carbon (i.e. the carbon atom of the phenyl ring that is bonded to C_α) resonances are centred at 145 ppm [363], the peak splittings are attributed to absorptions from isotactic, heterotactic and syndiotactic styrene pentad sequences [363, 364]. Backbone, β-methylene and α-methine, carbon resonances are observed over the 39-47 ppm chemical shift range [363, 364]. The triplet absorption centred at 77 ppm is from the solvent ($CDCl_3$). The 25 MHz ^{13}C NMR spectrum of the styrene/PMEC copolymer is similar to that of polystyrene homopolymer, with the exception that a weak resonance is observed at a chemical shift of 26 ppm. This absorption is considered to correspond to resonances from the methyl carbon atoms of the *t*-butyl group in PMEC (section 7.1.2). The relative peak intensities (e.g. from the 125 ppm absorption for styrene and from the 26 ppm resonance for PMEC) cannot be used to determine quantitative copolymer compositional data, however, as a consequence of nuclear Overhauser enhancements

(NOE's) [280, 347]. Additional ^{13}C resonances from PMEC are not observed in the 25 MHz ^{13}C NMR spectrum of the styrene/PMEC copolymer. The ^{13}C NMR spectra of the styrene/DBPF (figure 7.35) and styrene/ALPO (figure 7.36) copolymers appear to be identical to the polystyrene spectrum (figure 7.33). Absorptions from DBPF and ALPO comonomer units are not observed, indicating that both of these peroxides had been incorporated in copolymer samples to a lesser extent than had PMEC.

7.3.4 - DIFFUSE REFLECTANCE INFRARED FOURIER TRANSFORM (DRIFT) SPECTROSCOPY ANALYSIS OF PEROXIDE COPOLYMERS

Conventional FTIR spectroscopy has been used for both qualitative [365, 366] and quantitative [359, 360] determination of copolymer compositional values. The composition of a series of poly(ethylene-co-methyl acrylate) copolymers were determined by Meilchen et al. [357] from NMR/FTIR spectroscopy analysis. Mao et al. [360] have reported an absolute method for determination of copolymer compositions from FTIR analysis of copolymer solutions. FTIR absorbance with composition calibration curves [360] were determined from analysis of mixtures of the two, constituent, homopolymers, in solution [360]. Brown and Glass [368] determined the composition of isocyanate-containing copolymers from FTIR analysis of copolymer sample solutions. Calibration was performed via (dilute solution) FTIR analysis of a model compound [368]. Willis et al. [369] have accurately determined the composition of vinyl chloride/vinyl acetate copolymers from DRIFT spectroscopy analysis [369]. The calibration standards employed in this particular investigation were copolymers of known composition [369], however, and, hence, DRIFT analysis was not an absolute characterisation technique, in this instance. FTIR/DRIFT spectroscopy techniques would appear to have the potential to determine accurately the composition of styrene/peroxide copolymer samples with low peroxide content, materials that had been prepared in this investigation (sections 2.7.4 and 7.2). The intensity of an infrared absorption is related to the change in bond dipole moment that occurs on vibration [270] (section 2.8.5). Consequently, materials that solely contain covalent bonds between atoms of similar electronegativities, e.g. the C-C and C-H bonds of polystyrene, show relatively weak IR absorption bands [270] (section 3.5).

The stretching mode of the carbonyl group (as found in PMEC, DBPF and ALPO monomers) is of high molar absorptivity [270], however (section 2.8.5). It would, therefore, appear possible that styrene/peroxide copolymers, with peroxide contents (C) in the $0 < C \leq 5$ mole % range, could show relatively intense FTIR absorptions from polymer-bound peroxy carbonate or peroxy ester groups.

FTIR absorbance calibration curves for styrene/PMEC, styrene/DBPF and styrene/ALPO copolymer samples were obtained from FTIR analysis of ethylbenzene/PMEC, ethylbenzene/DBPF and ethylbenzene/ALPO (1, 2, 3, 4 and 5 mole % peroxide) mixtures (ethylbenzene was considered to be a suitable material for use as a model compound for PS group vibrations). The vibrational characteristics from FTIR analysis of ethylbenzene and from DRIFT absorptions of polystyrene have shown marked similarities (section 3.5), indicating that ethylbenzene does model several of the vibrations in polystyrene-based materials. Absorbance FTIR spectra of ethylbenzene, ethylbenzene/PMEC (4 mole % PMEC), ethylbenzene/DBPF (1.5 mole % DBPF), and ethylbenzene/ALPO (2 mole % ALPO) are shown in figures 7.37, 7.38, 7.39 and 7.40, respectively.

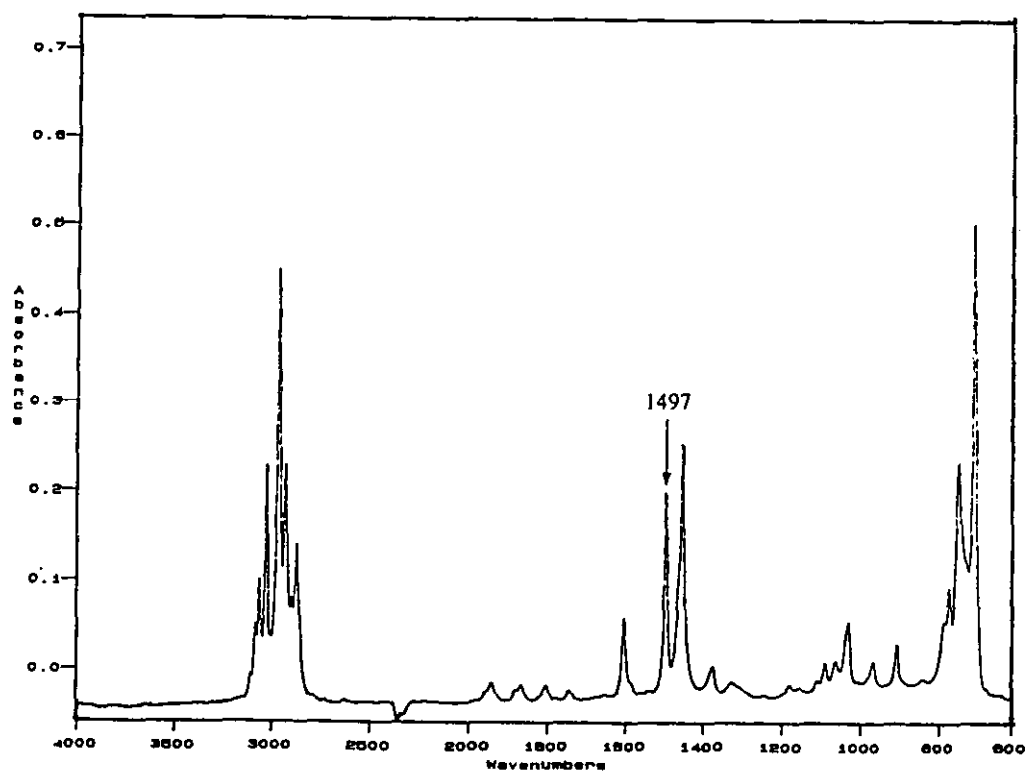## Figure 7.37 - Absorbance FTIR Spectrum of Ethylbenzene

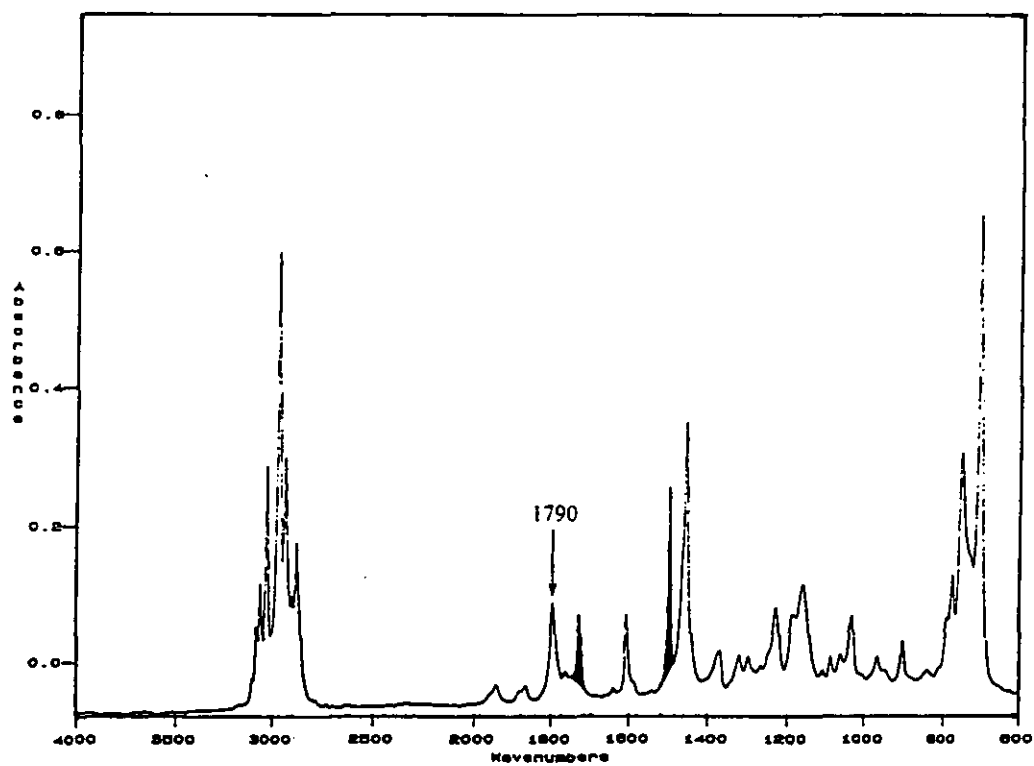**Figure 7.38 - Absorbance FTIR Spectrum of Ethylbenzene/PMEC (4 Mol%)**

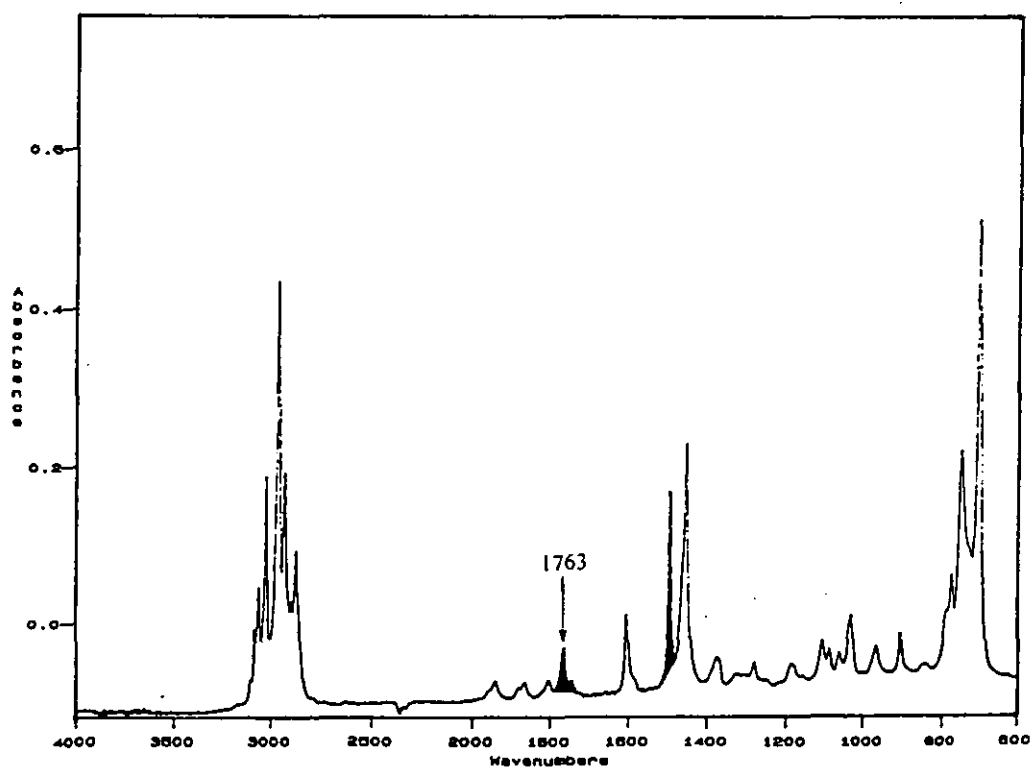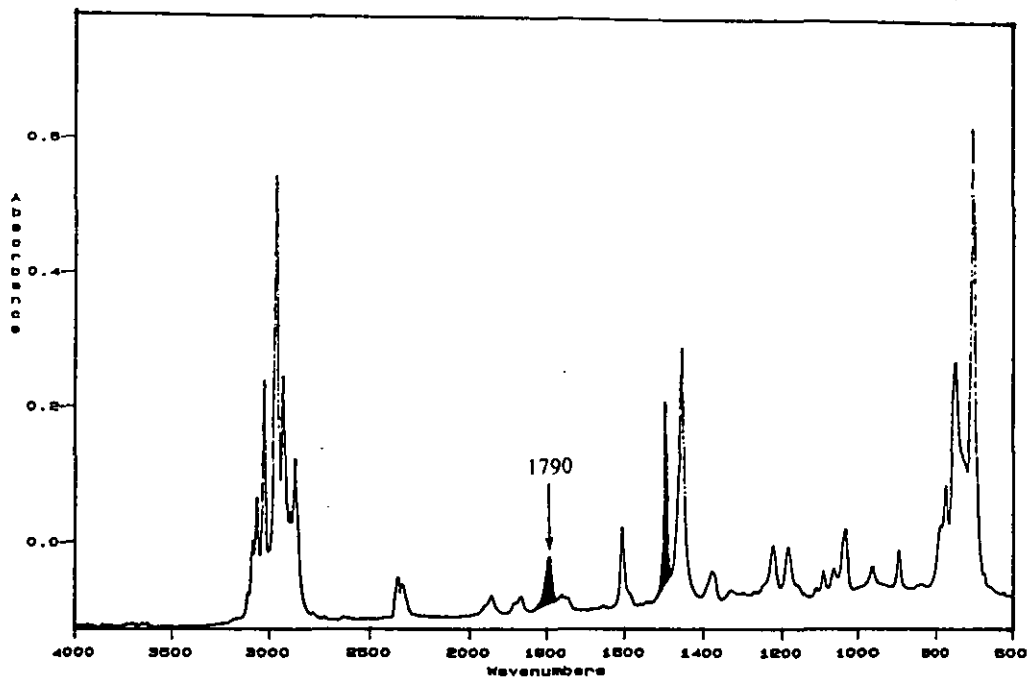**Figure 7.39 - Absorbance FTIR Spectrum of Ethylbenzene/DBPF (1.5 Mol%)**

Figure 7.40 - Absorbance FTIR Spectrum of Ethylbenzene/ALPO (2 Mole %)

The ethylbenzene/peroxide monomer mixtures exhibited the vibrational characteristics of pure ethylbenzene, with the exception that moderately strong absorptions, corresponding to the stretching mode of vibration for the carbonyl group in each peroxide monomer, were also observed from FTIR analysis. The intense peroxycarbonate carbonyl absorption from PMEC ($\bar{v}$ = 1790 cm^{-1}), the carbonyl group vibration from DBPF ($\bar{v}$ = 1763 cm^{-1}) and the C=O stretching mode of ALPO ($\bar{v}$ = 1790 cm^{-1}) were used for FTIR calibration curves (ethylbenzene does not show significant absorption behaviour in the 1750-1800 cm^{-1} region of the electromagnetic spectrum). The C-C stretching mode of vibration for the (monosubstituted) phenyl ring ($\bar{v}$ = 1497 cm^{-1}) in ethylbenzene [270, 292] was chosen as the second (FTIR absorbance) calibration band for ethylbenzene/peroxide mixtures. Absorbance (A) ratios [294], A_{1790}/A_{1497}, A_{1763}/A_{1497} and A^{*}_{1790}/A_{1497}, were determined from FTIR spectroscopy analysis of ethylbenzene/PMEC, ethylbenzene/DBPF and ethylbenzene/ALPO mixtures, respectively (table 7.22). Graphs of absorbance ratio [270, 294] versus peroxide concentration (section 2.8.5) for the ethylbenzene/PMEC (appendix 12), ethylbenzene/DBPF (appendix 13) and ethylbenzene/ALPO (appendix 14) calibrants were subsequently plotted.

Table 7.22 - Absorbance (A) Ratio with Peroxide Concentration (C)

Values from FTIR Analysis of Ethylbenzene/Peroxide Mixtures

Total Peroxide Content (Mole %)	A_{1790}/A_{1497} (PMEC)	A_{1763}/A_{1497} (DBPF)[1]	A^{*}_{1790}/A_{1497} (ALPO)
0	0.01	0.01	0.01
1	0.14	0.14	0.14
2	0.27	0.26	0.29
3	0.37	0.39	0.43
4	0.49	0.53	0.58
5	0.58		0.67

[1] Ethylbenzene/DBPF mixtures with 0.5, 1.0, 1.5 and 2.0 mole % DBPF were analysed, giving 1.0, 2.0, 3.0 and 4.0 mole % (total) peroxide concentrations, respectively. (An ethylbenzene/DBPF mixture with 2.5 mole% DBPF content was not analysed, due to the fact that only a small quantity of DBPF was available, and because DSC and $^{1}H/^{13}C$ NMR analysis had shown that the styrene/DBPF copolymer had a low peroxide content).

The absorbance ratio versus peroxide concentration graphs (appendices 12-14) all show linear relationships over the $0 \leq C \leq 4$ mole % range. Slight deviations from linearity are apparent at a concentration of 5 mole % for the ethylbenzene/ALPO mixture. Diffuse reflectance infrared Fourier transform (DRIFT) spectra (section 2.8.6) were recorded for dispersions (anhydrous KBr, 3 wt.% copolymer) of styrene/PMEC (figure 7.41), styrene/DBPF (figure 7.42) and styrene/ALPO copolymers (figure 7.43). The DRIFT spectrum of PS homopolymer is shown in figure 3.13 (section 3.5). The infrared absorptions of the styrene/peroxide copolymers show almost identical behaviour to the bands of polystyrene homopolymer (the DRIFT spectrum absorption characteristics of PS were discussed in section 3.5). Moderately intense DRIFT absorptions were also observed at 1792 and 1730 cm^{-1} (the two, major, carbonyl stretching vibrations of PMEC groups) radiation wavenumbers, for the styrene/PMEC copolymer sample.

Figure 7.41 - DRIFT Spectrum of Styrene/PMEC Copolymer

Figure 7.41 - DRIFT Spectrum of Styrene/PMEC Copolymer

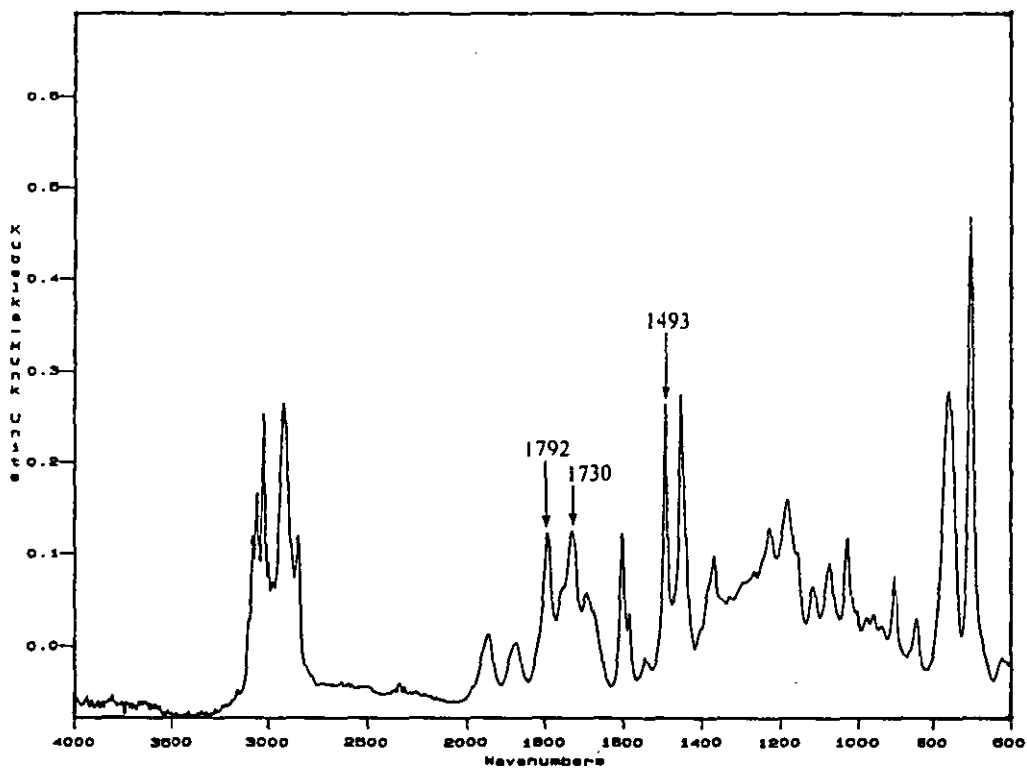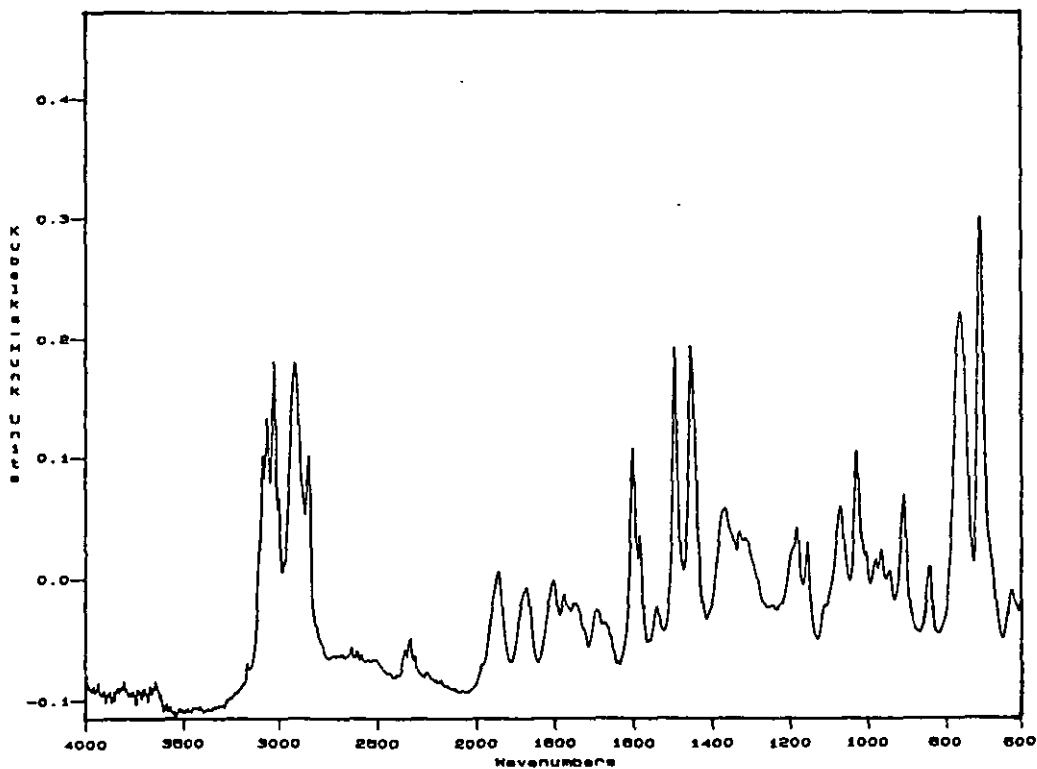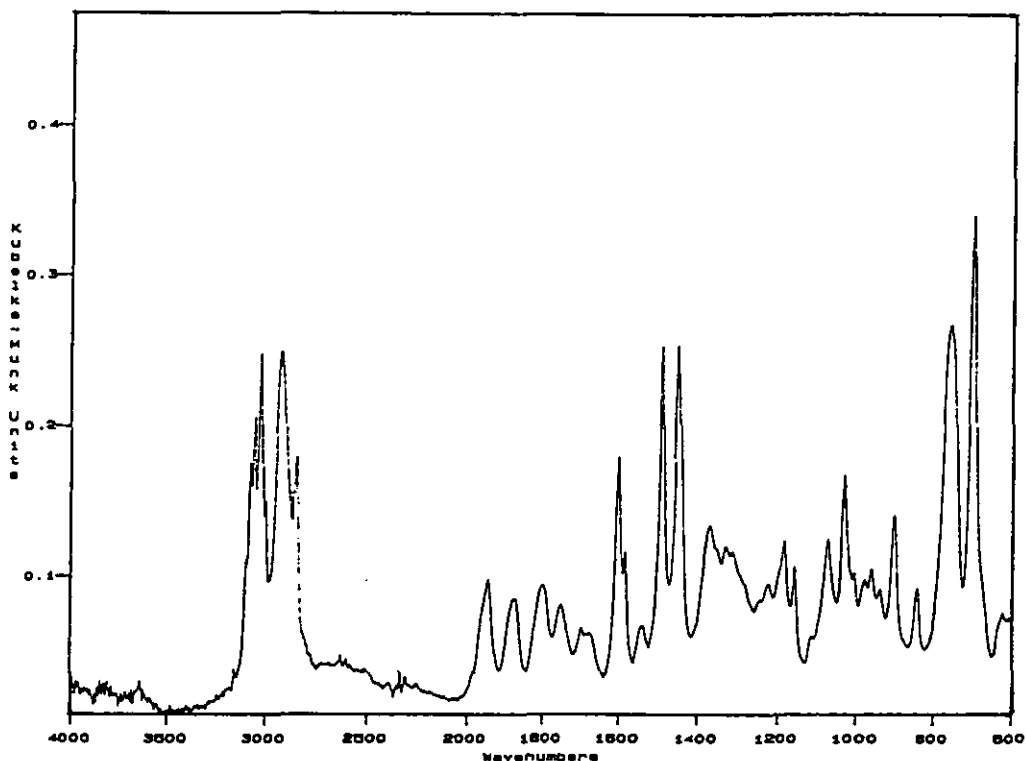## Figure 7.42 - DRIFT Spectrum of Styrene/DBPF Copolymer

Figure 7.42 - DRIFT Spectrum of Styrene/DBPF Copolymer

Figure 7.43 - DRIFT Spectrum of Styrene/ALPO Copolymer

The peroxycarbonate carbonyl stretching band of PMEC monomer ($\bar{v}$ = 1790 cm^{-1}) would appear to be the only suitable IR vibration for modelling the polymer-bound PMEC absorption ($\bar{v}$ = 1792 cm^{-1}) behaviour of styrene/PMEC copolymer samples with low peroxide content (C ≤ 5 mole %). The second, vinyl ester, carbonyl group absorption of PMEC monomer ($\bar{v}$ = 1724 cm^{-1}) was shifted to higher wavenumber on copolymerisation with styrene ($\bar{v}$ = 1730 cm^{-1}). The styrene/DBPF and styrene/ALPO copolymer DRIFT spectra are, ostensibly, identical to the spectrum of polystyrene homopolymer. Carbonyl absorptions were not observed from these two materials. DRIFT analysis had determined, therefore, that the mole fraction of peroxide was considerably higher for the styrene/PMEC copolymer, compared with the two other peroxide copolymer samples (as predicted from ^{1}H/^{13}C NMR and DSC analysis).

The DRIFT absorption bands from the styrene/PMEC copolymer sample are plotted in Kubelka-Munk (KM) [297, 370] units. The KM theory, for diffuse reflectance at scattering layers within powdered samples [297, 370], relates sample concentration to the intensity of scattered (IR) radiation.

For an infinitely thick layer, the Kubelka-Munk equation [370] may be written as:

$$f(R_\infty) = \frac{(1 - R_\infty)^2}{2R_\infty} = \frac{k}{s}$$

(7.13)

where $f(R_\infty)$ is the KM absorption intensity, R_∞ is the absolute reflectance of the layer, s is a scattering coefficient and k is the absorption index [297, 370].

Perfect diffuse reflectance standards are not available [297], however, and so the $f(R_\infty)$ and R_∞ terms in the KM relation (equation 7.13) should strictly be replaced by $f(R_\infty')$ and R_∞', units [297], respectively. Where:

$$R_\infty' = \frac{R_\infty (Sample)}{R_\infty (Standard)}$$

(7.14)

The R_∞(Sample) notation represents the reflectance spectrum of the sample and the R_∞(Standard) term represents the reflectance spectrum of the matrix (KBr). Finely ground KBr is an acceptable standard [297] (KBr was used to record the background DRIFT spectrum in this project) because it exhibits high diffuse reflectance over the 600-4,000 cm^{-1} IR wavenumber range [297, 371] (the wavelength region studied for PS and styrene/peroxide copolymer samples).

The KM theory predicts a linear relationship between the absorption index, k, and the peak value, $f(R_\infty')$, for each of the absorption bands [370], provided that the s factor remains constant. In practice, the s term is influenced by many experimental variables, which can include the average particle size of the matrix component [297, 372] and the powder's extent of compression during analysis [373]. Quantitative DRIFT absorption data are solely recovered, therefore, via the implementation of consistent experimental practices [297] (section 2.8.6). Uyemura and Maeda [374] have shown, for DRIFT analysis of dilute sample dispersions in low absorbing matrices, that the absorption index, k, is related to the molar concentration, c, of an absorption band, by:

$$k = (2.3026).(\varepsilon).(c)$$

(7.15)

where ε is the molar absorptivity and c is the molar concentration.

The peak value of $f(R_\infty')$ for a DRIFT absorption band is, therefore, related to the molar concentration, c, of the material [297, 370, 374], by:

$$f(R_\infty') = \frac{(2.3026).(\varepsilon).(c)}{s} \qquad (7.16)$$

Absorption of radiation by a sample of concentration, c (mol cm^{-3}), in a cell of thickness, l (cm), can often be determined by the Beer-Lambert relation [270]:

$$A = (\varepsilon).(l).(c) \qquad (7.17)$$

where A is defined as the absorbance of the sample and ε is the molar absorptivity of the absorbing species, at a given frequency.

The solution absorbance ratio for two IR bands (denoted as bands 1 and 2), A_1/A_2, can, therefore, under certain conditions [270], be given by:

$$\frac{A_1}{A_2} = \frac{(\varepsilon_1).(c_1)}{(\varepsilon_2).(c_2)} \qquad (7.18)$$

The KM peak value ratio for the same two absorption bands in the DRIFT analysis mode, $f(R_\infty')_1/f(R_\infty')_2$, can be given by [297, 370, 374]:

$$\frac{f(R_\infty')_1}{f(R_\infty')_2} = \frac{(\varepsilon_1).(c_1)}{(\varepsilon_2).(c_2)} \qquad (7.19)$$

The DRIFT spectroscopy peak ratio for the PMEC peroxycarbonate carbonyl group stretching frequency and the C-C stretching mode of vibration for the (monosubstituted) phenyl ring ($\bar{v} = 1493$ cm^{-1}) in the styrene/PMEC copolymer sample, $f(R_\infty')_{1792}/f(R_\infty')_{1493}$, was determined (table 7.23). The peroxide content of the styrene/PMEC copolymer was then estimated from the FTIR absorbance ratio (A_{1790}/A_{1497}) calibration curve (appendix 12), determined for ethylbenzene/PMEC mixtures.

Table 7.23 - Estimation of Peroxide Content in Styrene/PMEC Copolymer

DRIFT Peak Ratio, $f(R_\infty')_{1792}/f(R_\infty')_{1493}$	Peroxide Content, C (Mole %)
0.549	$C \approx 4.6$

The DRIFT/FTIR method employed for the determination of the styrene/PMEC copolymer composition was assumed to be qualitative in nature, as a consequence of the following considerations:

(I) - It was assumed that the molar absorptivity of the polymer-bound PMEC peroxycarbonate carbonyl absorption ($\bar{\nu} = 1792$ cm^{-1}) is identical to the corresponding vibration's absorptivity in PMEC monomer ($\bar{\nu} = 1790$ cm^{-1}), and that the absorptivity of the C-C stretching mode of vibration for the (monosubstituted) phenyl ring in the styrene/PMEC copolymer sample ($\bar{\nu} = 1493$ cm^{-1}), is identical to the molar absorptivity of the corresponding vibration in ethylbenzene ($\bar{\nu} = 1497$ cm^{-1}).

(II) - The, moderately intense, peroxycarbonate carbonyl group DRIFT absorption from the styrene/PMEC copolymer ($\bar{\nu} = 1792$ cm^{-1}) was found to overlap slightly with a weak band from polymer-bound styrene groups ($\bar{\nu} = 1803$ cm^{-1}).

(III) - It was assumed that comparable matrix average particle sizes were employed for the background (KBr) and styrene/PMEC copolymer sample (KBr dispersion) DRIFT spectra. (Comparisons between FTIR and DRIFT spectra are only valid when the KM scattering factor remains constant [297]).

In conclusion, copolymer conversion versus reaction time, ^{1}H and ^{13}C NMR spectroscopy, DRIFT spectroscopy and DSC observations showed that PMEC had been incorporated to a significantly greater extent than both DBPF and ALPO in styrene/peroxide copolymer samples. It was decided that PMEC should, therefore, be used for the synthesis of peroxide-functionalised polystyrene microgel particles.

7.4 - CHARACTERISATION OF PEROXIDE MICROGEL PARTICLES

Styrene/DVB/PMEC (0 and 0.25 mole % PMEC) emulsion polymerisations were performed over six hour periods at 75°C (section 2.7.5). Conversion samples were taken throughout these emulsion processes. The complete incorporation of PMEC molecules into microgel particles within the initial stages of the terpolymerisation was considered to be desirable. It was anticipated that centrally-functionalised peroxide microgel particles could then be synthesised (section 7.1.1). Microgel conversion versus polymerisation time data are given in table 7.24. The microgel conversion with polymerisation time behaviour is also illustrated in figure 7.44.

Table 7.24 - Microgel Emulsion Conversion Versus Polymerisation Time

Time (Minutes)	PS Microgel Yield (Weight %)	Peroxide Microgel Yield (Wt. %)
60	08	09
90	17	15
120	22	25
150	34	36
180	53	50
210	67	64
240	79	78
270	87	87
300	95	94
360	98	96

Consideration of initial, theoretical and experimental, terpolymer yields, 60 minutes after the emulsion polymerisation process had been initiated (i.e. after all of the peroxide monomer had been added), indicated that a very significant amount of the PMEC had been consumed during this "seed" period. A styrene/DVB feed was then added to the vessel, dropwise, over a further four hours. An additional sixty minute period of heating (section 2.7.5) was then employed. The styrene/DVB/PMEC terpolymerisation process proceeded to 96 weight % yield in total. DSC analysis of thermally-treated (section 2.7.6) PS microgel (figure 7.45) and PS/peroxide microgel samples (figure 7.46) was performed. A small exotherm was observed for the PS/DVB/PMEC microgel over a 130-210°C temperature range (no transition was observed for the PS microgel over this region), indicating that second-stage initiator (peroxide) groups were present in the PS/DVB/PMEC microgel sample.
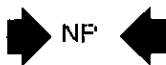
LIBRARY ORDER NO. Nº DE COMM. DE LA BIBL.	CUST. NO Nº DU CLIENT	FUND NO. Nº DU FOND	REPORT DATE DATE DU RAPPORT	QUANTITY QUANTITÉ
LB98010285	102805A0		02/08/2000	1

ISBN   0471988588

AUTHOR
AUTEUR

TITLE   Handbook of offender assessment and treatment / edited by Cl
TITRE   ive R.Hollin

REPORT
CODE   ➤ NP ⬅
RAPPORT
DE CODE

Publisher: John Wiley
        Due:
        Note:
Not Yet Published-Backordered

ORDER STATUS REPORT / RAPPORT SUR L'ÉTAT DE LA COMMANDE

THESIS

WASHBROOKE, S R.

" DEVELOPMENT OF AN
EXPERIMENTAL PATHWAY
FOR THE SYNTHESIS OF
ORGANIC SEQUENTIAL ... "

Washbrook, Simon Richard.

→ The development of an experimental pathway for the synthesis of organic requ (1998).

LU Thesis

Figure 7.44 - Graph of Microgel Yield Versus Polymerisation Time

Figure 7.44 - Graph of Microgel Yield Versus Polymerisation Time

Figure 7.45 - DSC Thermogram for Styrene/DVB (5 wt.% DVB) Microgel
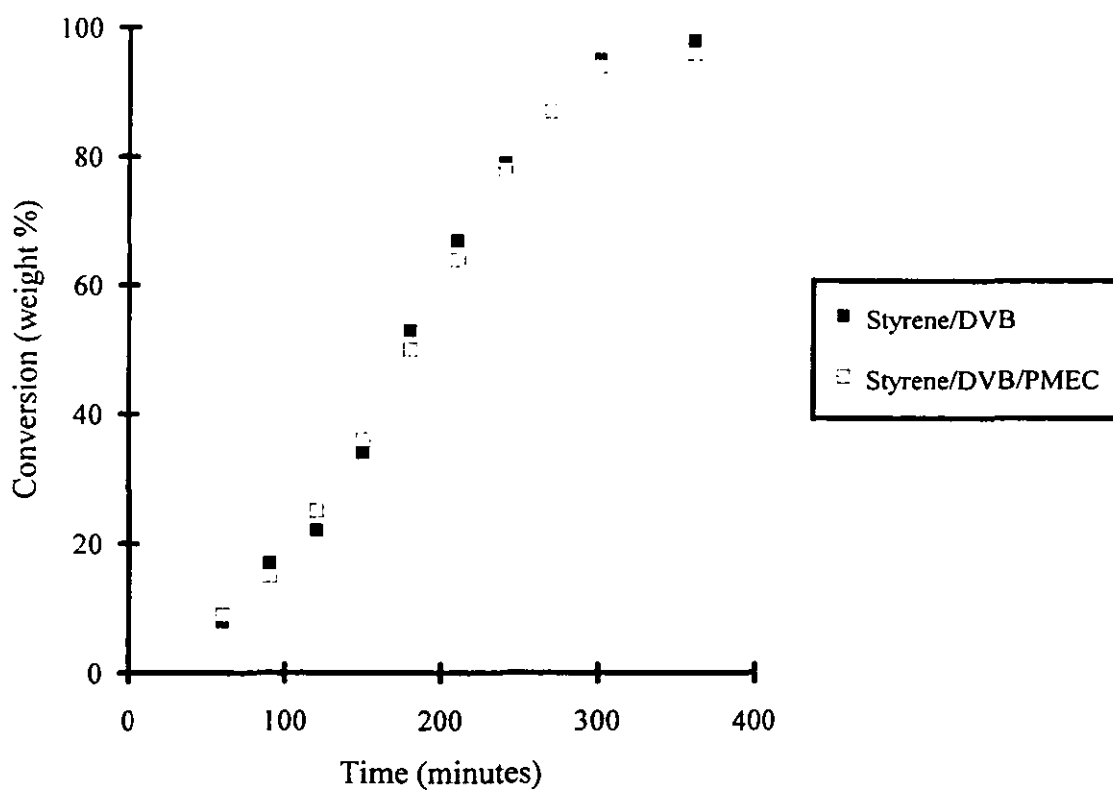

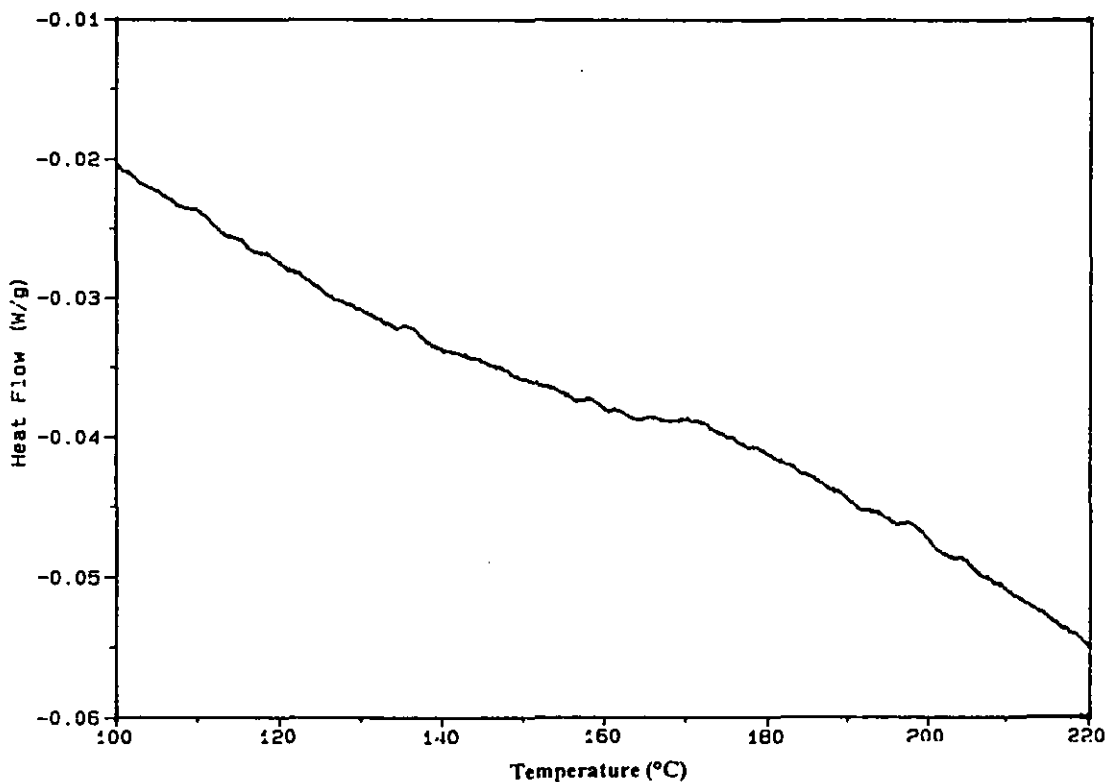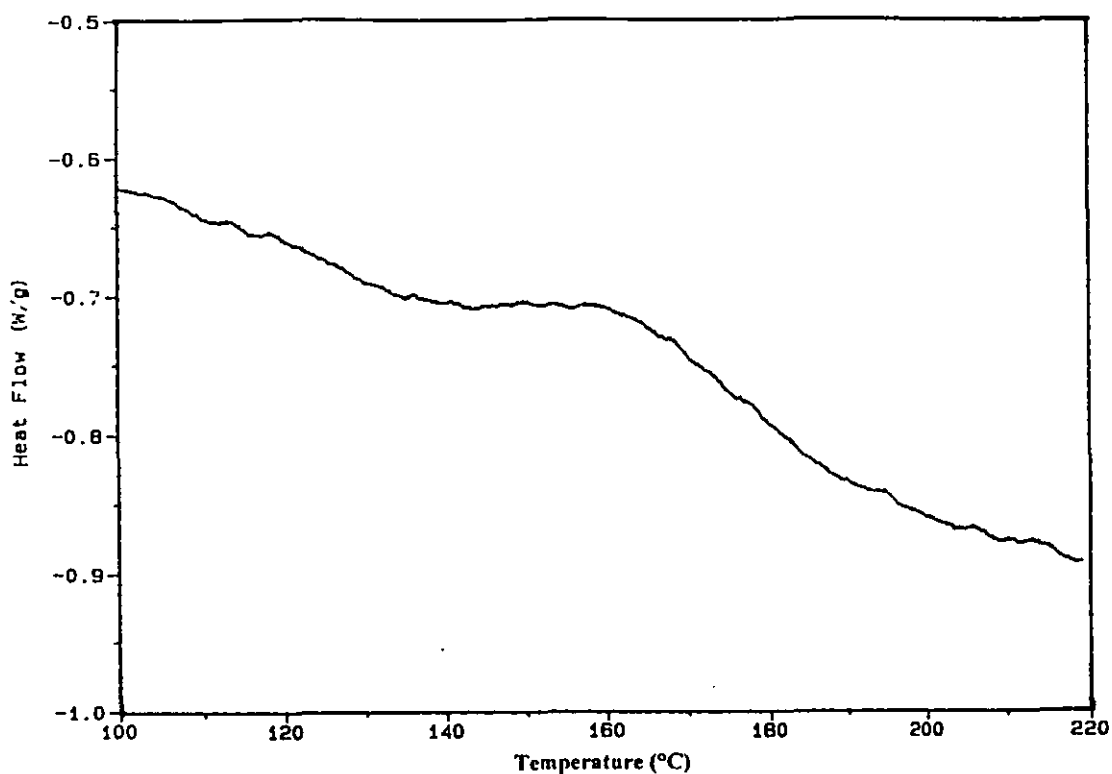Figure 7.45 - DSC Thermogram for Styrene/DVB (5 wt.% DVB) Microgel

Figure 7.46 - DSC Thermogram for Styrene/DVB/PMEC Microgel

7.5 - PEROXIDE MICROGEL AS POLYMERISATION INITIATOR

Anhydrous dispersions of the PS/DVB (5 wt.% DVB)/PMEC (0 and 0.25 mole % PMEC) particles in nBA/NPGDA (10 wt. % crosslinker) mixtures were prepared (section 2.7.7). Both dispersions were then heated at 110°C, under a nitrogen atmosphere. Complete macro-gelation of both dispersions occurred after approximately five hours of heating. It was not known if polymerisation in the PS/DVB dispersion system had been initiated by ACVA that was still present in the sample, or, if thermally-induced polymerisation of nBA/NPGDA had occurred. An anhydrous mixture of nBA/NPGDA was, therefore, heated at 110°C and macro-gelation was similarly found to occur after approximately five hours. It was concluded that the acrylic comonomers had thermally polymerised at the minimum temperature required for peroxide decomposition (i.e. at 110°C).

Consequently, an additional quantity (500 ppm) of hydroquinone monomethyl ether, MEHQ, was added to an anhydrous nBA/NPGDA sample and this mixture was heated for 10 hours at 110°C (section 2.7.7). The addition of inhibitor to the comonomer mixture was found to prevent/inhibit the thermally-induced acrylic polymerisation process. A dispersion of PS/DVB/PMEC (0.25 mole %) particles in anhydrous nBA/NPGDA, containing additional MEHQ (500 ppm), was, therefore, prepared, and the system was heated for 10 hours at 110°C. The addition of MEHQ was found to have prevented polymerisation occurring, to any significant extent, in this system. It would appear, therefore, that PMEC, ALPO and DBPF cannot be used as polymer-bound thermal free radical initiators for the synthesis of IPN microgel dispersions. ALPO and DBPF are both not suited to IPN microgel synthesis because they can not be incorporated efficiently within the first-stage polymer network, from emulsion terpolymerisation techniques. Thermal dissociation of the t-butylperoxy bond in network-bound PMEC units can be used to generate free radicals, but only at high temperatures (T ≥ 110°C). Significant, thermal, polymerisation of acrylic monomer was also observed at these temperatures, however.

CHAPTER 8

SUMMARY

8.1 - CONCLUSIONS FROM THIS INVESTIGATION

The following conclusions can be drawn from this research:

1. Low-viscosity organic polystyrene microgel dispersions are readily synthesised from the emulsion copolymerisation, latex flocculation, and organic diluent re-dispersion technique employed within this study.

2. Organic PnBA microgel dispersions can be synthesised from the emulsion copolymerisation, aqueous latex addition to dispersant, and water removal by distillation procedure developed. The organic diluent is required to be higher boiling than water. This phenomenon restricts the number of dispersants available for rubbery microgel systems.

3. Microgel re-dispersion only occurs when a suitable organic diluent is employed as dispersant (the liquid must be a solvent for the corresponding linear polymer).

4. The dispersion viscosity has been found to be influenced by the concentration of solids, the solubility parameter difference between the polymer and dispersant, and microgel crosslink-density (crosslink-densities are controlled by varying the difunctional comonomer concentration within the copolymerisation process).

5. Monomer solubility and gel swelling studies indicated that polymerisation of monomers within organic dispersions cannot exclusively-generate IPN particles (polymerisation loci will not be restricted to monomer-swollen microgels).

6. FTIR and ^{1}H/^{13}C NMR analysis determined that high purity t-butylperoxy-2-methacryloyloxyethyl carbonate (PMEC) was recovered in good yield from the reaction between the corresponding chloroformate and t-butylhydroperoxide.

7. DSC, ^{1}H/^{13}C NMR, DRIFT and GPC analysis determined that high molecular weight styrene/PMEC copolymer was synthesised from emulsion techniques.

8. Styrene/PMEC/DVB microgels were synthesised from emulsion polymerisation. Pendant microgel peroxide groups were developed to minimise polymerisation of monomers within the continuum of microgel/nBA dispersions. Thermally-induced polymerisation occurred at temperatures required for PMEC dissociation, however.

9. In principle, IPN microgel synthesis may result from similar techniques to those developed here in the future, provided that 'low temperature' free radical generation is attainable (e.g. photolysis of the PMEC groups listed in Point 8).

More-detailed conclusions from this research are included in the paragraphs below:

During this investigation a series of four PS latices prepared with 0, 1, 5, and 10 wt. % divinylbenzene was synthesised. Dynamic mechanical characterisation of these materials indicated that an increase in the concentration of DVB within the emulsion copolymerisation led to an increase in the material's T_g. Average molecular weight between crosslink values for PS (1 wt.% DVB) and PS (5 wt.% DVB) microgel formulations were estimated from Nielsen's [261] glass transition shift on crosslinking relation. The M_c values determined from DMTA T_g-shifts [261] were compared with theoretical M_cs [287], the average molecular weight between crosslinks for the corresponding "ideal" network samples, and good agreement was observed between theoretical and experimentally-determined values. Gel permeation chromatograms were recorded for dilute dispersions of the three PS microgel formulations and for a dilute polystyrene solution. The chromatogram peak was found to shift to higher elution volumes as the concentration of DVB in the microgel particles increased. This behaviour suggested that the crosslink-density of the microgel particles had increased as the DVB content increased. Dispersions of the three PS microgels were prepared in anhydrous cyclohexanone, toluene, n-butyl acrylate, tetrahydrofuran and benzyl alcohol (with ca. 5 wt.% solids for each dispersion). Rheological characterisation of the dispersions was performed at a temperature of 25°C. The viscosity behaviour of a PS solution in toluene (5 wt.% solids) was also examined. The viscosities of the three microgel dispersions in toluene were significantly lower than the homopolymer solution viscosity (at the same solid concentration and shear rate). This observation was considered to have resulted from a restriction in the number of available conformational states to these polymeric molecules by the microgel particles's network structure [203, 214, 227]. For each of the five dispersants examined, an increase in the particle's DVB concentration led to a reduction in the viscosity of the dispersion. This phenomenon indicated that microgel particles with the lowest crosslink-densities were swollen by diluent to the greatest extent. The relative ease in synthesising PS microgel dispersions, the variety of suitable diluents available, and the relatively low viscosities of these systems (at a 5 wt. % solids concentration), indicates that PS microgel dispersions can be used to investigate the synthesis of organic PS/PnBA IPN microgels.

Poly(*n*-butyl acrylate)-based microgels were synthesised from emulsion copolymerisation of *n*BA with 10 wt.% DVB, 10 wt.%, 20 wt.% ethylene glycol dimethacrylate (EGDMA) and 10 wt.%, 20 wt.% neopentyl glycol diacrylate (NPGDA). A P*n*BA homopolymer latex was also synthesised. Dried acrylic polymer films were characterised by dynamic mechanical thermal analysis. DMTA observations indicated that the incorporation of divinyl comonomer within latex particle formulations led to an increase in the material's T_g. Average molecular weight between crosslink values estimated from glass transitional shifts [261] were found to be higher than theoretical M_c values [287]. Organic acrylic microgel dispersions were prepared via vacuum distillation procedures [249]. Rheological characterisation of acrylic microgel dispersions (5 wt.% solids content) in *n*-butanol (*n*BuOH) and benzyl alcohol was performed at a temperature of 25°C. P*n*BA homopolymer solutions in *n*BuOH and benzyl alcohol were also tested on the rotational viscometer. The viscosity of each microgel dispersion was found to be significantly lower than the corresponding homopolymer solution viscosity. The viscosity reduction for microgel systems was considered to have resulted from the restricted mobility of polymer-chain sections [227] within microgel particles. Microgel dispersions showed shear-thinning behaviour over the shear rate range investigated. The high viscosity of acrylic microgel dispersions in benzyl alcohol ($\eta \approx 80$ cP), at a 5 weight % solid concentration, compared to organic PS dispersion viscosities, would appear to render acrylic materials as unsuitable for the preparation of first-stage IPN microgel precursors (*n*BuOH is a non-solvent for PS, copolymerisation of styrene/DVB within acrylic *n*BuOH dispersions would, most probably, lead to precipitation of IPNs).

Provided that second-stage comonomers are immiscible with the continuous phase of first-formed microgel dispersions, it should be possible to synthesise IPN microgel dispersions from quasi-emulsion second-stage copolymerisation. The solubility behaviour of styrene and *n*BA monomers (25°C) within a variety of different organic diluents was investigated, therefore. Formamide was the only liquid examined which was (practically) immiscible with both monomers. Each of the other organic liquid/monomer systems was found to be of one-phase, over all mixture compositions (25°C). Formamide has a high boiling point [248], and the material has also been

found to react with organic peroxides [248]. Consequently, none of the liquids examined appeared suitable for the synthesis of IPN microgels from second-stage, modified, quasi-emulsion copolymerisation processes [222, 223].

It was considered ideal that the introduction of second-stage comonomers within first-stage organic microgel dispersions should have led to exclusive adsorption of comonomers within first-formed microgel particles. Potential IPN microgel synthesis could have then been investigated with the employment of a continuum-soluble free radical initiator. An estimation of PS microgel particle swelling with monomer, within organic microgel dispersion systems, was made from equilibrium swelling of PS macrogel samples with a benzyl alcohol/nBA mixture (10 wt.% nBA). Macrogel samples recovered from bulk free radical copolymerisation processes were analysed by dynamic mechanical thermal analysis. DMTA observations indicated that the incorporation of increasing concentrations of DVB within the formulation lead to an increase in the macrogel's glass transition temperature (when compared to the T_g of polystyrene homopolymer). Estimations of macrogel M_c values were made from insertion of macrogel T_g-shifts into the Nielsen [261] relation. The PS (5 wt.% DVB) and PS (10 wt.% DVB) macrogel M_c values from DMTA characterisation [261] were comparable to the theoretical [287] average molecular weight between crosslink values for homogeneous network samples. Equilibrium swelling of PS macrogel samples was performed with anhydrous tetrahydrofuran, cyclohexanone, n-butyl acrylate, toluene and benzyl alcohol. For any given swelling agent, the volume fraction of network polymer at equilibrium (ϕ_2) was found to increase as the macrogel's DVB content increased. For THF, toluene, cyclohexanone and benzyl alcohol swelling data, the ϕ_2 value was found to increase as the solubility parameter difference between polystyrene and the liquid increased. The highest levels of liquid swelling, for a given macrogel sample, were found with THF, and the lowest degrees of swelling were found with benzyl alcohol. M_c values were evaluated from PS macrogel/toluene equilibrium swelling (25°C) experiments, from utilisation of the Flory-Rehner [167] approach. The crosslink-densities of the three PS macrogel samples estimated from equilibrium swelling appeared to be of comparable magnitude to their idealised values [287]. Samples from the three macrogels were swollen with a benzyl alcohol/nBA mixture (10 wt.% nBA) with 10 wt.% solids content employed

249

for each swelling experiment (120 hours at 25°C). The masses of macrogel, benzyl alcohol and nBA initially added to each vessel were recorded. After the period for equilibration, swollen macrogels were recovered, and their masses were then determined. FTIR spectra of benzyl alcohol/nBA mixtures (1, 2, 3, 4, 5, 6, 7, 8, 9 and 10 wt.% nBA) were recorded, for IR calibration purposes. Compositions of benzyl alcohol/nBA mixtures which had remained outside of gel components were determined from FTIR spectroscopy. Concentrations of nBA found within liquid mixtures recovered after equilibrium swelling were found to be, ostensibly, identical to the initial concentration of monomer in the swelling agent. It was concluded that nBA had not preferentially swollen the PS networks synthesised, therefore.

It was considered desirable to characterise acrylic macrogel samples prepared from batch, free radical, copolymerisation processes, as second-stage copolymerisations were to have been performed initially with batchwise addition of acrylic comonomer to first-stage PS microgel dispersions. Macrogel samples were analysed by dynamic mechanical thermal analysis. In general terms, the rheological behaviour of each acrylic macrogel sample mirrored the DMTA characteristics of its corresponding microgel formulation. The one notable exception to this observation was the PnBA (20 wt.% EGDMA) system. It was considered probable that either an "imperfect" network had resulted from copolymerisation of nBA with 20 weight % EGDMA under bulk, free radical, copolymerisation conditions, or that the macrogel was sufficiently highly crosslinked for the material's glass transition to have been suppressed completely [261]. Network M_c values estimated from T_g shifts [261] were found to be significantly higher than theoretical M_c values. The increase in glass transition temperature on crosslinking [261], for each of the five acrylic macrogels investigated, was significantly lower, therefore, than had been anticipated for the corresponding "ideal" network sample. It is possible that either acrylic gel glass transitions did not adhere to the Nielsen [261] estimation for T_g-shift/crosslink relations, or that the level of crosslinking within the acrylic copolymers synthesised was significantly diminished, when compared to the theoretical degree of crosslinking for each of the formulations. Several potential causes for a diminution in the degree of acrylic gel crosslinking were considered (if it is assumed that the Nielsen relation, generally, affords a fair estimation for crosslink-density values). It was thought

possible that divinyl comonomer incorporation had contributed to the formation of extensive chain branching [5, 11, 31, 261] within each material - the tertiary hydrogen in polymer-bound nBA repeat units has been found to readily abstract [304] during polymerisation. Reduced pendant vinyl bond reactivity effects [34, 35] could have potentially operated to a significant extent within each copolymerisation. Equilibrium swelling of acrylic macrogel samples (25°C) was performed with anhydrous styrene, n-butanol and benzyl alcohol. In general terms, the highest levels of liquid swelling, for any given macrogel sample, were found with styrene, and the lowest degrees of swelling were found with n-butanol. Average molecular weight between crosslink values for the five acrylic macrogel/styrene systems were estimated [167]. In general terms, the crosslink-densities of each acrylic macrogel appeared markedly lower than their ideal values. These findings mirrored those concluded from DMTA analysis.

The apparent absence of an organic diluent/monomer system suitable for second-stage polymerisations under modified quasi-emulsion conditions [222, 223], and the apparent non-preferential sorption of monomer in the PS/nBA/benzyl alcohol system (a mixture where the solubility parameter of the polymer network and monomer were comparable in magnitude, whereas the inert organic diluent was anticipated to have been significantly less compatible with the gel [310]), led to an investigation into the synthesis of PS microgel particles functionalised with second-stage polymerisation initiator fragments. These techniques were investigated in order to try and minimise the extent of second-stage polymerisation within the continuum. The peroxide monomers, t-butylperoxy-2-methacryloyloxyethyl carbonate (PMEC) [246], di-t-butylperoxy fumarate (DBPF) and t-butylperoxyallyl carbonate (ALPO) [246] were synthesised from the reaction between the corresponding chloroformate/acid chloride and t-butylhydroperoxide (t-BuOOH). Samples from the materials synthesised were analysed by 100 MHz ^{1}H NMR spectroscopy. Inspection of the ^{1}H NMR chemical shift, signal multiplicity and peak integral values inferred that high purity peroxides had been synthesised. It was considered that, in order to try and minimise the synthesis of PnBA macrogel, pendant second-stage (peroxide) free radical initiator molecules should have been "built-in" toward the centre of PS/DVB microgel particles. Ideal copolymerisation of peroxide monomer with styrene, to completion, would have been required if this synthetic procedure was to have been

viable. The suitability of each peroxide monomer for the synthesis of initiator-functionalised PS microgel particles was determined from styrene/peroxide (5 mole % peroxide) emulsion copolymerisations. A polystyrene latex was prepared under identical conditions. Samples were periodically taken from latices throughout these emulsion processes, and the non-volatile component of each aliquot was determined. Copolymer conversion versus reaction time data were determined from these non-volatile component values. The conversion versus time data for the styrene/PMEC copolymerisation followed the same behaviour as the PS emulsion system. This copolymerisation proceeded to very high yield. The styrene/ALPO emulsion copolymerisation was retarded in comparison with the PS polymerisation and the copolymerisation product was recovered in low yield. These observations were attributed to a degradative transfer [334, 335] to monomer process. The styrene/DBPF copolymerisation was retarded in comparison with the PS emulsion process and the copolymerisation proceeded to relatively low conversion. Purified copolymers were analysed by GPC. The chromatographic data showed that high molecular weight copolymer had been recovered from each copolymerisation process. Purified samples of each material were analysed by differential scanning calorimetry. DSC analysis indicated that each copolymer showed exothermic behaviour at temperatures above 120°C. An exotherm was not observed from the PS sample. The exotherms were considered to have arisen from the thermal decomposition of t-butylperoxy bonds [352]. The styrene/PMEC copolymer yielded the largest exotherm of the three copolymers and the styrene/DBPF copolymer generated the smallest exotherm. It was concluded that the styrene/PMEC sample had the largest peroxide content of the three copolymers (section 7.3.2). Dissociation rate constant with temperature relations determined from the styrene/PMEC thermogram [352] indicated that the minimum temperature, T, required for initiation of nBA/NPGDA copolymerisation was of the order of 110°C. Diffuse reflectance infrared Fourier transform (DRIFT) spectra were recorded for KBr dispersions of styrene/PMEC, styrene/DBPF and styrene/ALPO copolymers. The styrene/DBPF and styrene/ALPO copolymer DRIFT spectra were, ostensibly, identical to the spectrum of PS homopolymer. Moderately intense DRIFT absorptions were observed, at 1792 and 1730 cm^{-1} (the two, major, carbonyl stretching vibrations of PMEC groups) radiation wavenumbers, for the styrene/PMEC copolymer sample. The DRIFT spectroscopy

peak ratio for the PMEC peroxycarbonate carbonyl group stretching frequency and the C-C stretching mode of vibration for the phenyl ring ($\bar{\nu}$ = 1493 cm^{-1}) in the styrene/PMEC copolymer, f (R$_\infty$')$_{1792}$/f (R$_\infty$')$_{1493}$, was determined. An FTIR absorbance calibration curve for the styrene/PMEC copolymer sample was obtained from FTIR analysis of ethylbenzene/PMEC (1, 2, 3, 4 and 5 mole % peroxide) mixtures. The intense peroxycarbonate carbonyl absorption ($\bar{\nu}$ = 1790 cm^{-1}) from PMEC was used for the FTIR calibration curve. The C-C stretching mode of vibration for the phenyl ring ($\bar{\nu}$ = 1497 cm^{-1}) in ethylbenzene was chosen as the second calibration band for ethylbenzene/peroxide mixtures. A qualitative peroxide content of 4.6 mole % was estimated for the styrene/PMEC copolymer sample from the calibration results. Styrene/DVB/PMEC (0 and 0.25 mole % PMEC) emulsion terpolymerisations were performed over six hour periods at 75°C. The styrene/DVB/PMEC process proceeded to 96 weight % yield in total. DSC analysis of thermally-treated PS microgel and PS/peroxide microgel samples was performed. A small exotherm was observed for the PS/DVB/PMEC microgel at temperatures above 120°C (no transition was observed for the PS microgel over this region), indicating that second-stage initiator groups had been present in the PS/DVB/PMEC microgel sample. Anhydrous dispersions of the PS/DVB (5 wt.% DVB)/PMEC (0 and 0.25 mole % PMEC) particles in nBA/NPGDA (10 wt. % crosslinker) mixtures were prepared. Both dispersions were then heated at 110°C, under a nitrogen atmosphere. Complete macro-gelation of both dispersions occurred after approximately five hours of heating. An anhydrous mixture of nBA/NPGDA was similarly heated at 110°C and macro-gelation was found to occur after approximately five hours. It was concluded that the acrylic comonomers had thermally polymerised at the minimum temperature required for peroxide decomposition (i.e. at 110°C). It was considered that PMEC, ALPO and DBPF could not have been satisfactorily employed as polymer-bound thermal free radical initiators. ALPO and DBPF are both apparently not suited to IPN microgel synthesis since they were not efficiently incorporated within styrene/peroxide copolymer samples. Thermal dissociation of the *t*-butylperoxy bond in network-bound PMEC units apparently has the potential to generate free radicals, but only at high temperatures (T ≥ 110°C). Significant thermal polymerisation of acrylic monomer was observed at such temperatures, however.

8.2 - SUGGESTIONS FOR FUTURE WORK

In principle, there are three potential routes for synthesising IPN microgels via second-stage copolymerisations within the particles of an organic first-stage polymer microgel dispersion. Exclusive sorption of second-stage comonomers within first-formed microgel particles could potentially enable second-stage networks to be synthesised with the employment of conventional, continuum-soluble, free radical initiator. A second potential mode of IPN synthesis involves the employment of a dispersant/second-stage comonomer pair which are, practically, immiscible - the second network component would be subsequently synthesised via a quasi-emulsion copolymerisation process. The third potential route utilises initiator-functionalised microgel particles dispersed in homogeneous organic dispersant/second-stage comonomer mixtures. In terms of experimental brevity, the first of the three potential routes would be most desirable, if a suitable microgel/diluent/comonomer/initiator system were available. Initially, a series of microgels prepared from several distinct monomer components, e.g. PS, PMMA and poly(ethyl methacrylate) microgels, could be synthesised. Each material would be subsequently dispersed in a large number of distinct organic diluents. Several suitable second-stage monomers could then be chosen for addition to microgel dispersions. After sufficient time for equilibration, microgel particles could be sedimented by high-speed centrifugation, and the composition of the supernatant analysed. If a system could be found where significant quantities of second-stage monomer had preferentially partitioned within the first-formed particles, investigations into second-stage copolymerisations with the employment of a conventional free radical initiator could be undertaken. Microgels are a unique form of polymeric materials which show certain characteristics of both linear polymer molecules and macroscopic networks [47]. Preferential sorption of solvent by linear polymer molecules in dilute binary liquid mixtures [312-316] has been extensively investigated [312-322]. For a polymer solution in a thermodynamically good solvent [11], it is possible to vary the solvency of the medium by introducing controlled quantities of a second, theta, solvent [313]. The coefficient of selective adsorption [312, 313] of one of the two solvent components can be subsequently determined from analytical characterisation techniques (section 5.1). If organic microgels were to exhibit similar sorption

254

behaviour to their linear polymer analogues, an inert diluent which was a theta solvent for both of the corresponding linear polymers of the final IPN would, most probably, be required. The second-stage comonomer mixture would, however, most likely be required to be a thermodynamically good solvent for the first-stage microgel's linear polymer analogue. A high affinity between the first stage microgel and the second-stage comonomer component would appear to imply, however, that a high degree of compatibility between the two polymer components of the IPN would result. A significant level of incompatibility between the two polymer components is required if a true IPN, a material which exhibits a discernible heterogeneous phase structure, is to be generated from the synthetic process, however. The second potential route for the synthesis of organic IPN microgel dispersions utilises latex IPN techniques, i.e. the second-stage network component is generated via a second-stage quasi-emulsion copolymerisation process (section 1.6.4), with the exception that the continuous phase for the system would be non-aqueous in this instance. The miscibility characteristics of styrene and nBA monomers (25°C) with a number of organic diluents was determined within this investigation (section 4.5). Referral to the techniques of Okubo et al. [211, 221-223], who have synthesised composite PS/PDVB particles [221-223] via second-stage polymerisation of DVB within highly-polar ethanol/water mixtures, similarly implies that the solubility parameter of the disperse phase is required to be relatively high, compared to the solubility parameter of the second-stage monomer component, for the second-formed network component to be synthesised within the first-formed polymer particles. Utilisation of the techniques of Okubo et al. [221-223] for the synthesis of PS/PnBA microgel dispersions, could be investigated by NOF in the future. It is possible, however, that the replacement of the aqueous component with a highly-polar ethanol/water mixture may generate materials with similar structures to those prepared from conventional latex IPN techniques (section 1.6.4). The preparation of microgel particles functionalised with pendant free radical initiator fragments is the third potential route for the synthesis of IPN microgel dispersions (ideally, second-stage polymerisation initiator groups should be located toward the centre of the first-formed network particles). Such initiator-functionalised microgel particles could then be dispersed in second-stage comonomer/organic diluent mixtures, and copolymerisations within the first-stage network particles could then be attempted. Styrene/DVB/PMEC

(*t*-butylperoxy-2-methacryloyloxyethyl carbonate) microgels were synthesised via emulsion terpolymerisation in this investigation (section 7.5). Thermal dissociation of polymer-bound PMEC fragments ideally requires a temperature of 110°C, or higher, for the generation of free radicals at a sufficient rate for initiation of polymerisation (chapter 7). In the case of second-stage copolymerisations of *n*BA/NPGDA (section 7.5), the second-stage comonomers undergo thermal polymerisation at such high temperatures, however. It is possible that IPN synthesis could be investigated for the PS/DVB/PMEC microgel formulation dispersed within *n*BA/NPGDA via photoinitiated second-stage copolymerisation [353]. The generation of reactive, and "mobile", *t*-butoxyl radicals from photolysis of polymer-bound PMEC fragments would appear likely to cause significant degrees of copolymerisation within the continuum , however. In principle, if the synthesis of gel component outside of the first-formed microgel particles is to be minimised, homolytic bond scission of initiator fragments should lead to the generation of both polymer network-bound free radicals (radicals that are capable of initiating copolymerisations of second-stage comonomer) and inert, low molecular weight, radicals (free radicals which are inefficient at initiating polymerisation). Ajayaghosh [243] synthesised S-acryloyl O-ethyl xanthate, AX (figure 1.10, section 1.8), copolymers with methyl methacrylate (MMA) by AIBN-initiated solution copolymerisation (70°C) in benzene. Macroinitiators (copolymers containing pendant xanthate chromophores) were dissolved in benzene and photolysed, in the presence of MMA [243]. Poly(methyl methacrylate) was recovered (M_n = 40,000 g mol^{-1}) after 30 minutes of irradiation. S-acryloyl O-ethyl xanthate (AX) could be a suitable material for the generation of initiator-bound microgel particles. Photolysis of polymer-bound AX groups leads to the generation of reactive, keto, radicals (radicals that are capable of initiating polymerisation of MMA [243], for example) and "inert", low molecular weight, alkoxy thiocarbonyl thiyl, radicals [375]. It would appear possible that IPN microgel particles would also not be the exclusive product from such synthetic procedures. Free radical propagation during polymerisation and chain-transfer to monomer processes [11] would, most probably, ensure that free radicals would migrate toward the first-formed microgel particle surface. Complete macro-gelation of the system could then potentially occur rapidly. In principle, polymer-bound free radical inhibitor agents may also be required to be built toward the particle surface. Entrapment of reactive free radicals at the particle

surface, leading to the generation of inert free radicals, could possibly lead to a minimisation in the synthesis of second-stage gel component within the continuum. This technique would, most probably, involve a complex procedure, since not only would a suitable comonomer be required to terpolymerise efficiently with the first-stage comonomer components (e.g. with styrene/DVB comonomers) during the later stages of the first-stage emulsion process (ideally, such a comonomer would need to be more hydrophilic than styrene, for example), but the resulting mer units at the microgel surface would have to undergo a subsequent chemical-modification process, in order for polymer-bound free radical inhibitor fragments to be generated.

An additional route for synthesising IPN microgel particles that could be investigated in the future involves known, latex IPN (section 1.6.4), synthetic processes, whereas, in this instance, the first-formed microgel particles would be functionalised with second-stage photoinitiator moieties, ideally located toward the particle centre. After second-stage comonomers had been introduced to the microgel latex, and a period for swelling of the gel particles with comonomer had been completed, second-stage network formation could be initiated via photolysis of the system. Investigations into the influence of the first-formed microgel polymer type (e.g. styrene- or nBA-based), the crosslink-density of the first- and second-formed networks, the relative masses of the two polymer components, the duration of microgel swelling with comonomer before second-stage initiation of copolymerisation, the concentration and location of polymer-bound initiator groups within the first-formed microgel particles, and the duration of the photolysis process for the second-stage copolymerisation, on the overall particle morphology, could be instigated. Such aqueous IPN microgel particle dispersions could be subsequently converted to organic dispersions via distillation (section 4.4.1) or flocculation/re-dispersion (section 3.6) techniques. Although the synthesis of composite latex particles (section 1.6.3) and latex IPNs (section 1.6.4) has been widely reported in the scientific literature, the author is not aware of a detailed investigation into the influence of structured initiator-functionalised latex particles on composite latex particle morphologies having been undertaken, to this date.

REFERENCES

1)	J. E. Mark and B. Erman, *Rubberlike Elasticity A Molecular Primer*, Wiley-Interscience, New York, Chapters 1, 2 and 8, (1988).

2)	K. Adachi, T. Nakamoto and T. Kotaka, *Macromolecules*, **22**, 3106, (1989).

3)	J. E. Mark and J. Lal, *Elastomers and Rubber Elasticity*, American Chemical Society Publications, Washington D.C., p. 46, (1982).

4)	R. L. Zapp and P. Hous In *Rubber Technology*, Ed. M. Morton, 2nd Edition, Van Nostran Reinhold, New York, Chapter 14, (1973).

5)	H. L. Stephens In *Rubber Technology*, Ed. M. Morton, 2nd Edition, Van Nostran Reinhold, New York, Chapter 5, (1973).

6)	P. Weiss, G. Hild, J. Herz and P. Rempp, *Makromol. Chem.*, **135**, 249, (1970).

7)	J. E. Mark In *Physical Properties of Polymers*, Eds. J. E. Mark, A. Eisenberg, W. W. Graessley, L. Mandelkern and J. L. Koenig, American Chemical Society Publications, Washington D.C., Chapter 1, (1984).

8)	G. Friedmann, J. Herz and J. Brossas, *Polym. Bull.*, **6**, 251, (1982).

9)	J. A. Brydson, *Rubber Chemistry*, Applied Science, London, Chapter 6, (1978).

10)	A. Y. Coran In *Science and Technology of Rubber*, Ed. F. R. Eirich, Academic Press, New York, Chapter 11, (1978).

11)	F. W. Billmeyer, *Textbook of Polymer Science*, 3rd Edition, Wiley-Interscience, New York, Chapters 6 and 8, (1984).

12)	P. J. Flory, *Principles of Polymer Chemistry*, Cornell University Press, Ithaca, New York, Chapters 7, 12 and 14, (1953).

13)	P. K. Jarret, C. V. Benedict, J. P. Bell, J. A. Cameron and S. J. Huang, *Biomedical Applications of Polymers*, Eds. H. Hoffman and S. Shalaby, Plenum Press, New York, p. 181, (1984).

14)	F. A. Bovey, *The Effects of Ionizing Radiation on Natural and Synthetic High Polymers*, Interscience, New York, Chapter 4, (1958).

15)	M. Dole, *The Radiation Chemistry of Macromolecules*, Academic Press, New York, Chapter 1, (1972).

16)	M. Antonietti and H. Sillescu, *Macromolecules*, **18**, 1162, (1985).

17)	B. T. Storey, *J. Polym. Sci., Polym. Chem. Ed.*, **3**, 265, (1965).

18)	R. H. Wiley, J. Jin and T. Ahn, *J. Macromol. Sci., Chem.*, **3**, 1543, (1969).

19)	Y. Nitadori and T. Tsuruta, *Makromol. Chem.*, **179**, 2069, (1978).

20) C. Aso, *J. Polym. Sci.*, **39**, 475, (1959).

21) J.-E. Rosenberg and P. Flodin, *Macromolecules*, **19**, 1543, (1986).

22) H. Staudinger and W. Heuer, *Berichte*, **67**, 1164, (1934).

23) B. H. Zimm, F. P. Price and J. P. Bianchi, *J. Phys. Chem.*, **62**, 979, (1958).

24) G. C. Howard and C. A. Mingley, *J. Appl. Polym. Sci.*, **26**, 3845, (1981).

25) S. Loshaek and T. G. Fox, *J. Am. Chem. Soc.*, **75**, 3544, (1953).

26) A. R. Shultz, *J. Am. Chem. Soc.*, **80**, 1854, (1958).

27) S. Candau, J. Bastide and M. Delsanti, *Adv. Polym. Sci.*, **44**, 30, (1982).

28) R. H. Kienle and F. E. Petke, *J. Am. Chem. Soc.*, **62**, 1053, (1940).

29) P. J. Flory, *J. Am. Chem. Soc.*, **62**, 1057, (1940).

30) F. P. Price, J. H. Gibbs and B. H. Zimm, *J. Phys. Chem.*, **62**, 972, (1958).

31) P. J. Flory, *J. Am. Chem. Soc.*, **63**, 3083, (1941).

32) R. H. Wiley and E. E. Sale, *J. Polym. Sci.*, **42**, 491, (1960).

33) A. C. Shah, I. W. Parsons and R. N. Haward, *Polymer*, **21**, 825, (1980).

34) A. G. Mikos, C. G. Takoudis and N. A. Peppas, *Polymer*, **28**, 998, (1987).

35) D. T. Landin and C. W. Macosko, *Macromolecules*, **21**, 846, (1988).

36) N. A. Dotson, T. Diekmann, C. W. Macosko and M. Tirrell, *Macromolecules*, **25**, 4490, (1992).

37) W. H. Li, A. E. Hamielec and C. M. Crowe, *Polymer*, **30**, 1513, (1989).

38) W. H. Li, A. E. Hamielec and C. M. Crowe, *Polymer*, **30**, 1518, (1989).

39) G. Hild and R. Okasha, *Makromol. Chem.*, **186**, 93, (1985).

40) R. Okasha, G. Hild and P. Rempp, *Eur. Polym. J.*, **15**, 975, (1979).

41) M. Antonietti and C. Rosenauer, *Macromolecules*, **24**, 3434, (1991).

42) B. Walczynski, B. N. Kolarz and H. Galina, *Polym. Commun.*, **26**, 276, (1985).

43) H. Kast and W. Funke, *Makromol. Chem.*, **180**, 1335, (1979).

44) O. Okay, M. Kurz, K. Lutz and W. Funke, *Macromolecules*, **28**, 2728, (1995).

45) O. Okay, *Polymer*, **35**, 796, (1994).

46) W. Funke, *Adv. Org. Sci and Tech. Ser.* (*Proc. 6th Int. Conf. Org. Coat. Sci. Tech.*), 339, (1982).

47) W. E. Funke, *J. Coat. Tech.*, **60**, 69, (1988).

48) O. Olabisi, L. M. Robeson and M. T. Shaw, *Polymer-Polymer Miscibility*, Academic Press, New York, Chapter 2, (1979).

49)   D. R. Paul In *Multicomponent Polymer Materials*, Eds. D. R. Paul and L. H. Sperling, Advances in Chemistry 211, American Chemical Society, Washington D.C., p. 3, (1986).

50)   S. Krause In *Polymer Blends*, Eds. D. R. Paul and S. Newman, Academic Press, New York, Chapter 2, (1978).

51)   G. R. Williamson and B. Wright, *J. Polym. Sci., Part A*, **3**, 3885, (1965).

52)   L. A. Utracki In *Interpenetrating Polymer Networks*, Eds. D. Klempner, L. H. Sperling and L. A. Utracki, Advances in Chemistry 239, American Chemical Society, Washington D.C., p. 77, (1994).

53)   J. P. Kennedy and A. Vidal, *J. Polym. Sci., Polym. Chem. Ed.*, **13**, 1765, (1975).

54)   J. P. Kennedy, *J. Polym. Sci., Polym. Chem. Ed.*, **13**, 2213, (1975).

55)   L. A. Pilato, J. V. Koleske, B. L. Joesten and L. M. Robeson, *Polym. Prepr.*, **17**, 824, (1976).

56)   P. S. Tucker, J. W. Barlow and D. R. Paul, *Macromolecules*, **21**, 2794, (1988).

57)   H.-K. Lee, C.-K. Kang and W.-C. Zin, *Polymer*, **37**, 287, (1996).

58)   P. W. Atkins, *Physical Chemistry*, 3rd Edition, Oxford University Press, Chapter 9, (1986).

59)   J. W. Barlow, *Makromol. Chem., Macromol. Symp.*, **70/71**, 235, (1993).

60)   T. Sulzberg and R. J. Cotter, *J. Polym. Sci., A-1*, **8**, 2747, (1970).

61)   H. Sato and A. Nakajima, *Polym. J.*, **7**, 241, (1975).

62)   P. J. Flory, *J. Chem. Phys.*, **9**, 660, (1941).

63)   M. L. Huggins, *J. Chem. Phys.*, **9**, 440, (1941).

64)   P. J. Flory, *J. Chem. Phys.*, **10**, 51, (1942).

65)   J. M. G. Cowie, *Makromol Symp.*, **78**, 15, (1994).

66)   J. M. G. Cowie, V. M. C. Reid and I. J. McEwen, *Polymer*, **31**, 905, (1990).

67)   J. M. G. Cowie, G. Li and I. J. McEwen, *Polymer*, **35**, 5518, (1994).

68)   R. L. Scott, *J. Chem. Phys.*, **17**, 279, (1949).

69)   G. R. Brannock and D. R. Paul, *Macromolecules*, **23**, 5240, (1990).

70)   N. Nishimoto, H. Keskkula and D. R. Paul, *Polymer*, **30**, 1279, (1989).

71)   C. A. Cruz, J. W. Barlow and D. R. Paul, *Macromolecules*, **12**, 726, (1979).

72)   C. H. Lai, D. R. Paul and J. W. Barlow, *Macromolecules*, **21**, 2492, (1988).

73)   S. Rostami and D. J. Walsh, *Macromolecules*, **18**, 499, (1985).

74) J. V. Koleske and R. D. Lundberg, *J. Polym. Sci., Part A-2*, **7**, 795, (1969).

75) C. F. Hammer, *Macromolecules*, **4**, 69, (1971).

76) J. J. Hickman and R. M. Ikeda, *J. Polym. Sci., Polym. Phys. Ed.*, **11**, 1713, (1973).

77) L. M. Robeson and J. E. McGrath, *Polym. Eng. Sci.*, **17**, 300, (1977).

78) J. W. Schurer, A. deBoer and G. Challa, *Polymer*, **16**, 201, (1975).

79) S. J. Krause, *J. Macromol. Sci.-Rev. Macromol. Chem.*, **C7**, **2**, 251, (1972).

80) J. L. Halary, J. M. Ubrich, J. M. Nunzi, L. Monnerie and R. S. Stein, *Polymer*, **25**, 956, (1984).

81) G. M. Bartenev and G. S. Kongarov, *Rubber Chem. Technol.*, **36**, 668, (1963).

82) J. L. White and P. A. Mirau, *Macromolecules*, **26**, 3049, (1993).

83) M. Bank, J. Leffingwell and C. Thies, *J. Polym. Sci., A-2*, **10**, 1097, (1972).

84) P. A. Mirau, S. A. Heffner, G. Koegler and F. Bovey, *Polym. Int.*, **26**, 29, (1991).

85) P. A. Mirau, J. L. White and S. A. Heffner, *Macromol. Symp.*, **86**, 181, (1994).

86) P. Cifra, F. E. Karasz and W. J. MacKnight, *Macromolecules*, **22**, 3089, (1989).

87) W. Gibbs, *Collected Works*, Longman, Green and Co., New York, Vol. 1, Chapter 1, (1928).

88) S. Matsuda, *Polym. J.*, **23**, 435, (1991).

89) W. Ostwald, quoted by M. Volmer In *Kinetik der Phasenbildung*, Edwards, Ann Arbor, Michigan, Chapter 1, (1945).

90) I. M. Lifshitz and V. V. Slyozov, *J. Phys. Chem. Solids, Lett. Edn.*, **19**, 35, (1961).

91) J. W. Cahn and J. E. Hilliard, *J. Chem. Phys.*, **28**, 258, (1958).

92) J. W. Cahn and J. E. Hilliard, *J. Chem. Phys.*, **31**, 688, (1959).

93) L. H. Sperling, *Introduction to Physical Polymer Science*, Wiley-Interscience, New York, Chapter 2, (1992).

94) L. H. Sperling, *Interpenetrating Polymer Networks and Related Materials*, Plenum Press, New York, Chapters 1, 4, and 7, (1981).

95) T. Nishi, T. T. Wang and T. K. Kwei, *Macromolecules*, **8**, 227, (1975).

96) L. P. McMaster, *Adv. Chem. Ser.*, **142**, 43, (1975).

97) V. D. J. Stein, R. H. Jung, K. H. Illers and H. Hendus, *Angew. Makromol. Chem.*, **36**, 89, (1974).

98) L. H. Sperling, *J. Polym. Sci., Macromol. Rev.*, **12**, 141, (1977).

99) L. H. Sperling In *Multicomponent Polymer Materials*, Eds. D. R. Paul and L. H. Sperling, Advances in Chemistry 211, American Chemical Society, Washington D.C., p. 21, (1986).

100) L. H. Sperling In *Interpenetrating Polymer Networks*, Eds. D. Klempner, L. H. Sperling and L. A. Utracki, Advances in Chemistry 239, American Chemical Society, Washington D.C., p. 3, (1994).

101) L. H. Sperling, T.-W. Chiu and D. A. Thomas, *J. Appl. Polym. Sci.*, **17**, 2443, (1973).

102) J. A. Grates, D. A. Thomas, E. C. Hickey and L. H. Sperling, *J. Appl. Polym. Sci.*, **19**, 1731, (1975).

103) V. Huelck, D. A. Thomas and L. H. Sperling, *Macromolecules*, **5**, 340, (1972).

104) D. J. Hourston and J. A. McCluskey, *J. Appl. Polym. Sci.*, **31**, 645, (1986).

105) J. A. Manson and L. H. Sperling, *Polymer Blends and Composites*, Plenum Press, New York, p. 237, (1976).

106) R. M. Briber and B. J. Bauer, *Macromolecules*, **21**, 3296, (1988).

107) B. J. Bauer, R. M. Briber and C. C. Han, *Macromolecules*, **22**, 940, (1989).

108) M. I. Felisberti, L. L. Freeitas and R. Stadler, *Polymer*, **31**, 1441, (1990).

109) J. J. Fay, C. J. Murphy, D. A. Thomas and L. H. Sperling In *Sound and Vibration Damping with Polymers*, Eds. R. D. Corsaro and L. H. Sperling, ACS Symposium Series 424, American Chemical Society, Washington D.C., Chapter 3, (1990).

110) P. G. deGennes, *J. Phys.*, **40**, 69, (1979).

111) M. Narkis, Y. Talmon and M. Silverstein, *Polymer*, **26**, 1359, (1985).

112) C. J. McDonald, P. B. Smith, J. A. Roper, D. I. Lee and J. G. Galloway, *Colloid and Polym. Sci.*, **269**, 227, (1991).

113) D. J. Hourston and R. Satgurunathan, *J. Appl. Polym. Sci.*, **29**, 2969, (1984).

114) D. J. Hourston, R. Satgurunathan and H. Varma, *J. Appl. Polym. Sci.*, **31**, 1955, (1986).

115) D. J. Hourston, R. Satgurunathan and H. Varma, *J. Appl. Polym. Sci.*, **33**, 215, (1987).

116) D. J. Hourston, R. Satgurunathan and H. Varma, *J. Appl. Polym. Sci.*, **34**, 901, (1987).

117) A. K. Holdsworth and D. J. Hourston In *Interpenetrating Polymer Networks*, Eds. D. Klempner, L. H. Sperling and L. A. Utracki, Advances in Chemistry 239, American Chemical Society, Washington D.C., p. 449, (1994).

118) Z. Liucheng, L. Xiucuo and L. Tianchang, *J. Appl. Polym. Sci.*, **42**, 891, (1991).

119) L. H. Sperling, D. A. Thomas, J. E. Lorenz and E. J. Nagel, *J. Appl. Polym. Sci.*, **19**, 2225, (1975).

120) M. S. Silverstein and M. Narkis, *Polym. Eng. Sci.*, **29**, 824, (1989).

121) F. O. Eschbach and S. J. Huang In *Interpenetrating Polymer Networks*, Eds. D. Klempner, L. H. Sperling and L. A. Utracki, Advances in Chemistry 239, American Chemical Society, Washington D.C., p. 205, (1994).

122) J. K. Yeo, L. H. Sperling and D. A. Thomas, *J. Appl. Polym. Sci.*, **26**, 3283, (1981).

123) J. K. Yeo, L. H. Sperling and D. A. Thomas, *Polym. Eng. Sci.*, **21**, 696, (1981).

124) J. K. Yeo, L. H. Sperling and D. A. Thomas, *Polym. Eng. Sci.*, **22**, 190, (1982).

125) L. H. Sperling, D. W. Taylor, M. L. Kirkpatrick, H. F. George and D. R. Bardman, *J. Appl. Polym. Sci.*, **14**, 73, (1970).

126) L. H. Sperling, H. F. George, V. Huelck and D. A. Thomas, *J. Appl. Polym. Sci.*, **14**, 2815, (1970).

127) H. Adachi and T. Kotaka, *Polym. J.*, **14**, 379, (1982).

128) J. M. Widmaier and M. T. Tabka, *Eur. Polym. J.*, **28**, 499, (1992).

129) N. Parizel, G. Meyer and G. Weill, *Polymer*, **36**, 2323, (1995).

130) J. Lal, J. M. Widmaier, J. Bastide and F. Boue, *Macromolecules*, **27**, 6443, (1994).

131) P. J. Flory, *J. Am. Chem. Soc.*, **63**, 3096, (1941).

132) H. Tobita and K. Yamamoto, *Macromolecules*, **27**, 3389, (1994).

133) D. J. T. Hill, J. H. O'Donnell and P. W. O'Sullivan, *Macromolecules*, **18**, 9, (1985).

134) F. R. Mayo and F. M. Lewis, *J. Am. Chem. Soc.*, **66**, 1594, (1944).

135) G. Vandezande and A. Rudin, *Polym. Mat. Sci. Eng.*, **64**, 274, (1991).

136) M. S. El-Aasser In *An Introduction to Polymer Colloids*, Eds. F. Candau and R. H. Ottewill, Kluwer Academic Publishers, Dordrecht, p. 7, (1990).

137) W. A. Al-Shahib and A. S. Dunn, *J. Polym. Sci., Polym. Chem. Ed.*, **16**, 677, (1978).

138) W. C. Mast and C. H. Fischer, *Ind. Eng. Chem.*, **41**, 790, (1949).

139) J. A. Waters, *European Patent*, ERP **0327199**, (1989).

140) D. M. French, *J. Polym. Sci.*, **32**, 395, (1958).

141) A. Kashihara, K. Ishii, K. Kida, S. Ishikura and R. Mizuguchi, *Polym. Mat. Sci. Eng.*, **52**, 453, (1985).

142) E. W. Duck In *Encyclopedia of Polymer Science and Technology*, Eds. H. F. Mark, N. G. Gaylord and N. M. Bikales, Vol. 5, Wiley-Interscience, New York, p. 801, (1966).

143) H. J. Van Den Hul and J. W. Vanderhoff, *Br. Polym. J.*, **2**, 121, (1970).

144) Y. C. Chen, V. L. Dimonie and M. S. El-Aasser, *J. Appl. Polym. Sci.*, **42**, 1049, (1991).

145) C. S. Chern and G. W. Poehlein, *J. Polym. Sci., Polym. Chem. Ed.*, **25**, 617, (1987).

146) F. Hofmann, K. Dellbruck and K. Gottlob, *German Patent (Farbenfabriken Bayer A.G.)*, DRP **255129**, (1912).

147) W. D. Harkins, *J. Chem. Phys.*, **13**, 381, (1945).

148) W. D. Harkins, *J. Am. Chem. Soc.*, **69**, 1428, (1947).

149) W. D. Harkins, *J. Polym. Sci.*, **5**, 217, (1950).

150) M. Harada, M. Nomura, H. Kojima, W. Eguchi and S. Nagata, *J. Appl. Polym. Sci.*, **16**, 811, (1972).

151) W. V. Smith and R. H. Ewart, *J. Chem. Phys.*, **16**, 592, (1948).

152) W. V. Smith, *J. Am. Chem. Soc.*, **71**, 4077, (1949).

153) W. V. Smith, *J. Am. Chem. Soc.*, **70**, 3695, (1948).

154) L. Varela De La Rosa, E. D. Sudol, M. S. El-Aasser and A. Klein, *J. Polym. Sci., Polym. Chem. Ed.*, **34**, 461, (1996).

155) J. L. Gardon, *J. Polym. Sci. A-1*, **6**, 665, (1968).

156) R. M. Fitch and C. H. Tsai In *Polymer Colloids*, Ed. R. M. Fitch, Plenum Press, New York, p. 103, (1971).

157) J. Delgado, M. S. El-Aasser, C. A. Silebi and J. W. Vanderhoff, *J. Polym. Sci,. Polym. Chem. Ed.*, **24**, 861, (1986).

158) L. F. J. Noel, E. C. P. Brouwer, A. X. Van Herk and A. L. German, *J. Appl. Polym. Sci.*, **57**, 245, (1995).

159) K. Chujo, Y. Harada, S. Tokuhara and K. Tanaka, *J. Polym. Sci,. Part C*, **27**, 321, (1969).

160) M. P. Merkel, V. L. Dimonie, M. S. El-Aasser and J. W. Vanderhoff, *J. Polym. Sci,. Polym. Chem. Ed.*, **21**, 284, (1983).

161) J. Guillot In *Future Directions in Polymer Colloids*, Eds. M. S. El-Aasser and R. M. Fitch, NATO ASI, Series E, Applied Sciences No. 138, Nijhoff, The Hague, Chapter 4, (1987).

162) M. Morton, S. Kaizerman and M. W. Altier, *J. Colloid Sci.*, **9**, 300, (1954).

163) E. Vanzo, R. H. Marchessault and V. Stannett, *J. Colloid Sci.*, **20**, 62, (1965).

164) I. A. Maxwell, J. Kurja, G. H. J. Van Doremaele, A. L. German and B. R. Morrison, *Makromol. Chem.*, **193**, 2049, (1992).

165) I. A. Maxwell, J. Kurja, G. H. J. Van Doremaele and A.L. German, *Makromol. Chem.*, **193**, 2065, (1992).

166) A. M. Aerdts, M. W. A. Boei and A. L. German, *Polymer*, **34**, 574, (1993).

167) P. J. Flory and J. Rehner, *J. Chem. Phys.*, **11**, 521, (1943).

168) L. F. J. Noel, I. A. Maxwell and A. L. German, *Macromolecules*, **26**, 2911, (1993).

169) H. A. S. Schoonbrood, M. A. Van Den Boom, A. L. German and J. Hutovic, *J. Polym. Sci., Polym. Chem. Ed.*, **32**, 2311, (1994).

170) D. I. Lee, T. Kawamura and E. F. Stevens In *Future Directions in Polymer Colloids*, Eds. M. S. El-Aasser and R. M. Fitch, NATO ASI, Series E, Applied Sciences No. 138, Nijhoff, The Hague, p. 47, (1987).

171) I. Cho and K. W. Lee, *J. Appl. Polym. Sci.*, **30**, 1903, (1985).

172) M. Okubo, A. Yamada and T. Matsumoto, *J. Polym. Sci,. Polym. Chem. Ed.*, **16**, 3219, (1980).

173) C. Tongyu, X. Yongshen, S. Yuncheng, L. Fu, L. Xing and H. Yuhong, *J. Appl. Polym. Sci.*, **41**, 1965, (1990).

174) J. Clauss, K. Schmidt-Rohr, A. Adam, C. Boeffel and H. W. Spiess, *Macromolecules*, **25**, 5208, (1992).

175) L. W. Worgan, *J. Appl. Polym. Sci.*, **27**, 2033, (1982).

176) M. F. Mills, R. G. Gilbert and D. H. Napper, *Macromolecules*, **23**, 4247, (1990).

177) J. Berg, D. C. Sundberg and B. Kronberg, *Polym. Mat. Sci. Eng.*, **54**, 367, (1986).

178) S. Lee and A. Rudin, *Makromol. Chem., Rapid Commun.*, **10**, 655, (1989).

179) S. Lee and A. Rudin, *J. Polym. Sci,. Polym. Chem. Ed.*, **30**, 2211, (1992).

180) M. A. Winnik, C. Zhao, O. Shaffer and R. R. Shivers, *Langmuir*, **9**, 2053, (1993).

181) S. Shen, M. S. El-Aasser, V. L. Dimonie, J. W. Vanderhoff and E. D. Sudol, *J. Polym. Sci., Polym. Chem. Ed.*, **29**, 857, (1991).

182) D. Beyer, W. Lebek, W.-D. Hergerth and K. Schmutzler, *Colloid and Polym. Sci.*, **268**, 744, (1990).

183) M. P. Wai, R. A. Gelman, M. G. Fatica, R. H. Hoerl and G. D. Wignall, *Polymer*, **28**, 918, (1987).

184) J. L. Joensson, H. Hassander, L. H. Jansson and B. Toernell, *Macromolecules*, **24**, 126, (1991).

185) D. I. Lee and T. Ishikawa, *J. Polym. Sci., Polym. Chem. Ed.*, **21**, 147, (1983).

186) T. I. Min, A. Klein, M. S. El-Aasser and J. W. Vanderhoff, *J. Polym. Sci., Polym. Chem. Ed.*, **21**, 2845, (1983).

187) T. I. Min, T. Miyamoto and H. Inagaki, *Rubber Chem. Tech.*, **50**, 63, (1977).

188) T. I. Min, *Polymer (Korea)*, **2**, 146, (1978).

189) Y. Talmon and W. G. Miller, *J. Colloid Interface Sci.*, **67**, 284, (1978).

190) Y. Talmon, *Ultramicroscopy*, **14**, 533, (1984).

191) A. Chapiro in *Radiation Chemistry of Polymeric Systems*, Interscience, New York, Chapter 4, (1961).

192) F. A. Bovey and L. W. Jelinski, *J. Phys. Chem.*, **89**, 571, (1985).

193) F. Heatley, *Prog. in NMR Spectrosc.*, **13**, 47, (1979).

194) E. I. Du Pont de Nemours and Company, *Br. Pat.* **2 039 496A**, (1979).

195) J. S. Chiou and D. R. Paul, *J. Appl. Polym. Sci.*, **32**, 4793, (1986).

196) Y. J. Shur and B. Ranby, *J. Appl. Polym. Sci.*, **20**, 3121, (1976).

197) T. K. Kwei, T. Nishi and R. F. Roberts, *Macromolecules*, **7**, 667, (1974).

198) T. Nishi and T. T. Wang, *Macromolecules*, **8**, 909, (1975).

199) D. R. Paul, *J. Membrane Sci.*, **18**, 75, (1984).

200) R. Arshady, *J. Microencaps.*, **5**, 101, (1988).

201) W. Funke, W. Beer and U. Seitz, *Prog. Colloid and Polym. Sci.*, 57, 48, (1975).

202) Z. Ding, S. Ma, D. Kriz, J. J. Aklonis and R. Salovey, *J. Polym. Sci., Polym. Phys. Ed.*, 30, 1189, (1992).

203) J. L. Forget, C. Booth, P. H. Canham, M. Duggleby, T. A. King and C. Price, *J. Polym. Sci., Polym. Phys. Ed.*, 17, 1403, (1979).

204) M. Nair, *Prog. Org. Coat.*, 20, 53, (1992).

205) C. K. Ober and K. P. Lok, *Macromolecules*, 20, 268, (1987).

206) C. K. Ober, *Makromol. Chem., Macromol. Symp.*, 35/36, 87, (1990).

207) C. M. Tseng, Y. Y. Lu, M. S. El-Aasser and J. W. Vanderhoff, *J. Polym. Sci., Polym. Chem. Ed.*, 24, 2995, (1986).

208) B. Thomson, A. Rudin and G. Lajoie, *J. Polym. Sci., Polym. Chem. Ed.*, 33, 345, (1995).

209) K. Li and H. D. H. Stoever, *J. Polym. Sci., Polym. Chem. Ed.*, 31, 2473, (1993).

210) K. Li and H. D. H. Stoever, *J. Polym. Sci., Polym. Chem. Ed.*, 31, 3257, (1993).

211) M. Okubo, K. Ikegami and Y. Yamamoto, *Colloid and Polym. Sci.*, 267, 193, (1989).

212) F. M. B. Coutinho and D. Rabelo, *Eur. Polym. J.*, 28, 1593, (1992).

213) D. Rabelo and F. M. B. Coutinho, *Eur. Polym. J.*, 30, 675, (1994).

214) A. I. Medalia, *J. Polym. Sci.*, 6, 423, (1951).

215) H. Staudinger and E. Husemann, *Berichte*, 68, 1618, (1935).

216) Z. Ding, J. J. Aklonis and R. Salovey, *J. Polym. Sci., Polym. Phys. Ed.*, 29, 1035, (1991).

217) M. Antonietti, W. Bremser and M. Schmidt, *Macromolecules*, 23, 3796, (1990).

218) K. E. J. Barrett, *Dispersion Polymerization in Organic Media*, Wiley, New York, Chapters 1, 2 and 4, (1975).

219) M. D. Croucher and M. A. Winnik In *Future Directions in Polymer Colloids*, Eds. M. S. El-Aasser and R. M. Fitch, NATO ASI, Series E, Applied Sciences 138, Nijhoff, The Hague, p. 209, (1987).

220) J. V. Dawkins, G. G. Maghami, S. A. Shakir and J. S. Higgins, *Colloid and Polym. Sci.*, 264, 616, (1986).

221) M. Okubo, Y. Katayama and Y. Yamamoto, *Colloid and Polym. Sci.*, 269, 217, (1991).

222) M. Okubo, M. Shiozaki, M. Tsujihiro and Y. Tsukuda, *Colloid and Polym. Sci.*, **269**, 222, (1991).

223) M. Okubo and T. Nakagawa, *Colloid and Polym. Sci.*, **272**, 530, (1994).

224) C. M. Cheng, F. J. Micale, J. W. Vanderhoff and M. S. El-Aasser, *J. Polym. Sci., Polym. Chem. Ed.*, **30**, 235, (1992).

225) S. B. Downing, *Royal Soc. Chem., Special Publication*, **87**, 326, (1991).

226) C. W. A. Bromley, *J. Coat. Tech.*, **61**, 39, (1989).

227) V. E. Shashoua and R. G. Beaman, *J. Polym. Sci.*, **33**, 101, (1958).

228) B. E. Rodriguez and E. W. Kaler, *Langmuir*, **8**, 2376, (1992).

229) A. Einstein, *Ann. Physik.*, **17**, 459, (1905).

230) A. Einstein, *Ann. Physik.*, **19**, 271, (1906).

231) A. Einstein, *Ann. Physik.*, **34**, 591, (1911).

232) D. W. Van Krevelen, *Properties of Polymers: Their Estimation and Correlation with Chemical Structure*, 2nd Edition, Elsevier Scientific, Amsterdam, Chapter 7, (1976).

233) B. E. Rodriguez, E. W. Kaler and M. S. Wolfe, *Langmuir*, **8**, 2382, (1992).

234) R. Buscall, *Colloids and Surfaces, Physico. and Eng. Asp. Ed.*, **83**, 33, (1994).

235) R. Buscall, *Langmuir*, **8**, 2077, (1992).

236) K. Tharanikkarasu and G. Radhakrishnan, *Eur. Polym. J.*, **30**, 1351, (1994).

237) A. Ueda and S. Nagai, *J. Polym. Sci., Polym. Chem. Ed.*, **24**, 405, (1986).

238) B. Hazer, *Macromol. Chem. Phys.*, **196**, 1945, (1995).

239) H. Dicke and W. Heitz, *Colloid and Polym. Sci.*, **260**, 3, (1982).

240) R. Walz, B. Boemer and W. Heitz, *Makromol. Chem.*, **178**, 2527, (1977).

241) A. Ueda and S. Nagai, *J. Polym. Sci., Polym. Chem. Ed.*, **22**, 1611, (1984).

242) A. Ueda and S. Nagai, *J. Polym. Sci., Polym. Chem. Ed.*, **22**, 1783, (1984).

243) A. Ajayaghosh, *Polymer*, **36**, 2050, (1995).

244) O. Nuyken and R. Weidner, *Adv. Polym. Sci.*, **73/74**, 145, (1985).

245) O. Nuyken and R. Weidner, *Makromol. Chem.*, **189**, 1331, (1988).

246) T. Yamamoto, K. Aoshima, H. Ohmura, Y. Moriya, N. Suzuki and Y. Oshibe, *Polymer*, **32**, 19, (1991).

247) K. A. Kun and R. Kunin, *J. Polym. Sci., Part A-1*, **6**, 2689, (1968).

248) J. A. Riddick and W. B. Bunger, *Organic Solvents*, Wiley-Interscience, New York, Chapter 3, (1970).

249) K. Ishii, A. Kashihara, H. Kayano, S. Ishikura and R. Mizuguchi, *Polym. Mat. Sci. Eng.*, **52**, 448, (1985).

250) J. Mitchell, *Anal. Chem.*, **23**, 1069, (1951).

251) J. L. Angulo-Sanchez and P. Caballero-Mata, *Rubber Chem. Tech.*, **54**, 34, (1981).

252) J. Brandrup and E. H. Immergut (Eds.), *Polymer Handbook*, 2nd Edition, Wiley-Interscience, New York, III-242, (1975).

253) M. Ishidoya and H. Mizutani, *Private Communication*, (1995).

254) H. Taube, *J. Am. Chem. Soc.*, **64**, 161, (1942).

255) D. A. Smith, *Addition Polymers*, Butterworths, London, p. 33, (1968).

256) E. Turi, *Thermal Analysis in Polymer Characterization*, Wiley-Heyden, New York, Chapters 3 and 5, (1981).

257) S. M. Ellerstein, *Appl. Polym. Symp.*, **2**, 111, (1966).

258) N. T. Wakelyn and P. R. Young, *J. Appl. Polym. Sci.*, **10**, 1421, (1966).

259) B. Wunderlich, *Thermal Analysis*, Academic Press, San Diego, p. 123, (1990).

260) D. Campbell and J. R. White, *Polymer Characterization*, Chapman and Hall, London, p. 304, (1989).

261) L. E. Nielsen, *J. Macromol. Sci.*, **C3**, 69, (1969).

262) J. Sionakidis, L. H. Sperling and D. A. Thomas, *J. Appl. Polym. Sci.*, **24**, 1179, (1979).

263) J. K. Yeo, L. H. Sperling and D. A. Thomas, *Polym. Eng. Sci.*, **22**, 178, (1982).

264) I. M. Ward, *Mechanical Properties of Solid Polymers*, 2nd Edition, Wiley-Interscience, New York, Chapter 6, (1985).

265) M. L. Williams, R. F. Landel and J. D. Ferry, *J. Am. Chem. Soc.*, **77**, 3701, (1955).

266) P. J. Flory, *J. Chem. Phys.*, **17**, 303, (1949).

267) N. C. Billingham, *Molar Mass Measurements in Polymer Science*, Wiley, New York, Chapter 1, (1977).

268) J. Brandrup and E. H. Immergut (Eds.), *Polymer Handbook*, 2nd Edition, Wiley-Interscience, New York, IV-1, (1975).

269) A. R. Cooper In *Analysis of Polymer Systems*, Eds. L. S. Bark and N. S. Allen, Applied Science, London, Chapter 9, (1982).

270) N. B. Colthup, L. H. Daly and S. E. Wiberley, *Introduction to Infrared and Raman Spectroscopy*, Academic Press, New York, Chapter 2, (1975).

271) K. S. Seshadri and R. N. Jones, *Spectrochim. Acta.*, **19**, 1013, (1963).

272) S. R. Jin and G. C. Meyer, *Polymer*, **27**, 592, (1986).

273) M. Claybourn and P. Turner, *Polym. Mat. Sci. Eng.*, **64**, 193, (1991).

274) D. L. Allara, A. Baca and C. A. Pryde, *Macromolecules*, **11**, 1215, (1978).

275) S. R. Culler, M. T. McKenzie, L. J. Fina, H. Ishida and J. L. Koenig, *Appl. Spectrosc.*, **38**, 791, (1984).

276) M. P. Fuller and P. R. Griffiths, *Anal. Chem.*, **50**, 1906, (1978).

277) A. H. Fawcett, *Nuc. Magn. Reson.*, **22**, 333, (1993).

278) A. H. Fawcett, *Nuc. Magn. Reson.*, **23**, 306, (1994).

279) W. Kemp, *NMR In Chemistry*, Macmillan Education, London, Chapters 1, 3, 4 and 5, (1986).

280) R. J. Abraham, J. Fisher and P. Loftus, *Introduction To NMR Spectroscopy*, Wiley, New York, Chapters 5 and 6, (1988).

281) H. Z. Cummins and E. R. Pike, *Photon Correlation and Light Beating Spectroscopy*, Plenum Press, New York, p. 387, (1973).

282) B. J. Berne and R. Pecora, *Dynamic Light Scattering*, Wiley, New York, Chapters 2 and 6, (1976).

283) I. Tomka and G. Vancso In *Applied Polymer Analysis and Characterization*, Ed. J. Mitchell, Carl Hanser Verlag, Munich, p. 238, (1987).

284) G. W. Miller, *Thermal Analysis*, Academic Press, New York, p. 435, (1969).

285) A. K. Doolittle, *J. Appl. Phys.*, **22**, 471, (1951).

286) F. Bueche and J. C. Halpin, *J. Appl. Phys.*, **35**, 36, (1964).

287) J. Janacek and J. Hasa, *Collect. Czech. Chem. Commun.*, **31**, 2186, (1966).

288) K. Ueberreiter and G. Kanig, *J. Chem. Phys.*, **18**, 399, (1950).

289) T. G Fox and S. Loshaek, *J. Polym. Sci.*, **15**, 391, (1955).

290) H. D. Heinze, K. Schmieder, G. Schnell and K. A. Wolf, *Rubber Chem. Technol.*, **35**, 776, (1962).

291) J. Malinsky, J. Klaban and K. Dušek, *J. Macromol. Sci.-Chem.*, **5**, 1071, (1971).

292) M. Bartholin, G. Boissier and J. Dubois, *Makromol. Chem.*, **182**, 2075, (1981).

293) R. A. Nyquist, *Appl. Spectrosc.*, **38**, 264, (1984).

294) P. Nakanishi and P. H. Solomon, *Infrared Absorption Spectroscopy*, 2nd Edition, Holden-Day, Oakland, California, Chapter 2, (1977).

295) T. Batzilla, *Thesis*, University of Stuttgart, (1988).

296) R. R. Willey, *Appl. Spectrosc.*, **30**, 593, (1976).

297) P. J. Brimmer, P. R. Griffiths and N. J. Harrick, *Appl. Spectrosc.*, **40**, 258, (1986).

298) H. Davies, M. B. Huglin and S. J. O'Donohue, *Polymer*, **30**, 1379, (1989).

299) M. B. Huglin and M. A. Radwan, *Polymer*, **32**, 3381, (1991).

300) D. Mangaraj, S. K. Bhatnagar and S. B. Rath, *Makromol. Chem.*, **67**, 75, (1963).

301) J. Brandrup and E. H. Immergut (Eds.), *Polymer Handbook*, 2nd Edition, Wiley-Interscience, New York, IV-341, (1975).

302) F. P. Reding, J. A. Faulker and R. P. Whitman, *J. Polym. Sci.*, **57**, 483, (1962).

303) M. C. Shen and A. Eisenberg, *Progress in Solid State Chemistry*, Vol. 3, Pergamon Press, New York, p. 407, (1966).

304) P. A. Lovell, T. H. Shah and F. Heatley, *Polym. Mat. Sci. Eng.*, **64**, 278, (1991).

305) T. G Fox, *Bull. Am. Phys. Soc.*, **1**, 123, (1954).

306) N. W. Johnston, *J. Macromol. Sci.*, **A7(2)**, 531, (1973).

307) S. C. Temin, *J. Appl. Polym. Sci.*, **9**, 471, (1965).

308) P. C. Painter, M. M. Coleman and J. L. Koenig, *The Theory of Vibrational Spectroscopy and its Application to Polymeric Materials*, Wiley, New York, Chapters 1, 3 and 7, (1982).

309) E. T. Severs, *Rheology of Polymers*, Reinhold Publishing, New York, p. 67, (1962).

310) J. H. Hildebrand and R. L. Scott, *Regular Solutions*, Prentice-Hall, New Jersey, p. 218, (1962).

311) J. Brandrup and E. H. Immergut (Eds.), *Polymer Handbook*, 2nd Edition, Wiley-Interscience, New York, IV-241, (1975).

312) I. Katime, P. Garro and J. M. Teijon, *Eur. Polym. J.*, **11**, 881, (1975).

313) M. B. Huglin and M. A. Radwan, *Polymer*, **32**, 1293, (1991).

314) I. Katime, M. B. Huglin and P. M. Sasia, *Eur. Polym. J.*, **24**, 561, (1988).

315) P. Munk, M. T. Abijaoude and M. E. Halbrook, *J. Polym. Sci., Polym. Phys. Ed.*, **16**, 105, (1978).

316) F. Vira, K. Vira, F. Aroni and A. Dondos, *Eur. Polym. J.*, **10**, 891, (1974).

317) P. Munk, R. G. Allen and M. E. Halbrook, *J. Polym. Sci.*, **C42**, 1013, (1973).

318) A. Vrij and J. T. G. Overbeek, *J. Colloid Sci.*, **17**, 570, (1962).

319) M. B. Huglin and R. W. Richards, *Polymer*, **17**, 587, (1976).

320) P. Kratochvil, J. Pouchly and B. Sedlacek, *J. Polym. Sci., Polym. Phys. Ed.*, **10**, 2057, (1972).

321) J. Stejskal and P. Kratochvil, *J. Polym. Sci., Polym. Phys. Ed.*, **13**, 715, (1975).

322) C. Feyereisen, M. Morcellet and C. Loucheux, *Macromolecules*, **12**, 613, (1979).

323) J. M. G. Cowie and S. Bywater, *J. Macromol. Chem.*, **1**, 581, (1966).

324) I. Katime, A. Campos and J. M. T. Rivera, *Eur. Polym. J.*, **15**, 291, (1979).

325) H. Nomura and M. Onoda, *Polym. J.*, **14**, 249, (1982).

326) M. C. Gonzalez, F. Zamora, M. L. Leon and G. M. Guzman, *J. Polym. Sci., Polym. Lett. Ed.*, **20**, 375, (1982).

327) S. Lee, *Trends In Polymer Science*, **1**, 303, (1993).

328) J.-P. Queslel, F. Fontaine and L. Monnerie, *Polymer*, **29**, 1086, (1988).

329) H. D. H. Stoever and J. M. J. Frechet, *Macromolecules*, **24**, 883, (1991).

330) T. P. Davis and M. B. Huglin, *Macromolecules*, **22**, 2824, (1989).

331) G. Natta, *J. Polym. Sci.*, **16**, 143, (1955).

332) M. L. Huggins, *Ann. N. Y. Acad. Sci.*, **44**, 431, (1943).

333) T. P. Davis, M. B. Huglin and D. C. F. Yip, *Polymer*, **29**, 701, (1988).

334) J. Brandrup and E. H. Immergut (Eds.), *Polymer Handbook*, 2nd Edition, Wiley-Interscience, New York, VII-2, (1975).

335) G. M. Bristow and W. F. Watson, *Trans. Faraday Soc.*, **54**, 1731, (1958).

336) A. J. Chompff and S. Newman, *Polymer Networks - Structure and Mechanical Properties*, Plenum Press, New York, Chapters 3 and 14, (1971).

337) K. L. Hoy, *J. Coat. Tech.*, **51**, 27, (1979).

338) P. D. Bartlett and R. R. Hiatt, *J. Am. Chem. Soc.*, **80**, 1398, (1958).

339) T. Sato and T. Otsu, *Polymer*, **11**, 389, (1975).

340) A. G. Davies and K. J. Hunter, *J. Chem. Soc.*, 1808, (1953).

341) N. A. Milas and D. M. Surgenor, *J. Am. Chem. Soc.*, **68**, 205, (1946).

342) A. Streitwieser and C. H. Heathcock, *Introduction to Organic Chemistry*, 3rd Edition, Macmillan Publishing, New York, p. 455, (1985).

343) K. Fujimori and S. Oae, *J. Chem. Soc., Perkin Trans.*, **2**, 1335, (1989).

344) P. D. Bartlett and R. Altschul, *J. Am. Chem. Soc.*, **67**, 812, (1945).

345) M. Litt and F. R. Eirich, *J. Polym. Sci.*, **35**, 379, (1960).

346) B. Ranby, *Appl. Polym. Symp.*, **26**, 327, (1975).

347) F. Heatley, P. A. Lovell and J. McDonald, *Eur. Polym. J.*, **29**, 255, (1993).

348) T. Otsu, O. Ito, N. Toyoda and S. Mori, *Makromol. Chem., Rapid. Commun.*, **2**, 725, (1981).

349) T. Otsu, B. Yamada and T. Ishikawa, *Macromolecules*, **24**, 415, (1991).

350) M. Yoshioka, A. Matsumoto and T. Otsu, *Polym. J.*, **23**, 1249, (1991).

351) B. Yamada, M. Fujita and T. Otsu, *Makromol. Chem.*, **192**, 1829, (1991).

352) K. E. J. Barrett, *J. Appl. Polym. Sci.*, **11**, 1617, (1967).

353) W. Ando, *Organic Peroxides*, Wiley, New York, p. 456, (1992).

354) B. Barnett and W. E. Vaughan, *J. Phys. Colloid Chem.*, **51**, 926, (1947).

355) F. Strain, W. E. Bissinger, W. R. Dial, H. Rudoff, B. J. DeWitt, H. C. Stevens and J. H. Langston, *J. Am. Chem. Soc.*, **72**, 1254, (1950).

356) K. Ito, S. Iwase, K. Umehara and Y. Yamashita, *J. Macromol. Sci.-Chem.*, **1**, 891, (1967).

357) F. Heatley, G. Yu, C. Booth and T. G. Blease, *Eur. Polym. J.*, **27**, 573, (1991).

358) L. E. Bogan, *Macromolecules*, **24**, 4807, (1991).

359) Y. D. Semchikov, L. A. Smirnova, T. Y. Knyazeva, S. A. Bulgakova and V. I. Sherstyanykh, *Eur. Polym. J.*, **26**, 883, (1990).

360) R. Mao, M. B. Huglin and T. P. Davis, *Eur. Polym. J.*, **29**, 475, (1993).

361) F. A. Bovey, G. V. D. Tiers and G. Filipovich, *J. Polym. Sci.*, **38**, 73, (1959).

362) F. Heatley and F. A. Bovey, *Macromolecules*, **1**, 301, (1968).

363) F. A. Bovey, *High Resolution NMR of Macromolecules*, Academic Press, New York, p. 125, (1972).

364) L. F. Johnson, F. Heatley and F. A. Bovey, *Macromolecules*, **3**, 175, (1970).

365) J. Coates In *Computer Methods in UV, Visible and IR Spectroscopy*, Eds. W. O. George and H. A. Willis, RSC Publications, Cambridge, p. 95, (1990).

366) W.-M. Kulicke and H.-H. Horl, *Colloid and Polym. Sci.*, **263**, 530, (1985).

367) M. A. Meilchen, B. M. Hasch and M. A. McHugh, *Macromolecules*, **24**, 4874, (1991).

368) R. G. Brown and J. E. Glass, *J. Appl. Polym. Sci.*, **36**, 1909, (1988).

369) H. A. Willis, J. M. Chalmers and M. W. Mackenzie In *Computerized Quantitative Infrared Analysis*, Ed. G. L. McClure, STP **934**, ASTM, Philadelphia, p. 58, (1987).

370) P. Kubelka and F. Munk, *Z. Tech. Phys.*, **12**, 593, (1931).

371) M. P. Fuller and P. R. Griffiths, *Appl. Spectrosc.*, **34**, 533, (1980).

372) G. Kortum, *Reflectance Spectroscopy*, Springer Press, New York, p. 77, (1969).

373) S. A. Yeboah, S.-H. Wang and P. R. Griffiths, *Appl. Spectrosc.*, **40**, 259, (1984).

374) M. Uyemura and S. Maeda, *Bull. Chem. Soc. Japan*, **45**, 2225, (1972).

375) D. Weir, A. Ajayaghosh, M. Muneer and M. V. George, *J. Photochem. Photobiol. Chem.*, **52**, 425, (1990).

APPENDICES

Appendix 1

Coaxial Sensors for Haake VT500 Rheometer
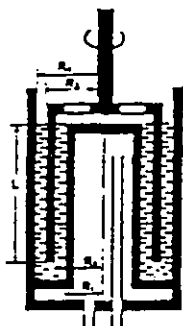
Sensor System	NV
System No.:	*1*
Inner Cylinder (Rotor) Radius R_2; R_3 (mm) Height L (mm)	17.85; 20.1 60
Outer Cylinder (Cup) Radius R_1; R_4 (mm)	17.5; 20.5
Radii Ratio R_a/R_i Gap Width (mm) Sample Volume V (cm^3) Temperature (°C)	1.02 0.35 9.0 −30/100
System Factors f M	 363 5410
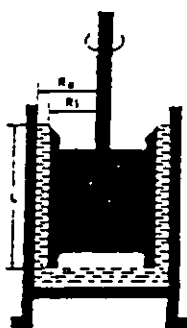
Sensor System	MV1	MV2	MV3
System No.:	*2*	*3*	*4*
Inner Cylinder (Rotor) Radius R_i (mm) Height L (mm)	20.04 60.0	18.4 60.0	15.2 60.0
Outer Cylinder (Cup) Radius R_a (mm)	21.0	21.0	21.0
Radii Ratio R_a/R_i Gap Width (mm) Sample Volume V (cm^3) Temperature (°C)	1.05 0.96 34.0	1.14 2.6 46.0 -30 / 100	1.38 5.8 66.0
System Factors f M	 657 2340	 768 900	 1110 440

277

PCS Size Distribution Curve for Aqueous PS (5 wt.% DVB) Microgel Latex

PS (5% DVB), ACVA

Live data
Cell type ZEM010
Data taken on 21/10/94 at 09:50:39
Merit 64.3 %   In range 99.1 %
Temperature 24.6   Viscosity 0.898 cP   Angle 90.0 deg
RI medium 1.34   RI particle 1.59 + Abs. 0.00

Cumulant Z Ave   49.3 nm   Polydispersity 0.059

Size distribution(s)

Diameter (nm) (x10^1)
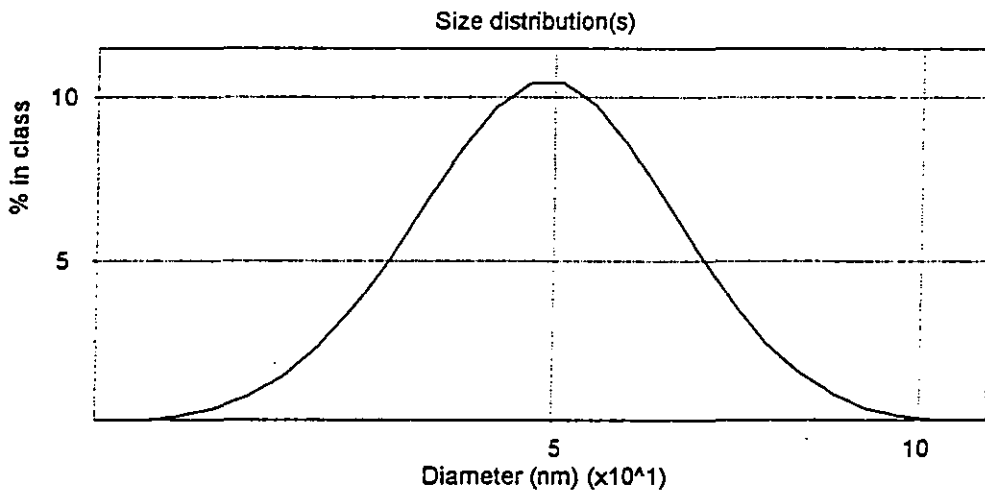
Size (nm)	% Intensity	Size (nm)	% Intensity	Size (nm)	% Intensity
23.5	0.1	39.3	6.8	65.6	5.3
25.1	0.2	41.9	8.4	69.9	3.7
26.7	0.4	44.7	9.7	74.5	2.5
28.5	0.8	47.6	10.4	79.5	1.5
30.4	1.5	50.8	10.5	84.7	0.9
32.4	2.4	54.1	9.8	90.3	0.5
34.6	3.6	57.7	8.5	96.3	0.2
36.8	5.1	61.5	6.9	102.7	0.1

Peak :   Mean 50.7 width 28.8 .

Analysis Monomodal   Fit 0.000445

Size Distribution Curve for Aqueous P*n*BA (20 wt.% EGDMA) Microgel Latex

PnBA (20% EGDM)

Live data
Cell type ZEM010
Data taken on 6/02/95 at 12:54:00
Merit 89.4 %   In range 84.8 %
Temperature 22.8   Viscosity 0.937 cP   Angle 90.0 deg
RI medium 1.33   RI particle 1.59 + Abs. 0.00

Cumulant Z Ave   41.7 nm   Polydispersity 0.214

Size distribution(s)
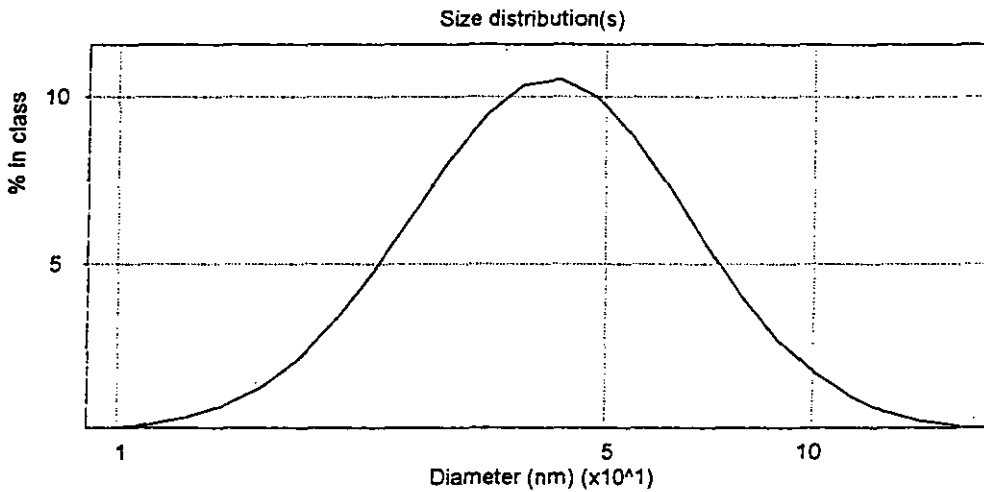
Size (nm)	% Intensity	Size (nm)	% Intensity	Size (nm)	% Intensity
9.9	0.1	26.4	6.4	70.0	5.6
11.2	0.2	29.8	8.1	79.1	4.1
12.7	0.4	33.7	9.5	89.4	2.7
14.3	0.7	38.0	10.3	101.0	1.7
16.2	1.3	43.0	10.5	114.1	1.0
18.3	2.2	48.6	10.0	128.9	0.5
20.7	3.3	54.9	8.8	145.6	0.3
23.4	4.8	62.0	7.3	164.5	0.1

Peak :   Mean 46.3 width 48.0

Analysis Monomodal   Fit 0.003587

Appendix 4

Transmittance FTIR Spectrum of Anhydrous *n*-Butanol
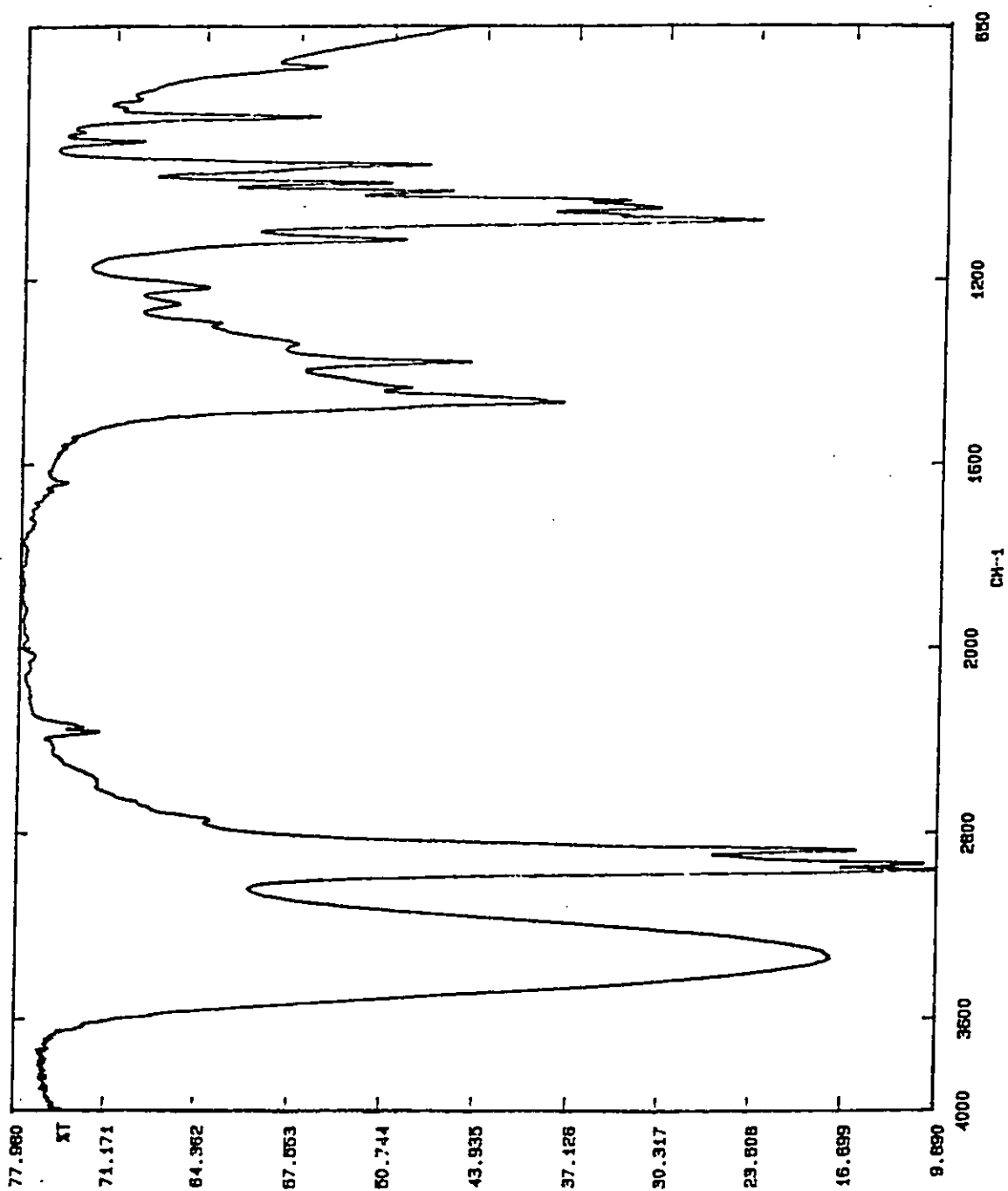
Appendix 5

Transmittance FTIR Spectrum of *n*-Butanol/H$_2$O Mixture (2 wt.% H$_2$O)
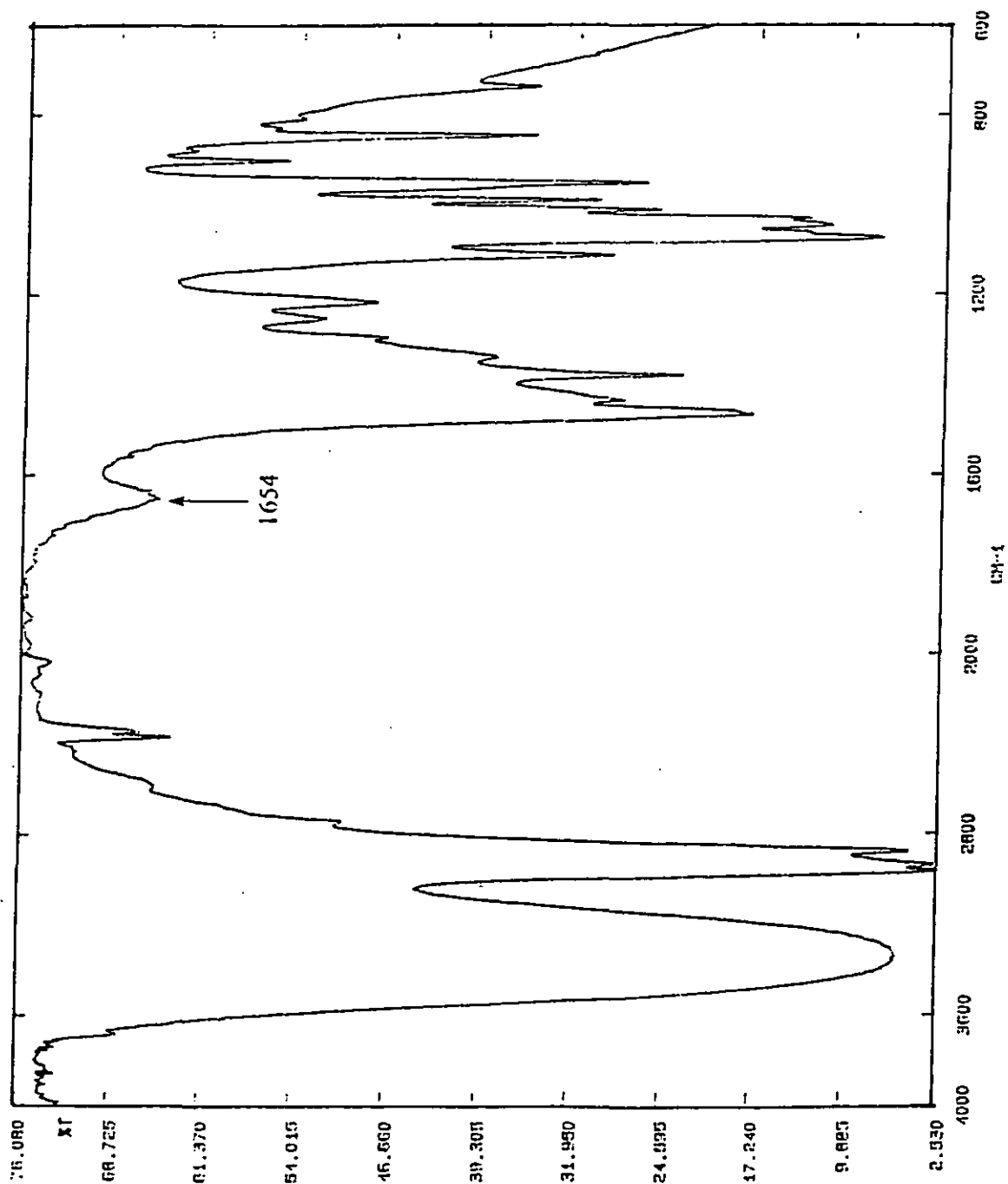
Appendix 6

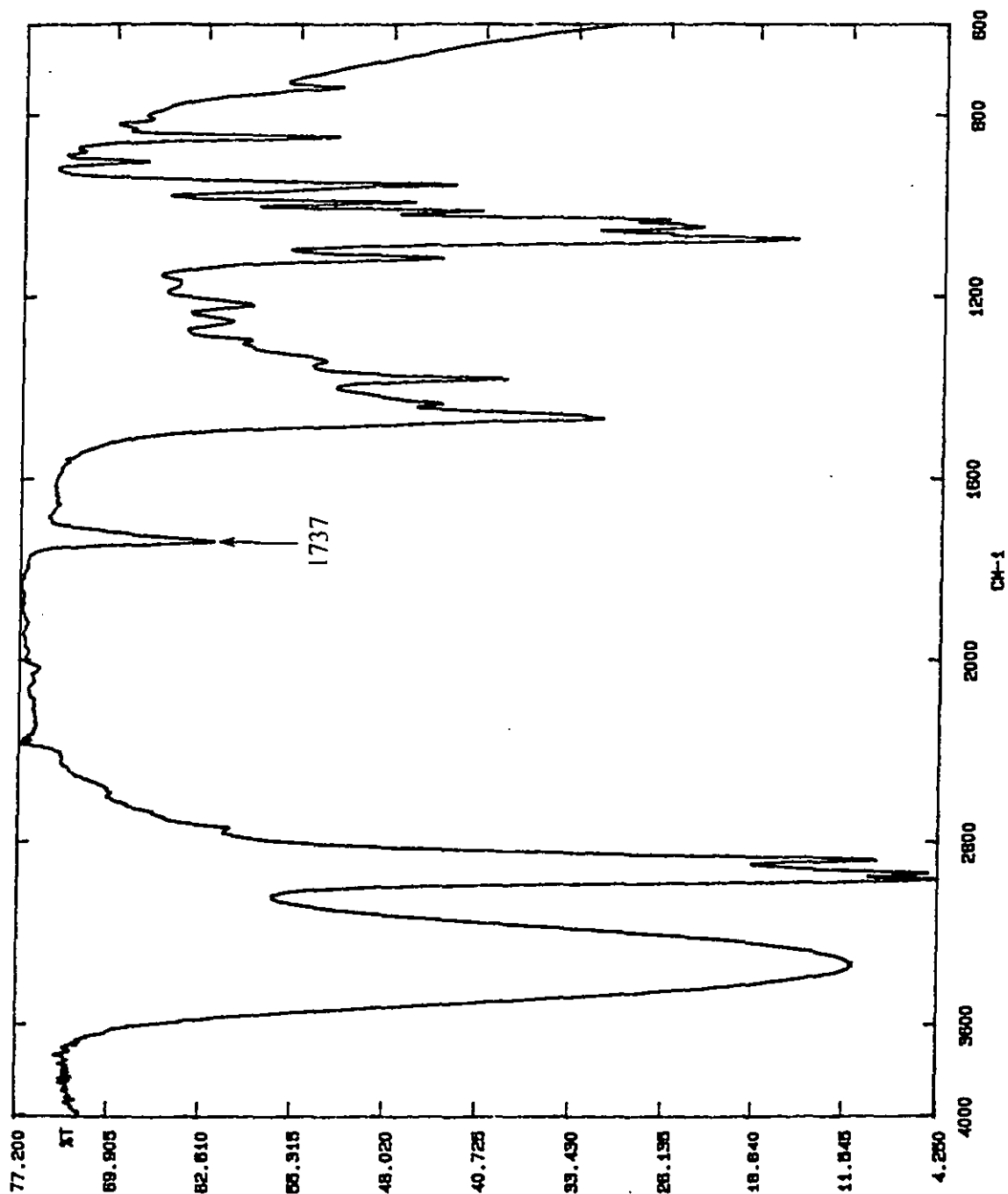## Transmittance FTIR Spectrum of Anhydrous Benzyl Alcohol
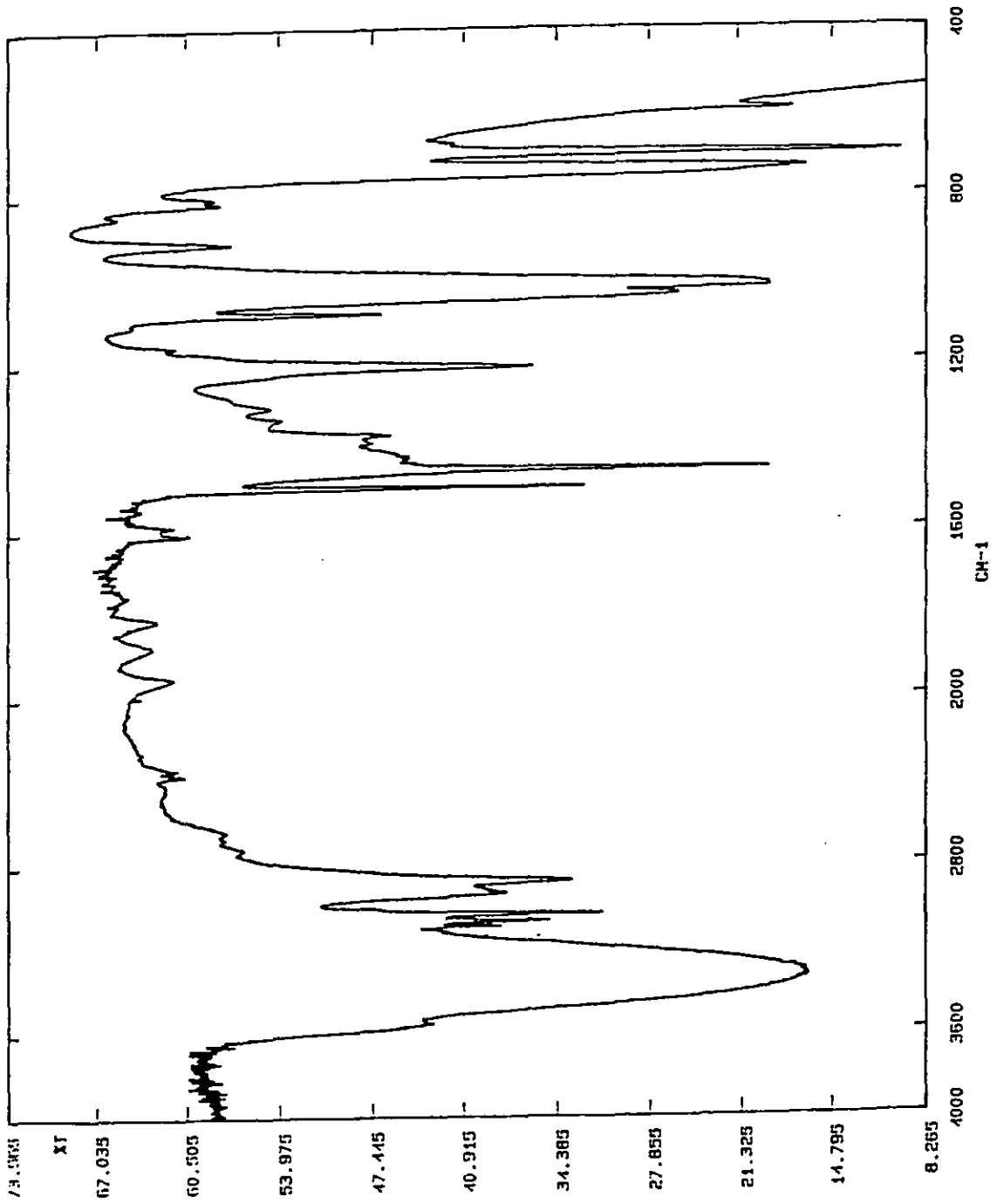
Appendix 7

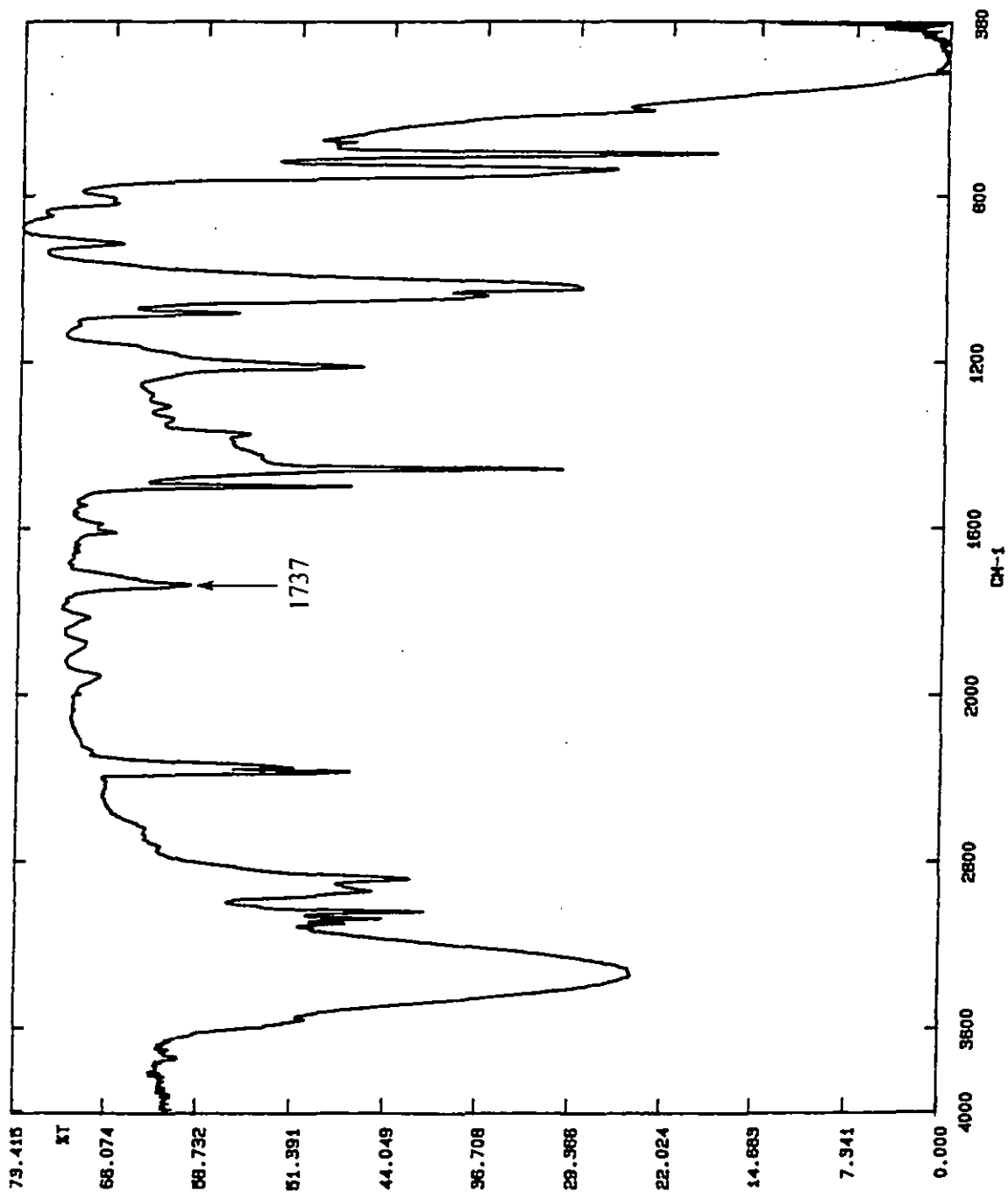## Transmittance FTIR Spectrum of Benzyl Alcohol/H_2O Mixture (5 wt.% H_2O)
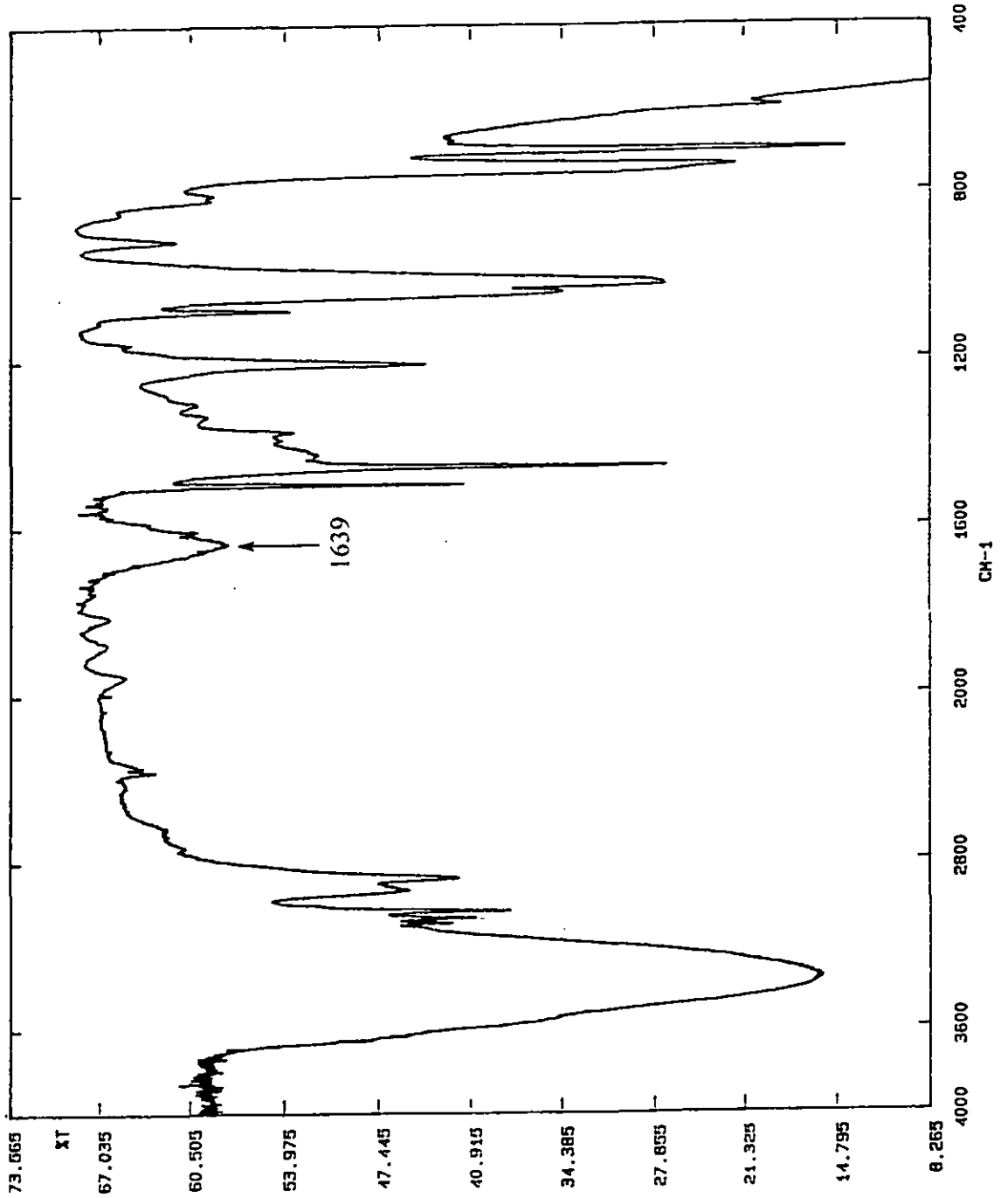
Appendix 8

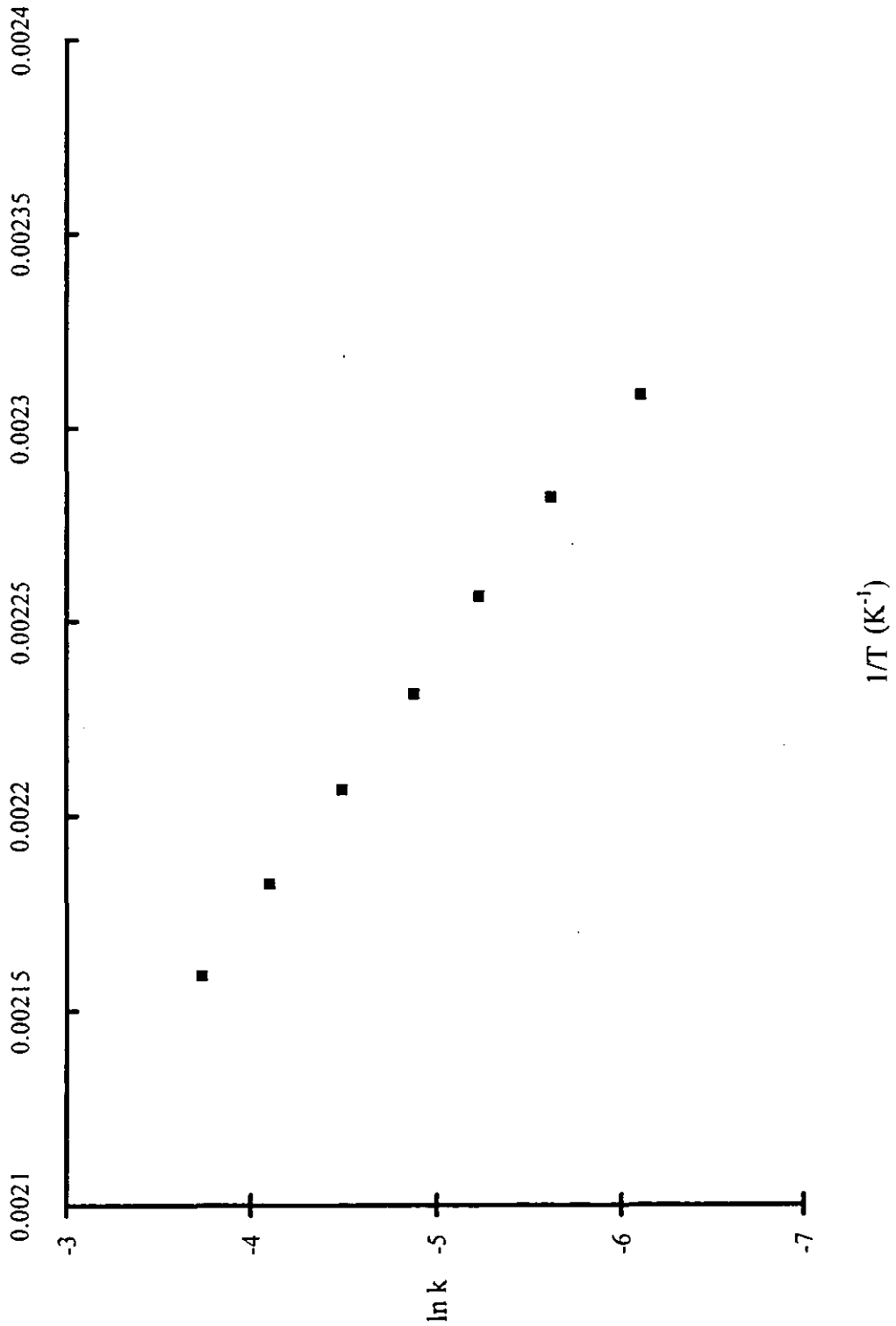FTIR Spectrum of P*n*BA (10 wt.% DVB) Microgel Dispersion in *n*-Butanol

FTIR Spectrum of P*n*BA (10 wt.% DVB) Microgel Dispersion in Benzyl Alcohol

Appendix 10

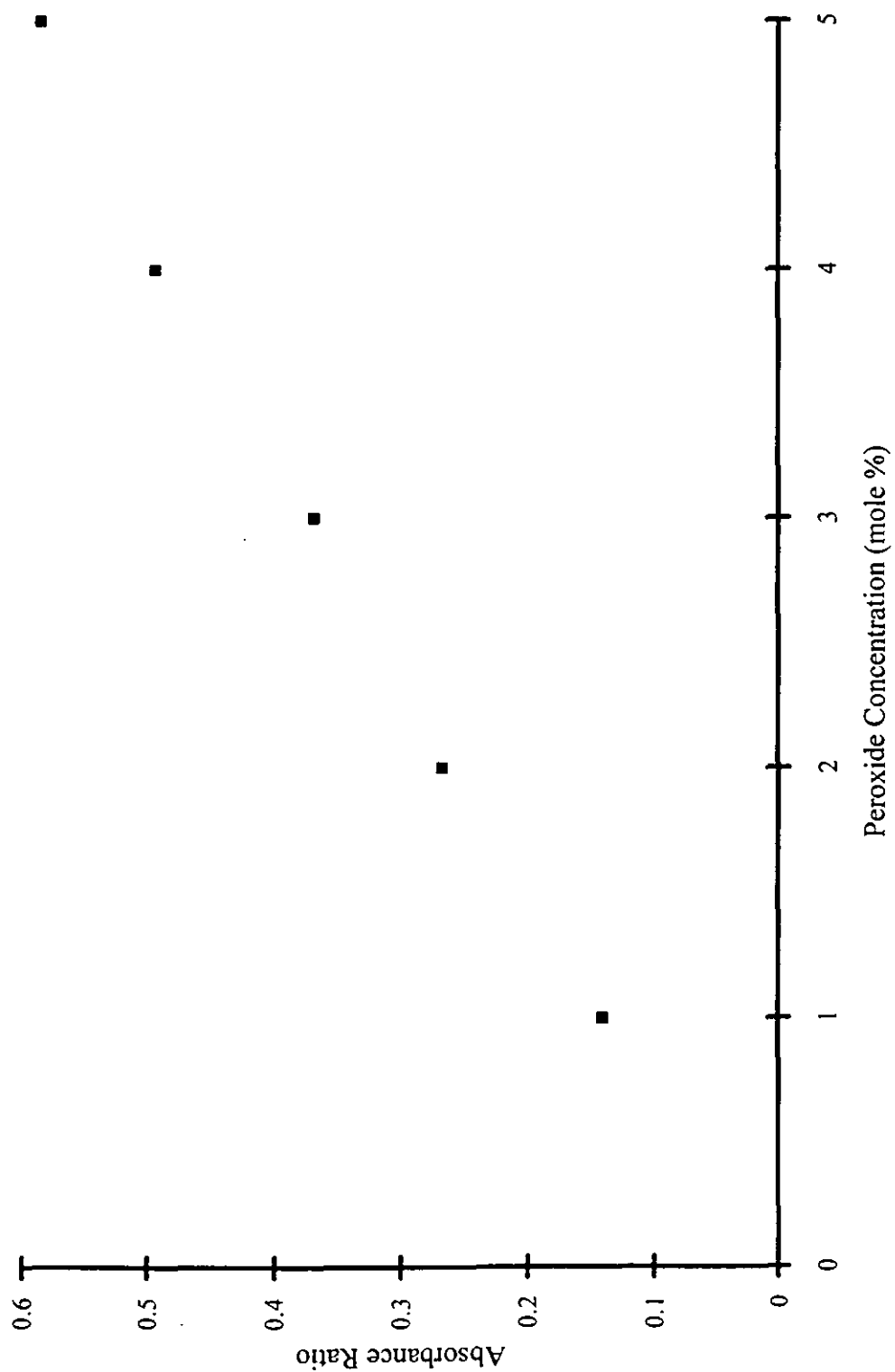Graph of ln K Versus 1/T for Thermal Dissociation of Styrene/PMEC
Copolymer Sample (DSC)

286

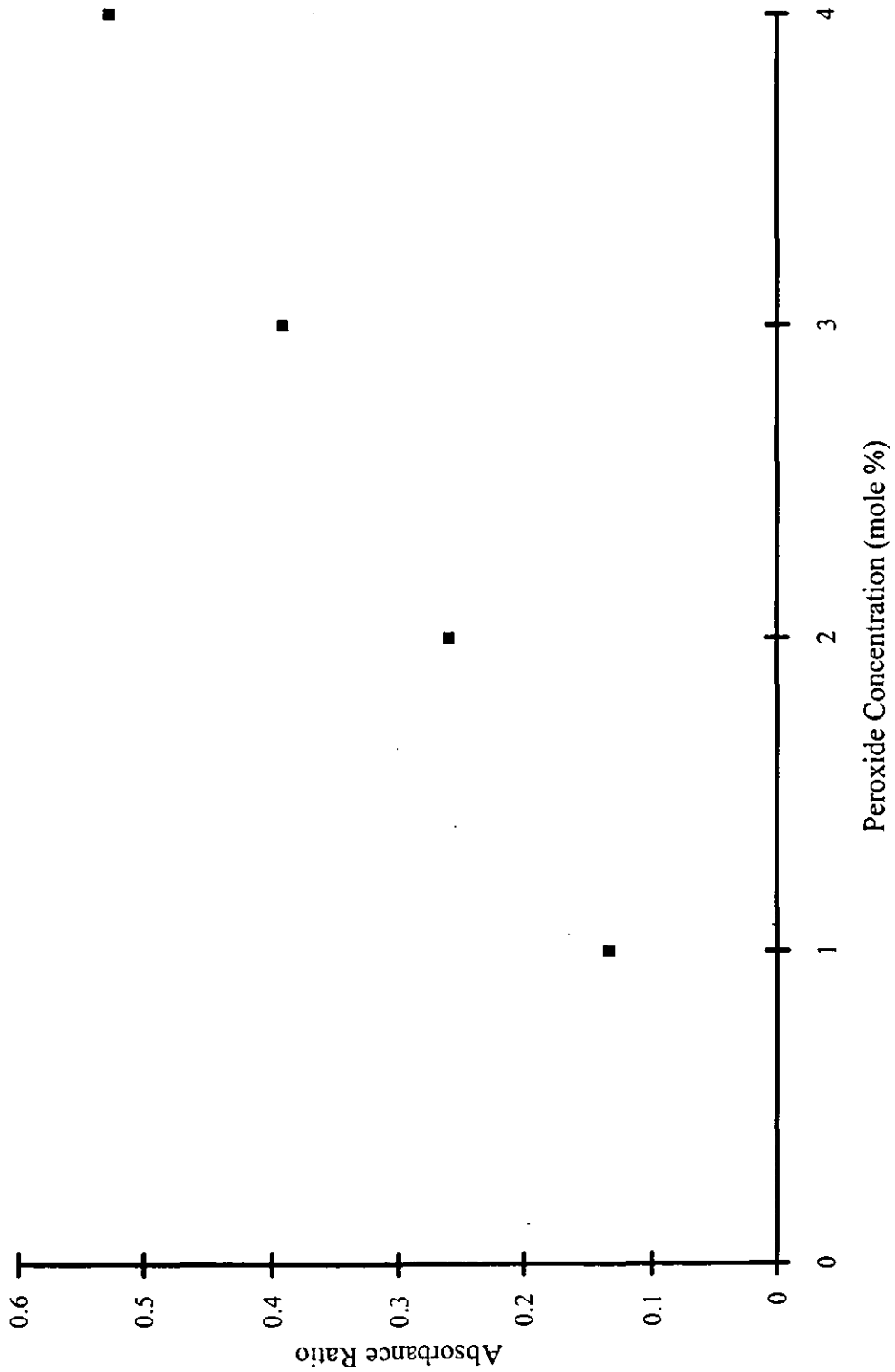Graph of ln K Versus 1/T for Thermal Dissociation of Styrene/DBPF
Copolymer Sample (DSC)
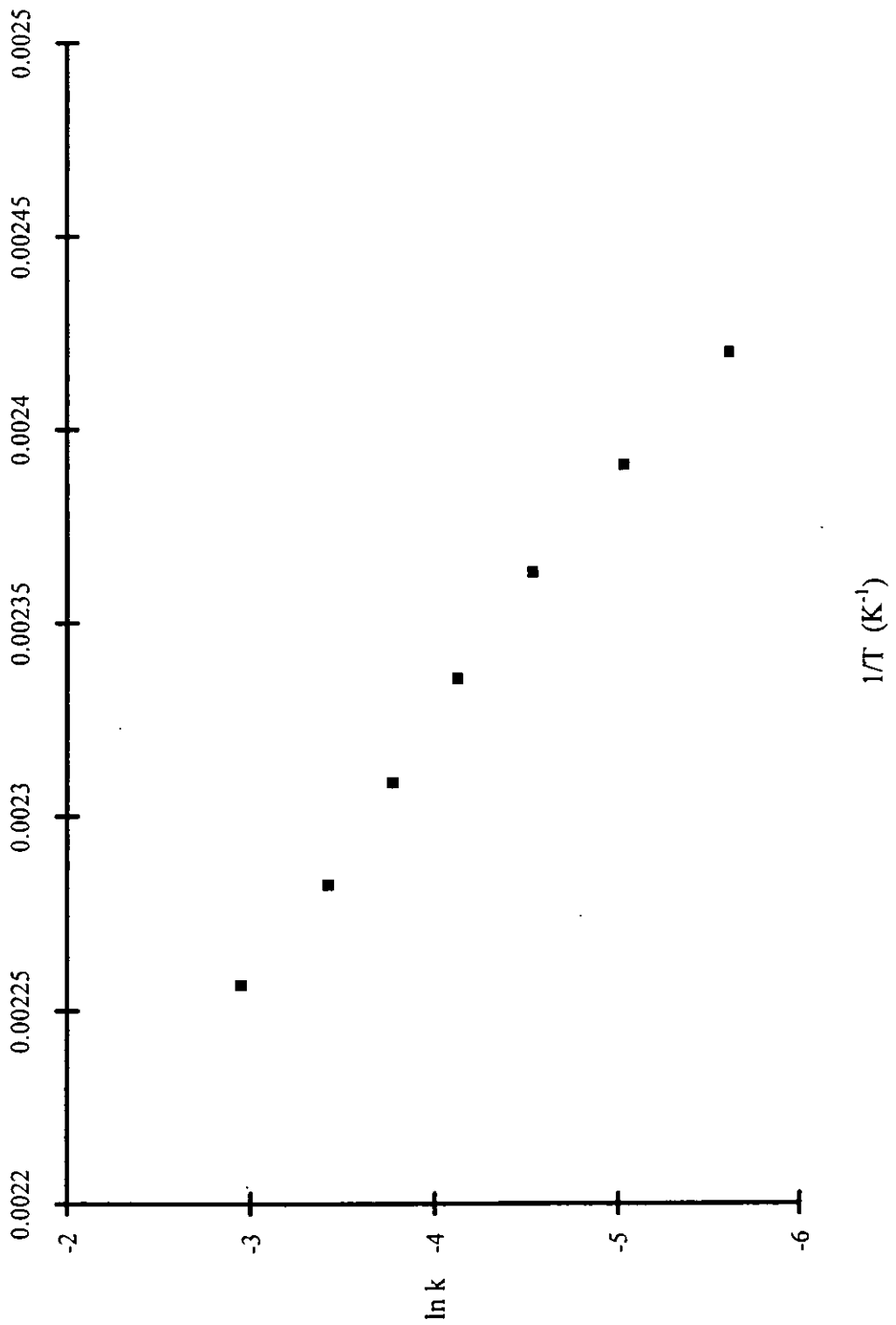
FTIR Absorbance Ratio Versus Peroxide Concentration Calibration Graph for Ethylbenzene/PMEC Mixtures

**FTIR Absorbance Ratio Versus Peroxide Concentration Calibration Graph
for Ethylbenzene/DBPF Mixtures**

**FTIR Absorbance Ratio Versus Peroxide Concentration Calibration Graph
for Ethylbenzene/ALPO Mixtures**